Technical University of Munich
Department of Electrical and Computer Engineering
Chair of Renewable and Sustainable Energy Systems (ENS)

Distribution Locational Marginal Price: Approximations, Solution Algorithm and Organization

Sarmad Hanif, M.Sc.

Vollständiger Abdruck der von der Fakultät für Elektrotechnik und Informationstechnik der Technischen Universität München zur Erlangung des akademischen Grades eines

Doktor-Ingenieurs (Dr.-Ing.)

genehmigten Dissertation.

Vorsitzender: Prof. Dr.-Ing. Ulf Schlichtmann

Prüfer der Dissertation

1. Prof. Dr. Thomas Hamacher
2. Prof. Hoay Beng Gooi, Ph.D.

Die Dissertation wurde am 14.06.2018 bei der Technischen Universität München eingereicht und durch die Fakultät für Elektrotechnik und Informationstechnik am 27.09.2018 angenommen.

Abstract

With the aim of de-carbonizing the power system and improving its economical operation, a rapid growth is seen towards the adoption of new technologies such as distributed generators and flexible loads. Physically, these technologies are integrated in distribution grids, which till date have been considered as the passive component of the power system — designed and operated based on a “fit and forget” philosophy. However, most distributed generators can be classified as highly variable renewable energy technologies whereas flexible loads are most naturally operated through profit-seeking entities without the aim of helping in improving the safety and security of the power system. These physical and operational requirements motivate a renewed approach towards the operation, maintenance and planning of distribution grids. This is one of the most pressing challenges currently faced by power systems around the world. This thesis is an attempt to addresses such a challenge in distribution grids, albeit on a formulation level. A framework to formulate distribution locational marginal price (DLMP) in distribution grids is proposed, a variant of the locational marginal price (LMP) at the transmission grid level.

In this thesis, a proposal is made to formulate, solve and organize distribution locational marginal price (DLMP) in a manner which is similar to the already existing transmission grid level locational marginal price (LMP). In this way, the proposed DLMP of this thesis has a higher practical realization, due to i) the readily transferable organizational lessons learned from implementing the LMP and ii) understanding/interpreting the price structure from the perspective of an electricity market. However, in contrast to transmission grids, distribution grids are very diverse in terms of their physical characteristics, presenting a challenge in readily adopting and deploying LMP concepts. This motivates the need for a new modeling and solution approach to calculate DLMPs in distribution grids, which is the main goal of this thesis. This thesis explores the state-of-the-art power flow modeling concepts for distribution grid, which caters for nonlinear power flows along with their diverse physical characteristics. The presented modeling concepts are explored in terms of their ability to provide power flow solution feasibility, robustness and approximation. These concepts are then utilized in proposing an optimization problem, mimicking a market framework at the distribution grid level. We term this framework as a local distribution grid market framework, which clears prices, i.e., DLMPs at each bus of the respective distribution grid on a day-ahead basis. Under the assumption of economically rational flexibility resources, the proposed market framework maximizes the overall social welfare of the distribution grid as well as for local flexibility resources. Moreover, the proposed local distribution grid market can cater for diverse physical characteristics of the distribution grids and varying flexibility resources types. By exploiting power flow approximation techniques and their solution feasibility concepts, a solution algorithm is proposed to solve the proposed local distribution grid market clearing problem. The proposed solution algorithm has the following advantages, it: i) aids in developing the DLMP formulation which closely resembles to the wholesale market, ii) incorporates the diverse physical characteristics of distribution grids and iii) efficiently allocates flexibility resources for both inter-temporal and instantaneous energy dispatch. To show the compatibility of the proposed method and its efficiency, tests are conducted on multiple benchmarked grid models and comparisons are made to the existing state-of-the-art relevant methodology.

Zusammenfassung

Mit dem Ziel, das Energiesystem zu entkohlen und seinen wirtschaftlichen Betrieb zu verbessern, wird ein rasches Wachstum in Richtung der Einführung neuer Technologien, wie verteilte Generatoren und flexible Lasten, beobachtet. Physikalisch sind diese Technologien in Verteilernetzen integriert, die bis heute als passive Komponente des Energiesystems betrachtet wurden – basierend auf einer "Fit and Forget" -Philosophie. Die meisten verteilten Generatoren können jedoch als hochvariable Technologien für

erneuerbare Energien klassifiziert werden, während flexible Lasten am natürlichsten durch Profit suchende Einheiten betrieben werden, ohne das Ziel zu haben, zur Verbesserung der Sicherheit des Energiesystems beizutragen. Diese physischen und betrieblichen Anforderungen motivieren zu einem neuen Ansatz für Betrieb, Wartung und Planung von Verteilnetzen. Dies ist eine der drängendsten Herausforderungen, denen sich Stromsysteme auf der ganzen Welt stellen müssen. Diese Arbeit ist ein Versuch, eine solche Herausforderung in Verteilungsnetzen zu lösen, wenn auch auf einer Formulierungsebene. Insbesondere wird ein Rahmen für die Formulierung des örtlichen Grenzpreises (DLMP) in Verteilungsnetzen vorgeschlagen, eine Variante des örtlichen Grenzpreises (LMP) auf der Übertragungsnetzebene.

In dieser Arbeit wird ein Vorschlag gemacht, um den lokalen Grenzpreis (DLMP) in einer Weise zu formulieren, zu lösen und zu organisieren, die ähnlich dem bereits existierenden Standortgrenzpreis (LMP) der Übertragungsnetzebene ist. Auf diese Weise hat der vorgeschlagene DLMP dieser Arbeit eine höhere praktische Realisierbarkeit, aufgrund i) der leicht übertragbaren organisatorischen Erkenntnisse aus der Umsetzung des LMP und ii) Verständnis / Interpretation der Preisstruktur aus der Perspektive eines Strommarktes. Im Gegensatz zu Übertragungsnetzen sind Verteilungsnetze jedoch sehr unterschiedlich in Bezug auf ihre physikalischen Eigenschaften, was eine Herausforderung darstellt, LMP-Konzepte leicht zu übernehmen und zu implementieren. Dies motiviert die Notwendigkeit eines neuen Modellierungs- und Lösungsansatzes zur Berechnung von DLMPs in Verteilungsnetzen, was das Hauptziel dieser Arbeit ist. Diese Dissertation untersucht die modernen Konzepte der Leistungsflussmodellierung für Verteilungsnetze, die nichtlineare Leistungsflüsse mit ihren unterschiedlichen physikalischen Eigenschaften berücksichtigen. Die vorgestellten Modellierungskonzepte werden im Hinblick auf ihre Fähigkeit untersucht, Machbarkeit, Robustheit und Approximation von Leistungsflusslösungen bereitzustellen. Diese Konzepte werden dann verwendet, um ein Optimierungsproblem vorzuschlagen, das ein Marktgerüst auf der Verteilnetzebene nachahmt. Wir bezeichnen diesen Rahmen als einen lokalen Verteilungsnetz-Marktrahmen, der die Preise, d. H. DLMPs, an jedem Bus des jeweiligen Verteilungsnetzes auf Day-Ahead-Basis freigibt. Unter der Annahme ökonomisch rationaler Flexibilitätsressourcen maximiert der vorgeschlagene Marktrahmen die allgemeine soziale Wohlfahrt des Verteilungsnetzes sowie die lokalen Flexibilitätsressourcen. Darüber hinaus ist der vorgeschlagene lokale Verteilnetzmarkt in der Lage, verschiedene physikalische Eigenschaften der Verteilungsnetze und unterschiedliche Arten von Flexibilitätsressourcen zu berücksichtigen. Durch die Nutzung von Power Flow Approximationstechniken und deren Lösungs-Machbarkeits-Konzepten wird ein Lösungsalgorithmus vorgeschlagen, um das vorgeschlagene Marktverrechnungsproblem des lokalen Verteilungsnetzes zu lösen. Der vorgeschlagene Lösungsalgorithmus weist die folgenden Vorteile auf: i) hilft bei der Entwicklung der DLMP-Formulierung, die dem Großhandelsmarkt sehr ähnlich ist, ii) die verschiedenen physikalischen Eigenschaften von Verteilungsnetzen einbezieht und iii) flexibel Ressourcen sowohl für den temporalen als auch für den sofortiger Energieversand Um die Kompatibilität der vorgeschlagenen Methode und ihre Effizienz zu demonstrieren, werden Tests an mehreren Benchmarked-Grid-Modellen durchgeführt und Vergleiche mit der bestehenden, dem aktuellen Stand der Technik entsprechenden Methodik durchgeführt.

Acknowledgements

There were many people who helped me during the course of this thesis. I am deeply humbled to have them in my life and I fear that this acknowledgment section might not do justice. Nevertheless, the following is my attempt.

First and foremost, I consider myself extremely lucky and fortunate to have Prof. Hamacher as my supervisor. He served as an immense source of inspiration, knowledge and guidance. On one hand, he was always open to new ideas, and on the other hand he could always convince you with his incredibly intuitive research dialog. Apart from work, he also showed, in a true sense, on how to achieve a good work and life balance, a lesson truly worth remembering for my entire life.

This PhD was conducted in Singapore while working for TUMCREATE. For this, I would like to thank Tobias for providing me with this wonderful opportunity. I would also like to extend my gratitude to Prof. Gooi, who was always supportive from the NTU side.

AT TUMCREATE, I could not have asked for a better team than ESTL (former RP8). A particular mention here are the ever enjoyable coffee table discussions I used to have with Juergen, Srikkanth, and Dante. I would also like to thank the management of TUMCREATE for supporting me with conference travels and administrative tasks.

When I moved to Singapore for my PhD thesis, it was also the start of my married life. I couldn't have asked for a better life partner as my wife. She was always patient, loving and caring and hence this thesis is dedicated to her. Last but not the least, my family back home is also to be thanked as they always were very supportive of me.

Contents

List of Figures

List of Tables

Acronyms

ADS Active Distribution System 13, 14, 15, 16, 18
AQP Approximate Quadratic Program 71, 72, 73, 76, 77, 81, 82, 107

CL Constant Load 65, 66

DER Distributed Energy Resource 14
DG Distributed Generator 7, 9, 12, 13, 14, 15, 16, 17, 19, 65, 66, 67, 69, 70, 73, 77, 81, 82, 83, 84, 85, 87, 91, 105, 106
DLMP Distribution Locational Marginal Price 12, 16, 17, 18, 19, 65, 67, 68, 69, 70, 71, 74, 77, 81, 82, 83, 82, 83, 84, 85, 86, 87, 90, 105, 106, 107
DSO Distribution System Operator 14, 15, 16, 17, 94, 95, 98, 106, 107

ED Economic Dispatch 23, 31, 32, 33, 35, 65, 66, 67, 68, 70, 77, 84, 91, 110
EV Electric Vehicle 13, 14

FL Flexible Load 7, 8, 9, 12, 13, 14, 15, 16, 17, 19, 65, 66, 67, 69, 70, 73, 81, 82, 83, 84, 91, 105, 106

HVAC Heating Ventillation and Air-Conditioning 13, 116, 117, 119

KKT Karush-Kuhn-Tucker 27, 28, 29

LMP Locational Marginal Price 15, 16, 17, 18, 33, 67
LP Linear Program 70, 72

PQ Constant source/load active and reactive power model (not dependent on voltages) 7, 9, 38, 39, 50, 53, 54, 55

QP Quadratic Program 70, 72, 76, 77, 81

SO System Operator 23, 30, 31, 32, 33

Nomenclature

Set of natural, real and complex numbers are respectively denoted through $\mathbb{N}, \mathbb{R}, \mathbb{C}$. Scalars are written in lower case, x, vectors are written in bold and lower case, $\mathbf{x}$, and matrices are written as bold and upper case, $\mathbf{X}$. For complex scalar $x \in \mathbb{C}$, it is composed of: $x = x_{re} + j x_{im}$, where $x_{re} := \Re(x)$ is the real part and $x_{im} := \Im(x)$ is the imaginary part of the complex quantity. Complex conjugate of $x \in \mathbb{C}$ is written as $\overline{x}$. For matrix $\mathbf{X}$, the operation $(\mathbf{X})_{\mathsf{n}}$ selects n rows and columns from $\mathbf{X}$. For the scalar $x \in \mathbb{R}$ and matrix $\mathbf{x}_{\mathsf{n}} \in \mathbb{R}^{\mathsf{n}}$ replicates scalar x n number of times. For vector $\mathbf{x} \in \mathbb{R}^{\mathsf{n}}$, the operation $\mathbf{X}_{\mathsf{n}\times\mathsf{n}} \in \mathbb{R}^{\mathsf{n}\times\mathsf{n}}$ places the vector $\mathbf{x}$ n times across its diagonal entries. Special case matrix $\mathbf{I}_{\mathsf{n}} \in \mathbb{R}^{\mathsf{n}\times\mathsf{n}}$ is an identity matrix of size $\mathsf{n} \times \mathsf{n}$. The operator $\mathrm{diag}(\mathbf{x})$ turns vector $\mathbf{x}$ to a matrix with $\mathbf{x}$ at its diagonal. The approximated and actual value of $\mathbf{x}$ is given by $\tilde{\mathbf{x}}$ and $\hat{\mathbf{x}}$, respectively.

Optimization Related

Notation	Description
$\mathcal{L}(\cdot)$	Lagrangian function with arguments $(\cdot)$
λ	Lagrange multiplier for equality constraint
μ	Lagrange multiplier for inequality constraint
$\nabla_x f(x)$	First derivative of $f(x)$ with respect to x
$\nabla_x^2 f(x)$	Second derivative of $f(x)$ with respect to x

Sets

Single-phase:

Notation	Description
$\mathsf{n} \in \mathbb{N}$	Number of PQ buses $\in \{1, \ldots, \mathsf{n}\}$
$\mathsf{N} \in \mathbb{N}$	Number of all buses (PQ and root-bus) in the grid $\in \{0, \ldots, \mathsf{n}\}$
$\mathsf{m} \in \mathbb{N}$	Number of lines in the grid $\in \{1, \ldots, \mathsf{m}\}$

Multi-phase:

Notation	Description
$\{a, b, c\} \in \mathbb{N}$	Set of possible phases for a bus
$3\mathsf{n} \in \mathbb{N}$	Number of PQ buses in the grid $\in \{1, \ldots, 3\mathsf{n}\}$
$3(\mathsf{n}+1) \in \mathbb{N}$	Number of all buses (PQ and root-bus) in the grid
$3\mathsf{m} \in \mathbb{N}$	Number of lines in the grid $\in \{1, \ldots, 3\mathsf{m}\}$

Economic Dispatch:

Notation	Description
$\mathsf{n}_t \in \mathbb{N}$	Time steps planning horizon, $\mathcal{T} = \{1, \ldots, \mathsf{n}_\mathsf{t}\}$
$\mathsf{n} \in \mathbb{N}$	Number of Distributed Generator (DG)s, Flexible Load (FL)s and fixed loads at all Constant source/load active and reactive power model (not dependent on voltages) (PQ) buses in the grid $\in \{1, \ldots, \mathsf{n}\}$

Parameters

Single-phase:

Notation	Description	Units
$(i,j) \in \mathbb{N}$	Line element connecting bus i and bus j	-
$\mathbf{A}^{\mathsf{f}}$	Sized m $\times$ N "from" buses incidence matrix	-
$\mathbf{A}^{\mathsf{t}}$	Sized m $\times$ N "to" buses incidence matrix	-
$b_{ij} \in \mathbb{R}$	Susceptance line element (i,j)	Ohm^{-1}
$r_{ij} \in \mathbb{R}$	Resistance of line element (i,j)	Ohm
$x_{ij} \in \mathbb{R}$	Reactance of line element (i,j)	Ohm
$y_{ij} \in \mathbb{C}$	Phase admittance of line element (i,j), $y_{ij} = 1/(r_{ij} + jx_{ij})$	Ohm^{-1}
$y_{sh} \in \mathbb{C}$	Shunt admittance of line element (i,j), $y_{sh} = jb_{ij}/2$	Ohm^{-1}
$\mathbf{Y} \in \mathbb{C}^{\mathsf{N}\times\mathsf{N}}$	Bus admittance matrix of the grid (root and n buses)	Ohm^{-1}
$\mathbf{Y}^{\mathsf{f}} \in \mathbb{C}^{\mathsf{m}\times\mathsf{N}}$	Bus admittance "from" matrix of the grid	Ohm^{-1}
$\mathbf{Y}^{\mathsf{t}} \in \mathbb{C}^{\mathsf{m}\times\mathsf{N}}$	Bus admittance "to" matrix of the grid	-

Multi-phase:

Notation	Description	Units
$(i,j) \in \mathbb{N}$	Line element connecting bus i and bus j	-
$\mathbf{A}^{\mathsf{f,abc}}$	Sized 3m $\times$ 3(n + 1) "from" buses incidence matrix	-
$\mathbf{A}^{\mathsf{t,abc}}$	Sized 3m $\times$ 3(n + 1) "to" buses incidence matrix	-
$b_{ij}^{aa} \in \mathbb{R}$	Self susceptance line element (i,j) phase a	Ohm^{-1}
$b_{ij}^{ab} \in \mathbb{R}$	Mutual susceptance line element (i,j) between phase a and b	Ohm^{-1}
$\mathbf{\Gamma} \in \mathbb{C}^{3\times3}$	Phase-ground to phase-phase conversion matrix	-
$\mathbf{H} \in \mathbb{C}^{3\mathsf{n}\times3\mathsf{n}}$	Matrix with $\mathbf{\Gamma}$ at its diagonals	-
$r_{ij}^{aa} \in \mathbb{R}$	Self resistance of line element (i,j) phase a	Ohm
$r_{ij}^{ab} \in \mathbb{R}$	Mutual resistance of line element (i,j) between phase a and b	Ohm
$x_{ij}^{ab} \in \mathbb{R}$	Mutual reactance of line element (i,j) between phase a and b	Ohm
$x_{ij}^{aa} \in \mathbb{R}$	Self reactance of line element (i,j) phase a	Ohm
$y_{ij}^{aa} \in \mathbb{C}$	Self phase admittance of line element (i,j) phase a	Ohm^{-1}
$y_{ij}^{ab} \in \mathbb{C}$	Mutual phase admittance of line element (i,j) between phase a and b	Ohm^{-1}
$y_{sh}^{aa} \in \mathbb{C}$	Self shunt admittance of line element (i,j) phase a	Ohm^{-1}
$y_{sh}^{ab} \in \mathbb{C}$	Mutual shunt admittance of line element (i,j) between phase a and b	Ohm^{-1}
$\mathbf{Y}_{ij}^{\mathsf{sh}} \in \mathbb{C}^3$	Multiphase shunt admittance matrix of line element (i,j)	Ohm^{-1}
$\mathbf{Y}_{ij}^{\mathsf{ph}} \in \mathbb{C}^3$	Multiphase phase admittance matrix of line element (i,j)	Ohm^{-1}
$\mathbf{Y}^{\mathsf{abc}} \in \mathbb{C}^{3(\mathsf{n}+1)\times3(\mathsf{n}+1)}$	Multiphase bus admittance matrix of the grid (root and n buses)	Ohm^{-1}
$\mathbf{Y}^{\mathsf{f,abc}} \in \mathbb{C}^{3\mathsf{m}\times3(\mathsf{n}+1)}$	Multiphase bus admittance "from" matrix of the grid	Ohm^{-1}
$\mathbf{Y}^{\mathsf{t,abc}} \in \mathbb{C}^{3\mathsf{m}\times3(\mathsf{n}+1)}$	Multiphase bus admittance "To" matrix of the grid	Ohm^{-1}

Economic dispatch[1]:

Notation	Description	Units
$\mathbf{a}_{y,t}^{\mathrm{fl/g}} \in \mathbb{R}^{\mathrm{n}}$	Positive price per unit vector, where $\mathbf{y}_t^{\mathrm{fl/g}} \in \{\mathbf{p}_t^{\mathrm{fl}}, \mathbf{p}_t^{\mathrm{g}}, \mathbf{q}_t^{\mathrm{g}}\}$ with $\mathbf{p}_t^{\mathrm{g}} \in \{p_t^0, \mathbf{p}_t^{\mathrm{dg}}\}$ and $\mathbf{q}_t^{\mathrm{g}} \in \{q_t^0, \mathbf{q}_t^{\mathrm{dg}}\}$	\$/MWh / \$/MVarh
$\mathbf{B}_{y,t}^{\mathrm{fl/g}} \in \mathbb{R}^{\mathrm{n}\times\mathrm{n}}$	Symmetric, positive definite matrix with small positive price sensitivity coefficients as diagonal entries, where $\mathbf{y}_t^{\mathrm{fl/g}} \in \{\mathbf{p}_t^{\mathrm{fl}}, \mathbf{p}_t^{\mathrm{g}}, \mathbf{q}_t^{\mathrm{g}}\}$ with $\mathbf{p}_t^{\mathrm{g}} \in \{p_t^0, \mathbf{p}_t^{\mathrm{dg}}\}$ and $\mathbf{q}_t^{\mathrm{g}} \in \{q_t^0, \mathbf{q}_t^{\mathrm{dg}}\}$	\$/MWh^2 / \$/MVarh^2
$\mathbf{c}_{y,t}^{\mathrm{fl/dg}} \in \mathbb{R}^{\mathrm{n}}$	Marginal cost of the form $\mathbf{a}_{y,t}^{\mathrm{fl/g}} + \mathbf{B}_{y,t}^{\mathrm{fl/g}}\mathbf{y}_t^{\mathrm{fl/g}}$, where $\mathbf{y}_t^{\mathrm{fl/g}} \in \{\mathbf{p}_t^{\mathrm{fl}}, \mathbf{p}_t^{\mathrm{g}}, \mathbf{q}_t^{\mathrm{g}}\}$ with $\mathbf{p}_t^{\mathrm{g}} \in \{p_t^0, \mathbf{p}_t^{\mathrm{dg}}\}$ and $\mathbf{q}_t^{\mathrm{g}} \in \{q_t^0, \mathbf{q}_t^{\mathrm{dg}}\}$	\$/MWh /\$/MVarh
$\mathbf{C}_t^{\mathrm{fl/g}}(\mathbf{y}_t^{\mathrm{fl/g}}) \in \mathbb{R}^{\mathrm{n}}$	Cost function of the form $(\mathbf{c}_{y,t}^{\mathrm{fl/dg}})^{\intercal}\mathbf{y}_t^{\mathrm{fl/g}}$ where $\mathbf{y}_t^{\mathrm{fl/g}} \in \{\mathbf{p}_t^{\mathrm{fl}}, \mathbf{p}_t^{\mathrm{g}}, \mathbf{q}_t^{\mathrm{g}}\}$ with $\mathbf{p}_t^{\mathrm{g}} \in \{p_t^0, \mathbf{p}_t^{\mathrm{dg}}\}$ and $\mathbf{q}_t^{\mathrm{g}} \in \{q_t^0, \mathbf{q}_t^{\mathrm{dg}}\}$	\$
$\mathbf{D}_t \in \mathbb{R}^{\mathrm{n}\times\mathrm{n}}$	Time-coupled drain matrix of FLs	Watt^{-1}
$\mathbf{z}_t \in \mathbb{R}^{\mathrm{n}}$	Disturbance experienced by FLs	-
$\mathbf{U}_t^{\mathrm{fl}}(\mathbf{p}_t^{\mathrm{fl}}) \in \mathbb{R}^{\mathrm{n}}$	Utility of providing flexibility from FLs, defined simply as negative cost of consumption $:= -\mathbf{C}_t^{\mathrm{fl}}(\mathbf{p}_t^{\mathrm{fl}})$	\$
$w_{p,t}(\mathbf{p}_t^{\mathrm{fl}}, \mathbf{p}_t^{\mathrm{g}}) \in \mathbb{R}^{\mathrm{n}}$	Overall social welfare for providing active power to the grid	\$
$w_{q,t}(\mathbf{q}_t^{\mathrm{g}}) \in \mathbb{R}^{\mathrm{n}}$	Overall social welfare for providing reactive power to the grid	\$

Variables

Single-phase:

Notation	Description	Units
$i_j \in \mathbb{C}$	Complex current injection at bus j	Ampere
$i_{ij} \in \mathbb{C}$	Complex current flow on line element (i, j), from bus i to j	Ampere
$\mathbf{i}_{\mathrm{L}} \in \mathbb{C}^{\mathrm{n}}$	Complex current injection for n PQ buses $:= (i_1, \ldots, i_{\mathrm{n}})^{\intercal}$	Ampere
$p_j \in \mathbb{R}$	Active power injection at bus j,	Watt
$\mathbf{p}_{\mathrm{L}} \in \mathbb{R}^{\mathrm{n}}$	Active power injections for n PQ buses $:= (p_1, \ldots, p_{\mathrm{n}})^{\intercal}$	Watt
$p_k^{\mathrm{f}} \in \mathbb{R}$	Active power flow "from" bus' line element k	Watt
$\mathbf{p}^{\mathrm{f}} \in \mathbb{R}^{\mathrm{m}}$	Active power "from" flows for all grid lines $:= (p_1^{\mathrm{f}}, \ldots, p_{\mathrm{m}}^{\mathrm{f}})^{\intercal}$	Watt
$p_k^{\mathrm{t}} \in \mathbb{R}$	Active power flow "to" bus' line element k	Watt
$\mathbf{p}^{\mathrm{t}} \in \mathbb{R}^{\mathrm{m}}$	Active power "to" flows for all grid lines $:= (p_1^{\mathrm{t}}, \ldots, p_{\mathrm{m}}^{\mathrm{t}})^{\intercal}$	Watt
$p^{\mathrm{l}} \in \mathbb{R}$	System active power losses	Watt
$q_j \in \mathbb{R}$	Reactive power injection at bus j	Var
$\mathbf{q}_{\mathrm{L}} \in \mathbb{R}^{\mathrm{n}}$	Reactive power injections for n PQ buses $:= (q_1, \ldots, q_{\mathrm{n}})^{\intercal}$	Var
$q_k^{\mathrm{f}} \in \mathbb{R}$	Reactive power flow "from" bus' line element $:= (q_1^{\mathrm{f}}, \ldots, q_{\mathrm{m}}^{\mathrm{f}})^{\intercal}$	Var
$\mathbf{q}^{\mathrm{f}} \in \mathbb{R}^{\mathrm{m}}$	Reactive power "from" flows for all grid lines	Var
$q_k^{\mathrm{t}} \in \mathbb{R}$	Reactive power flow "to" bus' line element	Var
$\mathbf{q}^{\mathrm{t}} \in \mathbb{R}^{\mathrm{m}}$	Reactive power "to" flows for all grid lines $:= (q_1^{\mathrm{t}}, \ldots, q_{\mathrm{m}}^{\mathrm{t}})^{\intercal}$	Var
$q^{\mathrm{l}} \in \mathbb{R}$	System reactive power losses	Var
$s_j \in \mathbb{C}$	Complex power injection at bus j, $:= p_i + jq_i$	VoltAmpere
$\mathbf{s}_{\mathrm{L}} \in \mathbb{C}^{\mathrm{n}}$	Complex power injections for n PQ buses $:= \mathbf{p}_{\mathrm{L}} + j\mathbf{q}_{\mathrm{L}}$	VoltAmpere
$s_k^{\mathrm{f}} \in \mathbb{C}$	Complex power flow "from" bus' line element $k := p_k^{\mathrm{f}} + jq^{\mathrm{f}}$	VoltAmpere
$\mathbf{s}^{\mathrm{f}} \in \mathbb{C}^{\mathrm{m}}$	Complex power "from" flows for all m lines $:= \mathbf{p}^{\mathrm{f}} + j\mathbf{q}^{\mathrm{f}}$	VoltAmpere

[1] We present nomenclature here for multi-period economic dispatch, mostly used in chapter 5. This is because as it already contains the model for single-period economic dispatch problem of chapter 4.

$s_k^{\mathsf{t}} \in \mathbb{C}$	Complex power flow "to" bus' line element $k := p_k^{\mathsf{t}} + jq_k^{\mathsf{t}}$	VoltAmpere
$\mathbf{s}^{\mathsf{t}} \in \mathbb{C}^{\mathsf{m}}$	Complex power "to" flows for all m lines, $:= \mathbf{p}^{\mathsf{t}} + j\mathbf{q}^{\mathsf{t}}$	VoltAmpere
$\mathbf{s}_{\mathsf{L}}^{\mathsf{inj}} \in \mathbb{R}^{2\mathsf{n}}$	Real-valued power injections $:= ((\mathbf{p}_{\mathsf{L}})^{\mathsf{T}}, (\mathbf{q}_{\mathsf{L}})^{\mathsf{T}})^{\mathsf{T}}$	[Watt;Var]
$s^{\mathsf{l}} \in \mathbb{C}$	System complex power losses, $s^{\mathsf{l}} = p^{\mathsf{l}} + jq^{\mathsf{l}}$	VoltAmpere
$\theta_j \in \mathbb{R}$	Voltage angle at bus j	Radian
$\theta_0 \in \mathbb{R}$	Voltage angle at root-bus	Radian
$\boldsymbol{\theta}_{\mathsf{L}} \in \mathbb{R}^{\mathsf{n}}$	Voltage angle for n PQ buses $:= (\theta_1, \ldots, \theta_{\mathsf{n}})^{\mathsf{T}}$	Radian
$u_j \in \mathbb{C}$	Complex voltage at bus $j := v_j e^{j\theta_j}$	Volt
$u_0 \in \mathbb{C}$	Complex voltage at root-bus	Volt
$\mathbf{u}_{\mathsf{L}} \in \mathbb{C}^{\mathsf{n}}$	Complex voltage for n PQ buses $:= (u_1, \ldots, u_{\mathsf{n}})^{\mathsf{T}}$	Volt
$v_j \in \mathbb{R}$	Voltage magnitude at bus j	Volt
$v_0 \in \mathbb{R}$	Voltage magnitude at root-bus	Volt
$\mathbf{v}_{\mathsf{L}} \in \mathbb{R}^{\mathsf{n}}$	Voltage magnitude for n PQ buses $:= (v_1, \ldots, v_{\mathsf{n}})^{\mathsf{T}}$	Volt

Multi-phase:

Notation	**Description**	**Units**
$i_j^a \in \mathbb{C}$	Complex current injection from phase a to ground of bus j	Ampere
$i_j^{ab} \in \mathbb{C}$	Complex current injection between phase a and b of bus j	Ampere
$\mathbf{i}_j^{\Delta} \in \mathbb{C}^3$	Complex delta current injection at bus $j := (i_j^{ab}, i_j^{bc}, i_j^{ca})^{\mathsf{T}}$	Ampere
$\mathbf{i}_{\mathsf{L}}^{\Delta} \in \mathbb{C}^{3\mathsf{n}}$	Complex delta current n PQ buses grid injections $:= ((\mathbf{i}_1^{\Delta})^{\mathsf{T}}, \ldots, (\mathbf{i}_{\mathsf{n}}^{\Delta})^{\mathsf{T}})^{\mathsf{T}}$	Ampere
$\mathbf{i}_j^{\mathsf{Y}} \in \mathbb{C}^3$	Complex wye current injection at bus $j := (i_j^a, i_j^b, i_j^c)^{\mathsf{T}}$	Ampere
$\mathbf{i}_{\mathsf{L}}^{\mathsf{Y}} \in \mathbb{C}^{3\mathsf{n}}$	Complex wye current n PQ buses grid injections $:= ((\mathbf{i}_1^{\mathsf{Y}})^{\mathsf{T}}, \ldots, (\mathbf{i}_{\mathsf{n}}^{\mathsf{Y}})^{\mathsf{T}})^{\mathsf{T}}$	Ampere
$i_{ij}^a \in \mathbb{C}$	Complex current flow on line element (i, j), from bus i to j of phase a	Ampere
$\mathbf{i}_{ij} \in \mathbb{C}^3$	Complex current flow on line element $(i, j) := (i_{ij}^a, i_{ij}^b, i_{ij}^c)^{\mathsf{T}}$	Ampere
$p_j^a \in \mathbb{R}$	Active power injection from phase a to ground of bus j	Watt
$\mathbf{p}_j^{\mathsf{Y}} \in \mathbb{R}^3$	Active power wye injections at bus $j := (p_j^a, p_j^b, p_j^c)^{\mathsf{T}}$	Watt
$\mathbf{p}_{\mathsf{L}}^{\mathsf{Y}} \in \mathbb{R}^{3\mathsf{n}}$	Active power wye injections for n PQ buses $:= ((\mathbf{p}_1^{\mathsf{Y}})^{\mathsf{T}}, \ldots, (\mathbf{p}_{\mathsf{n}}^{\mathsf{Y}})^{\mathsf{T}})$	Watt
$p_j^{ab} \in \mathbb{R}$	Active power injection between phase a and phase b of bus j	Watt
$\mathbf{p}_j^{\Delta} \in \mathbb{R}^3$	Active power delta injections at bus $j := (p_j^{ab}, p_j^{bc}, p_j^{ca})^{\mathsf{T}}$	Watt
$\mathbf{p}_{\mathsf{L}}^{\Delta} \in \mathbb{R}^{3\mathsf{n}}$	Active power delta injections for n PQ buses $:= ((\mathbf{p}_1^{\Delta})^{\mathsf{T}}, \ldots, (\mathbf{p}_{\mathsf{n}}^{\Delta})^{\mathsf{T}})$	Watt
$p_k^{\mathsf{f},a} \in \mathbb{R}$	Active power flow "from" bus' line element k phase a	Watt
$\mathbf{p}_k^{\mathsf{f,abc}} \in \mathbb{R}^3$	Active power flow "from" bus' line element $k := (p_k^{\mathsf{f},a}, p_k^{\mathsf{f},b}, p_k^{\mathsf{f},c})^{\mathsf{T}}$	Watt
$\mathbf{p}^{\mathsf{f,abc}} \in \mathbb{R}^{3\mathsf{m}}$	Active power "from" flows for all grid lines $:= ((\mathbf{p}_1^{\mathsf{f},abc})^{\mathsf{T}}, \ldots, (\mathbf{p}_{\mathsf{n}}^{\mathsf{f},abc})^{\mathsf{T}})^{\mathsf{T}}$	Watt
$p_k^{\mathsf{t},a} \in \mathbb{R}$	Active power flow "to" bus' line element k phase a	Watt
$\mathbf{p}_k^{\mathsf{t,abc}} \in \mathbb{R}^3$	Active power "to" bus' line element $k := (p_k^{\mathsf{t},a}, p_k^{\mathsf{t},b}, p_k^{\mathsf{t},c})^{\mathsf{T}}$	Watt
$\mathbf{p}^{\mathsf{t,abc}} \in \mathbb{R}^{3\mathsf{m}}$	Active power "to" flows for all grid lines $:= ((\mathbf{p}_1^{\mathsf{t},abc})^{\mathsf{T}}, \ldots, (\mathbf{p}_{\mathsf{n}}^{\mathsf{t},abc})^{\mathsf{T}})^{\mathsf{T}}$	Watt
$p^{\mathsf{l,abc}} \in \mathbb{R}$	Multiphase system active power losses	Watt

$q_j^a \in \mathbb{R}$	Reactive power injection from phase a to ground of bus j	Var
$\mathbf{q}_j^{\mathsf{Y}} \in \mathbb{R}^3$	Reactive power wye injections at bus $j := (q_j^a, q_j^b, p_j^c)^\intercal$	Var
$\mathbf{q}_{\mathsf{L}}^{\mathsf{Y}} \in \mathbb{R}^{3n}$	Reactive power wye injections for n PQ buses $:=$ $((\mathbf{q}_1^{\mathsf{Y}})^\intercal, \ldots, (\mathbf{q}_n^{\mathsf{Y}})^\intercal)$	Var
$q_j^{ab} \in \mathbb{R}$	Reactive power injection between phase a and phase b of bus j	Var
$\mathbf{q}_j^{\Delta} \in \mathbb{R}^3$	Reactive power delta injections at bus $j := (q_j^{ab}, q_j^{bc}, p_j^{ca})^\intercal$	Var
$\mathbf{q}_{\mathsf{L}}^{\Delta} \in \mathbb{R}^{3n}$	Reactive power delta injections for n PQ buses $:=$ $((\mathbf{q}_1^{\Delta})^\intercal, \ldots, (\mathbf{q}_n^{\Delta})^\intercal)$	Var
$q_k^{\mathsf{f},a} \in \mathbb{R}$	Reactive power flow "from" bus' line element k phase a	Var
$\mathbf{q}_k^{\mathsf{f},\mathsf{abc}} \in \mathbb{R}^3$	Reactive power flow "from" bus' line element k $:=$ $(q_k^{\mathsf{f},a}, q_k^{\mathsf{f},b}, q_k^{\mathsf{f},c})^\intercal$	Var
$\mathbf{q}^{\mathsf{f},\mathsf{abc}} \in \mathbb{R}^{3m}$	Reactive power "from" flows for all grid lines $:= ((\mathbf{q}_1^{\mathsf{f},abc})^\intercal, \ldots, (\mathbf{q}_n^{\mathsf{f},abc})^\intercal)^\intercal$	Var
$q_k^{\mathsf{t},a} \in \mathbb{R}$	Reactive power flow "to" bus' line element k phase a	Var
$\mathbf{q}_k^{\mathsf{t},\mathsf{abc}} \in \mathbb{R}^3$	Reactive power to "from" bus' line element k $:=$ $(q_k^{\mathsf{t},a}, p_k^{\mathsf{t},b}, p_k^{\mathsf{t},c})^\intercal$	Var
$\mathbf{q}^{\mathsf{t},\mathsf{abc}} \in \mathbb{R}^{3m}$	Reactive power "to" flows for all grid lines $:=$ $((\mathbf{q}_1^{\mathsf{t},abc})^\intercal, \ldots, (\mathbf{q}_n^{\mathsf{t},abc})^\intercal)^\intercal$	Var
$q^{\mathsf{l},\mathsf{abc}} \in \mathbb{R}$	Multiphase system reactive power losses	Var
$s_j^a \in \mathbb{R}$	Complex power injection from phase a to ground of bus j	VoltAmpere
$\mathbf{s}_j^{\mathsf{Y}} \in \mathbb{R}^3$	Complex power wye injections at bus $j := (s_j^a, s_j^b, s_j^c)^\intercal$	VoltAmpere
$\mathbf{s}_{\mathsf{L}}^{\mathsf{Y}} \in \mathbb{C}^{3n}$	Complex power delta injections for n PQ buses $:=$ $((\mathbf{s}_1^{\mathsf{Y}})^\intercal, \ldots, (\mathbf{s}_n^{\mathsf{Y}})^\intercal)$	VoltAmpere
$s_j^{ab} \in \mathbb{C}$	Complex power injection between phase a and phase b of bus j	VoltAmpere
$\mathbf{s}_j^{\Delta} \in \mathbb{C}^3$	Complex power delta injections at bus $j := (s_j^{ab}, s_j^{bc}, s_j^{ca})^\intercal$	VoltAmpere
$\mathbf{s}_{\mathsf{L}}^{\Delta} \in \mathbb{C}^{3n}$	Complex power delta injections for n PQ buses $:=$ $((\mathbf{s}_1^{\Delta})^\intercal, \ldots, (\mathbf{s}_n^{\Delta})^\intercal)$	VoltAmpere
$s^{\mathsf{l},\mathsf{abc}} \in \mathbb{C}$	Multiphase system complex power losses	VoltAmpere
$\mathbf{s}_{\mathsf{L}}^{\mathsf{inj},\mathsf{Y}} \in \mathbb{R}^{6n}$	Real-valued wye power injections $:= ((\mathbf{p}_{\mathsf{L}}^{\mathsf{Y}})^\intercal, (\mathbf{q}_{\mathsf{L}}^{\mathsf{Y}})^\intercal)^\intercal$	[Watt;Var]
$\mathbf{s}_{\mathsf{L}}^{\mathsf{inj},\Delta} \in \mathbb{R}^{6n}$	Real-valued delta power injections $:= ((\mathbf{p}_{\mathsf{L}}^{\Delta})^\intercal, (\mathbf{q}_{\mathsf{L}}^{\Delta})^\intercal)^\intercal$	[Watt;Var]
$\theta_j^a \in \mathbb{R}$	Voltage angle at bus j phase a	Radian
$\boldsymbol{\theta}_j \in \mathbb{R}^3$	Voltage angle at bus $j := (\theta_j^a, \theta_j^b, \theta_j^b)^\intercal$	Radian
$\boldsymbol{\theta}_0 \in \mathbb{R}^3$	Voltage angle at the root-bus $:= (\theta_0^a, \theta_0^b, \theta_0^b)^\intercal$	Radian
$\boldsymbol{\theta}_{\mathsf{L}}^{\mathsf{abc}} \in \mathbb{R}^{3n}$	Voltage angle for n PQ buses $:= ((\boldsymbol{\theta}_1)^\intercal, \ldots, (\boldsymbol{\theta}_n)^\intercal)^\intercal$	Radian
$u_j^a \in \mathbb{R}$	Complex voltage at bus j phase a, $:= v_j^a e^{j\theta_j^a}$	Volt
$\mathbf{u}_j \in \mathbb{R}^3$	Complex voltage at bus $j := (u_j^a, u_j^b, u_j^b)^\intercal$	Volt
$\mathbf{u}_0 \in \mathbb{R}^3$	Complex voltage at the root-bus $:= (u_0^a, u_0^b, u_0^b)^\intercal$	Volt
$\mathbf{u}_{\mathsf{L}}^{\mathsf{abc}} \in \mathbb{R}^{3n}$	Complex voltage for n PQ buses $:= ((\mathbf{v}_1)^\intercal, \ldots, (\mathbf{v}_n)^\intercal)^\intercal$	Volt
$v_j^a \in \mathbb{R}$	Voltage magnitude at bus j phase a	Volt
$\mathbf{v}_j \in \mathbb{R}^3$	Voltage magnitude at bus $j := (v_j^a, v_j^b, v_j^b)^\intercal$	Volt
$\mathbf{v}_0 \in \mathbb{R}^3$	Voltage magnitude at the root-bus $:= (v_0^a, u_0^b, u_0^b)^\intercal$	Volt
$\mathbf{v}_{\mathsf{L}}^{\mathsf{abc}} \in \mathbb{R}^{3n}$	Voltage magnitude for n PQ buses $:= ((\mathbf{v}_1)^\intercal, \ldots, (\mathbf{v}_n)^\intercal)^\intercal$	Volt

Economic Dispatch[2]:

Notation	Description	Units
$\mathbf{ch}_t \in \mathbb{R}^n$	State of charge for FLs	-
$\mathbf{p}_t^{\text{fl}} \in \mathbb{R}^n$	Active power of FLs $:= (p_{1,t}^{\text{fl}}, \ldots, p_{n,t}^{\text{fl}})^\intercal$	Watt
$\mathbf{p}_t^{\text{dg}} \in \mathbb{R}^n$	Active power of DGs $:= (p_{1,t}^{\text{dg}}, \ldots, p_{n,t}^{\text{dg}})^\intercal$	Watt
$\mathbf{p}_t^{\text{cl}} \in \mathbb{R}^n$	Active power of constant loads $:= (p_{1,t}^{\text{cl}}, \ldots, p_{n,t}^{\text{cl}})^\intercal$	Watt
$p_t^0 \in \mathbb{R}$	Active power from the root-bus	Watt
$\mathbf{q}_t^{\text{dg}} \in \mathbb{R}^n$	Reactive power of DGs $:= (q_{1,t}^{\text{dg}}, \ldots, q_{n,t}^{\text{dg}})^\intercal$	Var
$\mathbf{q}_t^{\text{fl}} \in \mathbb{R}^n$	Reactive power of FLs $:= (q_{1,t}^{\text{fl}}, \ldots, q_{n,t}^{\text{fl}})^\intercal$	Var
$\mathbf{q}_t^{\text{cl}} \in \mathbb{R}^n$	Reactive power of constant loads $:= (q_{1,t}^{\text{cl}}, \ldots, q_{n,t}^{\text{cl}})^\intercal$	Var
$q_t^0 \in \mathbb{R}$	Reactive power from the root-bus	Var

DLMP

Single-Phase

Notation	Description	Units
$\boldsymbol{\Pi}^{\text{Grid}}_{\mathbf{p}_t/\mathbf{q}_t} \in \mathbb{R}^n$	Final active/reactive power price (DLMP) cleared in the distribution grid market	\$/MWh / \$/MVarh
$\boldsymbol{\Pi}^{\text{Flex}}_{\mathbf{p}_t/\mathbf{q}_t} \in \mathbb{R}^n$	Marginal value of supplying active/reactive power from flexibility resources (DGs, FLs)	\$/MWh / \$/MVarh
$\boldsymbol{\Pi}^{\text{E/L/C/V}}_{\mathbf{p}_t} \in \mathbb{R}^n$	Energy/Loss/Congestion/Voltage component of $\boldsymbol{\Pi}^{\text{Grid}}_{\mathbf{p}_t}$	\$/MWh
$\boldsymbol{\Pi}^{\text{E/L/C/V}}_{\mathbf{q}_t} \in \mathbb{R}^n$	Energy/Loss/Congestion/Voltage component of $\boldsymbol{\Pi}^{\text{Grid}}_{\mathbf{q}_t}$	\$/MVarh

Multi-phase:

Notation	Description	Units
$\boldsymbol{\Pi}^{\text{Y, Grid}}_{\mathbf{p}/\mathbf{q}} \in \mathbb{R}^{3n}$	Final active/reactive power price (DLMP) cleared for wye connections in the distribution grid market	\$/MWh / \$/MVarh
$\boldsymbol{\Pi}^{\Delta,\text{Grid}}_{\mathbf{p}/\mathbf{q}} \in \mathbb{R}^{3n}$	Final active/reactive power price (DLMP) cleared for delta connections in the distribution grid market	\$/MWh / \$/MVarh
$\boldsymbol{\Pi}^{\text{Y, E/L/C/V}}_{\mathbf{p}} \in \mathbb{R}^{3n}$	Energy/Loss/Congestion/Voltage component of $\boldsymbol{\Pi}^{\text{Y, Grid}}_{\mathbf{p}}$	\$/MWh
$\boldsymbol{\Pi}^{\text{Y, E/L/C/V}}_{\mathbf{q}} \in \mathbb{R}^{3n}$	Energy/Loss/Congestion/Voltage component of $\boldsymbol{\Pi}^{\text{Y, Grid}}_{\mathbf{q}}$	\$/MVarh
$\boldsymbol{\Pi}^{\Delta,\text{E/L/C/V}}_{\mathbf{p}} \in \mathbb{R}^{3n}$	Energy/Loss/Congestion/Voltage component of $\boldsymbol{\Pi}^{\Delta,\text{Grid}}_{\mathbf{p}}$	\$/MWh
$\boldsymbol{\Pi}^{\Delta,\text{E/L/C/V}}_{\mathbf{q}} \in \mathbb{R}^{3n}$	Energy/Loss/Congestion/Voltage component of $\boldsymbol{\Pi}^{\Delta,\text{Grid}}_{\mathbf{q}}$	\$/MVarh

[2]We present nomenclature here for multi-period economic dispatch, mostly used in chapter 5. This is because as it already contains the model for single-period economic dispatch problem of chapter 4

Chapter 1

Introduction

1.1 Promises of Smart Grid and Emergence of Active Distribution System

Recently, most talks in electric power industry has been associated with the term “smart grid” [24, 36, 37]. The “smart grid” is an abstract concept, however with the promises of introducing:

- active unseen disturbance rejections;
- enable demand response technologies as well as higher consumer participation;
- integrate contemporary devices such as Flexible Load (FL)s and Distributed Generator (DG)s along with supporting storage devices; and
- optimize assets, improve power quality and increase observability,

into the grid. However, to achieve these features and enable a true “smart grid”, the following fundamental grid modernization components exist:

1. a higher requirement of sensing and metering infrastructure; and
2. a renewed design, operation and control philosophy for electricity distribution grids.

A simplified difference between conventional and emerging power systems can be seen in Fig. 1.1, where major physical integration of new technologies can be seen at the distribution grid level. Note that Fig. 1.1 presents an extremely simplified view point of the overall power system. There exists many exhaustive literatures on the overall power system operation and representation, for example [104, 29] for the transmission and [48] for distribution grids, interested readers are referred to them for more detail. Also, in Fig. 1.1, only a rough ball-park number is given with respect to voltage rating of transmission and distribution system. The exact voltages are system dependent and can be consulted for more interested reader, for example see [22] for primer on United States electricity system. In Fig. 1.1, we use the general term DG, which indicates smaller generators as compared to conventional large central transmission grid generators. Interested readers are referred to [23, 2] for more information on DGs. Similarly, the FL term in Fig. 1.1 can be referred as Electric Vehicle (EV) and Heating Ventillation and Air-Conditioning (HVAC), which are one of the most common representatives of Flexible Load (FL)s [86]. As most of these technologies are integrated in distribution grids, this is also where the focus of this thesis lies.

As shown in Fig. 1.1, in pursuit of modernizing the electric power industry, distribution grids have now been subjected to new assets and technologies, requiring a new operation

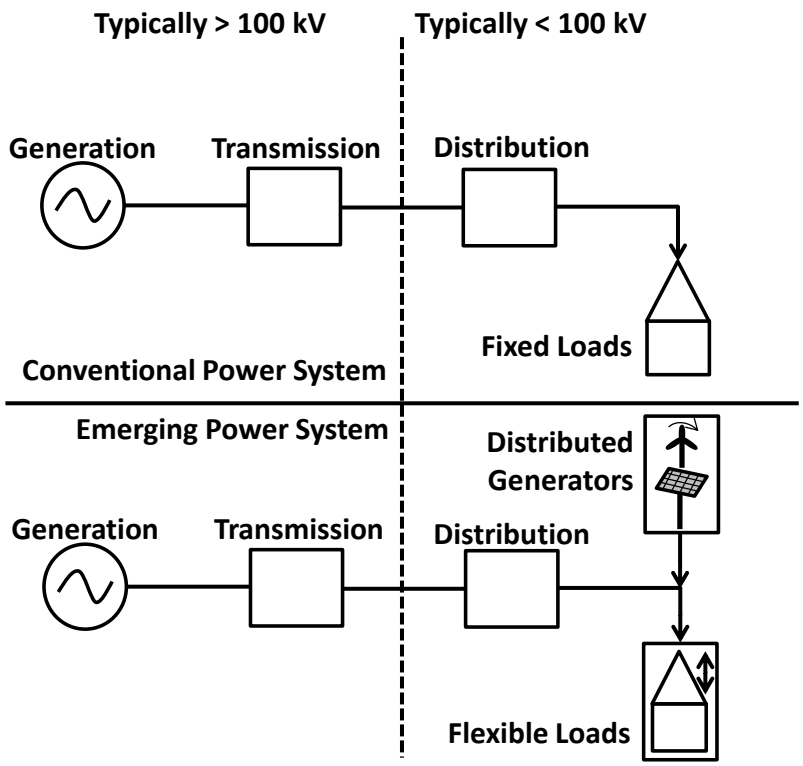

Figure 1.1: Comparison between conventional and emerging power systems.

and maintenance strategies. In principle, this causes distribution grids, a traditional passive component of the power system, to become more active. Traditionally the distribution grid was operated based on "fit and forget" strategy [48]. However, with the advent of FLs and DGs distribution grid is aimed to be an Active Distribution System (ADS). Interestingly, the term ADS has been adapted since 2012 from the original term "active distribution network", defined by CIGRE [83] in 2008 as:

"ADSs have systems in place to control a combination of Distributed Energy Resource (DER), defined as generators, loads, and storage, where the Distribution System Operator (DSO)[1] has the possibility of managing the electricity flows using a flexible network topology."

The drastic need for implementing a ADS is primarily due to the integration of uncontrollable DGs and rapidly varying FLs, which causes the traditional "pre-setting" of controllable equipment in the grid to fail. Hence, a higher coordination among various grid equipment is required and they should be updated more frequently. This poses a challenge to operate distribution grid in a reliable and efficient manner. Moreover, the rapid adoption trends of DGs and FLs over the year increases this challenge faced by distribution grids. At the end of the year 2017, Germany increased its installed capacity of DGs, i.e., solar photovoltaic and wind power amounted to 42'394 MW and 55'876 MW, respectively [43]. Similarly, EV fleet for the entire world reached surpassed two million vehicle mark in 2016 [42].

[1] We are going to present more explanation regarding the expected roles of the Distribution System Operator (DSO) in chapter 5.

Among many solution strategies and potential approaches, some of the main features of the ADS, as compared to traditional distribution grid are envisioned as:

- coordinated volt-var control of traditional (capacitor banks) and advanced (inverters of DGs) [74];
- demand response strategies for flexible loads or/and storages [75]; and
- active (more frequent) network reconfigurations algorithms [51].

To enable these advanced functionalities, it is envisioned that the ADS are capable to communicate electronically with its underlying equipment.

However, the question of which entity organizes these advanced functionalities in the ADS is still an ongoing discussion. Through the definition of this entity, the matters such as who control what and who pays/get paid what are then to be addressed in the ADS. As mentioned in the above definition of the ADS, most of the existing literature points out the emergence of the DSO to handle these issues [52, 71, 70, 93, 103]. In principle, the concept is somewhat similar to the Transmission System Operator, the entity responsible for scheduling power and managing transmission system level (wholesale) market. Similarly, the DSO is made responsible in the future distribution grid to oversee both advanced grid control mechanisms and market functionalities. The reports in [52, 71, 70] provides in detail the new responsibilities and roles for the DSO to aid in the modernization of the distribution grid. Some of the main responsibilities discussed in these reports for the DSO includes increasing system resilience, providing opportunities for end-user (consumer) participation in improving grid conditions and managing transactions among monetary driven entities such as retailers/aggregators. One way to automate these procedures is to set up a distribution grid market, which has been the topic for discussion in many utilities. For example, to name few, in New York [93] a more robust retail market has been in discussion whereas in Hawaii [92] it is suggested that utilities must evolve to handle both distribution grid operation and renewable energy integration. More information with respect to the overall distribution grid modernization and its acceptance in the utilities of United States can be found in [103].

1.2 Motivation

From the above mentioned promises of the smart grid along with intended features of the ADS, the next step is building a framework which integrates these technologies in a unified manner. Indeed, this envisioned framework benefits from the underlying communication infrastructure and electronically controlled advanced components of the ADS. The main goals of such a framework may aim for:

- a higher coordination and operation of both traditional (capacitor banks, transformers) and advanced (DGs and FLs) controllable assets to improve the technical efficiency of the ADS;
- the provision of higher utilization of underlying DGs and FLs to help de-carbonize the overall power system; and
- the improvement in the economic operation of the involved entities, while maintaining technical feasibility of the ADS.

With these goals defined, the envisioned framework then might also aid in recovering the cost of integrating advanced technologies in the ADS, while making sure that no compromise is made towards the overall grid reliability and its modernization.

In order to imagine such a framework for distribution systems, we might need to learn from the lessons learned while developing a sophisticated transmission system. In transmission system, one such mechanism, in the form of Locational Marginal Price (LMP), has laid the foundation of operating modern electric power industry in a cost/benefit manner. The LMP is a product of an optimization problem, interpreted as the cost to deliver the next megawatt hour to a certain transmission bus. The main concept of LMP was introduced in [88], where authors termed it as a spatial and temporal sport price which reflected the truest cost of the overall system. The spot price is recovered after solving for the maximum overall welfare of the system[2], while respective grid conditions. Based on this spot price at the respective bus, generators/loads sell/purchase energy. This framework of buying and selling the energy based on the spot price is then termed as wholesale electricity market[3]. Evidently, the LMP signal then serves as a tool to allocate costs of dispatching generation portfolios, driving future investments and also operating the overall power systems on a day-to-day basis in a more cost-effective manner.

Given the success of LMP in the transmission grid, extending it to the distribution grid might seem to be a viable option. However, even from a pure theoretical point of view, there exists many challenges with regards to adopting the current LMP model in distribution grids:

1. For transmission grids, the direct current approximations of power flows have shown to be adequate for regular transmission system operation [54, 40, 61, 60, 88]. This approximation is facilitated due to nature of transmission grid, where the actual power flows can be linearized up to certain accuracy as voltages usually do not vary much and are kept around their rated levels [104, 40, 54]. However, due to structural characteristics of distribution grids, the power flows are highly nonlinear and nonconvex. Moreover, the voltage profile in distribution grid is not flat, as compared to transmission grids. This renders the transmission grid approximations deployed for obtaining tractable and efficient LMP ineffective.
2. Distribution grids have different topologies (radial) as compared to transmission grids (meshed). In this regards, there exists a need for a new model which takes advantage of this topological difference.
3. Due to their structure, transmission systems are balanced and hence can be modeled as an equivalent single-phase positive sequence approach. However, distribution grids are diverse in their structure, i.e., they might have multiphase line elements, unbalanced loadings and various voltage levels. Hence, the envisioned DLMP model must be able to account for these characteristics.
4. The LMP models are developed based on instantaneous energy dispatch, i.e., single time-step. However, in the ADS flexibility resource, FLs and storage systems have been proposed to help aid in mitigating the effect of uncontrollable DGs. These systems have inter-temporal constraints, motivating the need for a multi-temporal modeling for this framework, as compared to the single time-step of the transmission grid LMP model.

1.3 State-of-the-art DLMP Formulations

Considering the above mentioned requirements for the desired framework to integrate advance functionalities in distribution grids, this section describes the recent literature.

[2] We provide more information regarding social welfare of the system, from the context of pricing in chapter 2

[3] The actual working and the products of wholesale electricity market varies and are dependent on the power system size and structures [1, 25]. However, they follow the same principle of spot pricing [88].

1.3.1 Equivalent Single-Phase DLMP Formulations

Realizing the need for DLMP as identified above, the earlier works are given in [12, 37, 82, 35, 34, 58, 41, 109, 90]. These works focused on a portion of symmetric and balanced distribution grids, hence modeling the distribution grid as an equivalent single-phase system[4]. Consistent with the organizational reports for the future distribution grids in [52, 71, 70, 93, 103], almost all theoretical works of [12, 37, 82, 35, 34, 58, 41, 109, 90] also appoint the DSO to be responsible for operating the envisioned local distribution grid market, while integrating flexibility resources (FLs and DGs). The coordination between FLs/DGs and the DSO is then established to find DLMPs, maximizing the individual as well as the overall surplus of the grid, i.e. a unique dispatch for FLs and DGs. Based on the given formulations of DLMPs, two broad methods can be classified as: (i) lossless-DLMPs and (ii) lossy-DLMPs.

Lossless-DLMPs

Recent lossless-DLMP formulations are reported in [35, 34, 58, 41]. These works present solution uniqueness and market equilibrium conditions for lossless-DLMPs with inter-temporal energy requirements from FLs and DGs. However, lossless power flow formulation used in these works is basically assumes a transmission grid LMP model to represent distribution grid DLMPs. However, the focus of these works has been in developing a local DSO run distribution grid market which efficiently allocates the local flexibility resources. With the help of simplified power flow models, the authors showed that the overall problem is in fact a strictly convex problem. Hence, the problem formulation of the local distribution grid market achieves a unique minimizer for the overall social welfare as well as individual entities. However, as mentioned earlier, high resistive/impedance ratios exist in distribution grids. This requires modeling of losses in the proven market equilibrium conditions of lossless-DLMPs [35, 34, 58, 41] is imperative. To this end, the authors have recently focused on developing lossy-DLMPs. As lossy-DLMPs are based on non-linear power flows to compute DLMPs, they are naturally more accurate in terms of representing grid conditions as compared to lossless-DLMPs.

Lossy-DLMPs

Recent works on lossy-DLMPs have considered i) linearized [3, 109], ii) convexified [82, 110], and iii) global power balance [82, 12, 90] variations of actual power flows. The linearized lossy-DLMP methods [3, 109] approximate actual power flows around an assumed fixed voltage magnitude across the distribution grid. Naturally, this inflicts an error in DLMPs at nodes farther away from the root-node, where a large voltage drop might occur. The convexified lossy-DLMP methods [82, 110] are more accurate as compared to linearized power flows, however, it does not translate to intuitive DLMP formulations [82]. This is important as the DSO must be able to interpret DLMPs and translate it into its financial settlements. The lossy-DLMPs in a most generic form are obtained from the global power balance formulation [12, 82, 90], allowing individual components of lossy-DLMPs to be analyzed in detail, which may help in interpreting DLMPs for distribution grids in a manner similar to the standardized LMP formulation of transmission grids [88]. However, for DLMPs, the challenge in this formulation lies in expressing power flows which have higher nonlinearities in distribution grids as compared to those of transmission grids [82]. Another important feature of transmission grid energy markets are that the final LMP value is represented as the sum of its energy, loss and (line flow) congestion components. However, from the above mentioned

[4] In chapter 3, we discuss grid modeling of both single-phase and multiphase systems in great detail.

lossy-DLMP formulations, only [82, 90, 3, 109] explicitly represent DLMP as the sum of its energy, loss and congestion component. Nevertheless, works in [82, 90] do not provide tractable formulation for nonlinear power flows and works in [3, 109] use static approximations (fixed voltages) which may inflict error in DLMP values. Hence there exists the need to develop a DLMP model which expresses DLMP at the node as components of its energy, system loss and congestion contribution to the grid along with sufficient accuracy of nonlinear power flows.

Market Equilibrium DLMPs

DLMPs achieving market equilibrium have been discussed mostly in the literature on lossless-DLMPs. However, investigations on lossy-DLMPs have mostly focused on incorporating nonlinearities in DLMPs and have not discussed market equilibrium conditions under the presence of both instantaneous and planned time horizon flexible resource dispatch. As flexibility resources (instantaneous and planned horizon dispatch) are envisioned to be an integral part of future grids and there must exist local distribution grid markets which is economically efficient, i.e., maximizing the overall grid surplus as well as the surplus of individual flexible resources.

1.3.2 DLMP Extensions to Multiphase Systems

Even though literature on single-phase DLMP attempts to provide insights into structure and formulation of DLMPs. The literature on multiphase DLMP model is not abundant. This is important as distribution grids can be quite diverse due to their multiphase and unbalance characteristics. Hence, single-phase DLMP models might not be readily adaptable to multiphase DLMPs. Recently, few works have been reported on three-phase DLMP models [106, 62, 102, 64]. Works in [106] deployed actual power flows systems and in [62] a convexified optimal power flow is developed to calculate DLMPs for three-phase distribution grids. The works in [102, 64] considered a linearized distribution grid model to calculate DLMPs. Most of these works considered equivalent three-phase systems. Moreover, none of these works discuss market equilibrium conditions along with its decomposition into its most general terms. As mentioned this decomposition is necessary to interpret DLMPs before charging the customers. Hence, there still has not been any work which considers combination of multiphase (single or three-phase) and/or unbalanced loadings of distribution grids in calculating DLMPs along with their decomposability and equilibrium as compared to equivalent single-phase DLMPs.

Based on the above identified relevant literature, the next section identifies the main research questions of this thesis.

1.4 Research Questions

In order to develop the above intended appropriate DLMP model, the main research questions this thesis answers are:

Question 1: How to obtain a tractable formulation for the DLMP model, considering highly nonlinear power flows of distribution grids as well as their diverse characteristics of having unbalanced loadings and multiphase lines?

Question 2: Can the DLMP model provide the same level of intuition, physical interpretation and calculation reliability as provided by the transmission grid level LMP model?

Question 3: Using the DLMP model as the fundamental component of the envisioned ADS framework, is it possible to organize a market mechanism for distribution grids, which ad-

dresses realistic grid constraints while achieving efficient resource allocation of the available flexibility resources?

Hence, this thesis is devoted to investigating an "appropriate" DLMP formulation for distribution grids. The term "appropriate" in the context of this thesis means that the resultant DLMP model must aim to achieve overall grid's social welfare maximization as well as for local flexibility resources (DGs and FLs), with the consideration of nonlinear distribution grid power flows and inter-temporal energy requirements. Moreover, the Distribution Locational Marginal Price (DLMP) model should aid in understanding and interpreting the final prices obtained from the local distribution grid market framework.

1.5 Thesis Contributions

In this thesis, we answer the above posed research questions. In doing so, the following contributions to the existing literature on DLMP is made in this thesis:

1. We present a tractable calculation methodology of DLMPs which accounts for i) nonlinear distribution grid power flows, ii) multi-period dispatch of FLs and DGs operation and iii) unbalanced and multiphase nature of distribution grids. The proposed methodology relies on approximation of distribution grid power flow, which fundamentally has similar characteristics for both equivalent single-phase as well as multiphase distribution grid models. Chapter 3 details the approximation procedure, whereas chapter 4 presents derivation of DLMP along with a solution algorithm to cater for non-linear power flows. In both chapters, the approximation procedures along with solution strategies have been performed for both equivalent single-phase and multiphase grids.
2. We exploit properties of convex optimization and power flow approximations to propose the DLMP formulation which is decomposable into intuitive energy, congestion, loss and voltage components. Hence, the proposed methodology is intuitive in its understanding and provides physical interpretation of grid conditions, improving its future practical realization. Chapter 4 details price decomposition for both equivalent single-phase and multiphase grid models, after utilizing the approximations from 3.
3. We show that there exists a possibility of distribution grid market framework, which efficiently allocates flexibility resources using DLMP as its final cleared price. The final cleared price is shown to exist in equilibrium with the overall grid conditions and under the assumption of rational FL and DGs maximizes the overall social welfare of the grid and for the individual entities in the grid. Chapter 2 outlines the basic role of convexity and interpretation of prices from the perspective of electricity market. Chapter 5 translates these concepts into the proposed local distribution grid market framework.

1.6 List of Publications

During this thesis, following publications were made, which directly and indirectly helped in identifying the main theme and research direction of the presented work:

Journal Publications

[1] **S. Hanif**, P. Creutzburg, C. Hackl, H. B. Gooi. Pricing Mechanism for Flexible Loads Using Distribution Grid Hedging Rights, for Special Issue on *Transactive Control of DER and Flexible Loads IEEE Transactions on Power Systems*, 2018. doi:10.1109/TPWRS.2018.2862149.

[2] **S. Hanif**, K. Zhang, C. Hackl, M. Barati, H. B. Gooi, T. Hamacher. Decomposition and Equilibrium Achieving Distribution Locational Marginal Pricing using Trust-Region Method, *IEEE Transactions on Smart Grid*, 2018. doi:10.1109/TSG.2018.2822766.

[3] **S. Hanif**, H. B. Gooi, T. Massier, T. Hamacher, T. Reindl. Distributed Congestion Management of Distribution Grids under Robust Flexible Buildings Operations, *IEEE Transactions on Power Systems*, Vol.:32, Issue: 6, 2017, doi:10.1109/TPWRS.2017.2660065.

[4] **S. Hanif**, T. Massier, H. B. Gooi, T. Hamacher, T. Reindl. Cost Optimal Integration of Flexible Buildings in Congested Distribution Grids, *IEEE Transactions on Power Systems*, Vol.:32, Issue: 3, 2016, doi:10.1109/TPWRS.2016.2605921.

Refereed Conference Publications

[5] **S. Hanif**, M. Barati, A. Kargarian, H. B. Gooi, T. Hamacher. Multiphase Distribution Locational Marginal Prices: Approximation and Decomposition, 2017. In: *IEEE Power and Energy Society General Meeting (PESGM 2018)*. (In press)

[6] S. Troitzsch, **S. Hanif**, T. Hamacher. Distributed Robust Reserve Scheduling in Congested Distribution Systems, 2018. In: *IEEE Power and Energy Society General Meeting (PESGM 2018)*. (In press)

[7] K. Zhang, **S. Hanif**, D. F. R. Melo. Clustering-based Decentralized Optimization Approaches for DC Optimal Power Flow. In: *The Innovative Smart Grid Technology (ISGT 2017)*, Dec 4 – 7, 2017. (In press)

[8] **S. Hanif**, C. Gruentgens, T. Massier, T. Hamacher, T. Reindl. Cost Optimal Operation for a Flexible Building with Local PV in a Singaporean Environment. In: *The 7th IEEE Innovative Smart Grid Technology (ISGT 2016)*, September 6 – 9, 2016. doi:10.1109/ISGT.2016.7781232

[9] **S. Hanif**, T. Massier, T. Hamacher, T. Reindl. Evaluating Demand Response Strategies in the Presence of Solar PV: Distribution Grid Perspective (**Best Paper Award**). In: *4th IEEE International conference on Smart Energy Grid Engineering (SEGE 2016)*, August 21 – 24, 2016. doi:10.1109/SEGE.2016.7589558

[10] **S. Hanif**, C. Gruentgens, T. Massier, T. Hamacher, T. Reindl. Quantifying the Effect on the Load Shifting Potential of Buildings due to Ancillary Service Provision. In: *IEEE Power and Energy Society General Meeting (PESGM 2016)*, July 21 – 24, 2016. doi:10.1109/PESGM.2016.7741402

[11] **S. Hanif**, D. F. R. Melo, T. Massier, T. Hamacher, T. Reindl. Robust Reserve Capacity Provision and Peak Load Reduction from Buildings in Smart Grids. In: *IEEE Power and Energy Society General Meeting (PESGM 2016)*, July 21 – 24, 2016. doi:10.1109/PESGM.2016.7741399

[12] **S. Hanif**, D. F. R. Melo, T. Massier, T. Hamacher, T. Reindl. Model Predictive Control Scheme for investigating Demand Side Flexibility in Singapore. In: *50th University Power Engineering Conference (UPEC 2015)*, September 1 – 4, 2015. doi:10.1109/UPEC.2015.7339769

[13] D. F. R. Melo, **S. Hanif**, T. Massier, G. H. Beng. Combination of renewable generation and flexible load aggregation for ancillary services provision. In: *50th University Power Engineering Conference (UPEC 2015)*, September 1 – 4, 2015. doi:10.1109/UPEC.2015.7339840

[14] J. Stich, **S. Hanif**, T. Massier, T. Hamacher, T. Reindl. Reducing the residual Power Supply of Singapore with Solar PV in Combination with Energy Storage. In: *5th International Conference on Sustainable Energy and Environment (SEE 2014)*, September 1 – 4, 2015.

Chapter 2

Market Modeling: Role of Convexity and Prices

In this chapter, we develop intuition of how prices are calculated in existing electricity markets. First, we show the role of convexity in interpreting the solution of an optimization problem. Dual functions are introduced to calculate prices and interpret its meaning for both the overall system and individual agents. A simplified Economic Dispatch (ED) problem is presented to formalize the role of a System Operator (SO) (could be either for distribution or transmission grid) and autonomous agents in the electricity market. In the end, we present a fully generalized ED and hence discuss practical challenges, prohibiting the ideal operation of electricity markets. The discussion in this section is inspired from [97, Chapter 6], lecture [45] and classical textbooks [94, 104].

2.1 Convex Optimization

In general, optimization problems are formulated to obtain an "objective" given some set of "constraints". Broadly speaking, in the manner how these objective (functions) and constraints are defined, also classify the type of optimization problem. Therefore, there exists many classifications regarding the types of optimization problems [78]. In this thesis, we focus on convex optimization problems [11]. The properties of convex optimization problems are well researched and as a consequence there exists many off-the-shelf software which can solve them readily. Hence, from the context of solution reliability and effectiveness, it is highly favorable to cast an optimization problem as convex. To this end, in this thesis, we are only going to present a brief overview of the convex optimization, which is also immensely relevant for the context of electricity markets.

2.1.1 Convex Function

To motivate our analysis, first, consider a scalar continuous real-valued function, $f(x) = x^2$, to be minimized over $x \in \mathbb{R}$. To find the minimum of this function, we can take help of two conditions, giving us ideas regarding the achieved minimum value, i.e. whether it is a locally or globally minimum:

1. Zero gradient of the function: $\nabla f(x) = 0, 2x^* = 0, x^* = 0$
2. Non-negative second derivative of the function: $\nabla^2 f(x) \geq 0, 2 > 0$

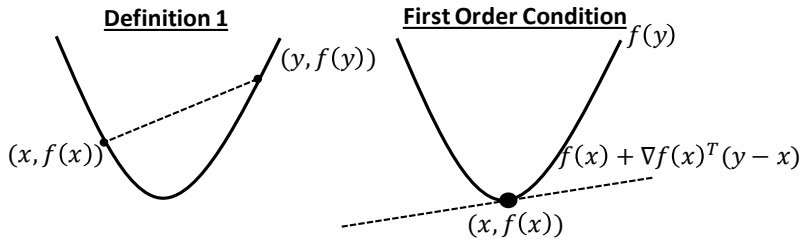

Figure 2.1: Illustration of Definition 1 (right) which shows line connecting two points on the graph must lie above the convex function. The first-order condition (left) shows that the tangent approximating a convex function is its global underestimator.

It is going to be apparent that the second condition is sufficient but not necessary. For both conditions met, the achieved optimal is not only a local minimum, but also a global minimum. However, the underlying principle which allows to conclude the optimality of the solution from the above presented two conditions is the convexity of $f(x)$, more formally defined as [11]:

Definition 1. A function $f : \mathbb{R}^n \to \mathbb{R}$ is convex if its domain (denoted $\mathcal{D}(f)$) is a convex set, and if, for all x,$y \in \mathcal{D}(f)$ and $0 \geq \theta \geq 1$,

$$f(\theta x + (1-\theta)y) \leq \theta f(x) + (1-\theta)f(y).$$

The Definition 1 is strictly convex, if the inequality condition becomes strict inequality for $x \neq y$ and $0 < \theta < 1$. Also, for f being convex, $-f$ is concave and vice versa.

Intuitively, the Definition 1 can be interpreted as if two points on the graph of a convex function are picked and a straight line is drawn through them, then this line will always lie above the actual function. Now, let's see how the above two conditions of our small example provided a global minimizer.

First-Order Condition: Let function $f : \mathbb{R}^n \to \mathbb{R}$ be differential, i.e., it has a gradient $\nabla_x f(x)$[1] for all $x \in \mathcal{D}(f)$. Then f is convex iff $\mathcal{D}(f)$ is a convex set and for all $x, y, \in \mathcal{D}(f)$,

$$f(y) \geq f(x) + \nabla_x f(x)^\intercal (y - x).$$

The right hand side of the above equation ($\nabla_x f(x)^\intercal (y - x)$) is also called first-order approximation to the function f at the point x. Similar to Definition 1, for strict convexity, the above inequality should be a strict inequality. For concave function the inequality should be reverse and for strict concavity it should be reversed and made strict inequality.

Intuitively, this means that for tangent drawn at any point on convex function f, it should always lie below its corresponding point on f.

[1]The gradient $\nabla_x f(x)$ means first derivative of $f(x)$ with respect to x, i.e., for a scalar case $\partial f(x)/\partial x$. For a generalized overview of gradient, and its context with respect to convex programs can be found in [11, Appendix A.4].

Second-Order Condition: Let function $f : \mathbb{R}^n \to \mathbb{R}$ be twice differential, i.e., it has a defined Hessian $\nabla_x^2 f(x)$ for all $x \in \mathcal{D}(f)$. Then f is convex iff $\mathcal{D}(f)$ is a convex set and its Hessian[2] is positive semidefinite for all $x, y, \in \mathcal{D}(f)$,

$$\nabla_x^2 f(x) \succeq 0.$$

Similarly, f is strictly convex for positive definite Hessian, concave for negative semidefinite Hessian and strictly concave for negative definite Hessian. The above notation of $\succeq$ in matrix does not imply component wise inequality.

To explain the above condition intuitively, consider a scalar twice differentiable function f. Then, the above condition states that the second derivative of f be non-negative.

Now from the above posed convexity conditions, we can informally infer that from the first order gradient solution, we have a local optimal x^* of $f(x^*)$. Hence, this condition is necessary for x^* to stand a chance of being considered as an optimal, no matter a local one. Now, considering that x^* also satisfies the second-order condition, it is sufficient to be considered as a global optimal. For a range of convex functions and sets, the interested readers are referred to [11].

2.1.2 Solving Convex Programs

From above discussion, we can conclude that the minimum of unconstrained function $f(x) = x^2$, i.e., $x^* = 0$, qualifies as a global minimum. Now we extend the discussion to solving $f(x)$ given set of constraints, compactly represented as:

$$\begin{aligned} \underset{x \in \mathbb{R}}{\text{minimize}} \quad & f(x) && && \text{(2.1a)} \\ \text{subject to} \quad & g_i(x) \leq 0, && i = 1, \ldots, l && \text{(2.1b)} \\ & h_j(x) = 0, && j = 1, \ldots, p && \text{(2.1c)} \end{aligned}$$

Now in order for (2.1) to be a convex program, $f : \mathbb{R} \to \mathbb{R}$, and $g_i : \mathbb{R} \to \mathbb{R}$ must be convex functions whereas, $h_j : \mathbb{R} \to \mathbb{R}$ must be affine functions[3]. And from our discussion above, we also have that any locally optimal solution to the convex program (2.1) is also globally optimal.

One Equality Constraint: An example

We demonstrate the solution procedure for a convex program through the following simple example of one equality constraint:

Example 2.1

$$\begin{aligned} \underset{x_1, x_2}{\text{minimize}} \quad & f(x_1, x_2) := x_1^2 + x_2^2 && \text{(2.2a)} \\ \text{subject to} \quad & h(x_1, x_2) := x_1 + x_2 - 2 = 0. && \text{(2.2b)} \end{aligned}$$

---

[2]The Hessian $\nabla_x^2 f(x)$ is the second derivative $f(x)$ with respect to x, i.e., for a scalar case $\partial^2 f(x)/\partial x$. For a generalized overview of Hessian, and its context with respect to convex programs can be found in [11, Appendix A.4].

[3]Affine function $h(x) = ax + b$ is a special set of convex function. Condition on $h(x) = 0$ to be affine comes from the fact that $h(x) = 0$ can be equivalently represented as $h(x) \leq 0$ and $-h(x) \leq 0$. So if $h(x)$ is convex, then $h(x) \leq 0$ is convex and $-h(x) \leq 0$ is concave. Therefore the only way to enforce $h(x) = 0$ is through the condition that $h(x)$ is affine as affine function are both convex and concave at the same time [11]

Intuitively, for $f(x_1, x_2)$ to be minimized, we would like it to be closer to the origin. However, the equality constraint (2.2b) is going to bind the solution at line $h(x_1, x_2)$. Graphically, the solution of (2.2) can be simply obtained as shown in Fig. 2.2. From Fig. 2.2, we can observe that at the solution point $(x_1^*, x_2^*) = (1, 1)$, the contour of $f(x_1, x_2) = 2$ just touches the constraint $h(x_1, x_2)$, i.e. any point below (above) this point the constraint misses (intersects twice) the contour functions. We would like to solve for this solution point, analytically. To this end, we present another observation of Fig. 2.2: At the solution (x_1^*, x_2^*) contours of the objective function $f(x_1, x_2)$ and the constraint function $h(x_1, x_2)$, have the same directed tangents, i.e., $\nabla f(x_1, x_2)$ and $\nabla h(x_1, x_2)$ are in the same direction. However, we don't know whether these directions have the same magnitude. This can be accounted using a multiplier λ, such that

$$\nabla f(x_1, x_2) = \lambda \nabla h(x_1, x_2) \tag{2.3}$$

The condition (2.3) must hold for the achieved solution of (2.2). With this, we have introduced a new unknown λ into our problem. Hence, in order to solve this analytically, we would require three equations. We achieve this by first representing (2.3) as a function:

$$\mathcal{L}(x_1, x_2, \lambda) = f(x_1, x_2) - \lambda h(x_1, x_2) = x_1^2 + x_2^2 - \lambda(x_1 + x_2 - 2) \tag{2.4}$$

then from the first-order of convexity, we have the following system of the equation and the solution for $x := (x_1, x_2, \lambda)$

$$\begin{bmatrix} \frac{\partial \mathcal{L}(x)}{\partial x_1} \\ \frac{\partial \mathcal{L}(x)}{\partial x_2} \\ \frac{\partial \mathcal{L}(x)}{\partial \lambda} \end{bmatrix} = \begin{bmatrix} 0 \\ 0 \\ 0 \end{bmatrix}, \underbrace{\begin{bmatrix} 2 & 0 & -1 \\ 0 & 2 & -1 \\ -1 & -1 & 0 \end{bmatrix}}_{A} \underbrace{\begin{bmatrix} x_1 \\ x_2 \\ \lambda \end{bmatrix}}_{x} = \underbrace{\begin{bmatrix} 0 \\ 0 \\ -2 \end{bmatrix}}_{b}, x^* = A^{-1}b, \begin{bmatrix} x_1^* \\ x_2^* \\ \lambda^* \end{bmatrix} = \begin{bmatrix} 1^* \\ 1^* \\ 2^* \end{bmatrix}. \tag{2.5}$$

Note that the last row of the above equation also satisfy the required optimality condition (2.3).

Similar analysis can be performed for the convex programs with multiple equality constraints.

One Equality and One Inequality Constraint: Generic

Now consider a simplified version of generic convex program (2.1) where only one equality and one inequality constraint exists:

$$\begin{aligned} \underset{x \in \mathbb{R}}{\text{minimize}} \quad & f(x) && \text{(2.6a)} \\ \text{subject to} \quad & g(x) \leq 0 && \text{(2.6b)} \\ & h(x) = 0 && \text{(2.6c)} \end{aligned}$$

An approach to solve the convex program with inequality constraints might be [45]:

1. Ignore the inequality constraint and solve it using the above defined method.
2. If inequality constraint is satisfied, then the inequality constraint was redundant.
3. If inequality constraint is not satisfied, then the inequality constraint must have been binding, i.e., the solution enforces inequality constraint to be an equality constraint, i.e. $g(x) = 0$.

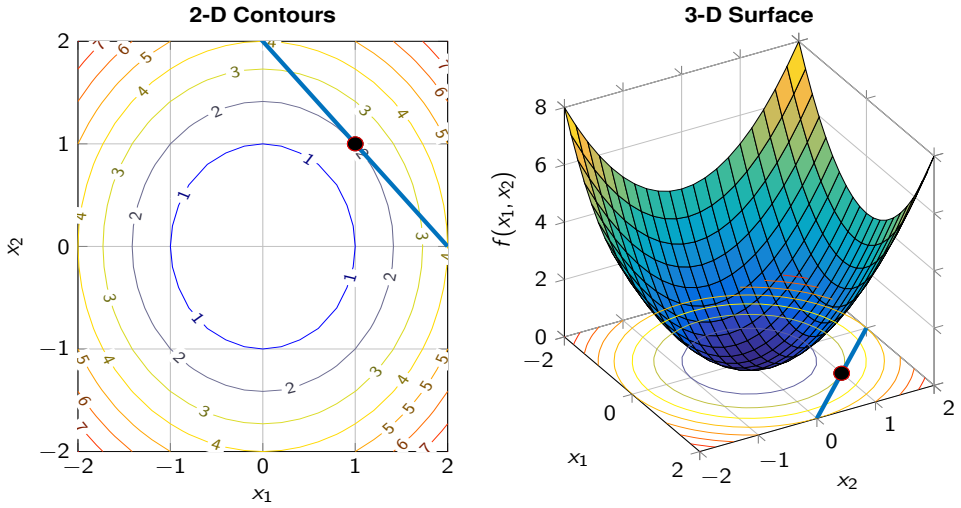

Figure 2.2: For varying values of the variable x_1 and x_2, 2-D contours show constant values of objective function, whereas 3-D surface shows the objective function value as a height along with its contours projected on the horizontal x_1-x_2 plane. The constraint (2.2b) is represented by the blue line and the dot on the line is the minimum of the convex program (2.2).

To analyze this, we write the $\mathcal{L}$ of (2.6) considering inequality constraint to be an equality constraint, i.e.,

$$\mathcal{L}(x, \lambda, \mu) = f(x) - \lambda h(x) - \mu g(x) \tag{2.7}$$

Now, for inequality condition not binding in (2.7), we have $\mu = 0$ and $g(x) \neq 0$. And for binding inequality constraint, we get $\mu \neq 0$ and $g(x) = 0$. Note that for both these scenarios to be enforced, we can simply have the relationship $\mu g(x) = 0$. Now, applying the first order necessary conditions which solves (2.7) for (x^*, λ^*, μ^*) we get:

$$\frac{\partial \mathcal{L}(x^*, \lambda^*, \mu^*)}{\partial x} = 0, \tag{2.8a}$$

$$\frac{\partial \mathcal{L}(x^*, \lambda^*, \mu^*)}{\partial \lambda} = 0, \tag{2.8b}$$

$$\frac{\partial \mathcal{L}(x^*, \lambda^*, \mu^*)}{\partial \mu} = 0, \tag{2.8c}$$

$$\mu^* g(x^*) = 0, \tag{2.8d}$$

$$\mu^* \geq 0, \tag{2.8e}$$

where in 2.8, apart from the first-order necessary conditions, (2.8d) and (2.8e) are also listed. The reason being, (2.8d) is a complimentary conditions which enforces that for inactive inequality constraint, its Lagrange multiplier is zero. The condition (2.8e) is included to make sure that the Lagrange multiplier is always nonnegative. The conditions in (2.8) hold true for the solution (x^*, λ^*, μ^*) to (2.6). Similarly, as the solution to the convex program (2.6) is a global minimum, the conditions in (2.8) are necessary and sufficient. The presented analysis on one equality and inequality constraint can simply be extended for multiple equality and inequality constraints.

Remark 2.1. The conditions shown in (2.8) are in the subsequent subsection generalized as Karush-Kuhn-Tucker (KKT) conditions [53].

2.1.3 Karush-Kuhn-Tucker Conditions

We generalize the conditions in (2.8) for generic convex programs (2.1) by first writing its corresponding $\mathcal{L}$,

$$\mathcal{L}(x, \lambda_i, \mu_i) = f(x) - \sum_{i=1}^{p} \lambda_i h_i(x) - \sum_{i=1}^{l} \mu_i g_i(x)$$

and then deriving the respective Karush-Kuhn-Tucker (KKT) conditions for optimality from it as:

$$\nabla_x \mathcal{L}(x, \lambda_i, \mu_i) = 0 \Rightarrow \nabla_x f(x) + \sum_{i=1}^{p} \lambda_i \nabla_x h_i(x) + \sum_{i=1}^{l} \mu_i \nabla_x g_i(x) = 0 \tag{2.9a}$$

$$\nabla_{\lambda_i} \mathcal{L}(x, \lambda_i, \mu_i) = 0 \Rightarrow h_i(x) = 0, i = 1, \ldots, p \tag{2.9b}$$

$$\nabla_{\mu_i} \mathcal{L}(x, \lambda_i, \mu_i) = 0 \Rightarrow g_i(x) \leq 0, i = 1, \ldots, l \tag{2.9c}$$

$$\mu_i g_i(x) = 0, i = 1, \ldots, l \tag{2.9d}$$

$$\mu_i \geq 0, i = 1, \ldots, l \tag{2.9e}$$

In (2.9), (2.9a) is known as stationary condition; (2.9b) and (2.9c) are known as primal feasible conditions; (2.9d) is known as complementary slackness and; (2.9e) is known as dual feasibility condition. For convex program (2.1), the optimal solution (x^*, λ^*, μ^*) is also a global solution and satisfies its KKT conditions (2.9).

Remark 2.2. In the literature, the multiplier λ is referred as Lagrange multiplier or dual variable, whereas the function $\mathcal{L}$ derived in (2.4) is called as Lagrangian function both these names have a significant usage in convex programs to be demonstrated next.

2.2 Market Price Fundamentals

We now attempt to understand electricity market operation. However, we do not aim to present exhaustive treatment of the organization and regulation of electricity markets. Instead, we focus on the central theme of the electricity market, i.e., price at which electricity is sold and bought.

2.2.1 Duality

Let's consider again the generic convex program of (2.1), now denoted as a primal problem solving for the primal variable x as:

$$\begin{aligned} P = \underset{x \in \mathbb{R}}{\text{minimize}} \quad & f(x) \\ \text{subject to} \quad & g_i(x) \leq 0, \qquad i = 1, \ldots, l;\ \mu_i \\ & h_i(x) = 0, \qquad i = 1, \ldots, p;\ \lambda_i \end{aligned} \tag{2.10}$$

Above, the respective Lagrange multipliers are stated to the right (after semicolon) of their respective constraints. Now, the Lagrangian of above problem is:

$$\mathcal{L}(x, \lambda_i, \mu_i) = f(x) - \sum_{i=1}^{p} \lambda_i h_i(x) - \sum_{i=1}^{l} \mu_i g_i(x),$$

and its dual function $l(\lambda_i, \mu_i)$ is then the unconstrained minimum of the Lagrangian with respect to the primal variable x,

$$l(\lambda_i, \mu_i) = \min_x \mathcal{L}(x, \lambda_i, \mu_i) = \nabla_x \mathcal{L}(x, \lambda_i, \mu_i) = 0.$$

Now for a feasible primal variable x and inequality Lagrange multiplier as $\mu_i \geq 0$[4], we can observe the following properties:

- $l(\lambda_i, \mu_i)$ is always concave, as it is affine in μ_i and λ_i;
- Similarly, we can then conclude that $l(\lambda_i, \mu_i) \leq P$ holds for all feasible x

This motivates us to define the dual optimization problem D, which finds the largest possible lower bound on the primal problem,

$$\begin{aligned} D = \quad & \underset{\mu_i \in \mathbb{R}^I, \lambda_i \in \mathbb{R}^p}{\text{maximize}} && l(\lambda_i, \mu_i) \\ & \text{subject to} && \mu_i \geq 0, \qquad i = 1, \ldots, I \end{aligned} \tag{2.11}$$

For the convex primal problem we have an important relationship of $D = P$, which means the same solution $(x^*, \mu_i^*, \lambda_i^*)$ from both primal and dual problems are achieved [11]. Hence, if we drop the maximization term in (2.11) and instead solve for $\min_x \mathcal{L}(x, \lambda_i, \mu_i) = \nabla_x \mathcal{L}(x, \lambda_i, \mu_i) = 0$, we arrive at the same solution for convex problems. In the end, we combining this interpretation with our KKT discussion, to informally conclude that for convex problems, the corresponding KKT conditions, presenting necessary and sufficient conditions for optimal $(x^*, \mu_i^*, \lambda_i^*)$, for convex programs yields both primal x^* and dual (μ_i^*, λ_i^*) optimal values.

2.2.2 Interpreting Duals as Market Price

Now we move with development of price intuition from the above explained duality concepts. Consider again the primal problem (2.10), with modified constraints as:

$$\begin{aligned} P = \ & \underset{x \in \mathbb{R}}{\text{minimize}} && f(x) \\ & \text{subject to} && g_i(x) \leq a, \qquad i = 1, \ldots, I;\ \mu_i \\ & && h_i(x) = b, \qquad i = 1, \ldots, p;\ \lambda_i \end{aligned} \tag{2.12}$$

The Lagrangian function for the above problem is then given as

$$\mathcal{L}(x, \lambda_i, \mu_i) = f(x) - \sum_{i=1}^{p} \lambda_i (h_i(x) - b) - \sum_{i=1}^{I} \mu_i (g_i(x) - a),$$

Now at the solution $(x^*, \lambda_i^*, \mu_i^*)$, we assume that infinitesimal change in constraints (a, b) has no affect in turning active to inactive constraints and vice versa, then we obtain the following relationships for dual variables after equating $\partial \mathcal{L}(x, \lambda_i, \mu_i)/\partial a = 0$ and $\partial \mathcal{L}(x, \lambda_i, \mu_i)/\partial b = 0$

$$\mu_i = -\frac{\partial P}{\partial a} \qquad \text{and} \qquad \lambda_i = -\frac{\partial P}{\partial b}.$$

[4]This nonnegative condition on inequality constraint's Lagrange multiplier is directly inspirit of our previous discussion on the treatment of inequality constraints.

These relationships state that the dual variables (μ_i^*, λ_i^*) represent the rate at which optimal value of the problem (2.12) changes when an infinitesimal change in their respective constraints is observed. With regards to economics, we can interpret this relationship in following manner: if P represents the economic operation cost, then the dual variables represent the price of their respective constraints. This is the key component in electricity markets which relates the cost of operating power systems with prices.

2.2.3 Efficient Economic Operation

In this subsection, we take a step closer towards the explanation of duals as a cornerstone of electricity market operations. In principle, we show how electricity markets revolve around duals incentivizing market participants to realize individual optimal solution, which in turn also enable overall social optimality. To motivate this, we consider now an example of two variables existing in the system, a generation variable p_1, flexible demand variable p_2 and fixed demand p_3. Ideally, generator wishes to minimize production cost of generating p_1, termed as $f(p_1)$ and flexible demand owner[5] aims to maximize the benefit of consuming p_2, termed as $f(p_2)$. In terms commonly referred in the literature, we can also say that $f(p_1)$ denotes the production cost curve for the generator whereas $f(p_2)$ denotes the demand curve for flexible demand owner. Assuming that a central entity, such as a SO, is in charge of operating the grid. Then the SO aims to maintain supply and demand balance while minimizing the cost (negative benefit) of energy production (consumption):

$$\begin{aligned} \underset{p_1,\, p_2}{\text{minimize}} \quad & f(p_1) - f(p_2) \\ \text{subject to} \quad & p_1 + p_2 = p_3 \qquad ; \lambda \end{aligned} \tag{2.13}$$

We can use the developed tools in the previous section to derive the Lagrangian of (2.13),

$$\mathcal{L}(p_1, p_2, \lambda) = f(p_1) - f(p_2) - \lambda(p_1 + p_2 - p_3)$$

The objective function $f(p_2) - f(p_1)$ is usually referred as social welfare. Hence, we aim to maximize the social welfare in (2.13) given the supply equals the demand (the only constraint). We again assume that (2.13) is convex. Now from the above discussion, we can recognize here too that upon the given solution, the dual variable λ can simply serve as a price, or from our context, the market clearing price. This price can be considered as the sensitivity of costs (negative benefits) functions. For generation variable p_1, given the price λ^* and demand variable p_2^* simply corresponds to:

$$\nabla_{p_1} \mathcal{L}(p_1, p_2^*, \lambda^*) = \frac{\partial f(p_1)}{\partial p_1} = \lambda^*$$

Now assuming strong duality holds for (2.13), then for variable p_1 the primal problem can be equivalently from its dual

$$\max_{\lambda} \min_{p_1} \mathcal{L}(p_1, \lambda) = \min_{p_1} f(p_1) - \lambda^* p_1,$$

where the maximization term in the above expression is dropped due to the assumption of strong duality, turning the dual into solving for the generation variable p_1, price λ^*. One way

[5] Usually, load serving entities, large consumers (mills, factories etc.) are able to participate in markets and demonstrate their demand flexibility.

of interpreting this is that price λ is able to align the objective of individual agent $f(p_1)$ with system condition, given the price reflects the grid conditions. Hence, it can be concluded that even though the production/consumption schedules can not be enforced, there exists a price which can autonomously help achieve the optimal behaviors from the agents. The next example elaborates this interaction of system price with individual agents under the condition of convexity.

Example 2.2

We demonstrate a simple example now with cost (negative benefit) functions in \$ as: $f(p_1) = ap_1^2 + bp_1 + c$ and $f(p_2) = d^2p_2 + ep_2 + f$ and the fixed demand $p_3 = 50$ in MW. As demonstrated in Sec. 2.1, the convex programs after being exposed to first-order condition can be solved as system of equations $x = A^{-1}b$. For (2.13), this gives us the coefficient of matrices:

$$A = \begin{bmatrix} 2a & 0 & -1 \\ 0 & -2d & -1 \\ 1 & 1 & 0 \end{bmatrix}, b = \begin{bmatrix} -b \\ e \\ 50 \end{bmatrix}.$$

Now for cost variables are assumed to be $a/d = 0.05/0.1$ in \$/MWh^2, $b/e = 0.1/0.2$ in \$/MWh and $c/f = 50/100$ in \$, we obtain the solution (p_1^*, p_2^*, λ^*) = (103 MW, -53 MW, 10.4 \$/MWh). The price λ is simply equal to sensitivity of each agent's objective function and its relationship with the overall obtained solution is given in Fig. 2.3. One can verify that at the optimal solution, we have $\lambda = \partial f(p_1)/\partial p_1 = -\partial f(p_2)/\partial p_2$.

Moreover, we also have the property of individual agent production/consumption problems, after including the cleared price λ to be exactly equal as the SO problem. For example, for generating unit $p1$, the optimal individual problem can be written simply as: $\min_{p_1} f(p_1) - \lambda p_1$, which from the first-order condition gives: $p_1^* = (\lambda^* - b)/2a$ and after substituting the values yield exactly the same solution as obtained from the overall social welfare problem, i.e. 103 MW.

From the above example,if $f(p)$ is taken as the production cost (negative benefit), then $\partial f(p)/\partial p$ is usually referred as the supply function offers (demand curve bids) [94, 97].

Remark 2.3. For the small example 2.2, we were able to manually obtain solution of duals (prices) by deploying first-order conditions and solving the system of linear equations. However, in practice these problems are solved through the deployment of a solver. These solvers also readily provide duals, which can then be interpreted as prices.

2.3 Economic Dispatch

The above presented example, simplified for brevity, can be interpreted as Economic Dispatch (ED), which is carried out by the SO as follows:

1. The producers/consumers submit offers/bids to the SO.
2. The SO collects these offers/bids and accordingly turns them into the sum of individual objectives such that the overall social welfare of the system is reflected.
3. The SO then solves for the social welfare, considering the system constraints.

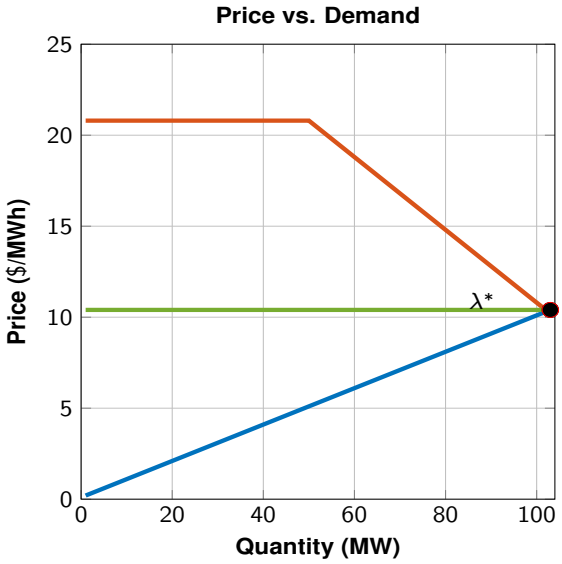

Figure 2.3: The relationship of price and demand for the given example. The figure is organized in a way to show that there exists no price elasticity from 0-50 MW, and then flexible consumers' *demand curve* exactly meets generation *supply function* where the price is cleared. In economics, the area between the optimal price and demand curve is known as consumer surplus and between supply function and optimal price as producer surplus. The sum of both areas are known as social welfare [94, 50].

4. The price is obtained from this solution, based on which producers are paid and consumers pay.

As an overview, we now present the ED problem in its full generality. For brevity, we take the transmission grid with n buses. Then, generic vectors for active $\mathbf{p} := (p_1, \ldots, p_n)$ and reactive power $\mathbf{q} := (q_1, \ldots, q_n)$ in the grid, which is known. Similarly, let complex voltages be $\mathbf{v} := (v_1, \ldots, v_n)$, which indicates actual power grid physical power flows, for given loading $(\mathbf{p}, \mathbf{q})$. The SO solve the following optimization problem, which aims to represent technical and economical transmission system operation:

$$\begin{aligned} \text{maximize} \quad & f(\mathbf{p}, \mathbf{q}, \mathbf{v}) && \text{(2.14a)} \\ \text{subject to} \quad & \mathbf{g}(\mathbf{p}, \mathbf{q}, \mathbf{v}) = \mathbf{0} : \boldsymbol{\lambda} && \text{(2.14b)} \\ & \mathbf{h}(\mathbf{p}, \mathbf{q}, \mathbf{v}) \leq \mathbf{0} : \boldsymbol{\mu} && \text{(2.14c)} \end{aligned}$$

where,

$f(\mathbf{p}, \mathbf{q}, \mathbf{v}) := \sum_i^n f_i(\mathbf{p}, \mathbf{q}, \mathbf{v})$ is the cost of the system, represented as the sum of individual costs for n buses[6]

$\mathbf{g}(\mathbf{p}, \mathbf{q}, \mathbf{v}) := \Big(g_1(\mathbf{p}, \mathbf{q}, \mathbf{v}), \ldots, g_{n1}(\mathbf{p}, \mathbf{q}, \mathbf{v})\Big)$ are $n1$ equality constraints representing physical power flows

$\mathbf{h}(\mathbf{p}, \mathbf{q}, \mathbf{v}) := \Big(h_1(\mathbf{p}, \mathbf{q}, \mathbf{v}), \ldots, h_{n2}(\mathbf{p}, \mathbf{q}, \mathbf{v})\Big)$ are $n2$ inequality constraints, such as thermal limits, voltage constraints etc,

[6]Usually, this cost can be interpreted as the short-run cost, represented as the cost of individual generating units.

and variables to the right of colon in (2.14b) and (2.14c) are their respective Lagrange multiplier and can be interpreted as their shadow prices.

To be discussed later, solving (2.14) is not a trivial task. However, we move towards obtaining the Locational Marginal Price (LMP), which establishes equilibrium between all market participants and grid conditions. Consider the Lagrangian $\mathcal{L}(\mathbf{p}, \mathbf{q}, \mathbf{v}, \boldsymbol{\lambda}, \boldsymbol{\mu})$ of (2.14):

$$\mathcal{L}(\mathbf{p}, \mathbf{q}, \mathbf{v}, \boldsymbol{\lambda}, \boldsymbol{\mu}) = f(\mathbf{p}, \mathbf{q}, \mathbf{v}) + \boldsymbol{\lambda}^{\mathsf{T}}\mathbf{g}(\mathbf{p}, \mathbf{q}, \mathbf{v}) + \boldsymbol{\mu}^{\mathsf{T}}\mathbf{h}(\mathbf{p}, \mathbf{q}, \mathbf{v}) \tag{2.15}$$

Consider a solution exists for (2.14), then from (2.15) we have active $\Pi^{\mathbf{p}}$ and reactive power $\Pi^{\mathbf{q}}$ LMP at each bus defined as:

$$\Pi^{\mathbf{p}} := \frac{\partial \mathcal{L}(\mathbf{p}, \mathbf{q}, \mathbf{v}, \boldsymbol{\lambda}, \boldsymbol{\mu})}{\partial \mathbf{p}}, \qquad \Pi^{\mathbf{q}} := \frac{\partial \mathcal{L}(\mathbf{p}, \mathbf{q}, \mathbf{v}, \boldsymbol{\lambda}, \boldsymbol{\mu})}{\partial \mathbf{q}} \tag{2.16}$$

From our previous discussions, given a convex program, the above mentioned ED generates a price (LMP) which not only incentivize individual agents to take optimal actions but also maximize the overall social welfare of the system. For example. 2.2, we have shown this property for an extremely simplified system. However, in a realistic electricity markets for implementing a globally optimal (in economic sense) ED, following challenges exist:

1. For any nonconvex objective or constraints in (2.13), the optimal individual agents decisions may not be in favor of the overall social welfare. For the case of power systems, this poses the biggest challenges with respect to physical power flows. This is because power flows are highly nonlinear and nonconvex in nature must be presented as convex functions. Otherwise, actual grid conditions might not be reflected in the price, causing suboptimal grid operation and hence overall ED schedules.
2. The individual agents are assumed to be *price-takers*. This means, they do not consider effect of their actions on the price clearing λ. However, there exists many power systems where agents purchasing/selling large quantities of energy might be able to exert market power.
3. The information might not be available for the SO or the individual agents to solve the central ED or the local agents problems. This can be caused due to many reasons, such as lack of communication infrastructure, privacy concerns and computation complexity.

From the above mentioned challenges, for transmission grids, the DC power flow linear approximations have shown to be adequate for regular transmission system operation [54, 40, 61, 60, 88]. This approximation is facilitated due to nature of transmission grid, where the actual power flows can be linearized up to certain accuracy as losses are not much and voltages are kept within rated levels [104, 40, 54]. However, for distribution grids, the power flows are highly nonlinear and nonconvex, due to higher losses and voltage drops. This renders the transmission grid approximations ineffective. Hence, in this thesis, we devote efforts to find approximation of distribution grid power flows in a manner, not only just convex, but also closer for easy interpretation of prices and establishing a distribution grid market.

Chapter 3

Distribution Grid Modeling: Load-Flow, Approximations and Extensions

As identified in the previous chapters, power flows are the main source of non-convexity in the ED. To this end, in this chapter we explore the power flow modeling for distribution grids. First, we present physical differences between the distribution and transmission grids. Then, the *load flow* problem for the single-phase equivalent distribution grid is described, along with methods to approximate it. The methodology for single-phase grids is then shown to be extensible to multi-phase distribution grids. A small discussion at the end of the chapter lays out the importance of the developed approximation method, with respect to setting up a market framework.

The main contributions of this chapter is bringing the state-of-the-art research on distribution grid solution feasibility [10, 8, 101, 5, 6] and approximations [9, 7], into i) a common framework for both single-phase and multi-phase grids, and ii) extending it to include approximation quantities relevant for calculating prices in a local distribution grid (to be introduced in the subsequent chapters).

3.1 Distribution versus Transmission Grid

As the focus of this thesis is on distribution grids, first let us revisit the main differences between distribution and transmission grids. In doing so, we motivate the need for developing a new power flow model representation in market clearing for distribution grids.

1. Transmission grids are organized in loops, whereas distribution grids are usually operated radially. Radial grids can be characterized as tree networks [48], having a unique ancestor to each bus. This means that only one branch exists between a particular bus and its ancestor Fig. 3.1. In principle, this means that the relationship between a bus and its ancestor is much simpler, as compared to loop flows of meshed networks in transmission grids.
2. Due to its respective components, distribution grids have a higher resistance to reactance ratio, i.e., R/X, as compared to transmission grids [48]. This property causes higher losses in distribution grids, as well as higher nonlinearity in power flows across the grid. Hence, lossless power flow approximations in transmission grids for calculating prices may not be suitable for distribution grids.

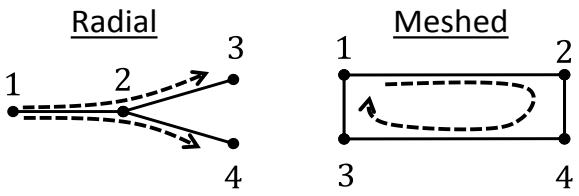

Figure 3.1: Comparison of radial grid (distribution grids) with meshed grid (transmission grid). As compared to meshed networks, in radial grids, power does not flow in loops. Moreover, in radial grids, each bus (e.g. bus 2) has a unique ancestor (bus 1) and multiple children nodes (bus 3 and 4).

3. Transmission grids are balanced, i.e. an equivalent single-phase model can be utilized to model it. However, distribution grids contain various single-phase, grounded and ungrounded supplies and unbalanced loads. This prohibits equivalent single-phase modeling of the transmission grids, to be readily deployed in distribution grids.

In light of the above mentioned differences of distribution grids with transmission grids, we present now distribution grid modeling and approximation procedure, relevant for setting up a distribution grid market and calculating prices.

3.2 Single-Phase Equivalent Distribution Grid Model

Similar to the works on approximate distribution grid solution [10, 4] and price calculations [82, 90, 3, 109, 110], we first consider the model of single-phase equivalent distribution grid.

3.2.1 Modeling Fundamentals

Before presenting the (distribution grid) *load-flow* problem, we first proceed by presenting the most commonly adopted assumptions in steady-state power system analysis:

Assumption 3.1. We limit our modeling for the steady state behavior, i.e., each complex signal is $y = xe^{j\angle x}$ with x as its root-mean-square value (magnitude) and $\angle x$ as its phase from a defined global reference (angle).

Assumption 3.2. The grid is considered a symmetric and balanced portion of the overall distribution grid.

Assumption 3.3. The grid is operated radially with one connection (root-bus) to the transmission grid.

Assumption 3.4. The grid consists of constant PQ models for all n bus. This means that all connected devices have independent dispatch of their active and reactive power, i.e. act as constant power sources/loads.

From **A. 3.1** and **3.2**, we have steady state at bus k described by complex voltage $u_i = v_i e^{j\theta_i} \in \mathbb{C}$, with magnitude $v_i \in \mathbb{R}$ and angle $\theta_i \in \mathbb{R}$. This complex voltage state of the grid is accompanied with the complex injection, more conveniently represented as $s_i = p_i + jq_i$,

where $p_i \in \mathbb{R}$ and $q_i \in \mathbb{R}$ are the active and reactive powers. From **A. 3.3**, we define set of buses as: $\{0, 1, \ldots, n\} \in N$, where 0 is the root-bus index whereas the rest are n PQ buses. For the whole grid, we get voltages as $\mathbf{u} := (u_0, (\mathbf{u}_L)^\intercal)^\intercal \in \mathbb{C}^N$, where $\mathbf{u}_L := (u_1, \ldots, u_n)^\intercal \in \mathbb{C}^n$ and $u_0 \in \mathbb{C}$ are the voltages for n buses and the root-bus, respectively. Similarly, we can define for the whole grid: complex power injections $\mathbf{s}_L := (s_0, (\mathbf{s}_L)^\intercal)^\intercal \in \mathbb{C}^N$, where $\mathbf{s} := (s_1, \ldots, s_n)^\intercal \in \mathbb{C}^n$ and $s_0 \in \mathbb{C}$ are defined for n buses and the root-bus, respectively and; complex current injections $\mathbf{i} := (i_0, (\mathbf{i}_L)^\intercal)^\intercal \in \mathbb{C}^N$, where $\mathbf{i} := (i_1, \ldots, i_n)^\intercal \in \mathbb{C}^n$ and $i_0 \in \mathbb{C}$ are defined for n buses and the root-bus, respectively. From **A. 3.4**, we have that injections at PQ model buses are imposed and not dependent on bus voltages [10], i.e. we have the following relationship:

$$\mathbf{s} = \mathrm{diag}(\mathbf{u})\bar{\mathbf{i}}, \tag{3.1a}$$

$$\mathbf{i} = \mathbf{Y}\mathbf{u}. \tag{3.1b}$$

which relates currents $\mathbf{i}$ to voltage $\mathbf{u}$ through the nodal admittance matrix $\mathbf{Y} \in \mathbb{C}^{N\times N}$. The following example demonstrates the above derivation.

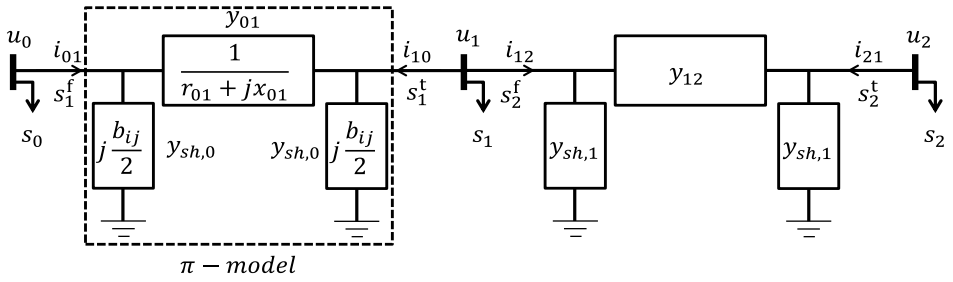

Figure 3.2: Exemplary three-bus single-phase equivalent distribution grid radial model, with adopted grid nomenclature. The adopted π-model [113] of the line (i, j) connecting nodes i and j is composed of series admittance $y_{ij} = 1/(r_{ij} + jx_{ij})$ and two equal halved shunt admittances $y_{sh,i} = jb_{ij}/2$, where r_{ij}, x_{ij} and b_{ij} are the resistance, reactance and susceptance of line (i, j). See Example 3.1 for derivation of (3.1), example 3.2 for the solution technique and example 3.3 for line flows. All quantities in this figure are in complex domain.

Example 3.1

We derive nodal injections (current and power) in a form given by (3.1) for the exemplary system of Fig. 3.2. For line element (i, j), consider the current i_{ij} is in the direction from bus i to j and i_{ji} is from bus j to i. From ohms' law, this gives us following relationship of current flowing in lines of the grid:

$$i_{01} = y_{sh,0}u_0 + y_{01}(u_0 - u_1), \qquad i_{10} = y_{sh,0}u_1 + y_{01}(u_1 - u_0),$$
$$i_{12} = y_{sh,1}u_1 + y_{12}(u_1 - u_2), \qquad i_{21} = y_{sh,1}u_2 + y_{12}(u_2 - u_1).$$

Now, we are interested in nodal quantities, which can be obtained using the Kirchoff law, which states that injected current at bus i, i_i, is equal to sum of all line currents considering

they are directly connected to bus i, i.e. $i_i = \sum_k i_{ik}, \forall k \in (i,k)$

$$\begin{aligned} i_0 &= i_{01}, & i_0 &= y_{sh,0}u_0 + y_{01}(u_0 - u_1), \\ i_1 &= i_{10} + i_{12}, & i_1 &= y_{sh,0}u_1 + y_{01}(u_1 - u_0) + y_{sh,1}u_1 + y_{12}(u_1 - u_2), \\ i_2 &= i_{21}, & i_2 &= y_{sh,1}u_2 + y_{12}(u_2 - u_1). \end{aligned}$$

In order to be consistent with (3.1b), we collect the above in appropriate vector forms to give:

$$\mathbf{i} = \mathbf{Y}\mathbf{u}, \qquad \text{where,}$$

$$\mathbf{i} = \begin{bmatrix} i_0 \\ i_1 \\ i_2 \end{bmatrix}, \mathbf{u} = \begin{bmatrix} u_0 \\ u_1 \\ u_2 \end{bmatrix}, \mathbf{Y} = \begin{bmatrix} y_{sh,0} + y_{01} & -y_{01} & 0 \\ -y_{01} & y_{sh,0} + y_{sh,1} + y_{01} + y_{12} & -y_{12} \\ 0 & -y_{12} & y_{sh,1} + y_{12} \end{bmatrix},$$

As complex power injection at node i is simply $s_i = u_i \bar{i_i}$, collecting it in vector form give us similar expression to (3.1a):

$$\mathbf{s} = \text{diag}(\mathbf{u})\bar{\mathbf{i}}, \text{where} \qquad \mathbf{s} = \begin{bmatrix} s_0 \\ s_1 \\ s_2 \end{bmatrix}.$$

Remark 3.1. The constant Constant source/load active and reactive power model (not dependent on voltages) (PQ) models are adopted due to their popularity in power system analysis for both classic [4] and recent distribution grid studies [10, 82, 109]. The constant PQ models can also be defined as voltage control bus through distributed generator placement. This is because the droop controller embedded in a distributed generator are usually capable of varying their corresponding PQ (active and reactive power) in correlation to their local voltage measurements. Nevertheless, the developed model can be extended to more advanced load models using the concepts provided in [5, 6].

Remark 3.2. The effect of different tap-settings of transformers can also be simply included in the nodal admittance $\mathbf{Y}$ matrix, as done usually in power flow softwares (for example, see [113, Fig. 3.1]).

3.2.2 The *Load-Flow* Problem

For distribution grids, we define the *load-flow* problem from (3.1) as: Given the specified loading $\mathbf{s}$ and the imposed voltage at the root-bus u_0[1], solve (3.1) to obtain complex voltages $\mathbf{u}$ for n buses.

Note that the *load-flow* problem which satisfy (3.1) implicitly solves for $\mathbf{i}$. Then, we can deploy quantities $(v_0, \mathbf{u}, \mathbf{i})$ to obtain root-bus injections, i.e. (i_0, s_0). To this end, we split the relationship in (3.1) between root-bus and the rest of buses. First, for the nodal admittance matrix $\mathbf{Y} \in \mathbb{C}^{N \times N}$, we have

$$\mathbf{Y} = \begin{bmatrix} \mathbf{Y}_{00} & \mathbf{Y}_{0L} \\ \mathbf{Y}_{L0} & \mathbf{Y}_{LL} \end{bmatrix} \tag{3.2}$$

[1] Usually, voltage magnitude v_0 is aimed to be kept at 1–1.05 per unit and angle θ_0 as a reference at 0 degrees.

where $\mathbf{Y}$: $\mathbf{Y}_{00} \in \mathbb{C}^1$, $\mathbf{Y}_{0L} \in \mathbb{C}^{1\times n}$, $\mathbf{Y}_{L0} \in \mathbb{C}^{n\times 1}$ and $\mathbf{Y}_{LL} \in \mathbb{C}^{n\times n}$. Then, for the grid equations (3.1), there exists the following structure,

$$\begin{bmatrix} s_0 \\ \mathbf{s}_L \end{bmatrix} = \begin{bmatrix} u_0 & \\ & \mathrm{diag}(\mathbf{u}_L) \end{bmatrix} \begin{bmatrix} \bar{i}_0 \\ \bar{\mathbf{i}}_L \end{bmatrix}, \tag{3.3a}$$

$$\begin{bmatrix} i_0 \\ \mathbf{i}_L \end{bmatrix} = \begin{bmatrix} \mathbf{Y}_{00} & \mathbf{Y}_{0L} \\ \mathbf{Y}_{L0} & \mathbf{Y}_{LL} \end{bmatrix} \begin{bmatrix} u_0 \\ \mathbf{u}_L \end{bmatrix}, \tag{3.3b}$$

which can be utilized to extract an equivalent problem from (3.1), in terms of only n PQ buses:

$$\mathbf{s}_L = \mathrm{diag}(\mathbf{u}_L)\bar{\mathbf{i}}_L, \tag{3.4a}$$

$$\mathbf{i}_L = \mathbf{Y}_{L0}u_0 + \mathbf{Y}_{LL}\mathbf{u}_L. \tag{3.4b}$$

After eliminating the complex current injections, we get the *load-flow* problem in only n PQ buses:

$$\mathbf{s}_L = \mathrm{diag}(\mathbf{u}_L)(\overline{\mathbf{Y}}_{L0}\bar{u}_0 + \overline{\mathbf{Y}}_{LL}\bar{\mathbf{u}}_L). \tag{3.5}$$

Even though the single-phase equivalent *load-flow* problem in (3.5) is nonlinear and non-convex, there exist numerous methodologies (Newton-Raphson, Guass-Siedel, forward-backward sweep) as well as readily available softwares to solve this problem for a large scale [113, 104]. In this thesis, we explore the recently proposed fixed-point iteration based methodology for solving the *load-flow* problem for distribution grids [10, 101, 8, 5, 6, 108], due to two main reasons:

1. The fixed-point based *load-flow* equation easily transforms into global approximation of load-flow equations. This is going to be discussed in Sec. 3.3.2.
2. The existence and uniqueness of the solution of the *load-flow* problem using fixed-point iteration has been recently shown in for both multi-phase [101, 8] and single-phase distribution grids [10, 6]. This is discussed next for single-phase equivalent grid.

From (3.5), separating solution variable $\mathbf{u}_L$ with injections $\mathbf{s}_L$ directly gives the following fixed-point equation:

$$\mathbf{u}_L = \mathbf{w} + {\mathbf{Y}_{LL}}^{-1}\mathrm{diag}(\bar{\mathbf{u}}_L)^{-1}\bar{\mathbf{s}}_L, \tag{3.6}$$

where $\mathbf{w} := -{\mathbf{Y}_{LL}}^{-1}\mathbf{Y}_{L0}u_0$ is the no-load voltage. Equation (3.6) is then the fixed-point equation, to be solved iteratively, for each iteration k as:

$$\mathbf{u}_L^{k+1} = \mathbf{G}(\mathbf{u}_L^k), \tag{3.7}$$

where $\mathbf{u}_L^k$ is voltage at iteration k, $\mathbf{s}_L$ is the loading (known injections), u^0 is the imposed root-bus voltage and $\mathbf{G}(\cdot)$ defined in (3.6). The following are the convergence properties of (3.7) [10]:

Solution Existence and Uniqueness We briefly explain now conditions for solution existence and uniqueness for (3.7), recently proposed in [101], which are more generalized

version of earlier works in [108, 10]. Consider a pair $(\hat{\mathbf{u}}_{\mathsf{L}}, \hat{\mathbf{s}}_{\mathsf{L}})$ satisfying (3.6), then there exists two conditions for the new set-point $\mathbf{s}_{\mathsf{L}}$:

$$\xi(\hat{\mathbf{s}}_{\mathsf{L}}) < u_{min}^2, \tag{3.8}$$

$$\Delta := (u_{min} - \frac{\xi(\hat{\mathbf{s}}_{\mathsf{L}})}{u_{min}})^2 - 4\xi(\mathbf{s}_{\mathsf{L}} - \hat{\mathbf{s}}_{\mathsf{L}}) > 0, \tag{3.9}$$

and given $\mathbf{u}_{\mathsf{L}} \in \mathcal{D}$, such that

$$\mathcal{D} := \{\mathbf{u}_{\mathsf{L}} : |\mathbf{u}_{\mathsf{L}} - \hat{\mathbf{u}}_{\mathsf{L}}| \leq \rho|\mathbf{w}|\}, \tag{3.10}$$

$$\rho := \frac{u_{min} - \frac{\xi(\hat{\mathbf{s}}_{\mathsf{L}})}{u_{min}} - \sqrt{\Delta}}{2}, \tag{3.11}$$

then there exists a unique $\mathbf{u}_{\mathsf{L}} \in \mathcal{D}$. In the above expressions

$$u_{min} := \min|\hat{\mathbf{u}}_{\mathsf{L}}/\mathbf{w}| \;\text{ and }\; \xi(\mathbf{s}_{\mathsf{L}}) := ||\mathbf{W}^{-1}\mathbf{Y}_{\mathsf{LL}}{}^{-1}\overline{\mathbf{W}}^{-1}\,\mathrm{diag}(\overline{\mathbf{s}_{\mathsf{L}}})||_\infty$$

where, $|\cdot|$ is the element-wise absolute operator for vector $(\cdot)$, matrix $\mathbf{A}$, $||\mathbf{A}||_\infty := \max_i \sum_j |a_{ij}|$ and $\mathbf{W} := \mathrm{diag}(\mathbf{w})$. In [101], the above shown conditions for unique solutions are proved by showing that the operator $\mathbf{G}$ in (3.7) is a contraction mapping: (i) $\mathbf{G}$ is a self-mapping of $\mathbf{u}_{\mathsf{L}}$ on $\mathcal{D}$ and (ii) $\mathbf{G}$ has contraction property, i.e. for solution $\mathbf{u}_{\mathsf{L}}^1, \mathbf{u}_{\mathsf{L}}^2 \in \mathcal{D}$, we have $||\mathbf{G}(\mathbf{u}_{\mathsf{L}}^2) - \mathbf{G}(\mathbf{u}_{\mathsf{L}}^1)||_\infty < ||\mathbf{u}_{\mathsf{L}}^2 - \mathbf{u}_{\mathsf{L}}^1||_\infty$.

The authors in [101] used the above derived uniqueness conditions to also obtain convenient initializing value $(\mathbf{u}_{\mathsf{L}}^0, \mathbf{s}_{\mathsf{L}}^0)$ for the successful convergence of the fixed-point algorithm (3.7). In particular, for the case when there exists no information regarding the condition of the grid exists, it was shown that the choice $(\mathbf{u}_{\mathsf{L}}^0, \mathbf{s}_{\mathsf{L}}^0) = (\mathbf{w}, \mathbf{0})$, i.e., no-load condition can be checked for solution existence and uniqueness. This can be simply seen by inserting $(\mathbf{u}_{\mathsf{L}}^0, \mathbf{s}_{\mathsf{L}}^0)$ in (3.8), (3.9), to obtain new set of unique solution guaranteeing equations:

$$\xi(\mathbf{0}) = \mathbf{0} < u_{min}^2, \tag{3.12}$$

$$\Delta := \xi(\mathbf{s}_{\mathsf{L}}) < 0.25. \tag{3.13}$$

Note that, as for no-load conditions $u_{min} = 1$, so condition (3.12) is always satisfied.

Example 3.2

Consider the grid data in Table. 3.1 for the exemplary system of Fig. 3.2. All values in Table. 3.1 are in per unit (p.u.)[a].

Table 3.1: Grid Data for Fig. 3.2.

Bus (i)	$\hat{p}_i$	$\mathrm{j}\hat{q}_i$	Line (i-j)	r_{ij}	x_{ij}
0	-	-	1 (0-1)	0.1	0.1
1	-1	-1j	2 (1-2)	0.1	0.1
2	0.5	0.5j			

In Table. 3.1, positive/negative load value means generation/consumption. Now, we evaluate two grid conditions to demonstrate the effectiveness of the fixed-point solution. First condition is at the original loading level $\hat{\mathbf{s}}_{\mathsf{L}}$ as given in Table. 3.1. Second condition is at new loading level of $\mathbf{s}_{\mathsf{L}} = 1.1\hat{\mathbf{s}}_{\mathsf{L}}$. For both conditions, Fig. 3.3 compares the fixed-point based solution in Fig. 3.2 against the Newton-Raphson based power flow solution [84].

For the original loading, the fixed-point method is initialized at $\mathbf{u}_{\mathsf{L}}^0 = (1.05, 1.05)$ and the root-node voltage magnitude and angles are fixed at 1.05 and 0radians. It can be seen in Fig. 3.3 that the solution from (3.6) is similar to the Newton-Raphson method. For second condition, we have initialized the fixed-point method at the rated solution pair, i.e. $(\hat{\mathbf{u}}_{\mathsf{L}}, \hat{\mathbf{s}}_{\mathsf{L}})$. The is done so that we can now interpret our solution guarantee conditions as follows: for given a new set point $\mathbf{s}_{\mathsf{L}}$ and the solution pair $(\hat{\mathbf{u}}_{\mathsf{L}}, \hat{\mathbf{s}}_{\mathsf{L}})$, the new solution $\mathbf{u}_{\mathsf{L}}$ is guaranteed to exist and be unique if it satisfies conditions (3.8), (3.9). Table 3.2 presents the required values for demonstrating the uniqueness of the new operating point $\mathbf{u}_{\mathsf{L}}$:

Table 3.2: Relevant quantities to check conditions (3.8), (3.9).

$\xi(\hat{\mathbf{s}}_{\mathsf{L}})$	$\xi(\mathbf{s}_{\mathsf{L}} - \hat{\mathbf{s}}_{\mathsf{L}})$	$\xi(\mathbf{s}_{\mathsf{L}})$	u_{min}^2	Δ	ρ
0.3628	0.0363	0.3991	0.8883	0.0851	0.0941

From Table 3.2, we have both conditions satisfied, i.e.,

$$\begin{aligned} \xi(\hat{\mathbf{s}}_{\mathsf{L}}) < u_{min}^2 \quad &\Leftrightarrow 0.3628 < 0.8883 \\ \Delta > 0 \quad &\Leftrightarrow 0.0851 > 0. \end{aligned}$$

Hence, this guarantees the existence and uniqueness of the solution $\mathbf{u}_{\mathsf{L}}$. This can be also observed from Fig. 3.4, where it can be seen that the new operating point $\mathbf{u}_{\mathsf{L}}$ lies in the feasible set $\mathcal{D}$. The feasible set is constructed using radius $\rho = 0.0941$.

Similarly, assuming we don't know the grid operating point, and we have to initialize the fixed-point algorithm with no-load operating condition, i.e., the pair $(\mathbf{w}, \mathbf{0})$, we can generate the unique solution guarantee within the power set-point interval $[0, \max(\mathbf{s}_{\mathsf{L}})]$. For the case of the considered grid, maximum limit of this interval is found to be $\max(\mathbf{s}_{\mathsf{L}}) = 1.3$. That means in this limit, both no-load solution guarantee conditions (3.12), (3.13) are satisfied.

[a]The per unit system is a calculation procedure in which all quantities of grid are converted to one equivalent unit, i.e., per unit (p.u.) In general, quantity x (p.u.) is calculated as: x (actual)/ x (base), where x (actual) is the quantity in actual units and x (base) is a base quantity of same unit but same for all components in the grid. For example, power of 1 MW (actual) on 1 MW (base) amounts to 1 p.u.

With the *load-flow* solution obtained $\hat{\mathbf{u}} := (u_0, (\hat{\mathbf{u}}_{\mathsf{L}})^{\mathsf{T}})^{\mathsf{T}}$ from (3.7), we represent the resulting complex line flows and complex system losses[2]

$$p^{\mathrm{f/t}} + jq^{\mathrm{f/t}} = \mathbf{s}^{\mathrm{f/t}} = \mathrm{diag}(\mathbf{A}^{\mathrm{f/t}}\hat{\mathbf{u}})\overline{\mathbf{Y}}^{\mathrm{f/t}}\overline{\hat{\mathbf{u}}}, \tag{3.14}$$

$$p^{\mathsf{l}} + jq^{\mathsf{l}} = s^{\mathsf{l}} = \hat{\mathbf{u}}^{\mathsf{T}}\overline{\mathbf{Y}\hat{\mathbf{u}}}, \tag{3.15}$$

In the above, we assume that grid has m number of lines with index $\{1, \ldots, \mathsf{m}\}$, making vector $\mathbf{s}^{\mathrm{f/t}} = (s_1^{\mathrm{f/t}}, \ldots, s_{\mathsf{m}}^{\mathrm{f/t}})^{\mathsf{T}} \in \mathbb{C}^{\mathsf{m}}$ to collect complex line flows "from"/"to" buses of the grid. The incidence matrix $\mathbf{A}^{\mathrm{f/t}}$ is an $\mathsf{m} \times \mathsf{n}$ matrix containing 1's at buses connected, zero elsewhere and the modified admittance matrix $\overline{\mathbf{Y}}^{\mathrm{f/t}} \in \mathbb{C}^{\mathsf{m}\times\mathsf{N}}$ appropriately selects contribution of bus voltages in calculating complex line flows "from"/"to" buses. The overall system loss $s^{\mathsf{l}} \in \mathbb{C}$ is a scalar. For derivation of (3.14) and (3.15), see example 3.3.

[2]Line flows and system losses are derived here because they play a key role in calculating energy prices.

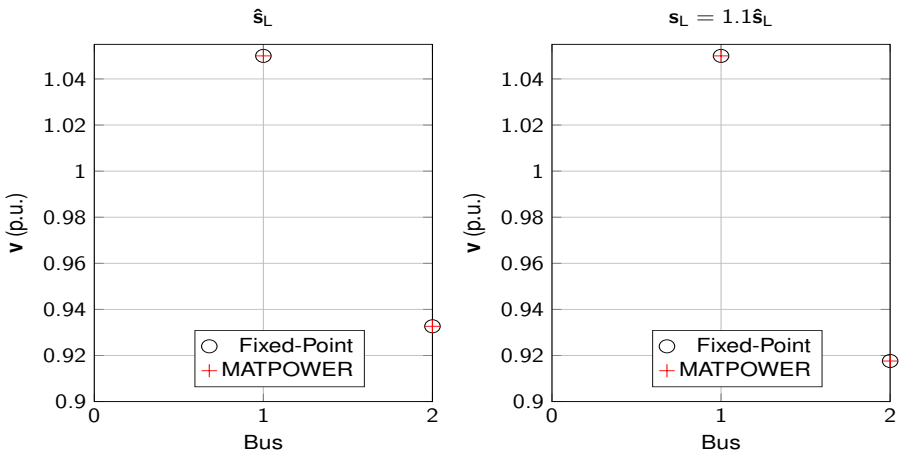

Figure 3.3: Voltage magnitude $\mathbf{v}$ comparison between the *load-flow* solution from fixed-point (3.7) and Newton-Raphson method [84].

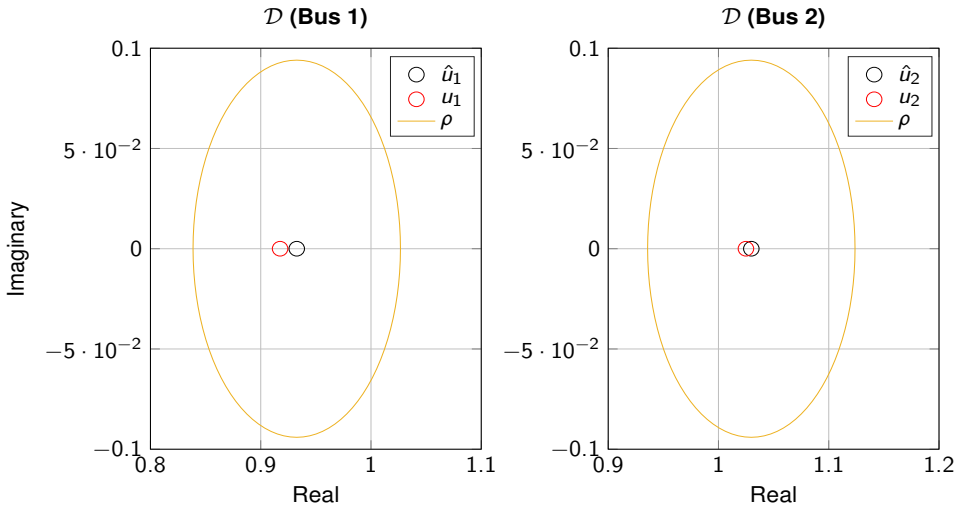

Figure 3.4: The identified domain for solution uniqueness of the new operating point $\mathbf{u}_L$, given the current operaing point $\hat{\mathbf{u}}_L$.

Example 3.3

We derive line flows in a form given by (3.14) for the exemplary system of Fig. 3.2. For line element $k \in (i,j)$, complex line flows direction "from" bus i to j is denoted as s_k^{f}. Hence, keeping the notation consistent, for the grid of Fig. 3.2, we have:

$$s_1^{\mathrm{f}} = u_0\overline{i_{01}}, \qquad s_2^{\mathrm{f}} = u_1\overline{i_{12}}$$

Recalling from example 3.1, line currents are defined as:

$$i_{01} = y_{sh,0}u_0 + y_{01}(u_0 - u_1), \qquad i_{12} = y_{sh,1}u_1 + y_{12}(u_1 - u_2),$$

giving us complex line flows in terms of voltages as:

$$s_1^{\mathrm{f}} = u_0\big(\overline{y_{sh,0}u_0} + \overline{y_{01}}(\overline{u_0} - \overline{u_1})\big), \qquad s_2^{\mathrm{f}} = u_1\big(\overline{y_{sh,1}u_1} + \overline{y_{12}}(\overline{u_1} - \overline{u_2})\big)$$

Now to obtain vector form of complex line flows "from" buses (3.14), we collect the above in appropriate vector forms to give:

$$\mathbf{s}^{\mathrm{f}} = \mathrm{diag}(A^{\mathrm{f}}\mathbf{u})\overline{\mathbf{Y}}^{\mathrm{f}}\overline{\mathbf{u}}, \qquad \text{where,}$$

$$\mathbf{s}^{\mathrm{f}} = \begin{bmatrix} s_1^{\mathrm{f}} \\ s_2^{\mathrm{f}} \end{bmatrix}, \mathbf{u} = \begin{bmatrix} u_0 \\ u_1 \\ u_2 \end{bmatrix}, \mathbf{Y}^{\mathrm{f}} = \begin{bmatrix} y_{sh,0} + y_{01} & -y_{01} & 0 \\ 0 & y_{sh,1} + y_{12} & -y_{12} \end{bmatrix}, \mathbf{A}^{\mathrm{f}} = \begin{bmatrix} 1 & 0 & 0 \\ 0 & 1 & 0 \end{bmatrix}.$$

Similarly, For line element $k \in (i, j)$, by denoting complex line flows from bus j to i as s_k^{t}, we can repeat the above procedure to derive its relationship as given in (3.14). For the grid of Fig. 3.2, the overall system losses can be derived as:

$$\begin{aligned} s^{\mathrm{l}} &= s_1^{\mathrm{f}} + s_1^{\mathrm{t}} + s_2^{\mathrm{f}} + s_2^{\mathrm{t}} \\ s^{\mathrm{l}} &= u_0\overline{i_{01}} + u_1\overline{i_{10}} + u_1\overline{i_{12}} + u_2\overline{i_{21}} \end{aligned}$$

Now we utilize line currents definitions from example 3.1, complex power flows definition from the above and combine them together to separately list the individual line losses:

$$\begin{aligned} s_1^{\mathrm{f}} + s_1^{\mathrm{t}} &= u_0\big(\overline{y_{sh,0}u_0} + \overline{y_{01}}(\overline{u_0} - \overline{u_1})\big) + u_1\big(\overline{y_{sh,0}u_1} + \overline{y_{01}}(\overline{u_1} - \overline{u_0})\big) \\ &= \begin{bmatrix} u_0 \\ u_1 \\ u_2 \end{bmatrix}^{\mathsf{T}} \begin{bmatrix} \overline{y_{sh,0}} + \overline{y_{01}} & -\overline{y_{01}} & 0 \\ -\overline{y_{01}} & \overline{y_{sh,0}} + \overline{y_{01}} & 0 \\ 0 & 0 & 0 \end{bmatrix} \begin{bmatrix} \overline{u_0} \\ \overline{u_1} \\ \overline{u_2} \end{bmatrix} \\ s_2^{\mathrm{f}} + s_2^{\mathrm{t}} &= u_1\big(\overline{y_{sh,1}u_1} + \overline{y_{12}}(\overline{u_1} - \overline{u_2})\big) + u_2\big(\overline{y_{sh,1}u_2} + \overline{y_{12}}(\overline{u_2} - \overline{u_1})\big) \\ &= \begin{bmatrix} u_0 \\ u_1 \\ u_2 \end{bmatrix}^{\mathsf{T}} \begin{bmatrix} 0 & 0 & 0 \\ 0 & \overline{y_{sh,1}} + \overline{y_{12}} & -\overline{y_{12}} \\ 0 & -\overline{y_{12}} & \overline{y_{sh,1}} + \overline{y_{12}} \end{bmatrix} \begin{bmatrix} \overline{u_0} \\ \overline{u_1} \\ \overline{u_2} \end{bmatrix} \\ s^{\mathrm{l}} = s_1^{\mathrm{f}} + s_1^{\mathrm{t}} + s_2^{\mathrm{f}} + s_2^{\mathrm{t}} &= \begin{bmatrix} u_0 \\ u_1 \\ u_2 \end{bmatrix}^{\mathsf{T}} \begin{bmatrix} \overline{y_{sh,0}} + \overline{y_{01}} & -\overline{y_{01}} & 0 \\ -\overline{y_{01}} & \overline{y_{sh,0}} + \overline{y_{01}} + \overline{y_{sh,1}} + \overline{y_{12}} & -\overline{y_{12}} \\ 0 & -\overline{y_{12}} & \overline{y_{sh,1}} + \overline{y_{12}} \end{bmatrix} \begin{bmatrix} \overline{u_0} \\ \overline{u_1} \\ \overline{u_2} \end{bmatrix} \\ s^{\mathrm{l}} &= \mathbf{u}^{\mathsf{T}}\overline{\mathbf{Y}}\overline{\mathbf{u}} \end{aligned}$$

Similar to (3.5), we also now split (3.14) and (3.15) to only present in terms of the desired solution variable $\hat{\mathbf{u}}_{\mathrm{L}}$. To this end, consider incidence matrix $\mathbf{A}^{\mathrm{f/t}}$ and admittance matrix $\overline{\mathbf{Y}}^{\mathrm{f/t}}$ to be arranged as follows:

$$\mathbf{A}^{\mathrm{f/t}} = \left(\mathbf{A}_0^{\mathrm{f/t}}, \mathbf{A}_{\mathrm{L}}^{\mathrm{f/t}}\right), \overline{\mathbf{Y}}^{\mathrm{f/t}} = \left(\overline{\mathbf{Y}}_0^{\mathrm{f/t}}, \overline{\mathbf{Y}}_{\mathrm{L}}^{\mathrm{f/t}}\right). \tag{3.16}$$

Then following the similar structure of (3.3), we get both complex line flows and system losses as a function of desired solution variables:

$$\mathbf{s}^{\mathrm{f/t}} = \mathrm{diag}(\mathbf{A}_0^{\mathrm{f/t}}u_0 + \mathbf{A}_{\mathrm{L}}^{\mathrm{f/t}}\hat{\mathbf{u}}_{\mathrm{L}})(\overline{\mathbf{Y}}_0^{\mathrm{f/t}}\overline{\hat{u}}_0 + \overline{\mathbf{Y}}_{\mathrm{L}}^{\mathrm{f/t}}\overline{\hat{\mathbf{u}}}_{\mathrm{L}}), \tag{3.17a}$$

$$s^{\mathrm{l}} = u_0(\overline{\mathbf{Y}}_{00}\overline{u}_0 + \overline{\mathbf{Y}}_{0\mathrm{L}}\overline{\hat{\mathbf{u}}}_{\mathrm{L}}) + (\hat{\mathbf{u}}_{\mathrm{L}})^{\mathsf{T}}(\overline{\mathbf{Y}}_{\mathrm{L}0}\overline{u}_0 + \overline{\mathbf{Y}}_{\mathrm{LL}}\overline{\hat{\mathbf{u}}}_{\mathrm{L}}). \tag{3.17b}$$

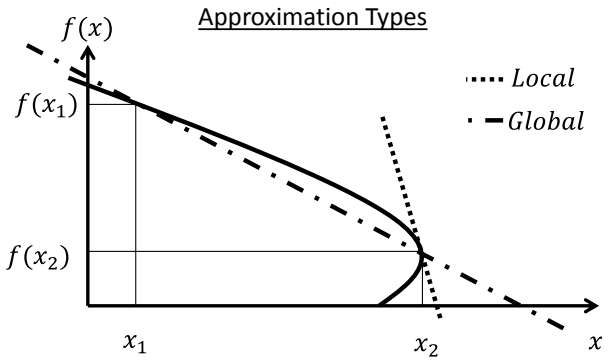

Figure 3.5: Comparison between local and global approximation types. It can be seen that the local approximation is the best approximation at a given point x_2, whereas the global approximation aims to give a more global behavior of the approximation function $f(x)$, which is the interpolation between points $(x_1, f(x_1))$ and $(x_2, f(x_2))$ [7].

3.3 Single-Phase Approximation Modeling

As an alternative to the complex-valued *load-flow* solution, we aim to find the following real-valued approximations:

$$\tilde{\mathbf{v}}_{\mathsf{L}} = \hat{\mathbf{a}} + \mathbf{M}^{\mathbf{v}}\mathbf{s}_{\mathsf{L}}^{\mathsf{inj}}, \tag{3.18a}$$

$$|\tilde{\mathbf{s}}^{\mathsf{f}}|^2 = \hat{\mathbf{b}} + \mathbf{M}^{\mathbf{s}^{\mathsf{f}}}\mathbf{s}_{\mathsf{L}}^{\mathsf{inj}}, \tag{3.18b}$$

$$|\tilde{\mathbf{s}}^{\mathsf{t}}|^2 = \hat{\mathbf{c}} + \mathbf{M}^{\mathbf{s}^{\mathsf{t}}}\mathbf{s}_{\mathsf{L}}^{\mathsf{inj}}, \tag{3.18c}$$

$$\tilde{p}^{\mathsf{l}} = \hat{d} + \mathbf{M}^{p^{\mathsf{l}}}\mathbf{s}_{\mathsf{L}}^{\mathsf{inj}}, \tag{3.18d}$$

$$\tilde{q}^{\mathsf{l}} = \hat{e} + \mathbf{M}^{q^{\mathsf{l}}}\mathbf{s}_{\mathsf{L}}^{\mathsf{inj}}, \tag{3.18e}$$

where $\mathbf{s}_{\mathsf{L}}^{\mathsf{inj}} := ((\mathbf{p}_{\mathsf{L}})^{\mathsf{T}}, (\mathbf{q}_{\mathsf{L}})^{\mathsf{T}})^{\mathsf{T}} \in \mathbb{R}^{2n}$ and $(\hat{\mathbf{a}}, \hat{\mathbf{b}}, \hat{\mathbf{c}}, \hat{d}, \hat{e})$ are appropriate constants. Note that (3.18) has a linear approximation structure, i.e. desired approximates $\tilde{(\cdot)}$ are related to real-valued grid injections $\mathbf{s}_{\mathsf{L}}^{\mathsf{inj}}$ as a function of their corresponding constant matrices $\mathbf{M}^{(\cdot)}$ and a fixed constant vector $\hat{(\cdot)}$.

The approximations in (3.18) are going to be deployed in the subsequent chapters for implementing optimal power flow and consequently electricity prices. To this end, next subsection presents two methods for obtaining these approximations. Qualitative difference between these two methods is provided in Fig 3.5.

3.3.1 Local Approximation

The first order complex-valued approximation of (3.5) w.r.t. complex injection $\mathbf{s}_{\mathsf{L}}$ can be obtained as:

$$\mathbf{U} = \mathrm{diag}(\overline{\mathbf{Y}}_{\mathsf{L0}}\overline{u}_0 + \overline{\mathbf{Y}}_{\mathsf{LL}}\overline{\mathbf{u}}_{\mathsf{L}})\frac{\partial \mathbf{u}_{\mathsf{L}}}{\partial \mathbf{s}_{\mathsf{L}}} + \mathrm{diag}(\mathbf{u}_{\mathsf{L}})\overline{\mathbf{Y}}_{\mathsf{LL}}\frac{\partial \overline{\mathbf{u}}_{\mathsf{L}}}{\partial \mathbf{s}_{\mathsf{L}}} \in \mathbb{C}^{n\times 2n}, \tag{3.19}$$

where $\mathbf{U} := (\mathbf{I}, j\mathbf{I}) \in \mathbb{C}^{n\times 2n}$. The above approximation is in a complex plane $(\mathbf{u}_{\mathsf{L}}, \mathbf{s}_{\mathsf{L}})$. However, from (3.18), we intend real-valued approximations in terms of augmented real-valued

injections $\mathbf{s}_{\mathsf{L}}^{\mathsf{inj}}$. To this end, we define a real-valued version of (3.19),

$$\mathbf{U}_{\mathsf{r}} = \mathbf{J}\,\mathbf{M}, \tag{3.20a}$$

$$\mathbf{M} = \mathbf{J}^{-1}\,\mathbf{U}_{\mathsf{r}}, \tag{3.20b}$$

where $\mathbf{U}_{\mathsf{r}} := \mathbf{I}_{2\mathsf{n}}$ and real-valued sensitivity matrix $\mathbf{M}$ arranged in terms of sensitivity of voltage magnitudes $\mathbf{v}_{\mathsf{L}}$ and angles $\boldsymbol{\theta}_{\mathsf{L}}$ with respect to active power $\mathbf{p}_{\mathsf{L}}$ and reactive power $\mathbf{q}_{\mathsf{L}}$injections,

$$\mathbf{M} := \begin{bmatrix} \frac{\partial \mathbf{v}_{\mathsf{L}}}{\partial \mathbf{p}_{\mathsf{L}}} & \frac{\partial \mathbf{v}_{\mathsf{L}}}{\partial \mathbf{q}_{\mathsf{L}}} \\ \frac{\partial \boldsymbol{\theta}_{\mathsf{L}}}{\partial \mathbf{p}_{\mathsf{L}}} & \frac{\partial \boldsymbol{\theta}_{\mathsf{L}}}{\partial \mathbf{q}_{\mathsf{L}}} \end{bmatrix} := \begin{bmatrix} \mathbf{M}^{\mathbf{v}} \\ \mathbf{M}^{\boldsymbol{\theta}} \end{bmatrix}. \tag{3.21}$$

The Jacobian $\mathbf{J}$ then follows,

$$\mathbf{J} := \Big(\langle \mathrm{diag}(\overline{\mathbf{Y}}_{\mathsf{L0}}\overline{u}_0 + \overline{\mathbf{Y}}_{\mathsf{LL}}\overline{\mathbf{u}}_{\mathsf{L}}) \rangle + \langle \mathrm{diag}(\mathbf{u}_{\mathsf{L}}) \rangle \mathbf{N} \langle \mathbf{Y}_{\mathsf{LL}} \rangle \Big) \mathbf{R}(\mathbf{u}_{\mathsf{L}}) \in \mathbb{R}^{2\mathsf{n}\times 2\mathsf{n}}, \tag{3.22}$$

where the above compact representation utilizes the following shorthands [9],

$$\mathbf{N} := \begin{bmatrix} \mathbf{I}_{\mathsf{n}} & \mathbf{O}_{\mathsf{n}\times\mathsf{n}} \\ \mathbf{O}_{\mathsf{n}\times\mathsf{n}} & -\mathbf{I}_{\mathsf{n}} \end{bmatrix},\ \langle \mathbf{A} \rangle := \begin{bmatrix} \Re(\mathbf{A}) & -\Im(\mathbf{A}) \\ \Im(\mathbf{A}) & \Re(\mathbf{A}) \end{bmatrix} \in \mathbb{R}^{2\mathsf{n}\times 2\mathsf{n}}, \tag{3.23a}$$

$$\mathbf{R}(\mathbf{u}_{\mathsf{L}}) := \begin{bmatrix} \mathrm{diag}(\cos \boldsymbol{\theta}_{\mathsf{L}}) & -\mathrm{diag}(\mathbf{v}_{\mathsf{L}})\,\mathrm{diag}(\sin \boldsymbol{\theta}_{\mathsf{L}}) \\ \mathrm{diag}(\sin \boldsymbol{\theta}_{\mathsf{L}}) & \mathrm{diag}(\mathbf{v}_{\mathsf{L}})\,\mathrm{diag}(\cos \boldsymbol{\theta}_{\mathsf{L}}) \end{bmatrix} \in \mathbb{R}^{2\mathsf{n}\times 2\mathsf{n}}. \tag{3.23b}$$

Matrix $\mathbf{I}_{\mathsf{n}} \in \mathbb{R}^{\mathsf{n}\times\mathsf{n}}$ is an identity matrix, i.e. with 1's at all diagonal. A small example to explain the shorthands of (3.23) follows.

Example 3.4

We utilize the notations of [9] to obtain compact representation of our Jacobian $\mathbf{J}$ in (3.22). We demonstrate the working of shorthands in (3.23) for small scalar cases.

First, equation (3.19) can be imagined as directly obtained from the product rule, where in a scalar form we have:

$$z = f(x,y)g(x,y), \qquad \frac{\partial z}{\partial x} = \frac{\partial f(x,y)}{\partial x} g(x,y) + \frac{\partial g(x,y)}{\partial x} f(x,y).$$

Now regarding the operator $\langle \cdot \rangle$, it is used to keep the real-valued nature of the formulation. To this end, consider function $f(x) = ax : \mathbb{R} \to \mathbb{R}$ for a complex constant $a \in C$ and a complex variable $x \in C$

$$\begin{aligned} f(x) &= (\Re(a) + j\Im(a))(\Re(x) + j\Im(x)), \\ &= \Re(a)\Re(x) - \Im(a)\Im(x) + j\Im(a)\Re(x) + j\Re(a)\Im(x) = \begin{bmatrix} \Re(a) & -\Im(a) \\ \Im(a) & \Re(a) \end{bmatrix} \begin{bmatrix} \Re(x) \\ \Im(x) \end{bmatrix}, \\ \frac{\partial f(x)}{\partial \begin{bmatrix} \Re(x) \\ \Im(x) \end{bmatrix}} &= \begin{bmatrix} \Re(a) & -\Im(a) \\ \Im(a) & \Re(a) \end{bmatrix} = \langle a \rangle \end{aligned}$$

The matrix $\mathbf{N}$ (let's denote it as N here for the scalar case) is used to represent complex

conjugate operation. This can be shown now for function $f(x) = a\overline{x}$

$$\begin{aligned} f(x) &= (\Re(a) + j\Im(a))(\Re(x) - j\Im(x)), \\ &= \Re(a)\Re(x) + \Im(a)\Im(x) + j\Im(a)\Re(x) - j\Re(a)\Im(x) = \begin{bmatrix} \Re(a) & \Im(a) \\ \Im(a) & -\Re(a) \end{bmatrix} \begin{bmatrix} \Re(x) \\ \Im(x) \end{bmatrix}, \\ \frac{\partial f(x)}{\partial \begin{bmatrix} \Re(x) \\ \Im(x) \end{bmatrix}} &= \begin{bmatrix} \Re(a) & -\Im(a) \\ \Im(a) & \Re(a) \end{bmatrix} \begin{bmatrix} 1 & 0 \\ 0 & -1 \end{bmatrix} = \langle a \rangle N \end{aligned}$$

Finally, the operator $\mathbf{R}(\mathbf{u}_\mathsf{L})$ (let's denote it as $R(u)$ here for the scalar case) is obtained by utilizing Euler's identity for the complex voltage

$$u = ve^{j\theta} = v\cos\theta + jv\sin\theta,$$

and then combining it with the above shown real-valued partial derivatives,

$$\begin{aligned} \begin{bmatrix} \Re(u) \\ \Im(u) \end{bmatrix} &= \begin{bmatrix} v\cos\theta \\ v\sin\theta \end{bmatrix} \\ \frac{\partial \begin{bmatrix} \Re(u) \\ \Im(u) \end{bmatrix}}{\partial \begin{bmatrix} v \\ \theta \end{bmatrix}} &= \begin{bmatrix} \cos\theta & -v\sin\theta \\ \sin\theta & v\cos\theta \end{bmatrix} = R(u) \end{aligned}$$

The Jacobian matrix $\mathbf{J}$ in (3.22) is shown to be invertible [101, 10], allowing us to solve the system of equations (3.20) for a given grid conditions $(\hat{\mathbf{s}}_\mathsf{L}^{\mathsf{inj}}, \hat{\mathbf{v}}_\mathsf{L}, \hat{\boldsymbol{\theta}}_\mathsf{L})$. The individual approximation quantities in (3.18) are obtained as given below:

Linear Voltage Magnitude (3.18a)**:** The sensitivity matrix $\mathbf{M}^{\mathbf{v}}$ is simply obtained as shown in (3.21). The vector $\hat{\mathbf{a}} := \hat{\mathbf{v}}_\mathsf{L} - \mathbf{M}^{\mathbf{v}}\hat{\mathbf{s}}^{\mathsf{inj}}$ which completes the approximation of (3.18a).

Linear Squared Line Flow (3.18b)**,** (3.18c)**:** First, consider squared line flows "from" buses expressed as:

$$|\mathbf{s}^{\mathsf{f}}|^2 := \mathrm{diag}(\overline{\mathbf{s}}^{\mathsf{f}})\mathbf{s}^{\mathsf{f}}.$$

To obtain (3.18b), we then proceed as:

$$\begin{aligned} \frac{\partial |\mathbf{s}^{\mathsf{f}}|^2}{\partial \mathbf{s}_\mathsf{L}^{\mathsf{inj}}} &= \mathrm{diag}(\overline{\mathbf{s}}^{\mathsf{f}})\frac{\partial \mathbf{s}^{\mathsf{f}}}{\partial \mathbf{s}_\mathsf{L}^{\mathsf{inj}}} + \mathrm{diag}(\mathbf{s}^{\mathsf{f}})\frac{\partial \overline{\mathbf{s}}^{\mathsf{f}}}{\partial \mathbf{s}_\mathsf{L}^{\mathsf{inj}}} \\ &= \mathrm{diag}\left(\Re(\mathbf{s}^{\mathsf{f}}) - j\Im(\mathbf{s}^{\mathsf{f}})\right)\left(\Re(\frac{\partial \mathbf{s}^{\mathsf{f}}}{\partial \mathbf{s}_\mathsf{L}^{\mathsf{inj}}}) + j\Im(\frac{\partial \mathbf{s}^{\mathsf{f}}}{\partial \mathbf{s}_\mathsf{L}^{\mathsf{inj}}})\right) + \mathrm{diag}\left(\Re(\mathbf{s}^{\mathsf{f}}) + j\Im(\mathbf{s}^{\mathsf{f}})\right)\left(\Re(\frac{\partial \mathbf{s}^{\mathsf{f}}}{\partial \mathbf{s}_\mathsf{L}^{\mathsf{inj}}}) - j\Im(\frac{\partial \mathbf{s}^{\mathsf{f}}}{\partial \mathbf{s}_\mathsf{L}^{\mathsf{inj}}})\right) \end{aligned}$$

where cross products cancels out to give the expression

$$\mathbf{M}^{\mathbf{s}^{\mathsf{f}}} := \frac{\partial |\mathbf{s}^{\mathsf{f}}|^2}{\partial \mathbf{s}_\mathsf{L}^{\mathsf{inj}}} := 2\Big(\mathrm{diag}\left(\Re(\mathbf{s}^{\mathsf{f}})\right)\Re(\frac{\partial \mathbf{s}^{\mathsf{f}}}{\partial \mathbf{s}_\mathsf{L}^{\mathsf{inj}}}) + \mathrm{diag}\left(\Im(\mathbf{s}^{\mathsf{f}})\right)\Im(\frac{\partial \mathbf{s}^{\mathsf{f}}}{\partial \mathbf{s}_\mathsf{L}^{\mathsf{inj}}})\Big) \tag{3.25a}$$

$$:= 2\Big(\mathrm{diag}\left(\Re(\mathbf{s}^{\mathsf{f}})\right), \mathrm{diag}\left(\Im(\mathbf{s}^{\mathsf{f}})\right)\Big) \begin{bmatrix} \Re(\frac{\partial \mathbf{s}^{\mathsf{f}}}{\partial \mathbf{s}_\mathsf{L}^{\mathsf{inj}}}) \\ \Im(\frac{\partial \mathbf{s}^{\mathsf{f}}}{\partial \mathbf{s}_\mathsf{L}^{\mathsf{inj}}}) \end{bmatrix}. \tag{3.25b}$$

Now, the required sensitivities from above are obtained as:

$$\begin{bmatrix} \Re(\frac{\partial \mathbf{s}_{\mathsf{f}}^{\mathsf{f}}}{\partial \mathbf{s}_{\mathsf{L}}^{\mathsf{inj}}}) \\ \Im(\frac{\partial \mathbf{s}_{\mathsf{f}}^{\mathsf{f}}}{\partial \mathbf{s}_{\mathsf{L}}^{\mathsf{inj}}}) \end{bmatrix} = \begin{bmatrix} \Re(\frac{\partial \mathbf{s}_{\mathsf{f}}^{\mathsf{f}}}{\partial \mathbf{u}_{\mathsf{L}}})\Re(\frac{\partial \mathbf{u}_{\mathsf{L}}}{\partial s^{\mathsf{inj}}}) \\ \Im(\frac{\partial \mathbf{s}_{\mathsf{f}}^{\mathsf{f}}}{\partial \mathbf{u}_{\mathsf{L}}})\Im(\frac{\partial \mathbf{u}_{\mathsf{L}}}{\partial s^{\mathsf{inj}}}) \end{bmatrix} = \begin{bmatrix} \Re(\frac{\partial \mathbf{s}_{\mathsf{f}}^{\mathsf{f}}}{\partial \mathbf{u}_{\mathsf{f}}}) \\ \Im(\frac{\partial \mathbf{s}_{\mathsf{f}}^{\mathsf{f}}}{\partial \mathbf{u}_{\mathsf{L}}}) \end{bmatrix} \mathbf{M} \tag{3.26}$$

where line flow sensitivity with respect to voltage can be obtained from the relationship of complex flows to voltages in (3.17a) and shorthands in (3.23):

$$\begin{bmatrix} \Re(\frac{\partial \mathbf{s}_{\mathsf{f}}^{\mathsf{f}}}{\partial \mathbf{u}_{\mathsf{f}}}) \\ \Im(\frac{\partial \mathbf{s}_{\mathsf{f}}^{\mathsf{f}}}{\partial \mathbf{u}_{\mathsf{L}}}) \end{bmatrix} = \Big(\langle \mathrm{diag}(\overline{\mathbf{Y}}_0^{\mathsf{f}}\overline{u}_0 + \overline{\mathbf{Y}}_{\mathsf{L}}^{\mathsf{f}}\overline{\mathbf{u}_{\mathsf{L}}})\mathbf{A}_{\mathsf{L}}^{\mathsf{f}}\rangle + \langle \mathrm{diag}(\mathbf{A}_0^{\mathsf{f}}u_0 + \mathbf{A}_{\mathsf{L}}^{\mathsf{f}}\mathbf{u}_{\mathsf{L}})\rangle \mathbf{N} \langle \mathbf{Y}_{\mathsf{L}}^{\mathsf{f}}\rangle \Big)\mathbf{R}(\mathbf{u}_{\mathsf{L}}) \in \mathbb{R}^{\mathsf{m}\times 2\mathsf{n}}. \tag{3.27}$$

Now by setting, $\hat{\mathbf{b}} := |\hat{\mathbf{s}}^{\mathsf{f}}|^2 - \mathbf{M}^{\mathbf{s}^{\mathsf{f}}}\hat{\mathbf{s}}^{\mathsf{inj}}$ we recover (3.18b), where $|\hat{\mathbf{s}}^{\mathsf{f}}|^2$ is the absolute flow squared obtained from the *load-flow* problem, i.e. for $\hat{\mathbf{u}}_{\mathsf{L}}$ satisfying (3.5). By inspection, we can see that the complex line flow sensitivities of (3.27) deploy the same structure as voltage sensitivity matrix $\mathbf{M}$, in order to be appropriately utilized in (3.26). An exactly similar procedure exists for obtaining complex line flow approximations for "to" buses (3.18c).

Linearized system losses (3.18d)**,** (3.18e) Similar to the above mentioned procedure, we proceed to obtain (3.18d), (3.18e) by first considering the following chain rule:

$$\begin{bmatrix} \mathbf{M}^{p^{\mathsf{l}}} \\ \mathbf{M}^{q^{\mathsf{l}}} \end{bmatrix} := \begin{bmatrix} \Re(\frac{\partial \mathbf{s}_{\mathsf{l}}^{\mathsf{l}}}{\partial \mathbf{s}_{\mathsf{L}}^{\mathsf{inj}}}) \\ \Im(\frac{\partial \mathbf{s}_{\mathsf{l}}^{\mathsf{l}}}{\partial \mathbf{s}_{\mathsf{L}}^{\mathsf{inj}}}) \end{bmatrix} = \begin{bmatrix} \Re(\frac{\partial \mathbf{s}_{\mathsf{l}}^{\mathsf{l}}}{\partial \mathbf{u}_{\mathsf{l}}})\Re(\frac{\partial \mathbf{u}_{\mathsf{L}}}{\partial s^{\mathsf{inj}}}) \\ \Im(\frac{\partial \mathbf{s}_{\mathsf{l}}^{\mathsf{l}}}{\partial \mathbf{u}_{\mathsf{L}}})\Im(\frac{\partial \mathbf{u}_{\mathsf{L}}}{\partial s^{\mathsf{inj}}}) \end{bmatrix} = \begin{bmatrix} \Re(\frac{\partial \mathbf{s}_{\mathsf{l}}^{\mathsf{l}}}{\partial \mathbf{u}_{\mathsf{l}}}) \\ \Im(\frac{\partial \mathbf{s}_{\mathsf{l}}^{\mathsf{l}}}{\partial \mathbf{u}_{\mathsf{L}}}) \end{bmatrix} \mathbf{M} \tag{3.28}$$

and,

$$\begin{bmatrix} \Re(\frac{\partial \mathbf{s}_{\mathsf{l}}^{\mathsf{l}}}{\partial \mathbf{u}_{\mathsf{l}}}) \\ \Im(\frac{\partial \mathbf{s}_{\mathsf{l}}^{\mathsf{l}}}{\partial \mathbf{u}_{\mathsf{L}}}) \end{bmatrix} = \Big(\langle u_0\rangle \mathbf{N}\langle \mathbf{Y}_{0\mathsf{L}}\rangle + \langle (\overline{\mathbf{Y}}_{\mathsf{L}0}\overline{u}_0 + \overline{\mathbf{Y}}_{\mathsf{LL}}\overline{\mathbf{u}}_{\mathsf{L}})^{\mathsf{T}} + \langle \hat{\mathbf{u}}_{\mathsf{L}}{}^{\mathsf{T}}\rangle \mathbf{N}\langle \mathbf{Y}_{\mathsf{LL}}\rangle \Big)\mathbf{R}(\mathbf{u}_{\mathsf{L}}) \in \mathbb{R}^{2\times 2\mathsf{n}}. \tag{3.29}$$

Now [(3.18d), (3.18e)] is obtained by setting

$$\begin{bmatrix} \hat{d} \\ \hat{e} \end{bmatrix} := \begin{bmatrix} \hat{p}^{\mathsf{l}} \\ \hat{q}^{\mathsf{l}} \end{bmatrix} - \begin{bmatrix} \mathbf{M}^{p^{\mathsf{l}}} \\ \mathbf{M}^{q^{\mathsf{l}}} \end{bmatrix} \hat{\mathbf{s}}^{\mathsf{inj}},$$

where $(\hat{p}^{\mathsf{l}}, \hat{q}^{\mathsf{l}})$ represent system active and reactive power losses, which satisfy the *load-flow* problem, i.e. for $\hat{\mathbf{u}}_{\mathsf{L}}$ satisfying (3.5).

3.3.2 Global Approximation

For the same set of approximates (3.18), we proceed now with their global approximation. As explained earlier that one of the advantages of the fixed-point structure of the *load-flow* problem is its utilization in obtaining global approximation of grid quantities. In particular, we present global approximation as an interpolation between two *load-flow* points, i.e., at the solution pair $(\hat{\mathbf{u}}_{\mathsf{L}}, \hat{\mathbf{s}}_{\mathsf{L}})$ and at no-load condition $(\mathbf{w}, \mathbf{0})$.

Consider the first iteration from the satisfied fixed point *load-flow* equation (3.6), then the complex-valued voltage sensitivity with respect to real-valued injections is simply obtained as:

$$\mathbf{M}^{\mathbb{C}} :=:= \frac{\partial \mathbf{u}_{\mathsf{L}}}{\partial \mathbf{s}_{\mathsf{L}}^{\mathsf{inj}}} := \Big(\frac{\partial \mathbf{u}_{\mathsf{L}}}{\partial \mathbf{p}_{\mathsf{L}}}, j\frac{\partial \mathbf{u}_{\mathsf{L}}}{\partial \mathbf{q}_{\mathsf{L}}}\Big) = \Big(\mathbf{Y}_{\mathsf{LL}}{}^{-1}\mathrm{diag}(\overline{\mathbf{u}}_{\mathsf{L}})^{-1}, -j\mathbf{Y}_{\mathsf{LL}}{}^{-1}\mathrm{diag}(\overline{\mathbf{u}}_{\mathsf{L}})^{-1}\Big) \in \mathbb{C}^{\mathsf{n}\times 2\mathsf{n}}. \tag{3.30}$$

Linear Voltage Magnitude (3.18a)**:** By utilizing the following partial derivative rule [8],

$$\frac{\partial |f(x)|}{\partial x} = \frac{1}{|f(x)|}\Re\Big(\overline{f(x)}\frac{\partial f(x)}{\partial x}\Big) \tag{3.31}$$

we obtain (3.18a) by defining:

$$\mathbf{M}^{\mathbf{v}} := \operatorname{diag}(\mathbf{v}_{\mathsf{L}})^{-1}\Re\Big(\operatorname{diag}(\overline{\mathbf{u}}_{\mathsf{L}})\mathbf{M}^{\mathbb{C}}\Big), \tag{3.32a}$$

$$\hat{\mathbf{a}} := \mathbf{v}_{\mathsf{L}} - \mathbf{M}^{\mathbf{v}}\hat{\mathbf{s}}_{\mathsf{L}}^{\mathsf{inj}}. \tag{3.32b}$$

Linear Squared Line Flow [(3.18b)**,** (3.18c)**]:** First, consider line flows "from" buses along with the following relationship already presented in (3.25),

$$\mathbf{M}^{\mathbf{s}^{\mathsf{f}}} := \frac{\partial |\mathbf{s}^{\mathsf{f}}|^2}{\partial \mathbf{s}_{\mathsf{L}}^{\mathsf{inj}}} := 2\Big(\operatorname{diag}\left(\Re(\mathbf{s}^{\mathsf{f}})\right), \operatorname{diag}\left(\Im(\mathbf{s}^{\mathsf{f}})\right)\Big)\begin{bmatrix}\Re(\frac{\partial \mathbf{s}^{\mathsf{f}}}{\partial \mathbf{s}_{\mathsf{L}}^{\mathsf{inj}}})\\ \Im(\frac{\partial \mathbf{s}^{\mathsf{f}}}{\partial \mathbf{s}_{\mathsf{L}}^{\mathsf{inj}}})\end{bmatrix}. \tag{3.33}$$

Now, we follow the chain rule of (3.26) to obtain the above required sensitivities. To this end, from (3.17a), we have the complex-valued sensitivity of line flows "from" with respect to voltages,

$$\frac{\partial \mathbf{s}^{\mathsf{f}}}{\partial \mathbf{u}_{\mathsf{L}}} := \operatorname{diag}(\overline{\mathbf{Y}}_0^{\mathsf{f}}\overline{u}_0 + \overline{\mathbf{Y}}_{\mathsf{L}}^{\mathsf{f}}\overline{\mathbf{u}_{\mathsf{L}}})\mathbf{A}_{\mathsf{L}}^{\mathsf{f}} + \operatorname{diag}(\mathbf{A}_0^{\mathsf{f}}\overline{u}_0 + \mathbf{A}_{\mathsf{L}}^{\mathsf{f}}\overline{\mathbf{u}}_{\mathsf{L}})\overline{\mathbf{Y}}_{\mathsf{L}}^{\mathsf{f}} \in \mathbb{C}^{\mathsf{m}\times\mathsf{n}}. \tag{3.34}$$

Now utilizing (3.30) and (3.26), we obtain:

$$\begin{bmatrix}\Re(\frac{\partial \mathbf{s}^{\mathsf{f}}}{\partial \mathbf{s}_{\mathsf{L}}^{\mathsf{inj}}})\\ \Im(\frac{\partial \mathbf{s}^{\mathsf{f}}}{\partial \mathbf{s}_{\mathsf{L}}^{\mathsf{inj}}})\end{bmatrix} := \begin{bmatrix}\Re\Big(\frac{\partial \mathbf{s}^{\mathsf{f}}}{\partial \mathbf{u}_{\mathsf{L}}}\cdot\mathbf{M}^{\mathbb{C}}\Big)\\ \Im\Big(\frac{\partial \mathbf{s}^{\mathsf{f}}}{\partial \mathbf{u}_{\mathsf{L}}}\cdot\mathbf{M}^{\mathbb{C}}\Big)\end{bmatrix} \in \mathbb{R}^{2\mathsf{m}\times 2\mathsf{n}}. \tag{3.35}$$

At no load, we have the sensitivity equation (3.34) turned as:

$$\frac{\partial \mathbf{s}^{\mathsf{f}}}{\partial \mathbf{w}} := \operatorname{diag}(\overline{\mathbf{Y}}_0^{\mathsf{f}}\overline{u}_0 + \overline{\mathbf{Y}}_{\mathsf{L}}^{\mathsf{f}}\overline{\mathbf{w}})\mathbf{A}_{\mathsf{L}}^{\mathsf{f}} + \operatorname{diag}(\mathbf{A}_0^{\mathsf{f}}\overline{u}_0 + \mathbf{A}_{\mathsf{L}}^{\mathsf{f}}\overline{\mathbf{w}})\overline{\mathbf{Y}}_{\mathsf{L}}^{\mathsf{f}} \in \mathbb{C}^{\mathsf{m}\times\mathsf{n}}, \tag{3.36}$$

with the required coefficient no load obtained as:

$$\hat{\mathbf{b}} := \begin{bmatrix}\Re\Big(\frac{\partial \mathbf{s}^{\mathsf{f}}}{\partial \mathbf{w}}\cdot\mathbf{w}\Big)\\ \Im\Big(\frac{\partial \mathbf{s}^{\mathsf{f}}}{\partial \mathbf{w}}\cdot\mathbf{w}\Big)\end{bmatrix} \in \mathbb{R}^{2\mathsf{m}}. \tag{3.37}$$

Exactly similar procedure exists for (3.18c) and is left here in the interest of space.

Linearized system losses (3.18d)**,** (3.18e)**:** First, consider the complex-valued system loss sensitivity of (3.17b) with respect to voltages as:

$$\frac{\partial \mathbf{s}^{\mathsf{l}}}{\partial \mathbf{u}_{\mathsf{L}}} := u_0\overline{\mathbf{Y}}_{0\mathsf{L}} + (\mathbf{Y}_{\mathsf{L}0}u_0 + \mathbf{Y}_{\mathsf{LL}}\mathbf{u}_{\mathsf{L}})^{\mathsf{T}} + \mathbf{u}_{\mathsf{L}}{}^{\mathsf{T}}\overline{\mathbf{Y}}_{\mathsf{LL}} \in \mathbb{C}^{1\times\mathsf{n}}. \tag{3.38}$$

Now follow the chain rule (3.28) and sensitivity (3.30), we get

$$\begin{bmatrix}\mathbf{M}^{p^{\mathsf{l}}}\\ \mathbf{M}^{q^{\mathsf{l}}}\end{bmatrix} := \begin{bmatrix}\Re(\frac{\partial \mathbf{s}^{\mathsf{l}}}{\partial \mathbf{s}_{\mathsf{L}}^{\mathsf{inj}}})\\ \Im(\frac{\partial \mathbf{s}^{\mathsf{l}}}{\partial \mathbf{s}_{\mathsf{L}}^{\mathsf{inj}}})\end{bmatrix} := \begin{bmatrix}\Re\Big(\frac{\partial \mathbf{s}^{\mathsf{l}}}{\partial \mathbf{u}_{\mathsf{L}}}\cdot\mathbf{M}^{\mathbb{C}}\Big)\\ \Im\Big(\frac{\partial \mathbf{s}^{\mathsf{l}}}{\partial \mathbf{u}_{\mathsf{L}}}\cdot\mathbf{M}^{\mathbb{C}}\Big)\end{bmatrix} \in \mathbb{R}^{2\times 2\mathsf{n}}. \tag{3.39}$$

In order to complete the loss approximation [(3.18d), (3.18e)], the required no-load condition (3.38) can now be written as:

$$\frac{\partial \mathbf{s}^{\mathsf{l}}}{\partial \mathbf{w}} := u_0 \overline{\mathbf{Y}}_{0\mathsf{L}} + (\mathbf{Y}_{\mathsf{L}0} u_0 + \mathbf{Y}_{\mathsf{LL}} \mathbf{w})^{\mathsf{T}} + \mathbf{w}^{\mathsf{T}} \overline{\mathbf{Y}}_{\mathsf{LL}} \in \mathbb{C}^{1\times \mathsf{n}}. \tag{3.40}$$

with the required no load coefficients now obtained as:

$$\begin{bmatrix} \hat{d} \\ \hat{e} \end{bmatrix} := \begin{bmatrix} \Re\left(\frac{\partial \mathbf{s}^{\mathsf{l}}}{\partial \mathbf{w}} \cdot \mathbf{w}\right) \\ \Im\left(\frac{\partial \mathbf{s}^{\mathsf{l}}}{\partial \mathbf{w}} \cdot \mathbf{w}\right) \end{bmatrix} \in \mathbb{R}. \tag{3.41}$$

.

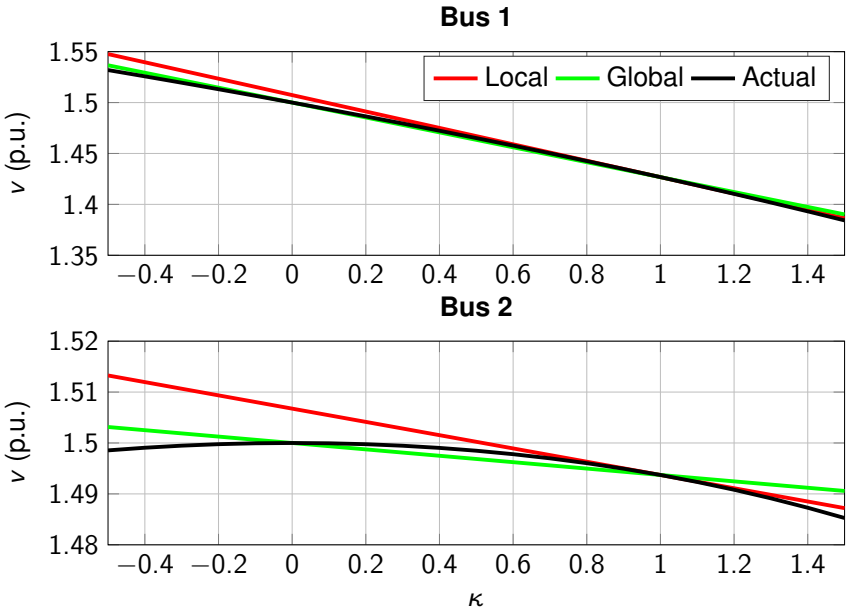

Figure 3.6: Voltage magnitude approximation for the exemplary grid.

Example 3.5

For the exemplary grid in Fig. 3.2 with data from example 3.3, we present verification for both local and global approximation methods. To this end, we do continuation analysis which varies grid loading as $\mathbf{s}_{\mathsf{L}} = \kappa \hat{\mathbf{s}}_{\mathsf{L}}$, where $\kappa \in [-0.5, 1.5]$ and $\hat{\mathbf{s}}_{\mathsf{L}}$ is the rated loading (see example 3.3) where a solution $\hat{\mathbf{u}}_{\mathsf{L}}$ exists. The voltage at the root-node is imposed at 1.5 p.u. For each step of the loading, the actual grid solution is obtained using the fixed-point *load-flow* equation (3.7). For both local and global approximation methods, Fig. 3.6, 3.7 and 3.8 respectively present approximation of voltage magnitude, absolute line square flow "from" buses and system active and reactive power loss. We omit "to" buses line flows in this example as the procedure for obtaining them, the obtained results and their characteristics are very similar to "from" bus line flows. Note that as no charging currents (zero capacitance in the pi-model) exists, the no-load conditions shows flat voltage(equal to 1 p.u.) and zero losses and line flows.

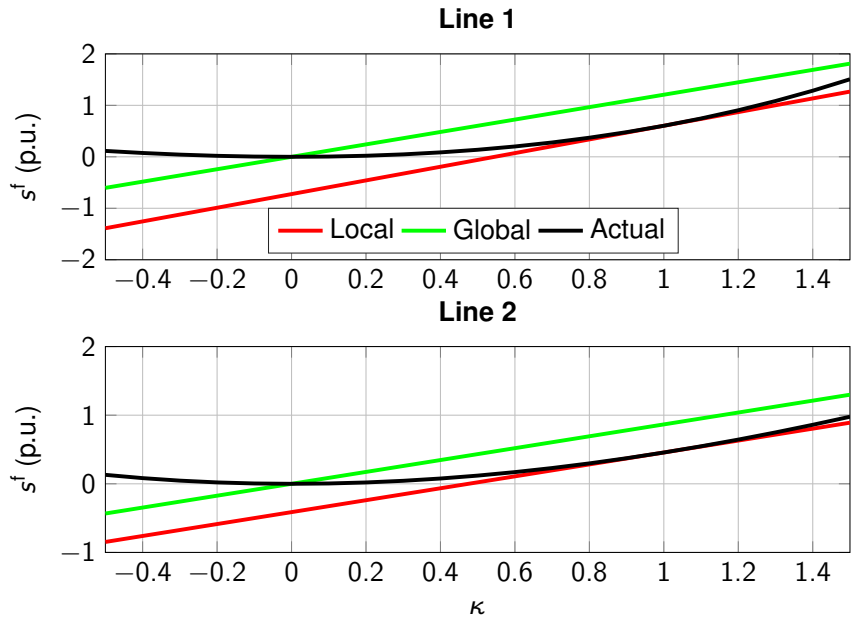

Figure 3.7: Absolute squared line flow "from" buses approximation for the exemplary grid.

For local approximation, the individual sensitivity matrices in (3.18) are found to be:

$$\begin{aligned}
\mathbf{M}^{\mathbf{v}} &= \begin{bmatrix} 0.0742 & 0.0678 & 0.0742 & 0.0678 \\ 0.0710 & 0.1290 & 0.0710 & 0.1290 \end{bmatrix}, \\
\mathbf{M}^{\mathbf{s}^{\mathrm{f}}} &= \begin{bmatrix} -1.2225 & -1.1176 & -1.2225 & -1.1176 \\ 0.0041 & 0.8770 & 0.0041 & 0.8770 \end{bmatrix}, \\
\mathbf{M}^{p^{\mathrm{l}}} &= \begin{pmatrix} -0.0565, & -0.0087, & -0.0565, & -0.0087 \end{pmatrix}, \\
\mathbf{M}^{q^{\mathrm{l}}} &= \begin{pmatrix} -0.0565, & -0.0087, & -0.0565, & -0.0087 \end{pmatrix}
\end{aligned}$$

and constants representing local grid conditions as:

$$\hat{\mathbf{a}} = \begin{bmatrix} 1.4268 \\ 1.4937 \end{bmatrix}, \quad \hat{\mathbf{b}} = \begin{bmatrix} 0.6033 \\ 0.4562 \end{bmatrix}, \quad \hat{d} = 0.0492, \hat{e} = 0.0492.$$

For global approximations, the individual sensitivity matrices are found to be as:

$$\begin{aligned}
\mathbf{M}^{\mathbf{v}} &= \begin{bmatrix} 0.0701 & 0.0669 & 0.0701 & 0.0669 \\ 0.0701 & 0.1339 & 0.0701 & 0.1339 \end{bmatrix}, \\
\mathbf{M}^{\mathbf{s}^{\mathrm{f}}} &= \begin{bmatrix} -1.1548 & -1.1031 & -1.1548 & -1.1031 \\ 0.0448 & 0.9552 & 0.0448 & 0.9552 \end{bmatrix}, \\
\mathbf{M}^{p^{\mathrm{l}}} &= \begin{pmatrix} 0, & 0, & -0.1027, & -0.0084 \end{pmatrix}, \\
\mathbf{M}^{q^{\mathrm{l}}} &= \begin{pmatrix} -0.1027, & -0.0084, & 0, & 0 \end{pmatrix},
\end{aligned}$$

and constant representing no-load grid condition as: $(\hat{\mathbf{a}}, \hat{\mathbf{b}}, \hat{d}, \hat{e}) = ((1.5, 1.5)^{\mathsf{T}}, (0, 0)^{\mathsf{T}}, 0, 0)$

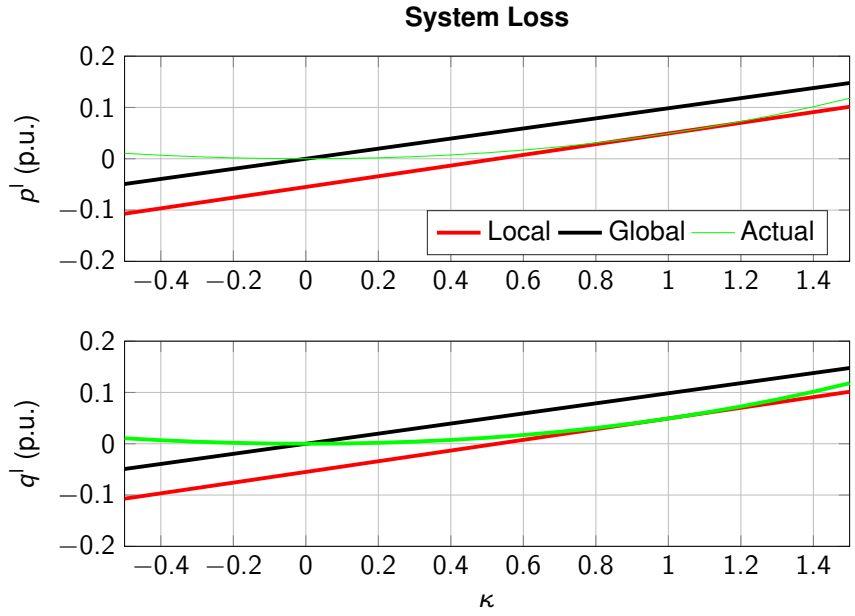

Figure 3.8: System active power loss (top) and reactive power loss (bottom) approximation for the exemplary grid.

From Fig. 3.7 and 3.8, we notice that for global approximation method, at the rated solution pair $(\hat{\mathbf{u}}_{\mathsf{L}}, \hat{\mathbf{s}}_{\mathsf{L}})$, the approximated quantities are actually double the rated value. For example, approximate active power loss $\tilde{p}^{\mathsf{l}}$ at rated loading $\hat{\mathbf{s}}_{\mathsf{L}}$ is twice the actual active power loss $\hat{p}^{\mathsf{l}}$, i.e., $\tilde{p}^{\mathsf{l}} = 2\hat{p}^{\mathsf{l}}$. Next, we show this property for global approximation method for the case of complex system losses s^{l} and absolute line squared flow "from" buses $|\tilde{\mathbf{s}}^{\mathsf{f}}|^2$. For brevity, we take the solution pair of the whole grid, i.e. $(\mathbf{u}, \mathbf{s}) := ((u_0, \mathbf{u}_{\mathsf{L}}), (s_0, \mathbf{s}_{\mathsf{L}}))$, instead of only PQ buses.

Double System Loss Approximation: Consider the overall total system loss approximation from (3.15) and its derivative with respect to injections:

$$s^{\mathsf{l}} = \mathbf{u}^{\mathsf{T}}\overline{\mathbf{Y}}\overline{\mathbf{u}}$$
$$\frac{\partial s^{\mathsf{l}}}{\partial \mathbf{s}} = (\overline{\mathbf{Y}}\overline{\mathbf{u}})^{\mathsf{T}}\frac{\partial \mathbf{u}}{\partial \mathbf{s}} + \mathbf{u}^{\mathsf{T}}\overline{\mathbf{Y}}\frac{\partial \overline{\mathbf{u}}}{\partial \mathbf{s}}$$

At the rated solution pair $(\hat{\mathbf{u}}, \hat{\mathbf{s}})$, we have $\frac{\partial \mathbf{u}}{\partial \hat{\mathbf{s}}} = \hat{\mathbf{u}}$. Hence, at the rated loading, where we intend to linearize the power flow at, we have the following global system loss sensitivity:

$$\frac{\partial s^{\mathsf{l}}}{\partial \hat{\mathbf{s}}} = (\overline{\mathbf{Y}\hat{\mathbf{u}}})^{\mathsf{T}}\hat{\mathbf{u}} + \hat{\mathbf{u}}^{\mathsf{T}}\overline{\mathbf{Y}\hat{\mathbf{u}}} = \hat{\mathbf{u}}^{\mathsf{T}}\overline{\mathbf{Y}\hat{\mathbf{u}}} + \hat{\mathbf{u}}^{\mathsf{T}}\overline{\mathbf{Y}\hat{\mathbf{u}}} = 2\hat{s}^{\mathsf{l}},$$

where one can observe $(\overline{\mathbf{Y}\hat{\mathbf{u}}})^{\mathsf{T}}\hat{\mathbf{u}} = \hat{\mathbf{u}}^{\mathsf{T}}\overline{\mathbf{Y}\hat{\mathbf{u}}}$. This proves the experimental observation of Fig. 3.8 where at rated loading we obtained double the rated losses $\hat{s}^{\mathsf{l}}$.

Double Absolute Line Flow Squared Approximation: Consider the squared line flow "from" buses definition $|\mathbf{s}^{\mathsf{f}}|^2 = \mathrm{diag}(\overline{\mathbf{s}}^{\mathsf{f}})\mathbf{s}^{\mathsf{f}}$, with its desired sensitivity in terms of injections as

$$\frac{\partial |\mathbf{s}^{\mathsf{f}}|^2}{\partial \mathbf{s}} = \mathrm{diag}(\overline{\mathbf{s}}^{\mathsf{f}})\frac{\partial \mathbf{s}^{\mathsf{f}}}{\partial \mathbf{s}} + \mathrm{diag}(\mathbf{s}^{\mathsf{f}})\frac{\partial \overline{\mathbf{s}}^{\mathsf{f}}}{\partial \mathbf{s}} = \mathrm{diag}(\overline{\mathbf{s}}^{\mathsf{f}})\frac{\partial \mathbf{s}^{\mathsf{f}}}{\partial \mathbf{s}} + \mathrm{diag}(\overline{\mathbf{s}}^{\mathsf{f}})\frac{\partial \mathbf{s}^{\mathsf{f}}}{\partial \mathbf{s}} = 2\,\mathrm{diag}(\overline{\mathbf{s}}^{\mathsf{f}})\frac{\partial \mathbf{s}^{\mathsf{f}}}{\partial \mathbf{s}} \tag{3.42}$$

Now we utilize line flow definition of $\mathbf{s}^{\mathrm{f}} = \mathrm{diag}(\mathbf{A}^{\mathrm{f}}\mathbf{u})\overline{\mathbf{Y}}^{\mathrm{f}}\overline{\mathbf{u}}$ from (3.14) and derive its sensitivity to injections:

$$\frac{\partial \mathbf{s}^{\mathrm{f}}}{\partial \mathbf{s}} = \mathrm{diag}(\overline{\mathbf{Y}}^{\mathrm{f}}\overline{\hat{\mathbf{u}}})\mathbf{A}^{\mathrm{f}}\frac{\partial \mathbf{u}}{\partial \mathbf{s}} + \mathrm{diag}(\mathbf{A}^{\mathrm{f}}\hat{\mathbf{u}})\overline{\mathbf{Y}}^{\mathrm{f}}\frac{\partial \overline{\mathbf{u}}}{\partial \mathbf{s}}.$$

At the rated solution pair $(\hat{\mathbf{u}}, \hat{\mathbf{s}})$, we have $\frac{\partial \mathbf{u}}{\partial \hat{\mathbf{s}}} = \hat{\mathbf{u}}$, giving us the above sensitivity at the rated-loading as:

$$\begin{aligned}\frac{\partial \mathbf{s}^{\mathrm{f}}}{\partial \mathbf{s}} &= \mathrm{diag}(\mathbf{A}^{\mathrm{f}}\hat{\mathbf{u}})\overline{\mathbf{Y}}^{\mathrm{f}}\overline{\hat{\mathbf{u}}} + \mathrm{diag}(\mathbf{A}^{\mathrm{f}}\hat{\mathbf{u}})\overline{\mathbf{Y}}^{\mathrm{f}}\overline{\hat{\mathbf{u}}} \\ &= 2\hat{\mathbf{s}}^{\mathrm{f}},\end{aligned}$$

where we have used the equivalence of $\mathrm{diag}(\mathbf{A}^{\mathrm{f}}\hat{\mathbf{u}})\overline{\mathbf{Y}}^{\mathrm{f}}\overline{\hat{\mathbf{u}}} = \mathrm{diag}(\overline{\mathbf{Y}}^{\mathrm{f}}\overline{\hat{\mathbf{u}}})\mathbf{A}^{\mathrm{f}}\hat{\mathbf{u}}$. By comparing the above results from the desired sensitivity term in (3.42), we prove the experimental observation in Fig. 3.7 where the global approximation produces twice the value of rated "from" buses line flows. Similar derivation exists for "to" buses line flows.

Remark 3.3. The doubled system losses obtained from the approximation procedure has also been noticed in transmission grid DC loss approximations [61, 54]. System operators account for this by introducing an offset term in their economic dispatch problem, which aims to cancel out this effect of doubled system loss. Interested readers are referred to [61, 54, 40], for more information regarding the calculation of this offset.

Remark 3.4. With the numerical evaluation of both method presented in example 3.5, we now qualitatively comment on complexity of both (local and global) approximation methodology [8]. In local approximation, for an n buses system, solving system of (3.20) which is in rectangular coordinates amount to computational complexity of $(4N)^2$ (see size of $\mathbf{M}$ in (3.21)). However, the global approximation, only algebraic multiplication is required, given $\mathbf{Y}_{\mathrm{LL}}^{-1}$ is precomputed. This shows the computational benefits of global approximation obtained through the fixed-point solution.

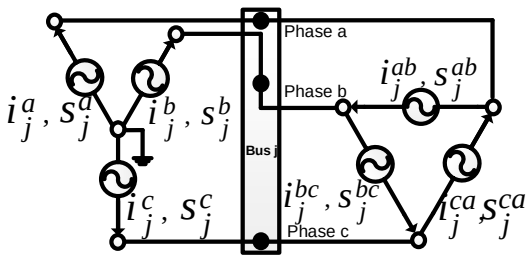

Figure 3.9: Exemplary three-phase grounded wye-connected (left) and delta-connected (right) sources with net current and complex power injections. Similar connections can be made for loads. Procedure to translate mixture of wye-connected and delta-connected sources/loads for both primary and secondary distribution transformer is given in [8].

3.4 Multi-Phase Distribution Grid Model

The above presented *load-flow* problem is now extended to include multi-phase characteristics of the distribution grid. From the previously described methods, we present the fixed-point

solution technique for the multi-phase *load-flow* problem and also present its natural deployment in obtaining the global approximation.

Assumption 3.5. For exposition simplicity, we first assume that the multi-phase grid is a full three-phase grid model.

However, we show in **R. 3.6** the procedure to relax this assumption. Moreover, consistent with **A. 3.3** and **3.4** we assume that distribution grid has one connection (root-bus) to the transmission grid along with n buses modeled as constant PQ model. However, as mentioned in **R. 3.1**, the results can be naturally extended to more generic load models [5].

With reference from Fig. 3.9, we proceed with the development of multi-phase grid notations.

For bus j in Fig. 3.9 with three-phases $\{a, b, c\}$, we have: complex net current injections for each phase-ground $\mathbf{i}_j^{\mathsf{Y}} := (i_j^a, i_j^b, i_j^c)^\intercal$ and phase-phase $\mathbf{i}_j^{\Delta} := (i_j^{ab}, i_j^{bc}, i_j^{ca})^\intercal$ connections along with net complex power injections from wye-connected $\mathbf{s}_j^{\mathsf{Y}} := (s_j^a, s_j^b, s_j^c)^\intercal$ and delta-connected $\mathbf{s}_j^{\Delta} := (s_j^{ab}, s_j^{bc}, s_j^{ca})^\intercal$ sources. Now for each phase-to-ground voltage represented as $\mathbf{u}_j := (u_j^{\mathsf{a}}, u_j^{\mathsf{b}}, u_j^{\mathsf{c}})^\intercal$, similar to (3.1a), we have the following from the Kirchoff Law (see Fig. 3.9 for the reference),

$$\mathbf{s}_j^{\Delta} = \operatorname{diag}(\mathbf{\Gamma}\mathbf{u}_j)\overline{\mathbf{i}_j^{\Delta}}, \tag{3.43a}$$

$$\mathbf{s}_j^{\mathsf{Y}} = \operatorname{diag}(\mathbf{u}_j)\overline{\mathbf{i}_j^{\mathsf{Y}}} - \operatorname{diag}(\mathbf{u}_j)\mathbf{\Gamma}^\intercal\overline{\mathbf{i}_j^{\Delta}} \tag{3.43b}$$

where,

$$\mathbf{\Gamma} := \begin{bmatrix} 1 & -1 & 0 \\ 0 & 1 & -1 \\ -1 & 0 & 1 \end{bmatrix}$$

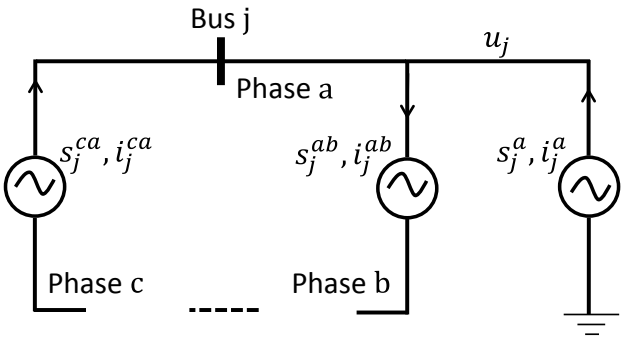

Figure 3.10: Illustration example for three-phase injections

Example 3.6

Fig. 3.10 is presented to explain combined delta and wye injections of (3.43). For bus j, we assume voltage between phase a to ground is u_j^a. At the intersection of phase a

in Fig. 3.10, we have the following nodal balance:

$$s_j^a = u_j^a \bar{i}_j^a + s_j^{\Delta,a},$$

where the injection contribution from connected delta devices to phase a of bus j is given as: $s_j^{\Delta,a} := u_j^a(\bar{i}_j^{ca} - \bar{i}_j^{ab})$. Substituting this result into the above equation gives us:

$$s_j^a = u_j^a i_j^a - u_j^a(\bar{i}_j^{ab} - \bar{i}_j^{ca}).$$

Similarly, we have u_j^b and u_j^c as the phase to ground voltage for phase b and c. The delta connections in Fig. 3.10, have the relationship of

$$s_j^{ab} = (u_j^a - u_j^b)\bar{i}_j^{ab}, \qquad s_j^{bc} = (u_j^b - u_j^c)\bar{i}_j^{bc}$$

Now, for full three-phase grid with desired injections for delta $\mathbf{s}_j^{\Delta} := (s_j^{ab}, s_j^{bc}, s_j^{ca})^\intercal$ and wye connections $\mathbf{s}_j^{Y} := (s_j^a, s_j^b, s_j^c)^\intercal$, the above results can be collected in a vector format which gives the relationship of (3.43).

3.4.1 Multi-Phase *Load-Flow* Problem

Similar to equivalent single-phase notation, we again consider one slack bus and n PQ buses for multi-phase *load-flow* solution. However, in single-phase modeling, we first presented full grid equations (including root-bus and n PQ buses (3.1)) and then shown their translation to represent only n buses. For multi-phase grid, we only directly present all equations in n buses. In order to extend grid equations of (3.43) for the whole grid except slack-bus, we have complex voltages as: $\mathbf{u}_L^{abc} := (\mathbf{u}_1^\intercal, \dots, \mathbf{u}_n^\intercal)^\intercal$, $\mathbf{i}_L^{Y} := (\mathbf{i}_1^\intercal, \dots, \mathbf{i}_n^\intercal)^\intercal$, $\mathbf{i}_L^{\Delta} := ((\mathbf{i}_1^{\Delta})^\intercal, \dots, (\mathbf{i}_1^{\Delta})^\intercal)^\intercal$, $\mathbf{s}_L^{Y} := ((\mathbf{s}_1^{Y})^\intercal, \dots, (\mathbf{s}_n^{Y})^\intercal)^\intercal$, $\mathbf{s}_L^{\Delta} := ((\mathbf{s}_1^{\Delta})^\intercal, \dots, (\mathbf{s}_n^{\Delta})^\intercal)^\intercal$ all having size $\mathbb{C}^{3n}$. The multi-phase *load-flow* problem is then to satisfy the following set of equations:

$$\operatorname{diag}(\mathbf{u}_L^{abc})\mathbf{H}^\intercal \bar{\mathbf{i}}_L^{\Delta} + \mathbf{s}_L^{Y} = \operatorname{diag}(\mathbf{u}_L^{abc})\bar{\mathbf{i}}_L^{Y}, \tag{3.44a}$$

$$\mathbf{s}_L^{\Delta} = \operatorname{diag}(\mathbf{H}\mathbf{u}_L^{abc})\bar{\mathbf{i}}_L^{\Delta}, \tag{3.44b}$$

$$\mathbf{i}_L^{Y} = \mathbf{Y}_{L0}^{abc}\mathbf{u}_0 + \mathbf{Y}_{LL}^{abc}\mathbf{u}_L^{abc}, \tag{3.44c}$$

where,

$$\mathbf{H} := \begin{bmatrix} \mathbf{\Gamma} & & \\ & \ddots & \\ & & \mathbf{\Gamma} \end{bmatrix}, \qquad \mathbf{Y}^{abc} := \begin{bmatrix} \mathbf{Y}_{00}^{abc} & \mathbf{Y}_{0L}^{abc} \\ \mathbf{Y}_{L0}^{abc} & \mathbf{Y}_{LL}^{abc} \end{bmatrix}$$

and $\mathbf{u}_0 := (u_0^a, u_0^b, u_0^c)^\intercal$ is the voltage at the root-bus and $\mathbf{Y}^{abc} \in \mathbb{C}^{3(n+1)\times 3(n+1)}$ is the bus admittance matrix of the whole grid (root-bus and n buses) with individual components from it extracted as: $\mathbf{Y}_{L0}^{abc} \in \mathbb{C}^{3n\times 3}$, $\mathbf{Y}_{0L}^{abc} \in \mathbb{C}^{3\times 3n}$, $\mathbf{Y}_{00}^{abc} \in \mathbb{C}^{3\times 3}$ and $\mathbf{Y}_{LL}^{abc} \in \mathbb{C}^{3n\times 3n}$.

Remark 3.5. Contrary to the superscript "Y", we denote phase to ground complex voltage as $\mathbf{u}_L^{abc}$. This on one hand keeps the notation consistent with the single-phase equivalent distribution grid notation and on the other hand establishes the fact that $\mathbf{u}_L^{abc}$ is the only solution variable of the multi-phase *load-flow* problem.

From (3.44), one can see that (3.44a) and (3.44b) are simply the augmented versions of the single bus injection formulations in (3.43). However, (3.44c) is a new equation which is explained in example 3.7.

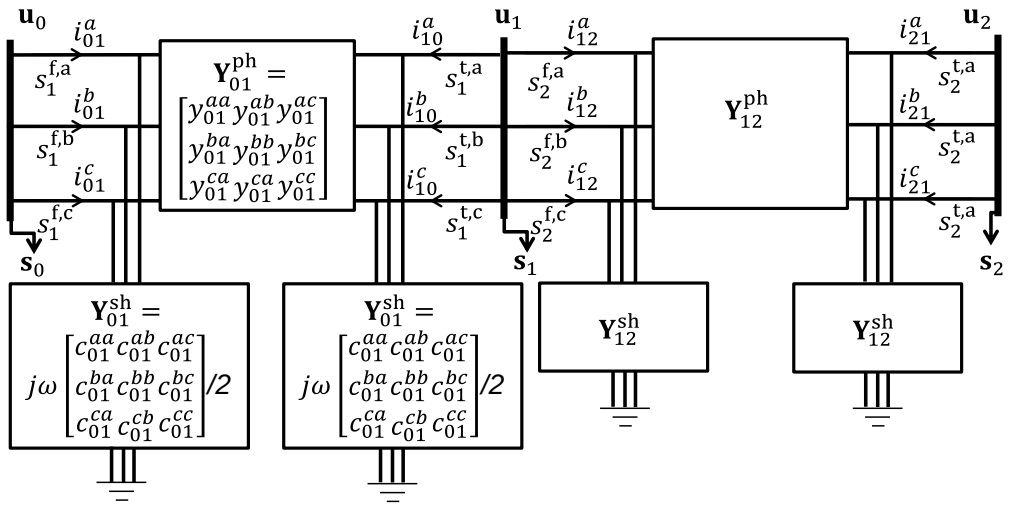

Figure 3.11: Exemplary three-phase grid model with three buses connected using two lines. The modeled distribution grid line elements represent a standard π-model for a generic three-phase line [48, 15, 112]. The vectors $\mathbf{s}_0$, $\mathbf{s}_1$, and $\mathbf{s}_2$ are generic injection variables which depending upon delta or wye connected sources/loads can be included in *load-flow* problem as shown in (3.44).

For bus i and j, the phase admittance matrix $\mathbf{Y}_{ij}^{\text{ph}}$ contains equivalent self admittances (e.g. y_{ij}^{aa} for phase a between bus i and j) and equivalent mutual admittances (e.g. y_{ij}^{ab} between phase a and b of the line between bus i and j). These equivalent admittances are obtained after performing Kron's reduction on the original three-phase conductor admittances, which also contain effect of ground and neutral nodes [48, chapter 6]. Similarly, shunt admittance matrix represent equivalent charging capacitance of the three-phase line element, which is then placed in equal halves at both ends of the line element (standard π model). The individual entities of shunt admittance matrix represent coupling between line element's phases, i.e., $j\omega c_{ij}^{aa}$ is the equivalent self shunt capacitance of phase a and $j\omega c_{ij}^{ab}$ is the equivalent mutual shunt capacitance between phase a and b of the line element connecting bus i and j. For calculating individual values of phase and shunt admittance matrices and their overall construction methodologies, interested readers are referred to [48, chapter 4-6].

Example 3.7

We now assume a grid with two three-phase distribution grid lines connecting three buses Fig. 3.11, where all buses contain three-phases. For line currents we have the relationship:

$$\mathbf{i}_{01} = \mathbf{Y}_{01}^{\text{sh}}\mathbf{u}_0 + \mathbf{Y}_{01}^{\text{ph}}(\mathbf{u}_0 - \mathbf{u}_1), \qquad \mathbf{i}_{10} = \mathbf{Y}_{01}^{\text{sh}}\mathbf{u}_1 + \mathbf{Y}_{01}^{\text{ph}}(\mathbf{u}_1 - \mathbf{u}_0)$$
$$\mathbf{i}_{12} = \mathbf{Y}_{12}^{\text{sh}}\mathbf{u}_1 + \mathbf{Y}_{12}^{\text{ph}}(\mathbf{u}_1 - \mathbf{u}_2), \qquad \mathbf{i}_{21} = \mathbf{Y}_{12}^{\text{sh}}\mathbf{u}_2 + \mathbf{Y}_{12}^{\text{ph}}(\mathbf{u}_2 - \mathbf{u}_1).$$

Above, phase to ground voltages and line currents contain all three phases. For example $\mathbf{u}_0 := (u_0^a, u_0^b, u_0^c)^\intercal$ and $\mathbf{i}_{01} := (i_{01}^a, i_{01}^b, i_{01}^c)^\intercal$. From Kirchoff's current law we have that for all k buses directly connected to bus j, i.e., $\sum_k \mathbf{i}_{j,k}$, the sum should be equal to zero:

$$\begin{aligned} \mathbf{i}_0 = \mathbf{i}_{01}, \qquad & \mathbf{i}_0 = \mathbf{Y}_{01}^{\text{sh}}\mathbf{u}_0 + \mathbf{Y}_{01}^{\text{ph}}(\mathbf{u}_0 - \mathbf{u}_1) \\ \mathbf{i}_1 = \mathbf{i}_{10} + \mathbf{i}_{12}, \qquad & \mathbf{i}_1 = \mathbf{Y}_{01}^{\text{sh}}\mathbf{u}_1 + \mathbf{Y}_{01}^{\text{ph}}(\mathbf{u}_1 - \mathbf{u}_0) + \mathbf{Y}_{12}^{\text{sh}}\mathbf{u}_1 + \mathbf{Y}_{12}^{\text{ph}}(\mathbf{u}_1 - \mathbf{u}_2) \\ \mathbf{i}_2 = \mathbf{i}_{21}, \qquad & \mathbf{i}_2 = \mathbf{Y}_{12}^{\text{sh}}\mathbf{u}_2 + \mathbf{Y}_{12}^{\text{ph}}(\mathbf{u}_2 - \mathbf{u}_1) \end{aligned}$$

Now collecting phase to ground current injections as: $\mathbf{i}^{\text{Y}} := (\mathbf{i}_0{}^\intercal, \mathbf{i}_1{}^\intercal, \mathbf{i}_2{}^\intercal)^\intercal$ and voltages as: $\mathbf{u}^{\text{abc}} := (\mathbf{u}_0{}^\intercal, \mathbf{u}_1{}^\intercal, \mathbf{u}_2{}^\intercal)^\intercal$, we can write the compact representation of above equations as:

$$\mathbf{i}^{\text{Y}} = \mathbf{Y}^{\text{abc}}\mathbf{u}^{\text{abc}}, \qquad \text{where}$$

$$\mathbf{Y}^{\text{abc}} = \begin{bmatrix} \mathbf{Y}_{01}^{\text{sh}} + \mathbf{Y}_{01}^{\text{ph}} & -\mathbf{Y}_{01}^{\text{ph}} & \mathbf{0}_{3\times 3} \\ -\mathbf{Y}_{01}^{\text{ph}} & \mathbf{Y}_{01}^{\text{sh}} + \mathbf{Y}_{01}^{\text{ph}} + \mathbf{Y}_{12}^{\text{sh}} + \mathbf{Y}_{12}^{\text{ph}} & -\mathbf{Y}_{12}^{\text{ph}} \\ \mathbf{0}_{3\times 3} & -\mathbf{Y}_{12}^{\text{ph}} & \mathbf{Y}_{12}^{\text{sh}} + \mathbf{Y}_{12}^{\text{ph}} \end{bmatrix}$$

Now in terms of representing above equations only in PQ buses, i.e., bus 1 and 2 in the example, we have the following relationship:

$$\mathbf{i}_{\text{L}}^{\text{Y}} = \mathbf{Y}_{\text{L0}}^{\text{abc}}\mathbf{u}_0 + \mathbf{Y}_{\text{LL}}^{\text{abc}}\mathbf{u}_{\text{L}}^{\text{abc}}, \qquad \text{where}$$

$$\mathbf{i}_{\text{L}}^{\text{Y}} = \begin{bmatrix} \mathbf{i}_1 \\ \mathbf{i}_2 \end{bmatrix}, \mathbf{u}_{\text{L}}^{\text{abc}} = \begin{bmatrix} \mathbf{u}_1 \\ \mathbf{u}_2 \end{bmatrix}, \mathbf{Y}_{\text{L0}}^{\text{abc}} = \begin{bmatrix} -\mathbf{Y}_{01}^{\text{ph}} \\ \mathbf{0}_{3\times 3} \end{bmatrix}, \mathbf{Y}_{\text{LL}}^{\text{abc}} = \begin{bmatrix} \mathbf{Y}_{01}^{\text{sh}} + \mathbf{Y}_{01}^{\text{ph}} + \mathbf{Y}_{12}^{\text{sh}} + \mathbf{Y}_{12}^{\text{ph}} & -\mathbf{Y}_{12}^{\text{ph}} \\ -\mathbf{Y}_{12}^{\text{ph}} & \mathbf{Y}_{12}^{\text{sh}} + \mathbf{Y}_{12}^{\text{ph}} \end{bmatrix}.$$

The above expression is exactly similar to (3.44c).

Similar to the single-phase *load-flow* problem in (3.6), the following fixed-point equation can be obtained for three-phase *load-flow* problem (3.44) [8]:

$$\mathbf{u}_{\text{L}}^{\text{abc}} = \mathbf{w}^{\text{abc}} + \mathbf{Y}_{\text{LL}}^{\text{abc}\,-1}\Big(\operatorname{diag}(\bar{\mathbf{u}}_{\text{L}}^{\text{abc}})^{-1}\bar{\mathbf{s}}_{\text{L}}^{\text{Y}} + \mathbf{H}^\intercal \operatorname{diag}(\mathbf{H}\bar{\mathbf{u}}_{\text{L}}^{\text{abc}})^{-1}\bar{\mathbf{s}}_{\text{L}}^{\Delta}\Big) \tag{3.45}$$

where $\mathbf{w}^{\text{abc}} := -\mathbf{Y}_{\text{LL}}^{\text{abc}\,-1}\mathbf{Y}_{\text{L0}}^{\text{abc}}\mathbf{u}_0$ is the no-load voltage and for given $(\mathbf{s}_{\text{L}}^{\Delta}, \mathbf{s}_{\text{L}}^{\text{Y}}, \mathbf{u}_0^{\text{abc}})$, can be solved for each iteration k as:

$$\mathbf{u}_{\text{L}}^{\text{abc}(k+1)} = \mathbf{G}_{\mathbf{s}^{\text{Y}}\mathbf{s}^{\Delta}}\Big(\mathbf{u}_{\text{L}}^{\text{abc}(k)}\Big) \tag{3.46}$$

with $\mathbf{G}_{\mathbf{s}^{\text{Y}}\mathbf{s}^{\Delta}}(\,\cdot\,)$ defined in (3.46). Similar to unique solution convergence for single-phase fixed-point operator $\mathbf{G}(\cdot)$ in (3.7). The conditions to guarantee solution uniqueness and existence for the multi-phase fixed point operator $\mathbf{G}_{\mathbf{s}^{\text{Y}}\mathbf{s}^{\Delta}}$ are given in [8, Theorem 1, 2]. Since, these proofs follow similar interpretations, as of single-phase solution uniqueness conditions, we do not pursue the proof of these theorems here. Instead, solution comparison of the fixed-point method of (3.46) with an open-source software, the open distribution system simulator (OpenDSS) [85], is given in example 3.8.

Example 3.8

For the exemplary system of Fig. 3.12, primary side (before transformer) of the grid is

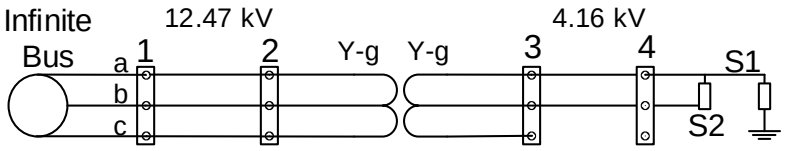

Figure 3.12: Modified IEEE 4-bus grid [47]. To illustrate multi-phase and unbalanced nature of the grid, phase c after bus 3 has been removed and mixture of wye and line to line (which is equivalent to single-phase delta connection) loads are included at bus 4. Example 3.8 describes solution values for this system.

rated at 12.47 kV (Line-Line)[a] and secondary side (after transformer) at 4.16 kV (Line-Line). The readers are referred to the openDSS script file in Appendix A.1.3 for more information regarding the modeled grid. It can be seen from Fig. 3.13 that the solution obtained from the fixed-point equation and openDSS is exactly similar.

[a] In this thesis, we always termed the voltage quantities, for example $\mathbf{u}^{abc}$, as line-neutral, which is simply Line-Line voltage/$\sqrt{3}$.

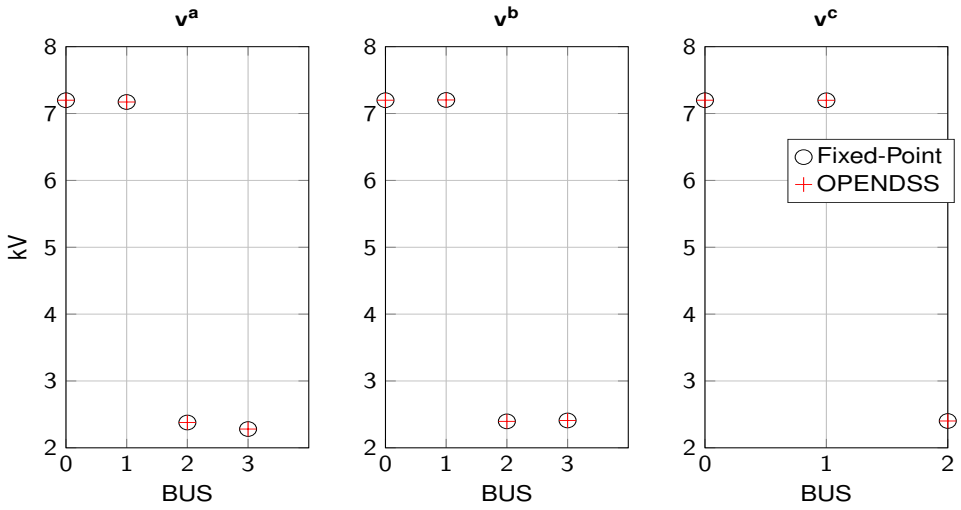

Figure 3.13: Comparison of voltage magnitude $\mathbf{v}^{(\cdot)}$ of phase $(\cdot)$ between the fixed point *load-flow* method (3.46) and openDSS [85].

Let $\hat{\mathbf{u}}^{abc} := (\mathbf{u}_0{}^{\mathsf{T}}, \hat{\mathbf{u}}_L^{abc\mathsf{T}})$ be the whole grid's voltage vector which contains the solution $\hat{\mathbf{u}}_L$ from solving (3.45). Then, we can formulate line flows and total system losses for three-phase distribution grids. To this end, we consider for grid with m three-phase distribution lines, having "from"/"to"buses complex line flows of $\mathbf{s}^{f,abc/t,abc} := ((\mathbf{s}_1^{f,abc/t,abc})^{\mathsf{T}}, \ldots, (\mathbf{s}_m^{f,abc/t,abc})^{\mathsf{T}})^{\mathsf{T}} \in \mathbb{C}^{3m}$

and total complex system loss $s^{\mathsf{l,abc}} \in \mathbb{C}$ as:

$$\mathbf{s}^{\mathsf{f,abc/t,abc}} = \mathrm{diag}(\mathbf{A}^{\mathsf{f,abc/t,abc}}\hat{\mathbf{u}}^{\mathsf{abc}})\mathbf{Y}^{\mathsf{f,abc/t,abc}}\overline{\hat{\mathbf{u}}}^{\mathsf{abc}}, \tag{3.47a}$$

$$s^{\mathsf{l,abc}} = \hat{\mathbf{u}}^{\mathsf{abc}\,\mathsf{T}}\overline{\mathbf{Y}}^{\mathsf{abc}}\overline{\hat{\mathbf{u}}}^{\mathsf{abc}}. \tag{3.47b}$$

Example 3.9

We derive now complex line flows for multi-phase grids in a form given by (3.47a) for the exemplary system of Fig. 3.11. We provide derivation for only "from" buses line flows as "to" buses follow exactly the same procedure. For line element $k \in (i, j)$, complex line flows direction "from" bus i to j is denoted as $\mathbf{s}_k^{\mathsf{f,abc}} :=:= (s_k^{\mathsf{f},a}, s_k^{\mathsf{f,b}}, s_k^{\mathsf{f,c}})^{\mathsf{T}}$. Hence, keeping the notation consistent, for the grid of Fig. 3.11, we have:

$$\mathbf{s}_1^{\mathsf{f,abc}} = \mathrm{diag}(\mathbf{u}_0)\overline{\mathbf{i}_{01}}, \qquad \mathbf{s}_2^{\mathsf{f,abc}} = \mathrm{diag}(\mathbf{u_1})\overline{\mathbf{i}_{12}}$$

Recalling multi-phase line currents from example 3.7:

$$\mathbf{i}_{01} = \mathbf{Y}_{01}^{\mathsf{sh}}\mathbf{u}_0 + \mathbf{Y}_{01}^{\mathsf{ph}}(\mathbf{u}_0 - \mathbf{u}_1), \qquad \mathbf{i}_{12} = \mathbf{Y}_{12}^{\mathsf{sh}}\mathbf{u}_1 + \mathbf{Y}_{12}^{\mathsf{ph}}(\mathbf{u}_1 - \mathbf{u}_2)$$

giving us complex line flows in terms of voltages as:

$$\mathbf{s}_1^{\mathsf{f,abc}} = \mathrm{diag}(\overline{\mathbf{u}}_0)(\overline{\mathbf{Y}}_{01}^{\mathsf{sh}}\mathbf{u}_0 + \overline{\mathbf{Y}}_{01}^{\mathsf{ph}}(\overline{\mathbf{u}}_0 - \overline{\mathbf{u}}_1)), \qquad \mathbf{s}_2^{\mathsf{f,abc}} = \mathrm{diag}(\overline{\mathbf{u}}_1)(\overline{\mathbf{Y}}_{12}^{\mathsf{sh}}\mathbf{u}_1 + \overline{\mathbf{Y}}_{12}^{\mathsf{ph}}(\overline{\mathbf{u}}_1 - \overline{\mathbf{u}}_2))$$

Now to obtain vector form of complex line flows "from" buses (3.47a), we collect the above in appropriate vector forms to give:

$$\mathbf{s}^{\mathsf{f,abc}} = \mathrm{diag}(\mathbf{A}^{\mathsf{f,abc}}\mathbf{u}^{\mathsf{abc}})\overline{\mathbf{Y}}^{\mathsf{f,abc}}\overline{\mathbf{u}}^{\mathsf{abc}}, \qquad \text{where,}$$

$$\mathbf{s}^{\mathsf{f,abc}} = \begin{bmatrix} s_1^{\mathsf{f},abc} \\ s_2^{\mathsf{f},abc} \end{bmatrix}, \mathbf{u}^{\mathsf{abc}} = \begin{bmatrix} \mathbf{u}_0 \\ \mathbf{u}_1 \\ \mathbf{u}_2 \end{bmatrix}, \mathbf{Y}^{\mathsf{f,abc}} = \begin{bmatrix} \mathbf{Y}_{01}^{sh} + \mathbf{Y}_{01}^{ph} & -\mathbf{Y}_{01}^{ph} & \mathbf{0}_{3\times3} \\ \mathbf{0}_{3\times3} & \mathbf{Y}_{12}^{sh} + \mathbf{Y}_{12}^{ph} & -\mathbf{Y}_{12}^{ph} \end{bmatrix},$$

$$\mathbf{A}^{\mathsf{f},abc} = \begin{bmatrix} I_3 & \mathbf{0}_{3\times3} & \mathbf{0}_{3\times3} \\ \mathbf{0}_{3\times3} & I_3 & \mathbf{0}_{3\times3} \end{bmatrix}.$$

For the grid of Fig. 3.11, the overall system losses can be derived as:

$$s^{\mathsf{l,abc}} = \mathbf{1}_3{}^{\mathsf{T}}(\mathbf{s}_1^{\mathsf{f,abc}} + \mathbf{s}_1^{\mathsf{t,abc}} + \mathbf{s}_2^{\mathsf{f,abc}} + \mathbf{s}_2^{\mathsf{t,abc}})$$

$$s^{\mathsf{l,abc}} = \mathbf{1}_3{}^{\mathsf{T}}(\mathrm{diag}(\mathbf{u}_0)\overline{\mathbf{i}_{01}} + \mathrm{diag}(\mathbf{u}_1)\overline{\mathbf{i}_{10}} + \mathrm{diag}(\mathbf{u}_1)\overline{\mathbf{i}_{12}} + \mathrm{diag}(\mathbf{u}_2)\overline{\mathbf{i}_{21}})$$

Now we utilize line currents definitions and complex power flows definition from exam-

ple 3.7 to combine them together to separately list the individual line losses:

$$
\begin{aligned}
s_1^{f,abc} + s_1^{t,abc} &= \mathbf{1}_3{}^{\mathsf{T}}\Big(\operatorname{diag}(\overline{\mathbf{u}}_0)(\overline{\mathbf{Y}}_{01}^{sh}\overline{\mathbf{u}}_0 + \overline{\mathbf{Y}}_{01}^{ph}(\overline{\mathbf{u}}_0 - \overline{\mathbf{u}}_1))\Big) \\
&\quad + \mathbf{1}_3{}^{\mathsf{T}}\Big(\operatorname{diag}(\overline{\mathbf{u}}_1)(\overline{\mathbf{Y}}_{01}^{sh}\overline{\mathbf{u}}_1 + \overline{\mathbf{Y}}_{01}^{ph}(\overline{\mathbf{u}}_1 - \overline{\mathbf{u}}_0))\Big) \\
&= \begin{bmatrix}\overline{\mathbf{u}}_0\\ \overline{\mathbf{u}}_1\\ \overline{\mathbf{u}}_2\end{bmatrix}^{\mathsf{T}} \begin{bmatrix}\overline{\mathbf{Y}}_{01}^{sh} + \overline{\mathbf{Y}}_{01}^{ph} & -\overline{\mathbf{Y}}_{01}^{ph} & \mathbf{0}_{3\times3}\\ -\overline{\mathbf{Y}}_{01}^{sh} & \overline{\mathbf{Y}}_{01}^{sh} + \overline{\mathbf{Y}}_{01}^{ph} & \mathbf{0}_{3\times3}\\ \mathbf{0}_{3\times3} & \mathbf{0}_{3\times3} & \mathbf{0}_{3\times3}\end{bmatrix} \begin{bmatrix}\overline{\mathbf{u}}_0\\ \overline{\mathbf{u}}_1\\ \overline{\mathbf{u}}_2\end{bmatrix} \\
s_2^{f,abc} + s_2^{t,abc} &= \mathbf{1}_3{}^{\mathsf{T}}\Big(\operatorname{diag}(\overline{\mathbf{u}}_1)(\overline{\mathbf{Y}}_{12}^{sh}\overline{\mathbf{u}}_1 + \overline{\mathbf{Y}}_{12}^{ph}(\overline{\mathbf{u}}_1 - \overline{\mathbf{u}}_2))\Big) \\
&\quad + \mathbf{1}_3{}^{\mathsf{T}}\Big(\operatorname{diag}(\overline{\mathbf{u}}_2)(\overline{\mathbf{Y}}_{12}^{sh}\overline{\mathbf{u}}_2 + \overline{\mathbf{Y}}_{12}^{ph}(\overline{\mathbf{u}}_2 - \overline{\mathbf{u}}_1))\Big) \\
&= \begin{bmatrix}\overline{\mathbf{u}}_0\\ \overline{\mathbf{u}}_1\\ \overline{\mathbf{u}}_2\end{bmatrix}^{\mathsf{T}} \begin{bmatrix}\mathbf{0}_{3\times3} & \mathbf{0}_{3\times3} & \mathbf{0}_{3\times3}\\ \mathbf{0}_{3\times3} & \overline{\mathbf{Y}}_{12}^{sh} + \overline{\mathbf{Y}}_{12}^{ph} & -\overline{\mathbf{Y}}_{12}^{ph}\\ \mathbf{0}_{3\times3} & -\overline{\mathbf{Y}}_{12}^{ph} & \overline{\mathbf{Y}}_{12}^{sh} + \overline{\mathbf{Y}}_{12}^{ph}\end{bmatrix} \begin{bmatrix}\overline{\mathbf{u}}_0\\ \overline{\mathbf{u}}_1\\ \overline{\mathbf{u}}_2\end{bmatrix} \\
s^{l} = s_1^{f} + s_1^{t} + s_2^{f} + s_2^{t} &= \begin{bmatrix}\overline{\mathbf{u}}_0\\ \overline{\mathbf{u}}_1\\ \overline{\mathbf{u}}_2\end{bmatrix}^{\mathsf{T}} \begin{bmatrix}\mathbf{Y}_{01}^{sh} + \mathbf{Y}_{01}^{ph} & -\mathbf{Y}_{01}^{ph} & \mathbf{0}_{3\times3}\\ -\mathbf{Y}_{01}^{ph} & \mathbf{Y}_{01}^{sh} + \mathbf{Y}_{01}^{ph} + \mathbf{Y}_{12}^{ph} + \mathbf{Y}_{12}^{ph} & -\mathbf{Y}_{12}^{ph}\\ \mathbf{0}_{3\times3} & -\mathbf{Y}_{12}^{ph} & \mathbf{Y}_{12}^{sh} + \mathbf{Y}_{12}^{ph}\end{bmatrix} \begin{bmatrix}\overline{\mathbf{u}}_0\\ \overline{\mathbf{u}}_1\\ \overline{\mathbf{u}}_2\end{bmatrix} \\
s^{l,abc} &= \overline{\mathbf{u}}^{abc\mathsf{T}}\overline{\mathbf{Y}}^{abc}\overline{\mathbf{u}}^{abc}.
\end{aligned}
$$

Note that in the above derivation, the introduction of conjugate between the changing of component-wise multiplication to vectorial form comes from the standard inner product rule of multiplying two complex vectors.

Similar to (3.44), we now split definitions in (3.47) in the desired solution variable $\hat{\mathbf{u}}_L$. To this end, consider incidence matrix $\mathbf{A}^{f,abc/t,abc}$, a $3m \times 3(n+1)$ matrix containing 1's at buses connected at the "from"/"to" ends of lines, zero elsewhere and admittance matrix $\overline{\mathbf{Y}}^{f,abc/t,abc} \in \mathbb{C}^{3m\times3(n+1)}$ to be arranged as follows:

$$
\mathbf{A}^{f,abc/t,abc} = \left(\mathbf{A}_0^{f,abc/t,abc}, \mathbf{A}_L^{f,abc/t,abc}\right), \overline{\mathbf{Y}}^{f,abc/t,abc} = \left(\overline{\mathbf{Y}}_0^{f,abc/t,abc}, \overline{\mathbf{Y}}_L^{f,abc/t,abc}\right). \tag{3.48}
$$

Then following the similar structure of (3.47), we get both complex line flows and system losses as a function of desired solution variables:

$$
\mathbf{s}^{f,abc/t,abc} = \operatorname{diag}(\mathbf{A}_0^{f,abc/t,abc}\mathbf{u}_0 + \mathbf{A}_L^{f,abc/t,abc}\hat{\mathbf{u}}_L^{abc})(\overline{\mathbf{Y}}_0^{f,abc/t,abc}\overline{\hat{\mathbf{u}}}_0 + \overline{\mathbf{Y}}_L^{f,abc/t,abc}\overline{\hat{\mathbf{u}}}_L^{abc}), \tag{3.49a}
$$

$$
s^{l,abc} = \overline{\mathbf{u}}_0{}^{\mathsf{T}}(\overline{\mathbf{Y}}_{00}^{abc}\overline{\mathbf{u}}_0 + \overline{\mathbf{Y}}_{0L}^{abc}\overline{\hat{\mathbf{u}}}_L^{abc}) + \overline{\hat{\mathbf{u}}}_L^{abc\mathsf{T}}(\overline{\mathbf{Y}}_{L0}^{abc}\overline{\mathbf{u}}_0 + \overline{\mathbf{Y}}_{LL}^{abc}\overline{\hat{\mathbf{u}}}_L^{abc}). \tag{3.49b}
$$

Remark 3.6. Equations in (3.44) can be easily modified to represent generic number of phases in the grid. For buses, the only required modification would be to appropriately collect vectors $\mathbf{s}_L^{\Delta}$, $\mathbf{s}_L^{Y}$ and $\mathbf{u}$ along with the reconstruction of matrix $\mathbf{H}$ as a $n^{\Delta} \times n^{Y}$ matrix, where n^{Y} is the total number of phases and n^{Δ} is the available phase-phase connections in the grid. Similarly, phase and shunt admittance matrices shall also be appropriately adjusted to represent it in the modified bus admittance matrix $\mathbf{Y}^{abc} \in n^{Y} \times n^{Y}$ to compliment the modified $\mathbf{H}$ matrix.

3.4.2 Multi-Phase Approximation Modeling

Similar to Sec. 3.3, we aim to find the following real-valued approximations for multi-phase grids, in order to be deployed later:

$$\tilde{\mathbf{v}}_{\mathsf{L}}^{\mathrm{abc}} = \hat{\mathbf{a}}^{\mathrm{abc}} + \mathbf{M}^{\mathbf{v}_{\mathsf{L}},\mathsf{Y}}\mathbf{s}_{\mathsf{L}}^{\mathrm{inj},\mathsf{Y}} + \mathbf{M}^{\mathbf{v}_{\mathsf{L}},\Delta}\mathbf{s}_{\mathsf{L}}^{\mathrm{inj},\Delta}, \tag{3.50a}$$

$$|\tilde{\mathbf{s}}^{\mathrm{f,abc}}|^2 = \hat{\mathbf{b}}^{\mathrm{abc}} + \mathbf{M}^{\mathbf{s}^{\mathrm{f}},\mathsf{Y}}\mathbf{s}_{\mathsf{L}}^{\mathrm{inj},\mathsf{Y}} + \mathbf{M}^{\mathbf{s}^{\mathrm{f}},\Delta}\mathbf{s}_{\mathsf{L}}^{\mathrm{inj},\Delta}, \tag{3.50b}$$

$$|\tilde{\mathbf{s}}^{\mathrm{t,abc}}|^2 = \hat{\mathbf{c}}^{\mathrm{abc}} + \mathbf{M}^{\mathbf{s}^{\mathrm{t}},\mathsf{Y}}\mathbf{s}_{\mathsf{L}}^{\mathrm{inj},\mathsf{Y}} + \mathbf{M}^{\mathbf{s}^{\mathrm{t}},\Delta}\mathbf{s}_{\mathsf{L}}^{\mathrm{inj},\Delta}, \tag{3.50c}$$

$$\tilde{p}^{\mathrm{l,abc}} = \hat{d}^{\mathrm{abc}} + \mathbf{M}^{p^{\mathrm{l}},\mathsf{Y}}\mathbf{s}_{\mathsf{L}}^{\mathrm{inj},\mathsf{Y}} + \mathbf{M}^{p^{\mathrm{l}},\Delta}\mathbf{s}_{\mathsf{L}}^{\mathrm{inj},\Delta}, \tag{3.50d}$$

$$\tilde{q}^{\mathrm{l,abc}} = \hat{e}^{\mathrm{abc}} + \mathbf{M}^{q^{\mathrm{l}},\mathsf{Y}}\mathbf{s}_{\mathsf{L}}^{\mathrm{inj},\mathsf{Y}} + \mathbf{M}^{q^{\mathrm{l}},\Delta}\mathbf{s}_{\mathsf{L}}^{\mathrm{inj},\Delta}, \tag{3.50e}$$

where $\mathbf{s}_{\mathsf{L}}^{\mathrm{inj},\mathsf{Y}} := ((\mathbf{p}_{\mathsf{L}}^{\mathsf{Y}})^\intercal, (\mathbf{q}_{\mathsf{L}}^{\mathsf{Y}})^\intercal)^\intercal \in \mathbb{R}^{6n}$, $\mathbf{s}_{\mathsf{L}}^{\mathrm{inj},\Delta} := ((\mathbf{p}_{\mathsf{L}}^{\Delta})^\intercal, (\mathbf{q}_{\mathsf{L}}^{\Delta})^\intercal)^\intercal \in \mathbb{R}^{6n}$ and $(\hat{\mathbf{a}}^{\mathrm{abc}}, \hat{\mathbf{b}}^{\mathrm{abc}}, \hat{\mathbf{c}}^{\mathrm{abc}}, \hat{d}^{\mathrm{abc}}, \hat{e}^{\mathrm{abc}})$ are appropriate constants. Similar to single-phase approximations (3.18), multi-phase grid approximations (3.50) also have a linear approximation structure, i.e. desired approximate $\tilde{(\cdot)}$ is related to grid injections $(\mathbf{s}_{\mathsf{L}}^{\mathrm{inj},\mathsf{Y}}, \mathbf{s}_{\mathsf{L}}^{\mathrm{inj},\Delta})$ through their corresponding constant matrices $(\mathbf{M}^{(\cdot),\mathsf{Y}}, \mathbf{M}^{(\cdot),\Delta})$. As mentioned earlier, for multi-phase systems we only present global approximation. However, for obtaining the local approximation, interest readers can follow:

1. Find system of equation describing complex-valued voltage sensitivities with respect to injections. For reference, see (3.20) for single-phase equivalent grid and [8, Sec. IV-A] for three systems.
2. With the complex valued sensitivities obtained, follow the steps given in Sec. 3.3.1 to obtain the rest of the approximations.

Now, we proceed with multi-phase *load-flow* global approximation. To this end, we utilize the fixed point variant of the multi-phase *load-flow* problem (3.45), giving the complex-valued voltage sensitivity with respect to both wye $\mathbf{M}^{\mathsf{Y}} \in \mathbb{C}^{3n\times 6n}$ and delta injections $\mathbf{M}^{\Delta} \in \mathbb{C}^{3n\times 6n}$ as:

$$\mathbf{M}^{\mathsf{Y}} := \Big(\frac{\partial \mathbf{u}_{\mathsf{L}}^{\mathrm{abc}}}{\partial \mathbf{p}_{\mathsf{L}}^{\mathsf{Y}}}, j\frac{\partial \mathbf{u}_{\mathsf{L}}^{\mathrm{abc}}}{\partial \mathbf{q}_{\mathsf{L}}^{\mathsf{Y}}}\Big) := \Big(\mathbf{Y}_{\mathsf{LL}}^{\mathrm{abc}\,-1}\mathrm{diag}(\overline{\mathbf{u}}_{\mathsf{L}}^{\mathrm{abc}})^{-1}, -j\mathbf{Y}_{\mathsf{LL}}^{\mathrm{abc}\,-1}\mathrm{diag}(\overline{\mathbf{u}}_{\mathsf{L}}^{\mathrm{abc}})^{-1}\Big), \tag{3.51a}$$

$$\mathbf{M}^{\Delta} := \Big(\frac{\partial \mathbf{u}_{\mathsf{L}}^{\mathrm{abc}}}{\partial \mathbf{p}_{\mathsf{L}}^{\Delta}}, j\frac{\partial \mathbf{u}_{\mathsf{L}}^{\mathrm{abc}}}{\partial \mathbf{q}_{\mathsf{L}}^{\Delta}}\Big) := \Big(\mathbf{Y}_{\mathsf{LL}}^{\mathrm{abc}\,-1}\mathbf{H}^\intercal\mathrm{diag}(\mathbf{H}\overline{\mathbf{u}}^{\mathrm{abc}})^{-1}, -j\mathbf{Y}_{\mathsf{LL}}^{\mathrm{abc}\,-1}\mathbf{H}^\intercal\mathrm{diag}(\mathbf{H}\overline{\mathbf{u}}^{\mathrm{abc}})^{-1}\Big). \tag{3.51b}$$

Linear Voltage Magnitude (3.50a) We again utilize the following rule

$$\frac{\partial |f(x)|}{\partial x} = \frac{1}{|f(x)|}\Re\Big(\overline{f(x)}\frac{\partial f(x)}{\partial x}\Big) \tag{3.52}$$

to obtain (3.50a) as:

$$\mathbf{M}^{\mathbf{v}_{\mathsf{L}},\mathsf{Y}} := \mathrm{diag}(\mathbf{v}_{\mathsf{L}}^{\mathrm{abc}})^{-1}\Re\Big(\mathrm{diag}(\overline{\mathbf{u}}_{\mathsf{L}}^{\mathrm{abc}})\mathbf{M}^{\mathsf{Y}}\Big), \tag{3.53a}$$

$$\mathbf{M}^{\mathbf{v}_{\mathsf{L}},\Delta} := \mathrm{diag}(\mathbf{v}_{\mathsf{L}}^{\mathrm{abc}})^{-1}\Re\Big(\mathrm{diag}(\overline{\mathbf{u}}_{\mathsf{L}}^{\mathrm{abc}})\mathbf{M}^{\Delta}\Big), \tag{3.53b}$$

$$\hat{\mathbf{a}}^{\mathrm{abc}} := \hat{\mathbf{v}}_{\mathsf{L}}^{\mathrm{abc}} - \mathbf{M}^{\mathbf{v}_{\mathsf{L}},\mathsf{Y}}\hat{\mathbf{s}}_{\mathsf{L}}^{\mathrm{inj},\mathsf{Y}} + \mathbf{M}^{\mathbf{v}_{\mathsf{L}},\Delta}\hat{\mathbf{s}}_{\mathsf{L}}^{\mathrm{inj},\Delta} \tag{3.53c}$$

Linear Squared Line Flow (3.50b)**,** (3.50c) First, consider sensitivities of line flows "from" buses. We start with the already presented sensitivity of line flows "from" with respect to injections for the single-phase equivalent model, already presented in (3.25) but repeated below for convenience:

$$\mathbf{M}^{\mathbf{s}^{\mathsf{f},\mathsf{abc}}} := \frac{\partial|\mathbf{s}^{\mathsf{f}}|^2}{\partial \mathbf{s}_{\mathsf{L}}^{\mathsf{inj}}} := 2\Big(\operatorname{diag}\left(\Re(\mathbf{s}^{\mathsf{f}})\right), \operatorname{diag}\left(\Im(\mathbf{s}^{\mathsf{f}})\right)\Big) \begin{bmatrix} \Re(\frac{\partial \mathbf{s}^{\mathsf{f}}}{\partial \mathbf{s}_{\mathsf{L}}^{\mathsf{inj}}}) \\ \Im(\frac{\partial \mathbf{s}^{\mathsf{f}}}{\partial \mathbf{s}_{\mathsf{L}}^{\mathsf{inj}}}) \end{bmatrix}.$$

For the multi-phase grid, the above relationship is simply changed to consider both wye, and delta connections as:

$$\mathbf{M}^{\mathbf{s}^{\mathsf{f},\mathsf{Y}}} := \frac{\partial|\mathbf{s}^{\mathsf{f},\mathsf{abc}}|^2}{\partial \mathbf{s}_{\mathsf{L}}^{\mathsf{Y}}} := 2\Big(\operatorname{diag}\left(\Re(\mathbf{s}^{\mathsf{f},\mathsf{abc}})\right), \operatorname{diag}\left(\Im(\mathbf{s}^{\mathsf{f},\mathsf{abc}})\right)\Big) \begin{bmatrix} \Re(\frac{\partial \mathbf{s}^{\mathsf{f},\mathsf{abc}}}{\partial \mathbf{s}_{\mathsf{L}}^{\mathsf{Y}}}) \\ \Im(\frac{\partial \mathbf{s}^{\mathsf{f},\mathsf{abc}}}{\partial \mathbf{s}_{\mathsf{L}}^{\mathsf{Y}}}) \end{bmatrix}, \tag{3.54a}$$

$$\mathbf{M}^{\mathbf{s}^{\mathsf{f},\Delta}} := \frac{\partial|\mathbf{s}^{\mathsf{f},\mathsf{abc}}|^2}{\partial \mathbf{s}_{\mathsf{L}}^{\Delta}} := 2\Big(\operatorname{diag}\left(\Re(\mathbf{s}^{\mathsf{f},\mathsf{abc}})\right), \operatorname{diag}\left(\Im(\mathbf{s}^{\mathsf{f},\mathsf{abc}})\right)\Big) \begin{bmatrix} \Re(\frac{\partial \mathbf{s}^{\mathsf{f},\mathsf{abc}}}{\partial \mathbf{s}_{\mathsf{L}}^{\Delta}}) \\ \Im(\frac{\partial \mathbf{s}^{\mathsf{f},\mathsf{abc}}}{\partial \mathbf{s}_{\mathsf{L}}^{\Delta}}) \end{bmatrix}. \tag{3.54b}$$

Now, we follow the chain rule of (3.26), used to obtain the equivalent single-phase model's sensitivities. To this end, first consider complex-valued sensitivity of line flows (3.47a) from with respect to voltage,

$$\frac{\partial \mathbf{s}^{\mathsf{f},\mathsf{abc}}}{\partial \mathbf{u}_{\mathsf{L}}^{\mathsf{abc}}} := \operatorname{diag}(\overline{\mathbf{Y}}_0^{\mathsf{f},\mathsf{abc}}\overline{\mathbf{u}}_0^{\mathsf{abc}} + \overline{\mathbf{Y}}_{\mathsf{L}}^{\mathsf{f},\mathsf{abc}}\overline{\mathbf{u}}_{\mathsf{L}}^{\mathsf{abc}})\mathbf{A}_{\mathsf{L}}^{\mathsf{f},\mathsf{abc}} + \operatorname{diag}(\mathbf{A}_0^{\mathsf{f},\mathsf{abc}}\overline{\mathbf{u}}_0^{\mathsf{abc}} + \mathbf{A}_{\mathsf{L}}^{\mathsf{f},\mathsf{abc}}\overline{\mathbf{u}}_{\mathsf{L}}^{\mathsf{abc}})\mathbf{Y}_{\mathsf{L}}^{\mathsf{f},\mathsf{abc}} \in \mathbb{C}^{3m\times 3n} \tag{3.55}$$

then combining it with (3.51) to obtain:

$$\begin{bmatrix} \Re(\frac{\partial \mathbf{s}^{\mathsf{f},\mathsf{abc}}}{\partial \mathbf{s}_{\mathsf{L}}^{\mathsf{Y}}}) \\ \Im(\frac{\partial \mathbf{s}^{\mathsf{f},\mathsf{abc}}}{\partial \mathbf{s}_{\mathsf{L}}^{\mathsf{Y}}}) \end{bmatrix} := \begin{bmatrix} \Re\Big(\frac{\partial \mathbf{s}^{\mathsf{f},\mathsf{abc}}}{\partial \mathbf{u}_{\mathsf{L}}^{\mathsf{abc}}} \cdot \mathbf{M}^{\mathsf{Y}}\Big) \\ \Im\Big(\frac{\partial \mathbf{s}^{\mathsf{f},\mathsf{abc}}}{\partial \mathbf{u}_{\mathsf{L}}^{\mathsf{abc}}} \cdot \mathbf{M}^{\mathsf{Y}}\Big) \end{bmatrix} \in \mathbb{R}^{6m\times 6n}. \tag{3.56a}$$

$$\begin{bmatrix} \Re(\frac{\partial \mathbf{s}^{\mathsf{f},\mathsf{abc}}}{\partial \mathbf{s}_{\mathsf{L}}^{\Delta}}) \\ \Im(\frac{\partial \mathbf{s}^{\mathsf{f},\mathsf{abc}}}{\partial \mathbf{s}_{\mathsf{L}}^{\Delta}}) \end{bmatrix} := \begin{bmatrix} \Re\Big(\frac{\partial \mathbf{s}^{\mathsf{f},\mathsf{abc}}}{\partial \mathbf{u}_{\mathsf{L}}^{\mathsf{abc}}} \cdot \mathbf{M}^{\Delta}\Big) \\ \Im\Big(\frac{\partial \mathbf{s}^{\mathsf{f},\mathsf{abc}}}{\partial \mathbf{u}_{\mathsf{L}}^{\mathsf{abc}}} \cdot \mathbf{M}^{\Delta}\Big) \end{bmatrix} \in \mathbb{R}^{6m\times 6n} \tag{3.56b}$$

For no-load condition, we have the no load version of the sensitivity term in (3.55), as

$$\frac{\partial \mathbf{s}^{\mathsf{f},\mathsf{abc}}}{\partial \mathbf{w}^{\mathsf{abc}}} := \operatorname{diag}(\overline{\mathbf{Y}}_0^{\mathsf{f},\mathsf{abc}}\overline{\mathbf{u}}_0^{\mathsf{abc}} + \overline{\mathbf{Y}}_{\mathsf{L}}^{\mathsf{f},\mathsf{abc}}\overline{\mathbf{w}}^{\mathsf{abc}})\mathbf{A}_{\mathsf{L}}^{\mathsf{f},\mathsf{abc}} + \operatorname{diag}(\mathbf{A}_0^{\mathsf{f},\mathsf{abc}}\overline{\mathbf{u}}_0^{\mathsf{abc}} + \mathbf{A}_{\mathsf{L}}^{\mathsf{f},\mathsf{abc}}\overline{\mathbf{w}}^{\mathsf{abc}})\mathbf{Y}_{\mathsf{L}}^{\mathsf{f},\mathsf{abc}} \in \mathbb{C}^{3m\times 3n} \tag{3.57}$$

with the required no load coefficient obtained as:

$$\hat{\mathbf{b}} := \begin{bmatrix} \Re\Big(\frac{\partial \mathbf{s}^{\mathsf{f}}}{\partial \mathbf{w}^{\mathsf{abc}}} \cdot \mathbf{w}^{\mathsf{abc}}\Big) \\ \Im\Big(\frac{\partial \mathbf{s}^{\mathsf{f}}}{\partial \mathbf{w}^{\mathsf{abc}}} \cdot \mathbf{w}^{\mathsf{abc}}\Big) \end{bmatrix} \in \mathbb{R}^{2m}. \tag{3.58}$$

Exactly similar procedure exists for (3.50c) and is left here in the interest of space.

Linearized system losses [(3.50d)**,** (3.50e)**]** First, consider the complex-valued system loss sensitivity of (3.47b) with respect to voltages as:

$$\frac{\partial s^{\mathrm{l,abc}}}{\partial \mathbf{u}_{\mathrm{L}}^{\mathrm{abc}}} := \mathbf{u}_{0}^{\mathrm{abc}\mathsf{T}}\overline{\mathbf{Y}}_{0\mathrm{L}}^{\mathrm{abc}} + (\mathbf{Y}_{\mathrm{L}0}^{\mathrm{abc}}\mathbf{u}_{0}^{\mathrm{abc}} + \mathbf{Y}_{\mathrm{LL}}^{\mathrm{abc}}\mathbf{u}_{\mathrm{L}}^{\mathrm{abc}})^{\mathsf{T}} + \mathbf{u}_{\mathrm{L}}^{\mathrm{abc}\mathsf{T}}\overline{\mathbf{Y}}_{\mathrm{LL}}^{\mathrm{abc}} \in \mathbb{C}^{1\times 3n}. \tag{3.59}$$

Similar to equivalent single-phase model, we follow the chain rule (3.28) and combine it with (3.51) to obtain:

$$\begin{bmatrix}\mathbf{M}^{p^{\mathrm{l,Y}}}\\ \mathbf{M}^{q^{\mathrm{l,Y}}}\end{bmatrix} := \begin{bmatrix}\Re(\frac{\partial \mathbf{s}_{\mathrm{L}}^{\mathrm{l}}}{\partial \mathbf{s}_{\mathrm{L}}^{\mathrm{Y}}})\\ \Im(\frac{\partial \mathbf{s}_{\mathrm{L}}^{\mathrm{l}}}{\partial \mathbf{s}_{\mathrm{L}}^{\mathrm{Y}}})\end{bmatrix} := \begin{bmatrix}\Re\Big(\frac{\partial \mathbf{s}^{\mathrm{l,abc}}}{\partial \mathbf{u}_{\mathrm{L}}^{\mathrm{abc}}}\cdot \mathbf{M}^{\mathrm{Y}}\Big)\\ \Im\Big(\frac{\partial \mathbf{s}^{\mathrm{l,abc}}}{\partial \mathbf{u}_{\mathrm{L}}^{\mathrm{abc}}}\cdot \mathbf{M}^{\mathrm{Y}}\Big)\end{bmatrix} \in \mathbb{R}^{2\times 6n} \tag{3.60a}$$

$$\begin{bmatrix}\mathbf{M}^{p^{\mathrm{l},\Delta}}\\ \mathbf{M}^{q^{\mathrm{l},\Delta}}\end{bmatrix} := \begin{bmatrix}\Re(\frac{\partial \mathbf{s}_{\mathrm{L}}^{\mathrm{l}}}{\partial \mathbf{s}_{\mathrm{L}}^{\Delta}})\\ \Im(\frac{\partial \mathbf{s}_{\mathrm{L}}^{\mathrm{l}}}{\partial \mathbf{s}_{\mathrm{L}}^{\Delta}})\end{bmatrix} := \begin{bmatrix}\Re\Big(\frac{\partial \mathbf{s}^{\mathrm{l,abc}}}{\partial \mathbf{u}_{\mathrm{L}}^{\mathrm{abc}}}\cdot \mathbf{M}^{\Delta}\Big)\\ \Im\Big(\frac{\partial \mathbf{s}^{\mathrm{l,abc}}}{\partial \mathbf{u}_{\mathrm{L}}^{\mathrm{abc}}}\cdot \mathbf{M}^{\Delta}\Big)\end{bmatrix} \in \mathbb{R}^{2\times 6n} \tag{3.60b}$$

Finally, in order to complete the loss approximation (3.50d), (3.50e), we obtain no-load loss sensitivity term as:

$$\frac{\partial s^{\mathrm{l,abc}}}{\partial \mathbf{w}_{\mathrm{L}}^{\mathrm{abc}}} := \mathbf{u}_{0}^{\mathrm{abc}\mathsf{T}}\overline{\mathbf{Y}}_{0\mathrm{L}}^{\mathrm{abc}} + (\mathbf{Y}_{\mathrm{L}0}^{\mathrm{abc}}\mathbf{u}_{0}^{\mathrm{abc}} + \mathbf{Y}_{\mathrm{LL}}^{\mathrm{abc}}\mathbf{w}^{\mathrm{abc}})^{\mathsf{T}} + \mathbf{w}^{\mathrm{abc}\mathsf{T}}\overline{\mathbf{Y}}_{\mathrm{LL}}^{\mathrm{abc}} \in \mathbb{C}^{1\times 3n}. \tag{3.61}$$

with the required coefficients now obtained as:

$$\begin{bmatrix}\hat{d}\\ \hat{e}\end{bmatrix} := \begin{bmatrix}\Re\Big(\frac{\partial \mathbf{s}^{\mathrm{l}}}{\partial \mathbf{w}^{\mathrm{abc}}}\cdot \mathbf{w}^{\mathrm{abc}}\Big)\\ \Im\Big(\frac{\partial \mathbf{s}^{\mathrm{l}}}{\partial \mathbf{w}^{\mathrm{abc}}}\cdot \mathbf{w}^{\mathrm{abc}}\Big)\end{bmatrix} \in \mathbb{R}. \tag{3.62}$$

Example 3.10

For the considered multi-phase grid in Fig. 3.12, we present verification for global approximation method. To this end, we do continuation analysis which varies grid loading as $\mathbf{s}_{\mathrm{L}}^{\mathrm{Y}} = \kappa\hat{\mathbf{s}}_{\mathrm{L}}^{\mathrm{Y}}$ and $\mathbf{s}_{\mathrm{L}}^{\Delta} = \kappa\hat{\mathbf{s}}_{\mathrm{L}}^{\Delta}$, where $\kappa \in [-0.5, 1.5]$ and $\hat{\mathbf{s}}_{\mathrm{L}}^{\mathrm{Y}}/\hat{\mathbf{s}}_{\mathrm{L}}^{\Delta}$ are the rated loading given in example 3.8, with a corresponding solution $\hat{\mathbf{u}}_{\mathrm{L}}^{\mathrm{abc}}$. The voltage at the root (bus 0) for all phases imposed at 7.1996 kV (Line-Neutral) or 12.47 kV (Line-Line). For each step of the loading, the actual grid solution is obtained using the fixed-point *load-flow* equation (3.46) Fig. 3.14, 3.15 and 3.16 respectively present approximation of voltage magnitude, absolute line square flow "from" buses and system active and reactive power loss. We omit "to" buses line flows in this example as the procedure for obtaining them, the obtained results and their characteristics are very similar to "from" bus line flows.

Remark 3.7. Recall that, for single-phase equivalent model, we have double system loss and absolute squared power flows, when estimated using global approximation method at the desired solution point. From example 3.10, it can be seen that similar behavior is observed for the multi-phase system. Hence, the similar doubled system loss and squared flows proof exists for multi-phase grid.

The approximation matrices derived in this chapter resembles similarity to the market indexes of transmission grid. For example, $\mathbf{M}^{p^{\mathrm{l}}}$ and $\mathbf{M}^{s^{\mathrm{f}}}$ can be considered as distribution

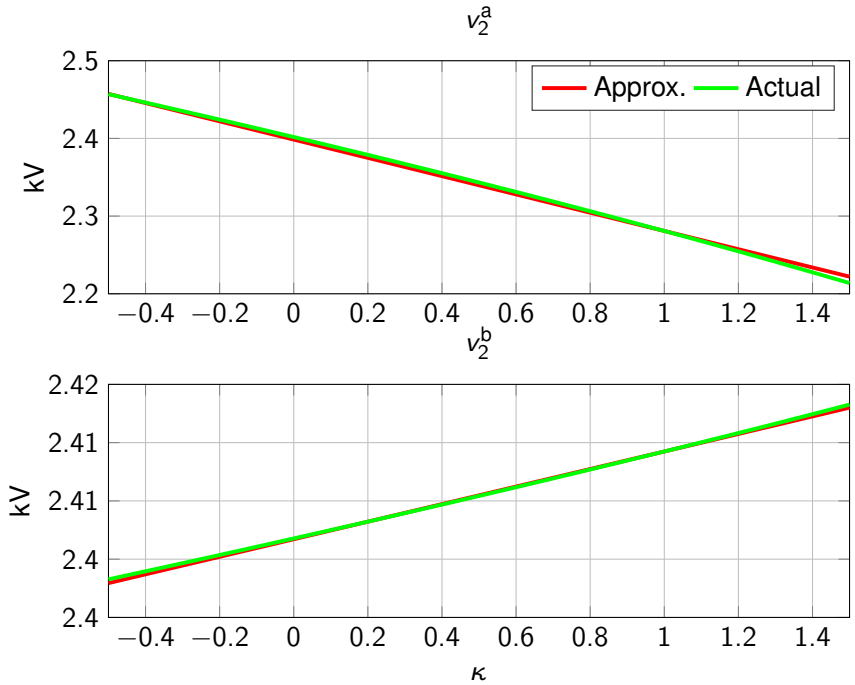

Figure 3.14: Voltage magnitude approximation for bus 2's phase a (top) and b (bottom) of the exemplary grid in Fig. 3.12.

grid's approximation of the famous Loss Factor (LF) and Power Transfer Distribution Factor (PTDF) matrices, deployed for calculating marginal loss and congestion prices in transmission grids [61, 54]. To this end, in the next chapter, we show how these approximations can help us in setting up distribution grid market framework. In doing so, we show that the derived sensitivity matrices of this chapter lend themselves naturally in decomposing the final price at the bus into its energy, loss, congestion and voltage components. As these decompositions are already existing for transmission grid wholesale markets, the presented market framework have a high chances of being favored when it comes to realizing distribution grid level markets. We show this in the next chapter.

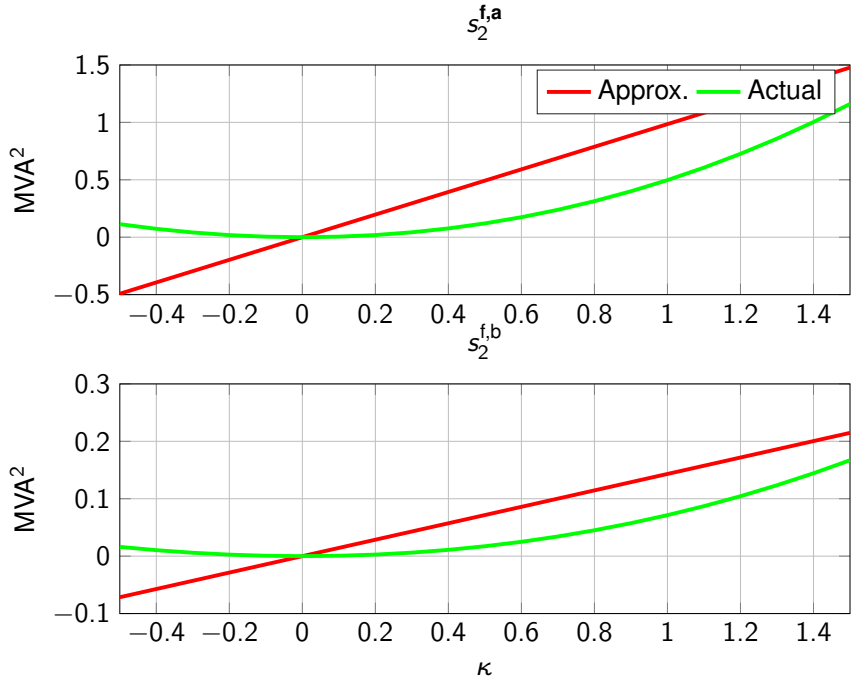

Figure 3.15: Absolute squared line flow “from” buses approximation for line 2’s phase a (top) and phase b (bottom) of the exemplary grid in Fig. 3.12.

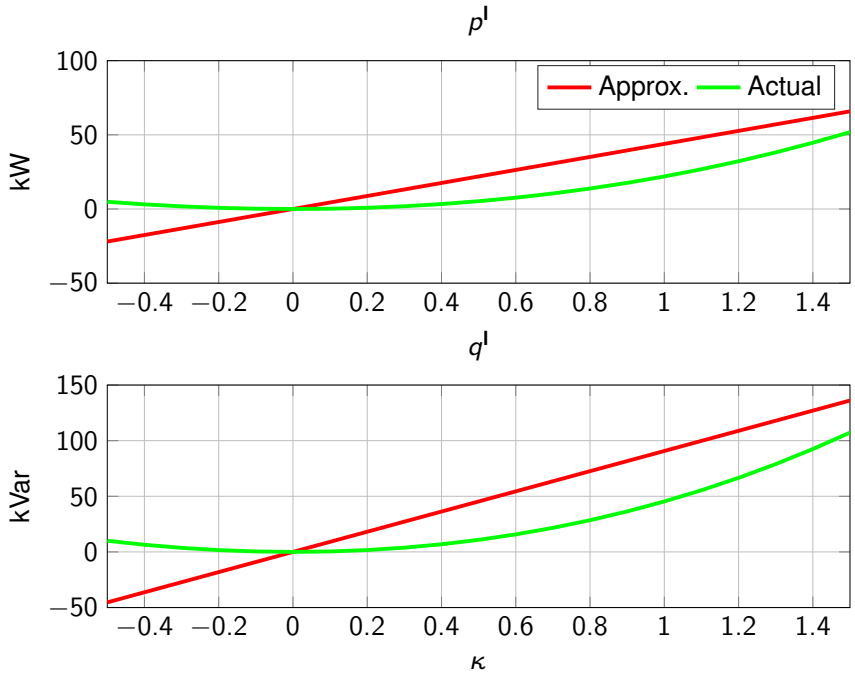

Figure 3.16: System active power loss (top) and reactive power loss (bottom) approximation of the exemplary grid in Fig. 3.12.

Chapter 4

Distribution Grid Economic Dispatch: Solution, Prices and Extensions

In this chapter, we collect concepts regarding convexity and grid approximation, presented in chapter 2 and 3 respectively and present Economic Dispatch (ED) problem for distribution grids. First, we deploy the optimality concepts of chapter 2 to derive the price, which resembles closely to the price formulation at the transmission level. We call this price as Distribution Locational Marginal Price (DLMP). Then, from the approximations derived in chapter 3, we provide a solution methodology for obtaining a Distribution Locational Marginal Price (DLMP). Regarding grid modeling, the explanation is first provided on equivalent single-phase grid models and then extended to multi-phase grid models.

The main contributions of this chapter are: i) proposing a tractable solution algorithm for calculating DLMPs and ii) utilizing approximation quantities developed in chapter 3 to aid in decomposing and physically interpreting DLMPs.

4.1 Distribution Grid Economic Dispatch Problem

In this section, Economic Dispatch (ED) for equivalent single-phase distribution grids is presented. First, a brief overview of the assumed system model is presented in Sec. 4.1.1. Then, Sec. 4.1.2 describes the optimization problem which is needed to be solved for achieving the ED in distribution grid. The main goal of this section is in deriving prices from the ED problem.

4.1.1 System Model

For the grid model, we use similar assumptions and notations as given in Sec. 3.1. However, we augment the grid model with flexibility resources, in order to be optimized in the ED problem. Apart from flexibility resources, we consider the grid to be also containing number of Constant Load (CL) which are always satisfied. The active powers of CLs are denoted as: $\mathbf{p}^{\mathrm{cl}} := (p_1^{\mathrm{cl}}, \ldots, p_n^{\mathrm{cl}})^\intercal$ and reactive power as: $\mathbf{q}^{\mathrm{cl}} := (q_1^{\mathrm{cl}}, \ldots, q_n^{\mathrm{cl}})^\intercal$. We also consider number of both Flexible Load (FL) and Distributed Generator (DG). The FLs are assumed to optimize their energy procurement cost of active powers $\mathbf{p}^{\mathrm{fl}} := (p_1^{\mathrm{fl}}, \ldots, p_n^{\mathrm{fl}})^\intercal$. As controlling reactive power $\mathbf{q}^{\mathrm{fl}} := (q_1^{\mathrm{fl}}, \ldots, q_n^{\mathrm{fl}})^\intercal$ is not a usual load behavior, it is kept as uncontrollable and modeled simply through a specified power factor. The DGs are assumed to optimize their instantaneous active powers $\mathbf{p}^{\mathrm{dg}} := (p_1^{\mathrm{dg}}, \ldots, p_n^{\mathrm{dg}})^\intercal$ and reactive powers $\mathbf{q}^{\mathrm{dg}} := (q_1^{\mathrm{dg}}, \ldots, q_n^{\mathrm{dg}})^\intercal$

independently [1]. Aggregation of low voltage PV systems with controllable active and reactive power support to the grid can be considered as a practical application of these types of DGs [109, 3, 97, 59].

Remark 4.1. For brevity, CLs and flexibility resources (FLs and DGs) are assumed of size n. However, one can see that the developed model is naturally extend-able to contain an arbitrary number of CLs, FLs and DGs. This is also demonstrated in (to be presented) examples of this chapter.

In the ED framework adopted in this chapter, it is assumed that DGs and FLs are price-taking, utility maximizing agents. To this end, the overall social welfare $w_p(\mathbf{p}^{\mathrm{fl}}, \mathbf{p}^{\mathrm{g}})$ as the aggregate benefit of DGs and FLs from the active power procurement is:

$$w_p(\mathbf{p}^{\mathrm{fl}}, \mathbf{p}^{\mathrm{g}}) = \Big(\mathbf{U}^{\mathrm{fl}}(\mathbf{p}^{\mathrm{fl}}) - \mathbf{C}^{\mathrm{g}}(\mathbf{p}^{\mathrm{g}})\Big), \tag{4.1}$$

where $\mathbf{p}^{\mathrm{g}} := (p^0, (\mathbf{p}^{\mathrm{dg}})^\intercal)^\intercal$ collects all individual DGs $\mathbf{p}^{\mathrm{dg}}$ and the root-bus p^0 with their marginal cost of supplying energy as $\mathbf{C}^{\mathrm{g}}(\mathbf{p}^{\mathrm{g}})$. The utility function of FLs is simply assumed as the negative cost of purchasing energy, i.e., $\mathbf{U}^{\mathrm{fl}}(\mathbf{p}^{\mathrm{fl}}) := -\mathbf{C}^{\mathrm{fl}}(\mathbf{p}^{\mathrm{fl}})$. See **R. 4.2** for the information regarding assumed cost/utility interpretations. We also consider reactive power costs in the model on the basis that reactive power pricing has been the subject of interest [12, 59, 28]. As only DGs optimize their reactive power dispatch, social welfare from reactive power procurement is:

$$w_q(\mathbf{q}^{\mathrm{g}}) = -\mathbf{C}^{\mathrm{g}}(\mathbf{q}^{\mathrm{g}}), \tag{4.2}$$

with total reactive power generations: $\mathbf{q}^{\mathrm{g}} := (q^0, (\mathbf{q}^{\mathrm{dg}})^\intercal)^\intercal$.

Remark 4.2. For all $x \in \{\mathrm{g}, \mathrm{fl}\}$ procuring power $y \in \{p, q\}$, costs are defined as $\mathbf{C}^x(\mathbf{y}^x) := \mathbf{c}_y^{x\intercal} \cdot \mathbf{y}^x$, where marginal cost is of the form $\mathbf{c}_y^x := \mathbf{a}_y^x + \mathbf{B}_y^x \mathbf{y}^x$ with a positive price per unit vector $\mathbf{a}_y^x \in \mathbb{R}^n$ (in \$/MWh) and symmetric, positive definite matrix $\mathbf{B}_y^x \in \mathbb{R}^{n\times n}$ of small positive price sensitivity coefficients (in \$/MWh^2), turning the social welfares introduced in (5.2) and (4.2) strictly convex. Regarding the cost interpretation, let λ be the cleared active power per unit price, then the cost/utility function for DGs/FLs in (5.2) is simply:

$$\mathbf{p}^{\mathrm{fl}} = \underset{\mathbf{p}^{\mathrm{fl}}\in\mathbb{R}^n}{\operatorname{argmax}}\ \mathbf{U}^{\mathrm{fl}}(\mathbf{p}^{\mathrm{fl}}) - \lambda\mathbf{p}^{\mathrm{fl}} = \max\left\{0, \left\{\mathbf{p}^{\mathrm{fl}} \mid \frac{\partial \mathbf{U}^{\mathrm{fl}}(\mathbf{p}^{\mathrm{fl}}))}{\partial \mathbf{p}^{\mathrm{fl}}} = \lambda\right\}\right\},$$
$$\mathbf{p}^{\mathrm{g}} = \underset{\mathbf{p}^{\mathrm{g}}\in\mathbb{R}^n}{\operatorname{argmax}}\ \lambda\mathbf{p}^{\mathrm{g}} - \mathbf{C}^{\mathrm{g}}(\mathbf{p}^{\mathrm{g}}) = \max\left\{0, \left\{\mathbf{p}^{\mathrm{g}} \mid \frac{\partial \mathbf{C}^{\mathrm{g}}(\mathbf{p}^{\mathrm{g}})}{\partial \mathbf{p}^{\mathrm{g}}} = \lambda\right\}\right\}.$$

Same interpretation holds for reactive power cost functions. Note that the above definitions are directly in spirit with the optimality discussion in Sec. 2.2.3, where it is shown how economically efficient ED is attained when independent price-taker agents' individual minimization problems turn to the overall social welfare of the system.

4.1.2 Economic Dispatch

From the generalized ED problem presented in Sec. 2.3, we now present its distribution grid variant. It is assumed that the distribution system operator (DSO) is responsible for running

[1] This assumption is realized through first specifying the maximum and minimum allowed power factor and then linearizing it to obtain reactive power dispatch capabilities [3].

the distribution grid ED, i.e. it collects all FLs'/DGs' individual supply/bid functions and then solves the following optimization problem:

$$\begin{aligned}
\text{maximize} \quad & w(\mathbf{p}^{\mathrm{fl}}, \mathbf{p}^{\mathrm{g}}, \mathbf{q}^{\mathrm{g}}) := w_p(\mathbf{p}^{\mathrm{fl}}, \mathbf{p}^{\mathrm{g}}) + w_q(\mathbf{q}^{\mathrm{g}}) && \text{(4.3a)}\\
\text{subject to} \quad & \mathbf{1}_{\mathrm{N}}^{\intercal}\mathbf{p}^{\mathrm{g}} - \mathbf{1}_{\mathrm{n}}^{\intercal}(\mathbf{p}^{\mathrm{cl}} + \mathbf{p}^{\mathrm{fl}}) = p^{\mathrm{l}} : \lambda^p && \text{(4.3b)}\\
& \mathbf{1}_{\mathrm{N}}^{\intercal}\mathbf{q}^{\mathrm{g}} - \mathbf{1}_{\mathrm{n}}^{\intercal}(\mathbf{q}^{\mathrm{cl}} + \mathbf{q}^{\mathrm{fl}}) = q^{\mathrm{l}} : \lambda^q && \text{(4.3c)}\\
& |\mathbf{s}^{\mathrm{f}}|^2 \leq (\mathbf{s}^{\mathrm{f}+})^2 && : \boldsymbol{\mu}_{s^{\mathrm{f}}}^{+} && \text{(4.3d)}\\
& |\mathbf{s}^{\mathrm{t}}|^2 \leq (\mathbf{s}^{\mathrm{t}+})^2 && : \boldsymbol{\mu}_{s^{\mathrm{t}}}^{+} && \text{(4.3e)}\\
& \mathbf{v}_{\mathrm{L}}^{-} \leq \mathbf{v}_{\mathrm{L}} \leq \mathbf{v}_{\mathrm{L}}^{+} && : \boldsymbol{\mu}_{\mathbf{v}_{\mathrm{L}}}^{-}, \boldsymbol{\mu}_{\mathbf{v}_{\mathrm{L}}}^{+} && \text{(4.3f)}\\
& \mathbf{p}^{\mathrm{dg}-} \leq \mathbf{p}^{\mathrm{dg}} \leq \mathbf{p}^{\mathrm{dg}+} && : \boldsymbol{\mu}_{\mathbf{p}}^{\mathrm{dg}-}, \boldsymbol{\mu}_{\mathbf{p}}^{\mathrm{dg}+} && \text{(4.3g)}\\
& \mathbf{q}^{\mathrm{dg}-} \leq \mathbf{q}^{\mathrm{dg}} \leq \mathbf{q}^{\mathrm{dg}+} && : \boldsymbol{\mu}_{\mathbf{q}}^{\mathrm{dg}-}, \boldsymbol{\mu}_{\mathbf{q}}^{\mathrm{dg}+} && \text{(4.3h)}\\
& \mathbf{p}^{\mathrm{fl}-} \leq \mathbf{p}^{\mathrm{fl}} \leq \mathbf{p}^{\mathrm{fl}+} && : \boldsymbol{\mu}_{\mathbf{p}}^{\mathrm{fl}-}, \boldsymbol{\mu}_{\mathbf{p}}^{\mathrm{fl}+} && \text{(4.3i)}
\end{aligned}$$

Constraints (4.3b) and (4.3c) respectively present global active and reactive power balance of the distribution grid. Consistent with the previous chapter, we denote active power loss as p^{l} and reactive power loss as q^{l}. Constraint (4.3i) dispatches FLs. All DGs' active/reactive power are constrained through (4.3g)/(4.3h), respectively. As mentioned in Sec. 4.1.1, the maximum and minimum reactive power limits are obtained with a ratio of reactive power to its corresponding nominal apparent power injections. Apparent power flowing in distribution grid lines from/to ends of the lines are constrained through (4.3d)/(4.3e). The variables listed to the right of each constraint (behind colon) are their respective Lagrangian multipliers. Note that the optimization problem in (4.3) is a classical global energy balance formulation, used to calculate LMPs [88, 82].

Remark 4.3. As classic marginal pricing [88] contains power flows as congestion components, we also opt for them. However, an extension of this model to consider thermal limits (in Amperage) can also be performed, as shown in [9, Appendix].

4.2 Distribution Locational Marginal Price

4.2.1 Derivation

Based on the ED problem in (4.3), this section derives DLMPs. First, we follow the generic procedure of Sec. 2.2.2, where the obtained prices achieved individual cost minimization and overall social welfare maximization. Consider Lagrangian of (4.3):

$$\begin{aligned}
&\mathcal{L}(\mathbf{p}^{\mathrm{g}}, \mathbf{p}^{\mathrm{fl}}, \mathbf{q}^{\mathrm{g}}, \lambda^p, \lambda^q, \boldsymbol{\mu}_{s^{\mathrm{f}}}^{+}, \boldsymbol{\mu}_{s^{\mathrm{t}}}^{+}, \boldsymbol{\mu}_{\mathbf{v}_{\mathrm{L}}}^{-}, \boldsymbol{\mu}_{\mathbf{v}_{\mathrm{L}}}^{+}, \boldsymbol{\mu}_{\mathbf{p}}^{\mathrm{dg}-}, \boldsymbol{\mu}_{\mathbf{p}}^{\mathrm{dg}+}, \boldsymbol{\mu}_{\mathbf{q}}^{\mathrm{dg}-}, \boldsymbol{\mu}_{\mathbf{q}}^{\mathrm{dg}+}, \boldsymbol{\mu}_{\mathbf{p}}^{\mathrm{fl}-}, \boldsymbol{\mu}_{\mathbf{p}}^{\mathrm{fl}+}) = w(\mathbf{p}^{\mathrm{fl}}, \mathbf{p}^{\mathrm{g}}, \mathbf{q}^{\mathrm{g}})\\
&- \lambda^p\left(\mathbf{1}_{\mathrm{N}}^{\intercal}\mathbf{p}^{\mathrm{g}} - \mathbf{1}_{\mathrm{n}}^{\intercal}(\mathbf{p}^{\mathrm{cl}} + \mathbf{p}^{\mathrm{fl}}) - p^{l}\right) - \lambda^q\left(\mathbf{1}_{\mathrm{N}}^{\intercal}\mathbf{q}^{\mathrm{g}} - \mathbf{1}_{\mathrm{n}}^{\intercal}(\mathbf{q}^{\mathrm{cl}} + \mathbf{q}^{\mathrm{fl}}) - q^{l}\right) - (\boldsymbol{\mu}_{s^{\mathrm{f}}}^{+})^{\intercal}\left(|\mathbf{s}^{\mathrm{f}}|^2 - (\mathbf{s}^{\mathrm{f}+})^2\right)\\
&- (\boldsymbol{\mu}_{s^{\mathrm{t}}}^{+})^{\intercal}\left(|\mathbf{s}^{\mathrm{f}}|^2 - |\mathbf{s}^{\mathrm{f}+}|^2\right) - (\boldsymbol{\mu}_{\mathbf{v}_{\mathrm{L}}}^{+})^{\intercal}\left(\mathbf{v}_{\mathrm{L}} - \mathbf{v}_{\mathrm{L}}^{+}\right) - (\boldsymbol{\mu}_{\mathbf{v}_{\mathrm{L}}}^{-})^{\intercal}\left(\mathbf{v}_{\mathrm{L}}^{-} - \mathbf{v}_{\mathrm{L}}\right)\\
&- (\boldsymbol{\mu}_{\mathbf{p}}^{\mathrm{dg}+})^{\intercal}\left(\mathbf{p}^{\mathrm{dg}} - \mathbf{p}^{\mathrm{dg}+}\right) - (\boldsymbol{\mu}_{\mathbf{p}}^{\mathrm{dg}-})^{\intercal}\left(\mathbf{p}^{\mathrm{dg}-} - \mathbf{p}^{\mathrm{dg}}\right) - (\boldsymbol{\mu}_{\mathbf{q}}^{\mathrm{dg}+})^{\intercal}\left(\mathbf{q}^{\mathrm{dg}} - \mathbf{q}^{\mathrm{dg}+}\right)\\
&- (\boldsymbol{\mu}_{\mathbf{q}}^{\mathrm{dg}-})^{\intercal}\left(\mathbf{q}^{\mathrm{dg}-} - \mathbf{q}^{\mathrm{dg}}\right) - (\boldsymbol{\mu}_{\mathbf{p}}^{\mathrm{fl}+})^{\intercal}\left(\mathbf{p}^{\mathrm{fl}} - \mathbf{q}^{\mathrm{fl}+}\right) - (\boldsymbol{\mu}_{\mathbf{p}}^{\mathrm{fl}-})^{\intercal}\left(\mathbf{p}^{\mathrm{fl}-} - \mathbf{p}^{\mathrm{fl}}\right) \qquad \text{(4.4)}
\end{aligned}$$

Now from the optimality conditions, for a given solution of (4.3), we have satisfaction of the following KKT conditions:

$$\frac{\partial w(\mathbf{p}^{\mathsf{fl}}, \mathbf{p}^{\mathsf{g}}, \mathbf{q}^{\mathsf{g}})}{\partial \mathbf{p}^{\mathsf{g}}} - \lambda^{p}\mathbf{1}_{\mathsf{N}} - (\frac{\partial p^{l}}{\partial \mathbf{p}^{\mathsf{g}}})^{\mathsf{T}}\lambda^{p} - (\frac{\partial q^{l}}{\partial \mathbf{p}^{\mathsf{g}}})^{\mathsf{T}}\lambda^{q} - (\frac{\partial |\mathbf{s}^{\mathsf{f}}|^2}{\partial \mathbf{p}^{\mathsf{g}}})^{\mathsf{T}}\boldsymbol{\mu}_{s^{\mathsf{f}}} - (\frac{\partial |\mathbf{s}^{\mathsf{t}}|^2}{\partial \mathbf{p}^{\mathsf{g}}})^{\mathsf{T}}\boldsymbol{\mu}_{s^{\mathsf{t}}}$$
$$-(\frac{\partial \mathbf{v}_{\mathsf{L}}}{\partial \mathbf{p}^{\mathsf{g}}})^{\mathsf{T}}(\boldsymbol{\mu}^{+}_{\mathbf{v}_{\mathsf{L}}} - \boldsymbol{\mu}^{-}_{\mathbf{v}_{\mathsf{L}}}) - (\boldsymbol{\mu}^{\mathsf{dg}+}_{\mathbf{p}} - \boldsymbol{\mu}^{\mathsf{dg}-}_{\mathbf{p}}) = \mathbf{0}, \tag{4.5a}$$

$$\frac{\partial w(\mathbf{p}^{\mathsf{fl}}, \mathbf{q}^{\mathsf{g}}, \mathbf{q}^{\mathsf{g}})}{\partial \mathbf{q}^{\mathsf{g}}} - \lambda^{q}\mathbf{1}_{\mathsf{N}} - (\frac{\partial p^{l}}{\partial \mathbf{q}^{\mathsf{g}}})^{\mathsf{T}}\lambda^{p} - (\frac{\partial q^{l}}{\partial \mathbf{q}^{\mathsf{g}}})^{\mathsf{T}}\lambda^{q} - (\frac{\partial |\mathbf{s}^{\mathsf{f}}|^2}{\partial \mathbf{q}^{\mathsf{g}}})^{\mathsf{T}}\boldsymbol{\mu}_{s^{\mathsf{f}}} - (\frac{\partial |\mathbf{s}^{\mathsf{t}}|^2}{\partial \mathbf{q}^{\mathsf{g}}})^{\mathsf{T}}\boldsymbol{\mu}_{s^{\mathsf{t}}}$$
$$-(\frac{\partial \mathbf{v}_{\mathsf{L}}}{\partial \mathbf{q}^{\mathsf{g}}})^{\mathsf{T}}(\boldsymbol{\mu}^{+}_{\mathbf{v}_{\mathsf{L}}} - \boldsymbol{\mu}^{-}_{\mathbf{v}_{\mathsf{L}}}) - (\boldsymbol{\mu}^{\mathsf{dg}+}_{\mathbf{q}} - \boldsymbol{\mu}^{\mathsf{dg}-}_{\mathbf{q}}) = \mathbf{0}, \tag{4.5b}$$

$$\frac{\partial w(\mathbf{p}^{\mathsf{fl}}, \mathbf{p}^{\mathsf{g}}, \mathbf{q}^{\mathsf{g}})}{\partial \mathbf{p}^{\mathsf{fl}}} + \lambda^{p}\mathbf{1}_{\mathsf{n}} + (\frac{\partial p^{l}}{\partial \mathbf{p}^{\mathsf{fl}}})^{\mathsf{T}}\lambda^{p} + (\frac{\partial q^{l}}{\partial \mathbf{p}^{\mathsf{fl}}})^{\mathsf{T}}\lambda^{q} + (\frac{\partial |\mathbf{s}^{\mathsf{f}}|^2}{\partial \mathbf{p}^{\mathsf{fl}}})^{\mathsf{T}}\boldsymbol{\mu}_{s^{\mathsf{f}}} + (\frac{\partial |\mathbf{s}^{\mathsf{t}}|^2}{\partial \mathbf{p}^{\mathsf{fl}}})^{\mathsf{T}}\boldsymbol{\mu}_{s^{\mathsf{t}}}$$
$$+(\frac{\partial \mathbf{v}_{\mathsf{L}}}{\partial \mathbf{p}^{\mathsf{fl}}})^{\mathsf{T}}(\boldsymbol{\mu}^{+}_{\mathbf{v}_{\mathsf{L}}} - \boldsymbol{\mu}^{-}_{\mathbf{v}_{\mathsf{L}}}) + (\boldsymbol{\mu}^{\mathsf{fl}+}_{\mathbf{p}} - \boldsymbol{\mu}^{\mathsf{fl}-}_{\mathbf{p}}) = \mathbf{0}, \tag{4.5c}$$

$$\boldsymbol{\mu}_{s^{\mathsf{f}}}(|\underline{\mathbf{s}}^{\mathsf{f}}|^2 - (\mathbf{s}^{\mathsf{f}+})^2) = 0, \tag{4.5d}$$
$$\boldsymbol{\mu}_{s^{\mathsf{f}}}(|\underline{\mathbf{s}}^{\mathsf{t}}|^2 - (\mathbf{s}^{\mathsf{t}+})^2) = 0, \tag{4.5e}$$
$$\boldsymbol{\mu}^{+}_{\mathbf{v}_{\mathsf{L}}}(\mathbf{v}_{\mathsf{L}} - \mathbf{v}^{+}_{\mathsf{L}}) = \mathbf{0}, \tag{4.5f}$$
$$\boldsymbol{\mu}^{-}_{\mathbf{v}_{\mathsf{L}}}(-\mathbf{v}_{\mathsf{L}} + \mathbf{v}^{-}_{\mathsf{L}}) = \mathbf{0}, \tag{4.5g}$$
$$\boldsymbol{\mu}^{\mathsf{dg}+}_{\mathbf{p}}(\mathbf{p}^{\mathsf{dg}} - \mathbf{p}^{\mathsf{dg}+}) = \mathbf{0}, \tag{4.5h}$$
$$\boldsymbol{\mu}^{\mathsf{dg}-}_{\mathbf{p}}(-\mathbf{p}^{\mathsf{dg}} + \mathbf{p}^{\mathsf{dg}+}) = \mathbf{0}, \tag{4.5i}$$
$$\boldsymbol{\mu}^{\mathsf{dg}+}_{\mathbf{q}}(\mathbf{q}^{\mathsf{dg}} - \mathbf{q}^{\mathsf{dg}+}) = \mathbf{0}, \tag{4.5j}$$
$$\boldsymbol{\mu}^{\mathsf{dg}-}_{\mathbf{q}}(-\mathbf{q}^{\mathsf{dg}} + \mathbf{q}^{\mathsf{dg}+}) = \mathbf{0}, \tag{4.5k}$$
$$\boldsymbol{\mu}^{\mathsf{fl}+}_{\mathbf{p}}(\mathbf{p}^{\mathsf{fl}} - \mathbf{p}^{\mathsf{fl}+}) = \mathbf{0}, \tag{4.5l}$$
$$\boldsymbol{\mu}^{\mathsf{fl}-}_{\mathbf{p}}(-\mathbf{p}^{\mathsf{fl}} + \mathbf{p}^{\mathsf{fl}+}) = \mathbf{0}, \tag{4.5m}$$

along with primal feasibility conditions [(4.3b) – (4.3i)] and all inequality Lagrange multipliers to be non-negative, i.e.,

$$\Big((\boldsymbol{\mu}^{+}_{s^{\mathsf{f}}})^{\mathsf{T}}, (\boldsymbol{\mu}^{+}_{s^{\mathsf{t}}})^{\mathsf{T}}, (\boldsymbol{\mu}^{-}_{\mathbf{v}_{\mathsf{L}}})^{\mathsf{T}}, (\boldsymbol{\mu}^{+}_{\mathbf{v}_{\mathsf{L}}})^{\mathsf{T}}, (\boldsymbol{\mu}^{\mathsf{dg}-}_{\mathbf{p}})^{\mathsf{T}}, (\boldsymbol{\mu}^{\mathsf{dg}+}_{\mathbf{p}})^{\mathsf{T}}, (\boldsymbol{\mu}^{\mathsf{dg}-}_{\mathbf{q}})^{\mathsf{T}}, (\boldsymbol{\mu}^{\mathsf{dg}+}_{\mathbf{q}})^{\mathsf{T}}, (\boldsymbol{\mu}^{\mathsf{fl}-}_{\mathbf{p}})^{\mathsf{T}}, (\boldsymbol{\mu}^{\mathsf{fl}+}_{\mathbf{p}})^{\mathsf{T}}\Big)^{\mathsf{T}} \succeq \mathbf{0}.$$

Note that compared to stationary conditions (4.5a), (4.5b), in stationary conditions (4.5c), the sign reversal is due to convention that demand is actually a negative injection, i.e., for generic injection variable $\mathbf{p}$ we have the convention $\mathbf{p} := \mathbf{p}^{\mathsf{g}} - \mathbf{p}^{\mathsf{fl}}$. Hence, for any grid variable $(\cdot)$, the derivative follows the rule:

$$\frac{\partial \mathcal{L}}{\partial \mathbf{p}^{\mathsf{fl}}} = \frac{\partial \mathcal{L}}{\partial (\cdot)}\frac{\partial (\cdot)}{\partial \mathbf{p}^{\mathsf{fl}}},$$

where partial derivative of the grid variable $(\cdot)$ is obtained as:

$$\frac{\partial (\cdot)}{\partial \mathbf{p}^{\mathsf{fl}}} = \frac{\partial (\cdot)}{\partial \mathbf{p}}\frac{\partial \mathbf{p}}{\partial \mathbf{p}^{\mathsf{fl}}} = \frac{\partial (\cdot)}{\partial \mathbf{p}}(-1).$$

As explained in the demonstrative example 2.2, the optimal price recovered from ED problem enforces condition of all supply functions (from generators) to be equal to the bid functions (from flexible demand). We follow the similar line of arguments to find DLMPs in (4.3) as follows.

First, we obtain the relationship of root-bus with respect to power deliverance to the distribution grids. Note that in (4.5), the only stationary conditions providing the relationship to the root-bus is given in (4.5a). Moreover, from the distribution grid modeling setup explained in chapter 3, we have voltages at the root-bus fixed, and not as the solution of the *load-flow* problem. Hence, with respect to root-bus there exists no sensitivity of root-bus with respect to the *load-flow* solution variables, i.e. all sensitivity terms in (4.5a) are zero, except the cost term (first term in (4.5a)). Hence, at the root-bus, we have the following relationship.

$$c_p^0 = \lambda^p, \qquad \text{and} \qquad c_q^0 = \lambda^q, \tag{4.6}$$

where consistent from the definition in **R. 4.2**, c_p^0 and c_q^0 are the marginal cost of providing power at the root-bus.

Second, we define the marginal value of supplying active and reactive power by flexibility resources, i.e. active power from DGs $\boldsymbol{\Pi}^{\text{flex}}_{\mathbf{p}^{\text{dg}}}$ and FLs $\boldsymbol{\Pi}^{\text{flex}}_{\mathbf{p}^{\text{fl}}}$ and reactive power by generation $\boldsymbol{\Pi}^{\text{Flex}}_{\mathbf{q}^{\text{g}}}$ as:

$$\boldsymbol{\Pi}^{\text{Flex}}_{\mathbf{p}^{\text{dg}}} := -\mathbf{c}^{\text{dg}}_{\mathbf{p}} + \boldsymbol{\mu}^{\text{dg}+}_{\mathbf{p}} - \boldsymbol{\mu}^{\text{dg}-}_{\mathbf{p}}, \tag{4.7}$$

$$\boldsymbol{\Pi}^{\text{Flex}}_{\mathbf{q}^{\text{g}}} := -\mathbf{c}^{\text{dg}}_{\mathbf{q}} + \boldsymbol{\mu}^{\text{dg}+}_{\mathbf{q}} - \boldsymbol{\mu}^{\text{dg}-}_{\mathbf{q}}, \tag{4.8}$$

$$\boldsymbol{\Pi}^{\text{Flex}}_{\mathbf{p}^{\text{fl}}} := \mathbf{c}^{\text{dg}}_{\mathbf{p}} - \boldsymbol{\mu}^{\text{fl}+}_{\mathbf{p}} + \boldsymbol{\mu}^{\text{fl}-}_{\mathbf{p}}. \tag{4.9}$$

In the above definitions, it can be observed that marginal values of supplying flexibility resources are simply linear combinations of their internal marginal costs ($\mathbf{c}^{\text{dg}}_{\mathbf{p}}, \mathbf{c}^{\text{dg}}_{\mathbf{q}}, \mathbf{c}^{\text{fl}}_{\mathbf{p}}$) of energy procurement and maximum and minimum dispatch limitations ($\boldsymbol{\mu}^{\text{dg}+}_{\mathbf{p}}, \boldsymbol{\mu}^{\text{dg}-}_{\mathbf{p}}, \boldsymbol{\mu}^{\text{dg}+}_{\mathbf{q}}, \boldsymbol{\mu}^{\text{dg}-}_{\mathbf{q}}, \boldsymbol{\mu}^{\text{fl}+}_{\mathbf{p}}, \boldsymbol{\mu}^{\text{fl}-}_{\mathbf{p}}$). Hence, it can be concluded that these marginal values represent internal constraints of all flexibility resources.

Finally, from the definition of grid cleared price, the DLMP must exist in equilibrium with marginal value of satisfying grid conditions and supplying dispatch from flexibility resources. This can be written as the following equivalence condition:

$$\boldsymbol{\Pi}^{\text{Grid}}_{\mathbf{p}} = \boldsymbol{\Pi}^{\text{Flex}}_{\mathbf{p}^{\text{dg}}} = \Pi^{\text{Flex}}_{\mathbf{p}^{\text{fl}}}, \tag{4.10}$$

$$\boldsymbol{\Pi}^{\text{Grid}}_{\mathbf{q}} = \boldsymbol{\Pi}^{\text{Flex}}_{\mathbf{q}^{\text{g}}} \tag{4.11}$$

where $\boldsymbol{\Pi}^{\text{Grid}}_{\mathbf{p}}$/$\boldsymbol{\Pi}^{\text{Grid}}_{\mathbf{q}}$ represent marginal value of delivering active/reactive power at all grid buses. We call this value DLMP, as this value exists in equilibrium with grid conditions and marginal values of flexibility resources. To this end, we obtain DLMP using the following manipulations:

1. by substituting [(4.7) – (4.9)] into stationary KKT conditions (4.5a) – (4.5c),
2. utilizing the equilibrium conditions [(4.10), (4.11)] and
3. using the equivalence of marginal value of delivering power at root-bus (4.6).

This yields the following expression of DLMP for all n grid buses:

$$\boldsymbol{\Pi}^{\text{Grid}}_{\mathbf{p}} = c_p^0 \mathbf{1}_{\text{n}} + (\frac{\partial p^{\prime}}{\partial \mathbf{p}})^{\intercal} c_p^0 + (\frac{\partial q^{\prime}}{\partial \mathbf{p}})^{\intercal} c_q^0 + (\frac{\partial |\mathbf{s}^{\text{f}}|^2}{\partial \mathbf{p}})^{\intercal} \boldsymbol{\mu}_{s^{\text{f}}} + (\frac{\partial |\mathbf{s}^{\text{t}}|^2}{\partial \mathbf{p}})^{\intercal} \boldsymbol{\mu}_{s^{\text{t}}} + (\frac{\partial \mathbf{v}_{\text{L}}}{\partial \mathbf{p}})^{\intercal} (\boldsymbol{\mu}^{+}_{\mathbf{v}_{\text{L}}} - \boldsymbol{\mu}^{-}_{\mathbf{v}_{\text{L}}}) \tag{4.12}$$

$$\boldsymbol{\Pi}^{\text{Grid}}_{\mathbf{q}} = c_q^0 \mathbf{1}_{\text{n}} + (\frac{\partial p^{\prime}}{\partial \mathbf{q}})^{\intercal} c_p^0 + (\frac{\partial q^{\prime}}{\partial \mathbf{q}})^{\intercal} c_q^0 + (\frac{\partial |\mathbf{s}^{\text{f}}|^2}{\partial \mathbf{q}})^{\intercal} \boldsymbol{\mu}_{s^{\text{f}}} + (\frac{\partial |\mathbf{s}^{\text{t}}|^2}{\partial \mathbf{q}})^{\intercal} \boldsymbol{\mu}_{s^{\text{t}}} + (\frac{\partial \mathbf{v}_{\text{L}}}{\partial \mathbf{q}})^{\intercal} (\boldsymbol{\mu}^{+}_{\mathbf{v}_{\text{L}}} - \boldsymbol{\mu}^{-}_{\mathbf{v}_{\text{L}}}) \tag{4.13}$$

Note that, one can verify that the above expression is generic in grid injections $\mathbf{p}/\mathbf{q} = \mathbf{p}^{\mathsf{g}} - \mathbf{p}^{\mathsf{fl}}/\mathbf{q}^{\mathsf{g}} - \mathbf{q}^{\mathsf{fl}}$, i.e., the derivation holds true for positive/negative power injections, i.e., for both DGs ($\mathbf{p}^{\mathsf{g}}, \mathbf{q}^{\mathsf{g}}$) and FLs $\mathbf{p}^{\mathsf{fl}}$.

4.2.2 Decomposition

The DLMP values in [(4.12), (4.13)] are decomposable into energy $\boldsymbol{\pi}^{\mathsf{E}}_{\mathbf{p}}/\boldsymbol{\pi}^{\mathsf{E}}_{\mathbf{q}}$, loss $\boldsymbol{\pi}^{\mathsf{L}}_{\mathbf{p}}/\boldsymbol{\pi}^{\mathsf{L}}_{\mathbf{q}}$, congestion $\boldsymbol{\pi}^{\mathsf{C}}_{\mathbf{p}}/\boldsymbol{\pi}^{\mathsf{C}}_{\mathbf{q}}$ and voltage components $\boldsymbol{\pi}^{\mathsf{V}}_{\mathbf{p}}/\boldsymbol{\pi}^{\mathsf{V}}_{\mathbf{q}}$:

$$\boldsymbol{\pi}^{\mathsf{Grid}}_{\mathbf{p}} = \boldsymbol{\pi}^{\mathsf{E}}_{\mathbf{p}} + \boldsymbol{\pi}^{\mathsf{L}}_{\mathbf{p}} + \boldsymbol{\pi}^{\mathsf{C}}_{\mathbf{p}} + \boldsymbol{\pi}^{\mathsf{V}}_{\mathbf{p}} \tag{4.14}$$

$$\boldsymbol{\pi}^{\mathsf{Grid}}_{\mathbf{q}} = \boldsymbol{\pi}^{\mathsf{E}}_{\mathbf{q}} + \boldsymbol{\pi}^{\mathsf{L}}_{\mathbf{q}} + \boldsymbol{\pi}^{\mathsf{C}}_{\mathbf{q}} + \boldsymbol{\pi}^{\mathsf{V}}_{\mathbf{q}} \tag{4.15}$$

where active power terms are:

$$\boldsymbol{\pi}^{\mathsf{E}}_{\mathbf{p}} := c^0_p \mathbf{1}_{\mathsf{n}}, \tag{4.16a}$$

$$\boldsymbol{\pi}^{\mathsf{L}}_{\mathbf{p}} := (\frac{\partial p^l}{\partial \mathbf{p}})^{\mathsf{T}} c^0_p + (\frac{\partial q^l}{\partial \mathbf{p}})^{\mathsf{T}} c^0_q, \tag{4.16b}$$

$$\boldsymbol{\pi}^{\mathsf{C}}_{\mathbf{p}} := (\frac{\partial |\mathbf{s}^{\mathsf{f}}|^2}{\partial \mathbf{p}})^{\mathsf{T}} \boldsymbol{\mu}_{s^{\mathsf{f}}} + (\frac{\partial |\mathbf{s}^{\mathsf{t}}|^2}{\partial \mathbf{p}})^{\mathsf{T}} \boldsymbol{\mu}_{s^{\mathsf{t}}}, \tag{4.16c}$$

$$\boldsymbol{\pi}^{\mathsf{V}}_{\mathbf{p}} := (\frac{\partial \mathbf{v}_{\mathsf{L}}}{\partial \mathbf{p}})^{\mathsf{T}} (\boldsymbol{\mu}^{+}_{\mathbf{v}_{\mathsf{L}}} - \boldsymbol{\mu}^{-}_{\mathbf{v}_{\mathsf{L}}}), \tag{4.16d}$$

and similarly reactive power terms are:

$$\boldsymbol{\pi}^{\mathsf{E}}_{\mathbf{q}} := c^0_q \mathbf{1}_{\mathsf{n}} \tag{4.17a}$$

$$\boldsymbol{\pi}^{\mathsf{L}}_{\mathbf{q}} := (\frac{\partial p^l}{\partial \mathbf{q}})^{\mathsf{T}} c^0_p + (\frac{\partial q^l}{\partial \mathbf{q}})^{\mathsf{T}} c^0_q \tag{4.17b}$$

$$\boldsymbol{\pi}^{\mathsf{C}}_{\mathbf{q}} := (\frac{\partial |\mathbf{s}^{\mathsf{f}}|^2}{\partial \mathbf{q}})^{\mathsf{T}} \boldsymbol{\mu}_{s^{\mathsf{f}}} + (\frac{\partial |\mathbf{s}^{\mathsf{t}}|^2}{\partial \mathbf{q}})^{\mathsf{T}} \boldsymbol{\mu}_{s^{\mathsf{t}}} \tag{4.17c}$$

$$\boldsymbol{\pi}^{\mathsf{V}}_{\mathbf{q}} := (\frac{\partial \mathbf{v}_{\mathsf{L}}}{\partial \mathbf{q}})^{\mathsf{T}} (\boldsymbol{\mu}^{+}_{\mathbf{v}_{\mathsf{L}}} - \boldsymbol{\mu}^{-}_{\mathbf{v}_{\mathsf{L}}}) \tag{4.17d}$$

4.2.3 Discussion

The DLMP derived in [(4.12), (4.13)] with its decomposition provided in [(4.16), (4.17)] is able to represent price as contribution of each bus towards grid conditions, i.e. energy, loss, congestion and voltage. In this way, better justification of the imposed price for the respective bus can be made. For example, a bus causing voltage to bind at lower/upper limits due to its injected has also to be charged for its contribution to voltage binding in the grid. This structure is very similar to already existing transmission grid level electricity market price, where the final price conveyed to the loads/generators is decomposed into their contribution to energy, loss and congestion components [2]. Hence, it can be concluded that the DLMP structure of [(4.12), (4.13)] is able to provide the impact of crucial grid conditions on the cleared prices. Moreover, due to the similar structure adopted in transmission grid, the proposed DLMP structure of this thesis maintains high practical relevance. As the tools and knowledge developed over the years from transmission level pricing can be simply transfered to DLMP.

[2] We wish to emphasize here that voltage contributions in transmission level pricing has still not been included because usually transmission grids have a reliable voltage profile. However, as voltage issues are more common for distribution grids, we believe their contribution in the final price to be passed on to the user must be incorporated.

4.2.4 Challenges

In order to be deployed in a practical settings, a reliable and robust solution methodology is required to calculate DLMP. On the transmission level, this has been achieved by adopting an approximation of power flows, i.e., DC *load-flow* model, where it is assumed that voltage across the grid is flat (same) [61, 54]. With the inclusion of DC *load-flow*, the resultant ED problem is a LP/QP problem. These problems have a reliable solution methodology and consequently price calculation, as many off-the-shelf software exists to solve them [11, 30, 65]. However, in distribution grids, due to higher losses, a DC *load-flow* model is inefficient and generally not accurate. Moreover, with the advent of DGs/FLs in distribution grids, the injection/loading can vary drastically which makes the assumption of constant voltage profile too strong [26, 3, 63]. Hence, for DLMP recovery, a great barrier exist in solving (4.3) in its given form. Mainly the main non-convexity can be seen to arise from constraints (4.3b)–(4.3f) [see grid modeling parts of chapter 3]. Due to this, the DLMP determination from (4.3) is difficult as off-the-shelf solvers can not solve it in this form. This reduces solution reliability and future practical realization of the proposed DLMPs.

4.3 Solution Algorithm: Methodology

To construct the solution methodology, which is not only as intuitive as the DLMP structure [(4.12), (4.13)], but also mitigates grid nonlinearities, we proceed as follows:

1. perform approximate power flow equations developed in chapter 3 and deploy them to obtain an an approximate convex problem variant of (4.3); and
2. iteratively optimize the approximate convex program and obtain new approximate power flow solution points, so that it moves in a trust-region solution space, i.e., where the approximate grid model matches closely to the actual grid model.

Next, we explain the above mentioned solution methodology steps in detail.

4.3.1 Approximate Quadratic Program

In order to develop an Approximate Quadratic Program (AQP), we repeat below for convenience our previously developed approximations $\tilde{\mathbf{x}} := ((\tilde{\mathbf{v}}_{\mathsf{L}})^{\mathsf{T}}, (\tilde{\mathbf{s}}^{\mathsf{f}})^{\mathsf{T}}, (\tilde{\mathbf{s}}^{\mathsf{t}})^{\mathsf{T}}, (\tilde{p}^{\mathsf{l}})^{\mathsf{T}}, (\tilde{q}^{\mathsf{l}})^{\mathsf{T}})^{\mathsf{T}}$,

$$\tilde{\mathbf{v}}_{\mathsf{L}} = \hat{\mathbf{a}} + \mathbf{M}^{\mathbf{v}_{\mathsf{L}}}\mathbf{s}_{\mathsf{L}}^{\mathsf{inj}}, \tag{4.18a}$$

$$|\tilde{\mathbf{s}}^{\mathsf{f}}|^2 = \hat{\mathbf{b}} + \mathbf{M}^{\mathbf{s}^{\mathsf{f}}}\mathbf{s}_{\mathsf{L}}^{\mathsf{inj}}, \tag{4.18b}$$

$$|\tilde{\mathbf{s}}^{\mathsf{t}}|^2 = \hat{\mathbf{c}} + \mathbf{M}^{\mathbf{s}^{\mathsf{t}}}\mathbf{s}_{\mathsf{L}}^{\mathsf{inj}}, \tag{4.18c}$$

$$\tilde{p}^{\mathsf{l}} = \hat{d} + \mathbf{M}^{p^{\mathsf{l}}}\mathbf{s}_{\mathsf{L}}^{\mathsf{inj}}, \tag{4.18d}$$

$$\tilde{q}^{\mathsf{l}} = \hat{e} + \mathbf{M}^{q^{\mathsf{l}}}\mathbf{s}_{\mathsf{L}}^{\mathsf{inj}}, \tag{4.18e}$$

obtained using actual states $\hat{\mathbf{x}} := ((\hat{\mathbf{v}}_{\mathsf{L}})^{\mathsf{T}}, (\hat{\mathbf{s}}^{\mathsf{f}})^{\mathsf{T}}, (\hat{\mathbf{s}}^{\mathsf{t}})^{\mathsf{T}}, (\hat{p}^{\mathsf{l}})^{\mathsf{T}}, (\hat{q}^{\mathsf{l}})^{\mathsf{T}})^{\mathsf{T}}$ satisfying the following equations:

$$\hat{\mathbf{u}}_{\mathsf{L}} = -\mathbf{Y}_{\mathsf{LL}}{}^{-1}\mathbf{Y}_{\mathsf{L}0}u_0 + \mathbf{Y}_{\mathsf{LL}}{}^{-1}\mathrm{diag}(\bar{\hat{\mathbf{u}}}_{\mathsf{L}})^{-1}\bar{\hat{\mathbf{s}}}_{\mathsf{L}}, \tag{4.19a}$$

$$\hat{\mathbf{s}}^{\mathsf{f/t}} = \mathrm{diag}(\mathbf{A}_0^{\mathsf{f/t}}u_0 + \mathbf{A}_{\mathsf{L}}^{\mathsf{f/t}}\hat{\mathbf{u}}_{\mathsf{L}})(\overline{\mathbf{Y}}_0^{\mathsf{f/t}}\bar{\hat{u}}_0 + \overline{\mathbf{Y}}_{\mathsf{L}}^{\mathsf{f/t}}\bar{\hat{\mathbf{u}}}_{\mathsf{L}}), \tag{4.19b}$$

$$\hat{p}^{\mathsf{l}} + j\hat{q}^{\mathsf{l}} = \hat{s}^{\mathsf{l}} = u_0(\overline{\mathbf{Y}}_{00}\bar{u}_0 + \overline{\mathbf{Y}}_{0\mathsf{L}}\bar{\hat{\mathbf{u}}}_{\mathsf{L}}) + (\hat{\mathbf{u}}_{\mathsf{L}})^{\mathsf{T}}(\overline{\mathbf{Y}}_{\mathsf{L}0}\bar{u}_0 + \overline{\mathbf{Y}}_{\mathsf{LL}}\bar{\hat{\mathbf{u}}}_{\mathsf{L}}). \tag{4.19c}$$

Refer to chapter 3 for more information regarding the above equations. After substituting the approximation of (4.18) in the original nonconvex problem (4.3), we obtain the following AQP:

$$\begin{aligned}
\text{maximize} \quad & w(\tilde{\mathbf{p}}^{\mathsf{fl}}, \tilde{\mathbf{p}}^{\mathsf{g}}, \tilde{\mathbf{q}}^{\mathsf{g}}) := w_p(\tilde{\mathbf{p}}^{\mathsf{fl}}, \tilde{\mathbf{p}}^{\mathsf{g}}) + w_q(\tilde{\mathbf{q}}^{\mathsf{g}}) && \text{(4.20a)}\\
\text{subject to} \quad & \mathbf{1}_{\mathsf{N}}^{\mathsf{T}}\tilde{\mathbf{p}}^{\mathsf{g}} - \mathbf{1}_{\mathsf{n}}^{\mathsf{T}}(\tilde{\mathbf{p}}^{\mathsf{cl}} + \tilde{\mathbf{p}}^{\mathsf{fl}}) = \tilde{p}^{\mathsf{l}} : \lambda^{p} && \text{(4.20b)}\\
& \mathbf{1}_{\mathsf{N}}^{\mathsf{T}}\tilde{\mathbf{q}}^{\mathsf{g}} - \mathbf{1}_{\mathsf{n}}^{\mathsf{T}}(\tilde{\mathbf{q}}^{\mathsf{cl}} + \tilde{\mathbf{q}}^{\mathsf{fl}}) = \tilde{q}^{\mathsf{l}} : \lambda^{q} && \text{(4.20c)}\\
& |\tilde{\mathbf{s}}^{\mathsf{f}}|^2 \leq (\mathbf{s}^{\mathsf{f}+})^2 && : \boldsymbol{\mu}_{s^{\mathsf{f}}}^{+} \quad \text{(4.20d)}\\
& |\tilde{\mathbf{s}}^{\mathsf{t}}|^2 \leq (\mathbf{s}^{\mathsf{t}+})^2 && : \boldsymbol{\mu}_{s^{\mathsf{t}}}^{+} \quad \text{(4.20e)}\\
& \mathbf{v}_{\mathsf{L}}^{-} \leq \tilde{\mathbf{v}}_{\mathsf{L}} \leq \mathbf{v}_{\mathsf{L}}^{+} && : \boldsymbol{\mu}_{\mathbf{v}_{\mathsf{L}}}^{-}, \boldsymbol{\mu}_{\mathbf{v}_{\mathsf{L}}}^{+} \quad \text{(4.20f)}\\
& \mathbf{p}^{\mathsf{dg}-} \leq \tilde{\mathbf{p}}^{\mathsf{dg}} \leq \mathbf{p}^{\mathsf{dg}+} && : \boldsymbol{\mu}_{\mathbf{p}}^{\mathsf{dg}-}, \boldsymbol{\mu}_{\mathbf{p}}^{\mathsf{dg}+} \quad \text{(4.20g)}\\
& \mathbf{q}^{\mathsf{dg}-} \leq \tilde{\mathbf{q}}^{\mathsf{dg}} \leq \mathbf{q}^{\mathsf{dg}+} && : \boldsymbol{\mu}_{\mathbf{q}}^{\mathsf{dg}-}, \boldsymbol{\mu}_{\mathbf{q}}^{\mathsf{dg}+} \quad \text{(4.20h)}\\
& \mathbf{p}^{\mathsf{fl}-} \leq \tilde{\mathbf{p}}^{\mathsf{fl}} \leq \mathbf{p}^{\mathsf{fl}+} && : \boldsymbol{\mu}_{\mathbf{p}}^{\mathsf{fl}-}, \boldsymbol{\mu}_{\mathbf{p}}^{\mathsf{fl}+} \quad \text{(4.20i)}
\end{aligned}$$

Assuming that there exists a flexibility resource dispatch $\hat{\mathbf{s}}^{\mathsf{disp}} := ((\hat{\mathbf{p}}^{\mathsf{g}})^{\mathsf{T}}, (\hat{\mathbf{p}}^{\mathsf{fl}})^{\mathsf{T}}, (\hat{\mathbf{q}}^{\mathsf{g}})^{\mathsf{T}})^{\mathsf{T}}$ which satisfy grid power flows (4.19), then (4.20) calculates a new dispatch $\tilde{\mathbf{s}}^{\mathsf{disp}} := ((\tilde{\mathbf{p}}^{\mathsf{g}})^{\mathsf{T}}, (\tilde{\mathbf{p}}^{\mathsf{fl}})^{\mathsf{T}}, (\tilde{\mathbf{q}}^{\mathsf{g}})^{\mathsf{T}})^{\mathsf{T}}$ in the direction of maximum overall social welfare.

Remark 4.4. The AQP in (4.20) is a QP, because its objective function (4.20a) has a positive definite Hessian term (see **R. 4.2**) along with constraints which are affine in the dispatch variables (4.18). QPs have a property of being strictly convex, i.e. the recovered solution from QP is a global minimizer (see chapter 2). Note that adopting this property is not mere a technicality, as (to be introduced later) it is going to be the cornerstone in our discussion on price calculations. Note that if the objective function of (4.20a) had been linear, then the resultant problem (4.20) would have been an LP. As mentioned before, both LPs and QPs have freely available off-the-shelf solvers, able to provide timely solutions for very large programs.

4.3.2 Trust-Region Algorithm

We present now a trust-region algorithm [17], [79, chapter 4] to obtain methodical iterative procedure for improving the solution from AQP (4.20). The trust-region methods have been applied to optimal power flow problems [27, 91, 44, 89]. However, they have not yet been deployed for radial distribution grids with fixed-point solution guarantees (see grid modeling part of chapter 3), which is the focus of this thesis. In general, trust-region based algorithm mitigates the approximation inaccuracy, i.e. the approximate dispatch $\tilde{\mathbf{s}}^{\mathsf{disp}}$ obtained from AQP (4.20), i.e., $\tilde{\mathbf{s}}^{\mathsf{disp}}$ may move the grid approximation quantities, i.e., $\tilde{\mathbf{x}}$ in (4.18) too far from the operating point $\hat{\mathbf{x}}$. This renders the linearization (done around the operation point) in (4.18) inaccurate[3], i.e., not giving an accurate reflection of the original power flow equations (4.19).

Algorithm 1 describes a trust-region based methodology in 4 steps. The steps improve the approximate solution of the AQP in an iterative manner for each iteration m. The explanation of each step follows:

Step 1 – *Trust-region Minimization*: In this step, the AQP is modified by augmenting its inequality constraints to include a permissible value (a trust-region) which restrict their

[3] As we recall that both local and global approximations when moved away from the operating point yields an error with respect to actual grid operation.

movement. So clearly, we would like the algorithm to remember the previous state of the problem as well as predicting its movement in future states [79]. To this end, let us redefine the approximate state and dispatch quantities as the measure of change in their operating state at the current iteration (m), i.e., $\tilde{\mathbf{x}}(m) = \hat{\mathbf{x}}(m) + \Delta\mathbf{x}(m)$ and dispatch quantities $\tilde{\mathbf{s}}^{\text{disp}}(m) = \hat{\mathbf{s}}^{\text{disp}}(m) + \Delta\mathbf{s}^{\text{disp}}(m)$, then the modified AQP (4.20) for each iteration m becomes:

$$\text{maximize} \quad w(\tilde{\mathbf{s}}^{\text{disp}}(m)) := w(\hat{\mathbf{s}}^{\text{disp}}(m)) + w(\Delta\mathbf{s}^{\text{disp}}(m)) \tag{4.21a}$$

$$\text{subject to} \quad (4.20\text{b}) - (4.20\text{i}) \tag{4.21b}$$

$$-\delta \leq \Delta\mathbf{s}^{\text{disp}}(m) \leq \delta \tag{4.21c}$$

$$-\delta \leq \Delta\mathbf{x}^{\text{disp}}(m) \leq \delta \tag{4.21d}$$

where the trust-region is now denoted by a radius $\delta > 0$.

Remark 4.5. In (4.21), the constraints [(4.20b) - (4.20i)] are consistent with the new constraints [(4.21c), (4.20d)]. This is because, recall from chapter 3, that the structure of approximations in (4.18) is: $\tilde{(\cdot)} = \hat{(\cdot)} + \mathbf{M}^{(\cdot)}\mathbf{s}_{\text{L}}^{\text{inj}}$. This can be rearrange and simply represented as :

$$\Delta(\cdot) = \mathbf{M}^{(\cdot)}\Delta\mathbf{s}_{\text{L}}^{\text{inj}}$$

where by definition of grid injections the only change in injection is due to flexible DGs and FLs,

$$\Delta\mathbf{s}_{\text{L}}^{\text{inj}} := \Delta\mathbf{p}^{\text{dg}} - \Delta\mathbf{p}^{\text{fl}} - \mathbf{p}^{\text{cl}} + j(\Delta\mathbf{q}^{\text{dg}} - \Delta\mathbf{q}^{\text{fl}} - \mathbf{q}^{\text{cl}})$$

where

$$\Delta\mathbf{p}^{\text{dg/fl}} = \tilde{\mathbf{p}}^{\text{dg/fl}} - \hat{\mathbf{p}}^{\text{dg/fl}}.$$

Also note that this also implies that inequality constraints in [(4.20b) - (4.20i)] are only going to be active when $(\Delta\mathbf{s}^{\text{disp}}(m), \Delta\mathbf{x}(m))$ causes the movement of the original quantities $(\hat{\mathbf{s}}^{\text{disp}}(m), \hat{\mathbf{x}}(m))$ to reach their allowable limits at iteration m. Finally, by observation, it can still be seen that the modified AQP is still a QP[4], and within the allowable given trust-region radius δ finds a global minimum (see **R. 4.4**).

Step 2 – *Feasible Solution Projection*: Using the dispatch result from the step-1, at iteration $m-1$, we project the newly calculated dispatch for iteration m $\tilde{\mathbf{s}}^{\text{disp}}(m-1)$ to the actual power flows (4.19). This is done by subjecting the new injection to obtain the *load-flow* solution from (4.19). This might yield a new state $\hat{\mathbf{x}}(m+1)$ for iteration $m+1$. This is because depending upon the approximation quality of the model, change in the root-bus injection might happen, as the root-bus acts as a slack-bus, which compensates for any difference in the approximated state $\tilde{\mathbf{x}}(m)$ and actual grid state $\hat{\mathbf{x}}(m)$. This projected dispatch which satisfies grid equations is then denoted as $\hat{\mathbf{s}}^{\text{disp}}(m)$.

Step 3 – *Trust-Region Evaluation and Update*: In this step, we evaluate the trust-region radius for the current iteration m using the following criteria:

$$\sigma(m) = \frac{w(\hat{\mathbf{s}}^{\text{disp}}(m-1)) - w(\hat{\mathbf{s}}^{\text{disp}}(m))}{w(\hat{\mathbf{s}}^{\text{disp}}(m-1)) - w(\tilde{\mathbf{s}}^{\text{disp}}(m))}. \tag{4.22}$$

The numerator shows the actual reduction in the objective function, whereas the denominator shows the predicted reduction in the objective function. In principle, it is evaluated,

[4]This is because constraints of the modified AQP are still affine in the decision variable and the objective function has a positive definite Hessian (see the definition of objective function in **R. 4.2**.

for two consecutive iterations, whether the ratio of change in actual system progression (numerator) to the change in the approximate system progression is comparable. Some observations regarding the trust-region evaluation step follows (for the generic implementation, see Algorithm 1). The higher value of $\sigma(m)$ represents a good agreement between approximation and actual system and hence advocates an increase in the size of the trust-region. For $\sigma(m) < 0$, the trust-region step must be reduced [79]. For our case, this means that the new projected dispatch (at iteration m) is higher than the previously projected dispatch value (at iteration $m-1$), i.e., $w(\hat{\mathbf{s}}^{\text{disp}}(m)) > w(\hat{\mathbf{s}}^{\text{disp}}(m-1))$. For the approximated dispatch showing a decrease in its objective value as compared to the feasible solution, i.e., $w(\hat{\mathbf{s}}^{\text{disp}}(m)) < w(\hat{\mathbf{s}}^{\text{disp}}(m-1))$, we also do not expand the trust-region as the approximated model is still not accurate enough. Similarly, for $\sigma = 0$, we also reduce the trust-region size.

Step 4 – *Evaluate Solution Progress*: Finally, if the solution at the current iteration makes a satisfactory progress towards the optimal solution, i.e., yields improvement as compared to the previous iteration's objective function, we accept the solution and move to the next iteration. Otherwise, we repeat the above steps using the modified trust-region $\sigma(m)$. A safe heuristic measure to ensure that the progress in the objective function is made at the current iteration is $\sigma(m) > 0$ (see Algorithm 1 for more generic implementation.).

The trust-region algorithm is terminated when a change in dispatch $|\Delta\tilde{\mathbf{s}}^{\text{disp}}(m)|_\infty := \max |\tilde{\mathbf{s}}^{\text{disp}}(m) - \tilde{\mathbf{s}}^{\text{disp}}(m-1)|$ where $|\cdot|$ is the absolute operator, is below a certain threshold ϵ. From the perspective of power system problems adopted for trust-region method, more information regarding the choice of γ, ϵ, η, τ and $\delta_{\max}$, can be found in [27, 91, 89]. The above mentioned steps in an algorithmic form are presented in Algorithm 1.

4.3.3 Final DLMP Model

Upon convergence of Algorithm 1, the final DLMP model in its decomposed components of energy $\boldsymbol{\pi}^{\text{E}}_{\mathbf{p}}/\boldsymbol{\pi}^{\text{E}}_{\mathbf{q}}$, loss $\boldsymbol{\pi}^{\text{L}}_{\mathbf{p}}/\boldsymbol{\pi}^{\text{L}}_{\mathbf{q}}$, congestion $\boldsymbol{\pi}^{\text{C}}_{\mathbf{p}}/\boldsymbol{\pi}^{\text{C}}_{\mathbf{q}}$ and voltage components $\boldsymbol{\pi}^{\text{V}}_{\mathbf{p}}/\boldsymbol{\pi}^{\text{V}}_{\mathbf{q}}$ is:

$$\boldsymbol{\pi}^{\text{Grid}}_{\mathbf{p}} = \boldsymbol{\pi}^{\text{E}}_{\mathbf{p}} + \boldsymbol{\pi}^{\text{L}}_{\mathbf{p}} + \boldsymbol{\pi}^{\text{C}}_{\mathbf{p}} + \boldsymbol{\pi}^{\text{V}}_{\mathbf{p}} \tag{4.23}$$

$$\boldsymbol{\pi}^{\text{Grid}}_{\mathbf{q}} = \boldsymbol{\pi}^{\text{E}}_{\mathbf{q}} + \boldsymbol{\pi}^{\text{L}}_{\mathbf{q}} + \boldsymbol{\pi}^{\text{C}}_{\mathbf{q}} + \boldsymbol{\pi}^{\text{V}}_{\mathbf{q}} \tag{4.24}$$

where its can be observed that active power terms:

$$\boldsymbol{\pi}^{\text{E}}_{\mathbf{p}} := c^0_p \mathbf{1}_{\text{n}}, \tag{4.25a}$$

$$\boldsymbol{\pi}^{\text{L}}_{\mathbf{p}} := (\mathbf{M}^{p^{\text{l}}})^{\intercal}_{\mathbf{p}} c^0_p + (\mathbf{M}^{q^{\text{l}}})^{\intercal}_{\mathbf{p}} c^0_q, \tag{4.25b}$$

$$\boldsymbol{\pi}^{\text{C}}_{\mathbf{p}} := (\mathbf{M}^{\mathbf{s}^{\text{f}}})^{\intercal}_{\mathbf{p}} \boldsymbol{\mu}_{s^{\text{f}}} + (\mathbf{M}^{\mathbf{s}^{\text{t}}})^{\intercal}_{\mathbf{p}} \boldsymbol{\mu}_{s^{\text{t}}}, \tag{4.25c}$$

$$\boldsymbol{\pi}^{\text{V}}_{\mathbf{p}} := (\mathbf{M}^{\mathbf{v}_{\text{L}}})^{\intercal}_{\mathbf{p}} (\boldsymbol{\mu}^{+}_{\mathbf{v}_{\text{L}}} - \boldsymbol{\mu}^{-}_{\mathbf{v}_{\text{L}}}), \tag{4.25d}$$

and reactive power terms:

$$\boldsymbol{\pi}^{\text{E}}_{\mathbf{q}} := c^0_q \mathbf{1}_{\text{n}} \tag{4.26a}$$

$$\boldsymbol{\pi}^{\text{L}}_{\mathbf{q}} := (\mathbf{M}^{p^{\text{l}}})^{\intercal}_{\mathbf{q}} c^0_p + (\mathbf{M}^{q^{\text{l}}})^{\intercal}_{\mathbf{q}} c^0_q \tag{4.26b}$$

$$\boldsymbol{\pi}^{\text{C}}_{\mathbf{q}} := (\mathbf{M}^{\mathbf{s}^{\text{f}}})^{\intercal}_{\mathbf{q}} \boldsymbol{\mu}_{s^{\text{f}}} + (\mathbf{M}^{\mathbf{s}^{\text{t}}})^{\intercal}_{\mathbf{q}} \boldsymbol{\mu}_{s^{\text{t}}} \tag{4.26c}$$

$$\boldsymbol{\pi}^{\text{V}}_{\mathbf{q}} := (\mathbf{M}^{\mathbf{v}_{\text{L}}})^{\intercal}_{\mathbf{q}} (\boldsymbol{\mu}^{+}_{\mathbf{v}_{\text{L}}} - \boldsymbol{\mu}^{-}_{\mathbf{v}_{\text{L}}}) \tag{4.26d}$$

contain the approximated sensitivity matrices from (4.18). Note that matrix $\mathbf{M}^{[\cdot]}_{\mathbf{p}/\mathbf{q}}$ simply corresponds to active/reactive injection entries of $\mathbf{M}^{[\cdot]}$.

Algorithm 1: Trust-Region Algorithm

Input Using initial dispatch quantities $\hat{\mathbf{s}}^{\text{disp}}(0)$ perform a base case power flow to obtain feasible state $\hat{\mathbf{x}}(0)$ satisfying (4.19)
while $|\Delta\tilde{\mathbf{s}}^{disp}(m)|_\infty \geq \epsilon$ **do**
  Step 1 – *Trust-region Minimization*;
  From a feasible $\hat{\mathbf{x}}(m)$, obtain approximates from (4.18) and solve (4.20) to get $\tilde{\mathbf{s}}^{\text{disp}}(m)$;
  Step 2: *Feasible Solution Projection ;*
  Using $\tilde{\mathbf{s}}^{\text{disp}}(m)$ solve (4.19) to obtain a new feasible state $\hat{\mathbf{x}}(m)$ and a corresponding feasible dispatch $\hat{\mathbf{s}}^{\text{disp}}(m)$;
  Step 3: *Trust Region Evaluation and Update;*
  if $\sigma(m) \leq \eta$ **then** /* bad approx. */
    $\delta(m+1) = \gamma \cdot \delta(m)$;
  else if $\sigma(m) > (1-\eta)$ **then** /* good approx. */
    $\delta(m+1) = \min(2\delta(m), \delta_{\max})$;
  else
    $\delta(m+1) = \delta(m)$;
  end
  Step 4: *Evaluate Solution Progress ;*
  if $\sigma(m) > \tau$ **then**
    $m = m+1$;
    Accept the iteration, set new states as $\hat{\mathbf{x}}(m)$;
  else
    Reject the iteration and repeat using the modified region;
  end
end

4.4 Solution Algorithm: Discussion

In this subsection, we discuss how the proposed solution methodology of Algorithm 1 can be analyzed from the viewpoint of already presented concepts of i) solution uniqueness (Sec. 3.2.2) and ii) convexity (chapter 2).

4.4.1 Solution Existence & Uniqueness

Recall that for the fixed-point *load-flow* solution of (4.19), we have solution existence and uniqueness under the satisfaction of two conditions. We repeat these conditions below for convenience.

$$\xi(\hat{\mathbf{s}}_{\mathsf{L}}) < u_{min}^2, \tag{4.27}$$

$$\Delta := (u_{min} - \frac{\xi(\hat{\mathbf{s}}_{\mathsf{L}})}{u_{min}})^2 - 4\xi(\mathbf{s}_{\mathsf{L}} - \hat{\mathbf{s}}_{\mathsf{L}}) > 0, \tag{4.28}$$

within the set

$$\mathcal{D} := \{\mathbf{u}_{\mathsf{L}} : |\mathbf{u}_{\mathsf{L}} - \hat{\mathbf{u}}_{\mathsf{L}}| \leq \rho|\mathbf{w}|\}, \tag{4.29}$$

$$\rho := \frac{u_{min} - \frac{\xi(\hat{\mathbf{s}}_{\mathsf{L}})}{u_{min}} - \sqrt{\Delta}}{2}, \tag{4.30}$$

which guarantees a unique solution $\mathbf{u}_{\mathsf{L}} \in \mathcal{D}$ and the pair $(\mathbf{u}_{\mathsf{L}}, \mathbf{s}_{\mathsf{L}})$ satisfies (3.6) (see Sec. 3.2.2 for more information). Note that conditions [(3.8), (3.9)] are parameterized in the solution pair $(\hat{\mathbf{u}}_{\mathsf{L}}, \hat{\mathbf{s}}_{\mathsf{L}})$ satisfying the *load-flow* problem along with a new arbitrarily requested set-point $\mathbf{s}_{\mathsf{L}}$. With regards to Algorithm 1, this is equivalent to being parameterized in actual states and dispatch $(\hat{\mathbf{x}}, \hat{\mathbf{s}}^{\text{disp}})$ satisfying grid equations and a new requested set-point $\tilde{\mathbf{s}}^{\text{disp}}$ calculated from step 1 of Algorithm 1. Hence, it can be concluded that the satisfaction of [(4.27), (4.28)] ensures that the feasible solution projection, i.e., step 2 of the Algorithm 1 always exists and yields a unique solution. This is an important result from the perspective of the proposed algorithm as the feasible solution projection (step 2 of Algorithm 1) is deployed in subsequent steps to measure the improvement in the solution obtained from the modified AQP (4.21a). Moreover, it has been shown in [101] that for practical operating range of the distribution grid, the conditions in [(3.8), (3.9)] are usually satisfied. We also observe the same in this thesis (to be shown in subsequent examples and results).

Also note that Algorithm 1 is initialized using a base case *load-flow*. For the case of uncertain base case *load-flow*, we can also initialize Algorithm 1 using a cold start, i.e., at no-load condition $(\mathbf{w}, \mathbf{0})$. Recall that this is obtained by inserting $(\mathbf{u}_{\mathsf{L}}^0, \mathbf{s}_{\mathsf{L}}^0)$ in [(4.27), (4.28)], to obtain new set of unique solution guaranteeing equations:

$$\xi(\mathbf{0}) = \mathbf{0} < u_{min}^2, \tag{4.31}$$

$$\Delta := \xi(\mathbf{s}_{\mathsf{L}}) < 0.25. \tag{4.32}$$

To summarize, the above conditions can be conveniently used for the scenario when no base case operating conditions existing to initialize Algorithm 1. Hence, upon satisfaction of conditions [(4.31), (4.32)], we can begin Algorithm 1 with no-load condition $(\mathbf{w}, \mathbf{0})$.

4.4.2 Solution Progression

Assume that at iteration m, the dispatch $\hat{\mathbf{s}}^{\text{disp}}(m)$ satisfies [(4.27), (4.28)], then from the above discussion we know that the new candidate set-point $\tilde{\mathbf{s}}^{\text{disp}}(m)$ yields a unique projection on the actual grid power flows. Moreover, with regards to solution optimality of the new candidate set-point $\tilde{\mathbf{s}}^{\text{disp}}(m)$, it is in itself a global minimizer of the modified AQP (4.21), within the allowable trust-region radius δ. This is simply because the modified AQP is still a QP (see **R. 4.5**). This means that considering a feasible starting point of Algorithm 1, at the completion of step 1, $\tilde{\mathbf{s}}^{*\text{disp}}$ is a unique optimizer. Then throughout Algorithm 1, we ensure that for each iteration m a new candidate dispatch $\tilde{\mathbf{s}}^{\text{disp}}(m)$ under [(4.27), (4.28)] maintains solution uniqueness, while improving solution quality in terms of objective function (see (4.22)). Holistically, this means that the algorithm finds new successive operating points with the aim to lower the value of the objective functions (4.21a), where the operating point satisfies *load-flow* solution exists. Now observing the termination conditions of Algorithm 1, one can see that this criteria corresponds to the point where solving (4.21a) and projecting on (4.19) yields no improvement, while conditions [(3.8), (3.9)] hold. This is true for two conditions, either the point found is a local minimum or a global minimum. Hence, it can be concluded that in the worst-case the proposed algorithm 1 finds a local minimum of the overall nonconvex problem (4.3) or in the

best case a global minimum [11]. For radial grids and under practical operating conditions, works of [10, 101, 6] have shown that the resultant power flow solution space is convex. Since exploring the solution space is not the key focus here, we are not going to pursue it in detail in this thesis. However, the results section of this chapter support these claims and provides similar solution quality as compared to a benchmark optimal power flow software [113].

4.4.3 Practical Implications

The above described solution methodology handles non-convexity of the original program (4.3) in two steps: (i) AC power flow calculation (step 2) and (ii) convex program solution (step 1). Both these steps have off-the-shelf software, which can be readily deployed to obtain reliable solution methodology[5]. Hence, the above described solution methodology has a high solution robustness and reliability. Moreover, the approximations developed in chapter 3 are also directly deployed for solving the convex program as well as calculating DLMPs. This aids in the ease of price interpretation. The solution methodology adopted in this thesis is different to recent propositions of convex relaxation of power flows [97]. However, in appendix A.2, we show that convex relaxation approach might not translate to intuitive DLMP formulation and interpretation.

4.5 Results of the Proposed Solution Methodology

In this section, we demonstrate the above described solution strategy for solving the original nonconvex problem (4.3) and recovering DLMPs [(4.25), (4.26)] from it. In doing so, we are going to compare the results with MATPOWER [84][6].

Example 4.1

First, we present the analysis on the single-phase equivalent three-bus system of example 3.2. More information of this grid can be found in appendix A.1.1. As evident from the MATPOWER case file of appendix A.1.1, we have modified the test case by inserting a DG at bus 2 and setting marginal value of active and reactive power supply by both DGs (at bus 2 and root-bus (bus 0)) at 10 \$/MWh and 1 \$/MVarh, respectively. A small price sensitivity coefficient of $1 \cdot 10^{-4}$ \$/MWh^2(MVarh^2) is chosen to keep the objective function strictly convex and hence the modified AQP as a QP (see **R. 4.2**). We demonstrate two scenario. Scenario-1 contains no congestion whereas Scenario-2 is implemented by limiting power flow on the line from bus 1 to bus 2 by 0.65 MVA. For both cases, we assume there is no scarcity of generation, i.e., there is no maximum limit on active and reactive power generation. For both cases, upon convergence of Algorithm 1, we demonstrate all components of active and reactive power DLMP model, derived in [(4.25), (4.26)] in Table 4.1 and 4.2 respectively.

Table 4.1: Active power DLMPs (in \$/MWh) for scenario 1 (top) and 2 (bottom) for all grid buses i.

[5] For example, the convex optimization can be solved using [31] and AC power flow calculation can be performed using [84].

[6] For MATPOWER, we experienced same results from both semi-definite and interior point solvers. For more information regarding the solution methodologies of MATPOWER, interested readers are referred to [113, 84].

i	$\boldsymbol{\pi}_{\mathbf{p}}^{\mathsf{E}}$	$\boldsymbol{\pi}_{\mathbf{p}}^{\mathsf{L}}$	$\boldsymbol{\pi}_{\mathbf{p}}^{\mathsf{C}}$	$\boldsymbol{\pi}_{\mathbf{p}}^{\mathsf{V}}$	$\boldsymbol{\pi}_{\mathbf{p}}^{\mathsf{Grid}}$	$\boldsymbol{\pi}_{\mathbf{p}}^{\mathsf{MAT}}$	$\mathbf{c}_p^{\mathsf{dg}}$	$\boldsymbol{\mu}_{\mathbf{p}}^{\mathsf{dg}+} - \boldsymbol{\mu}_{\mathbf{p}}^{\mathsf{dg}-}$	$\boldsymbol{\pi}_{\mathbf{p}^{\mathsf{dg}}}^{\mathsf{Flex}}$
0		0	0	0	**10**	**10**	10	0	**10**
1	10	0.5934	0	-0.0279	**10.566**	**10.566**	–	–	–
2		0.0507	0	-0.0507	**10**	**10**	10	0	**10**
0		0	0	0	**10**	**10**	10	0	**10**
1	10	0.668	0	0	**10.668**	**10.668**	–	–	–
2		0.173	-0.173	0	**10**	**10**	10	0	**10**

In Table 4.1, $\boldsymbol{\pi}_{\mathbf{p}}^{\mathsf{MAT}}$ is the final DLMP value obtained from MATPOWER. Shown in bold in Table 4.1, it can be observed that flexible DLMPs $\boldsymbol{\pi}_{\mathbf{p}^{\mathsf{dg}}}^{\mathsf{Flex}}$ representing the internal flexible bus dynamics exist in equilibrium with the grid cleared DLMPs, i.e., $\boldsymbol{\pi}_{\mathbf{p}}^{\mathsf{Grid}} = \boldsymbol{\pi}_{\mathbf{p}^{\mathsf{dg}}}^{\mathsf{Flex}}$ and they are equal to the benchmarked MATPOWER solution. This on one hand verifies the DLMP model's equilibrium conditions (4.11) and on the other hand shows capability of Algorithm 1 to handle the non-convex ED program (4.3) reliably. Hence, the value of objective function along with dispatch of generator is similar and are not mentioned here to save space. Some comments on the behavior of DLMP components follow. In Table. 4.1, a negative value of the DLMP component at a bus means that a unit increase demand at that bus increases the objective value of the non-convex ED problem (4.3a). For example, positive loss components $\boldsymbol{\pi}_{\mathbf{p}}^{\mathsf{L}}$ at bus 1 and 2 means that unit increase in demand at bus 1 and 2 increases the cost of the overall system by this amount. This is exactly why this component has been termed as marginal loss in transmission grid market calculations [61]. Another interesting observation from Table. 4.1 is that originally (Scenario 1) there exists nonzero voltage binding component of DLMP,i.e. $\boldsymbol{\pi}_{\mathbf{p}}^{\mathsf{V}}$. This was because the DG, due to no constraints on line flow from bus 2 to bus 1 in Scenario 1, dispatched power which caused voltage at its bus (bus 2) to reach the maximum value of 1.5 p.u.. Now due to imposed line flow constraint of 0.65 MVA, the DG dispatches less power, which removes the voltage binding and consequently removes the DLMP voltage component. However, as compared to Scenario 1, the final cleared DLMP value at bus 1 is increased $10.668 > 10.565$ for Scenario 2. This is because due to line flow congestion, extra power has to come from the root-bus, which would have been provided more cost-effectively (as in Scenario 1) by DG (at bus 2). This can also be verified by comparing objective function values (costs) for both Scenario 1 and 2. Indeed, for Scenario 2 the calculated objective function value is 11.552 \$, whereas in Scenario 1 the final objective function value is 11.537 \$. This amounts to 0.13% increase in the cost when the grid operates from non-congested to congested scenario, i.e., from Scenario 1 to Scenario-2. Similar observations can be inferred regarding reactive power DLMPs, given in Table 4.2.

Table 4.2: Reactive power DLMPs (in \$/MVarh) for scenario 1 (top) and 2 (bottom) for all grid buses i.

i	$\boldsymbol{\pi}_{\mathbf{q}}^{\mathrm{E}}$	$\boldsymbol{\pi}_{\mathbf{q}}^{\mathrm{L}}$	$\boldsymbol{\pi}_{\mathbf{q}}^{\mathrm{C}}$	$\boldsymbol{\pi}_{\mathbf{q}}^{\mathrm{V}}$	$\boldsymbol{\pi}_{\mathbf{q}}^{\mathrm{Grid}}$	$\boldsymbol{\pi}_{\mathbf{q}}^{\mathrm{MAT}}$	$\mathbf{c}_q^{\mathrm{dg}}$	$\boldsymbol{\mu}_{\mathbf{q}}^{\mathrm{dg}+} - \boldsymbol{\mu}_{\mathbf{q}}^{\mathrm{dg}-}$	$\boldsymbol{\pi}_{\mathbf{q}^{\mathrm{dg}}}^{\mathrm{Flex}}$
0		0	0	0	**1**	**1**	1	0	**1**
1	1	0.593	0	-0.027	**1.566**	**1.566**	–	–	–
2		0.050	0	-0.050	**1**	**10**	1	0	**1**
0		0	0	0	**1**	**1**	1	0	**1**
1	1	0.668	0	0	**1.668**	**1.668**	–	–	–
2		0.173	-0.173	0	**1**	**1**	1	0	**1**

Next, we see algorithm performance for Scenario 2 (with congestion). The reason for analyzing Scenario 2 is that it demonstrates all constraints in the optimization problem being active, consequently posing a higher challenge to find a solution as compared to non-congested scenario (Scenario-1). Fig. 4.1 shows the progress of control variable error. For the given system, the maximum error in control variable reaches the value of $1 \cdot 10^{-5}$ in 5 seconds (within 15 iterations). However, we use no-load conditions to initialize Algorithm 1 to simulate the worst-case initialization scenario (zero dispatch values). The number of iterations can be reduced by intelligently initializing Algorithm 1, i.e., selecting a base-case which is closer to the actual operating condition.

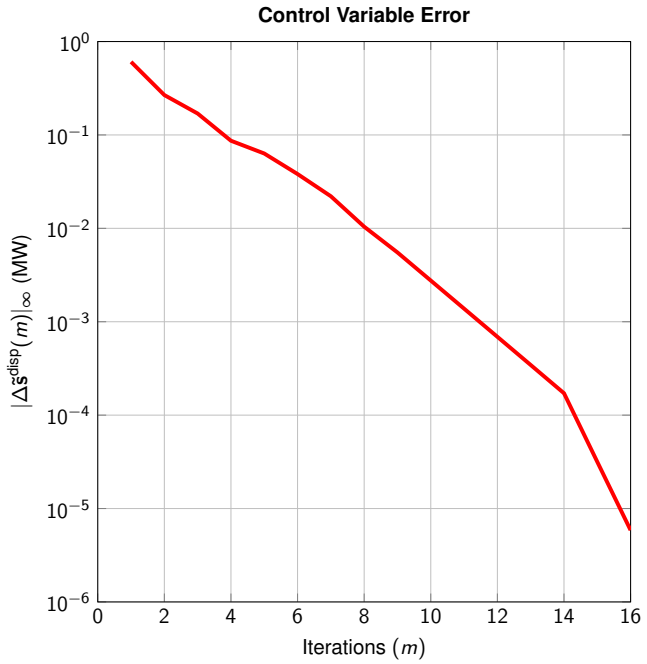

Figure 4.1: Control variable progression for each iteration (m) of Algorithm 1 for 3-bus grid.

Fig. 4.2 shows the dispatched active/reactive generations for both root-bus (p^0/q^0) and DG at bus 2 ($p_1^{\mathrm{dg}}/q_1^{\mathrm{dg}}$) for each iteration of Algorithm 1. It can also be seen here that we initialize Algorithm 1 using zero dispatch value for both generations. Moreover, it can be verified that at the termination of Algorithm 1, the final dispatch value calculated from Algorithm 1 ($\tilde{(\cdot)}$) and MATPOWER's interior point non-convex program ($\hat{(\cdot)}$) is exactly the

same, i.e., $(\tilde{p}^0, \tilde{p}_1^{dg}, \tilde{q}^0, \tilde{q}_1^{dg}) = (\hat{p}^0, \hat{p}_1^{dg}, \hat{q}^0, \hat{q}_1^{dg})$. The same results are also obtained when MATPOWER's solver is switched from interior point to semi-definite programming.

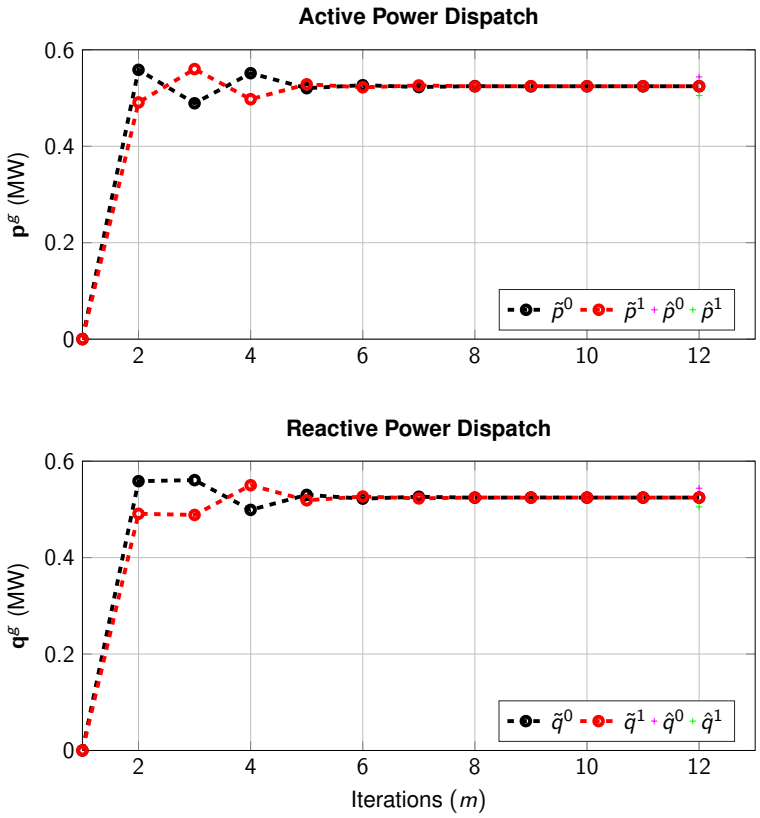

Figure 4.2: Dispatched active/reactive generations for both root-bus (p^0/q^0) and DG (p_1^{dg}/q_1^{dg}) for each iteration (m) of Algorithm 1 for 3-bus grid.

Fig. 4.3 simulates verification of conditions [(4.27), (4.28)] at each iteration m. The values in Fig. 4.3 are calculated as follow. For a pair $(\hat{\mathbf{u}}_L(m-1), \hat{\mathbf{s}}_L(m-1))$, satisfying (4.19) we calculate whether the new dispatched candidate (injections) $\tilde{\mathbf{s}}_L(m)$ from step 1 can be successfully projected to actual power flow solution space (step-2) for iteration m. To this end, we check conditions [(4.27), (4.28)] which are then parameterized in a satisfied solution pair $(\hat{\mathbf{u}}_L(m-1), \hat{\mathbf{s}}_L(m-1))$ and a new candidate $\tilde{\mathbf{s}}_L(m)$. Fig. 4.3 experimentally verifies this, where it can be seen that both conditions [(4.27), (4.28)] are satisfied for each iteration of Algorithm 1. Main takeaway from this experiment is that one can comment that throughout Algorithm 1 for each iteration m a unique solution exists within the defined trust-region radius δ. Moving on, Algorithm 1 moved towards optimal (minimum cost in this example) solution. Eventually, at the termination of Algorithm 1, objective function and consequently control variables ceases to change Fig. 4.1 and Fig. 4.2. Note that the final dispatch value from Fig. 4.2 provides exactly same values as MATPOWER's semi-definite programming, which has been shown to provide a global optimal. This also provides experimental verification of our concluding remarks of Sec. 4.4.2, where we mentioned that, due to convexity of solution space for radial grids under normal operation conditions, the proposed Algorithm 1 converges to a global optimal.

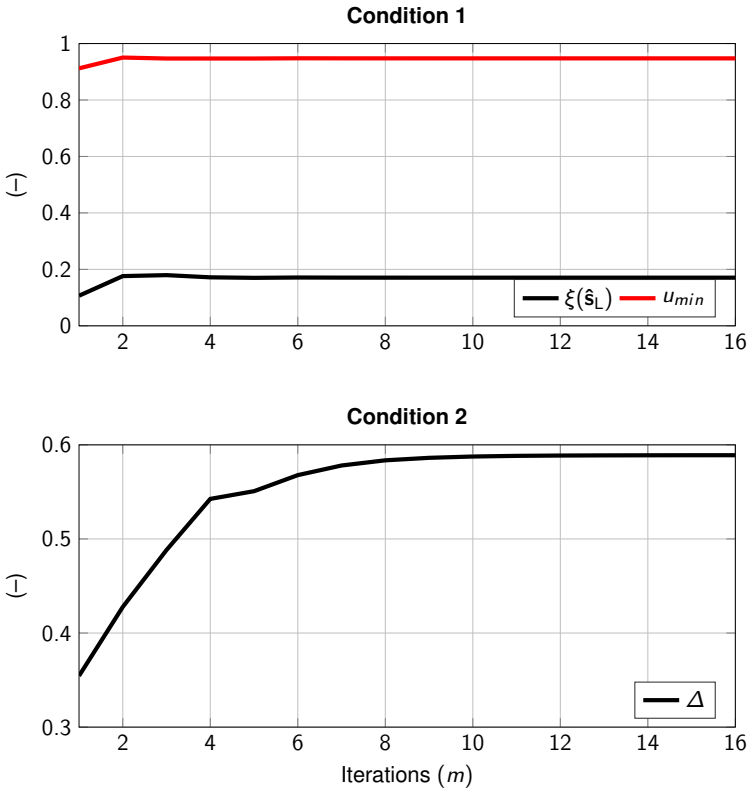

Figure 4.3: Verification of solution uniqueness conditions [(4.27), (4.28)] for each iteration (m) of Algorithm 1 for 3-bus grid.

4.5.1 Model Comparisons

In this subsection we compare the proposed solution methodology of DLMP, with state-of-the-art methods from the literature. To this end, we compare in Fig. 4.4, the proposed methodology of Sec. 4.3 (AQP) against an i) approximate (linearized) DLMP model (AQP[7]) [109] and ii) an interior point[8] MATPOWER model (MAT) [84].

As AQP in [109] has been tested extensively for 33-bus system, we also perform DLMP comparisons on the same grid. Moreover, to present realistic assessment, we introduce both DGs and FLs in the 33-bus system. See Fig. 5.2 for pictorial representation of the grid and Sec. A.1.2 in appendix for the MATPOWER code. DGs and FLs have dispatch capabilities as follows; (1) the active and reactive power dispatch for DGs are within range $[0, 0.5]$ MW and $[-0.3, 0.3]$ MVar and (2) the active power dispatch for FLs is within the range $[-1.47, 0]$ MW (derived from [35]). Two DGs are introduced and placed at bus 22 and bus 18 whereas two FLs are selected and placed at bus 33 and bus 25. In this way, each DG and FL is placed closer and far-off from the root-bus. The marginal value of supplying power to the grid from root-bus is fixed at 10 \$/MWh and 3 \$/Mvar. A small price sensitivity coefficient of $1 \cdot 10^{-4}$ \$/MWh^2(MVarh^2) is chosen to keep the objective function strictly convex and hence the modified AQP as a QP (see **R. 4.2**). Similar to example 4.1 we simulate two scenarios. In principle,

[7] We also call this method AQP as we named (4.20). This is because, similar to AQP of (4.20), the final model in [109] is also a quadratic program.

[8] The semi-definite solver of MATPOWER provided the same results. See Sec. 4.4.2 for more information.

we manipulate supply/bid functions of DGs/FLs to obtain DLMPs with congestion (scenario 2) and without congestion (scenario 1).

Scenario-1*:* For all flexible buses (DGs/FLs) and the root-bus, this case fixes the active and reactive power marginal costs at 10 \$/MWh and 3 \$/MVarh. From Fig. 4.4 it can be seen that the proposed AQP-TR, utilizing trust-region iterations, provides an improved solution quality compared to the AQP, and exactly similar solution as non-convex ACOPF (MAT). The improvement from AQP is is because for buses far from the root-bus large voltage drops exist causing higher errors in linearization, which is performed around a flat nodal voltage profile (1 p.u) and negligible angle difference. As FLs, due to their locations, with same marginal values to DGs are not dispatched, next we present *Scenario*-2 to evaluate their presence on DLMPs.

Scenario-2*:* In this case, marginal utility for all FLs are increased to 15 \$/MWh, all remaining settings are similar to *Scenario*-1. The proposed LMOPF method again achieves almost identical dispatch quantities and DLMPs as compared to the non-convex ACOPF solution [84]. The large power drawn by the FLs now binds the lower voltage and line flow limit at bus 25 and 33.

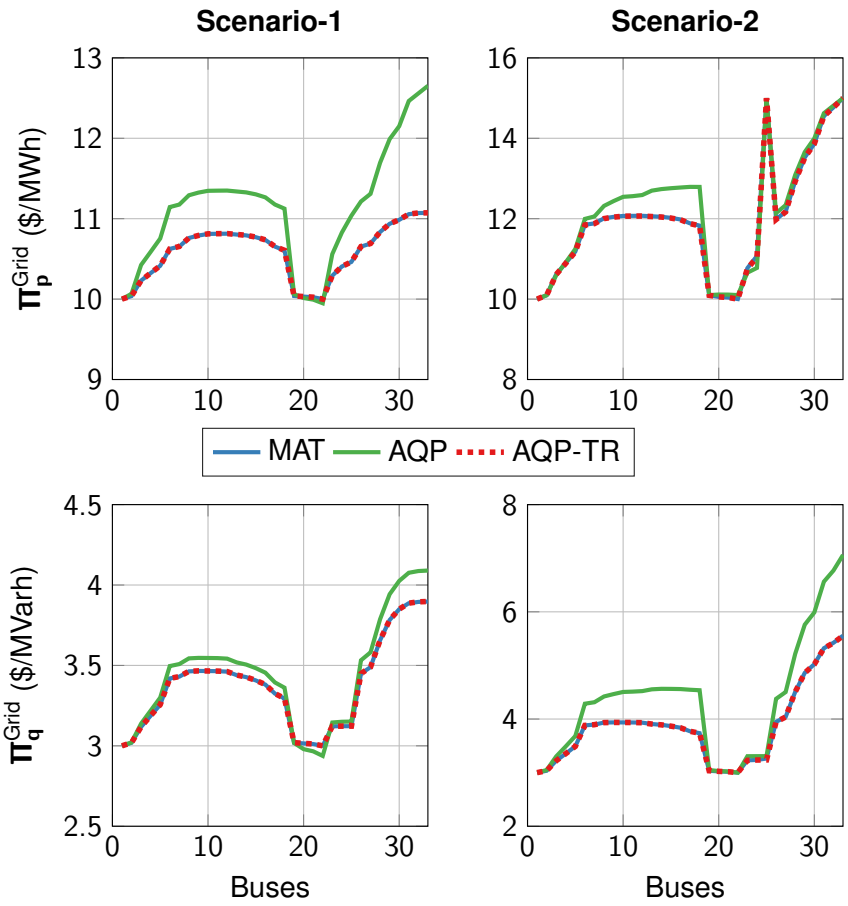

Figure 4.4: Active (top) and reactive power (bottom) DLMP comparisons on 33-bus grid, obtained using MATPOWER (MAT) [84]; a linear grid model (AQP) [109]; and the proposed methodology of Sec. 4.3 (AQP-TR).

The general observation from both scenarios is that for buses 19-22, similar DLMPs are

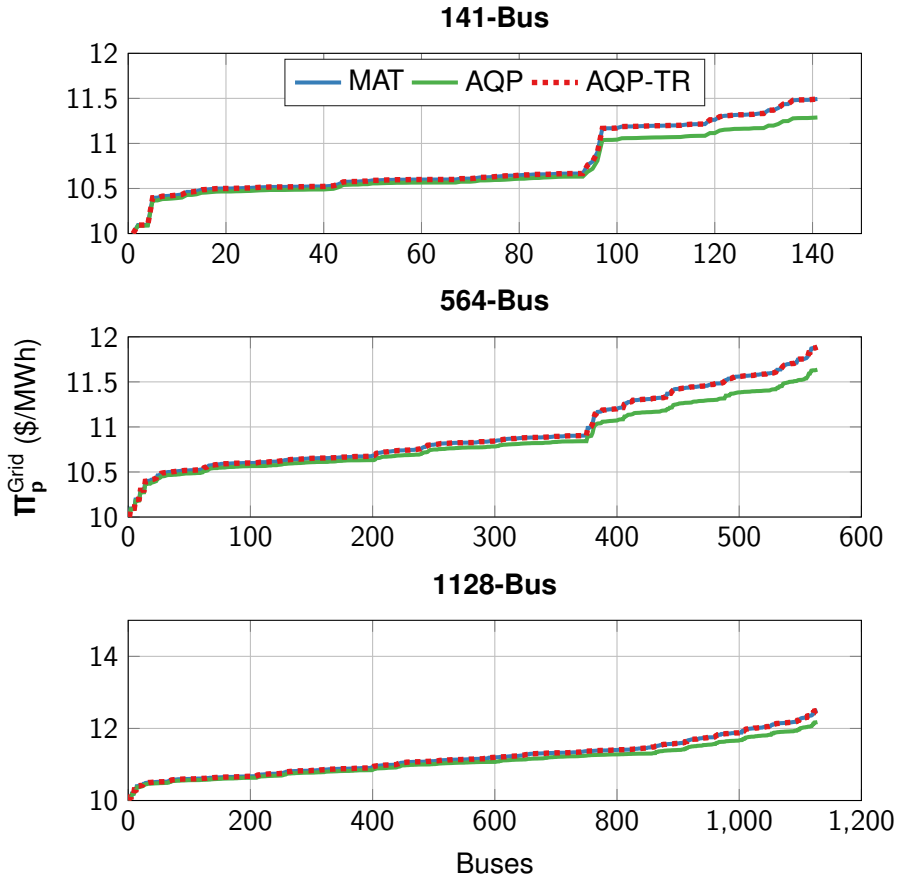

Figure 4.5: Active power DLMP comparison between the proposed LMOPF, ACOPF [84] and LIOPF [109] for 141-buses (top), 564-buses (middle) and 1128-buses (bottom) grid.

obtained from all three methods. This happens because voltage magnitudes are close to their upper voltage limits and binding at bus 22, making its feed-in branch experiencing DLMPs at its marginal cost, i.e. 10 $/MWh and 3 $/MVarh. For Case-2, this effect is also caused by line flow constraint binding at bus 33, causing the respective DLMPs to be closer to FLs' marginal utility value, i.e. 15 $/MWh. It was also confirmed that, for both scenarios, regardless of the initialization point, the proposed Algorithm 1 method always converged to the same dispatch and consequently DLMPs within only 4 iterations.

4.5.2 Model Scalability

To show the scalability of the proposed model, we implement the proposed model on three distribution grids containing 141-buses [49], 564-buses and 1128-buses. For all the grids, the marginal cost settings for DGs/FLs are kept similar to those of *Scenario-2* of Sec. 4.5.1. We construct the 564-buses and the 1128-buses grid by duplicating the 141-buses grid, while preserving its original root-bus [109]. Similarly, the number of DGs/FLs in the 564-buses grid and the 1128-buses grid are proportionally increased as compared to 141-buses grid. In this way, we not only evaluate the feasible solution projection step but also the trust-region minimization step of the proposed model (See Algorithm 1).

The scalability of the proposed method along with comparison of solution quality with

other methods in the literature is shown in Fig. 4.5. We only present active power DLMPs in Fig. 4.5 as reactive power DLMPs show similar results and are left out here to save space. Similar to Fig. 4.4, Fig. 4.5 reiterates that the proposed model achieves the same results as MATPOWER's interior point ACOPF model, while outperforming the state-of-the-art linearized model [109]. Table. 4.3 details the information regarding the simulated grids and the resultant computation efforts of the proposed model. It can be seen that the proposed model scales well with the increase in the size of the grid and the number of flexibility resources (DGs/FLs).

Table 4.3: Proposed Model Scalability

buses	DGs	FLs	Iteration	Time (sec.)
141	2	2	3	1.5
564	8	8	3	3.3
1128	16	16	4	13.3

4.6 Multi-Phase Economic Dispatch Problem

4.6.1 Multi-Phase System Model

In this section, we present extension of the proposed DLMP model of Sec. 4.2 for multi-phase grid models. All assumptions regarding cost functions of flexible resources (DGs/FLs) of single-phase system model (see **R. 4.1**) is also preserved for multi-phase grid model. However, we make a simplification that we only consider DGs as a flexible resource, while considering possibility of DGs having both wye and delta connections.

Combining the multi-phase grid notation of Sec. 3.4, with DGs, we have: let wye-/delta-connected active and reactive power injections as $\mathbf{p}_{\mathsf{L}}^{\mathsf{Y}/\Delta} := \Re(\mathbf{s}_{\mathsf{L}}^{\mathsf{Y}/\Delta})$ and $\mathbf{q}_{\mathsf{L}}^{\mathsf{Y}/\Delta} := \Im(\mathbf{s}_{\mathsf{L}}^{\mathsf{Y}/\Delta})$, where in particular, $\mathbf{p}_{\mathsf{L}}^{\mathsf{Y}/\Delta} := ((\mathbf{p}_{g,1}^{\mathsf{Y}/\Delta} - \mathbf{p}_{l,1}^{\mathsf{Y}/\Delta})^\intercal, \ldots, (\mathbf{p}_{g,n}^{\mathsf{Y}/\Delta} - \mathbf{p}_{l,n}^{\mathsf{Y}/\Delta})^\intercal)^\intercal$, $\mathbf{q}_{\mathsf{L}}^{\mathsf{Y}/\Delta} := ((\mathbf{q}_{g,1}^{\mathsf{Y}/\Delta} - \mathbf{q}_{l,1}^{\mathsf{Y}/\Delta})^\intercal, \ldots, (\mathbf{q}_{g,n}^{\mathsf{Y}/\Delta} - \mathbf{q}_{l,n}^{\mathsf{Y}/\Delta})^\intercal)^\intercal$ where $\mathbf{p}_g^{\mathsf{Y}/\Delta}$, $\mathbf{p}_l^{\mathsf{Y}/\Delta}$, $\mathbf{q}_g^{\mathsf{Y}/\Delta}$ and $\mathbf{q}_l^{\mathsf{Y}/\Delta}$ of size $\mathbb{R}^{3n}$ are active power generation, active power demand, reactive power generation and reactive power demand, respectively. We make $p^l/q^l := \Re(s^l)/\Im(s^l)$ as active/reactive power grid losses and $\mathbf{p}^0/\mathbf{q}^0 := \Re(\mathbf{s}^0)/\Im(\mathbf{s}^0) \in \mathbb{R}^3$ as active/reactive power injection from the bulk-transmission to the distribution grid's slack bus. First, upon solution of multi-phase *load-flow* problem, we have a solution $\hat{\mathbf{u}}_{\mathsf{L}}^{\mathsf{abc}}$ for given injections $(\hat{\mathbf{s}}_{\mathsf{L}}^{\Delta}, \hat{\mathbf{s}}_{\mathsf{L}}^{\mathsf{Y}})$, resulting in line flows and system losses $(\hat{\mathbf{s}}^{\mathsf{f,abc/t,abc}}, \hat{s}^{\mathsf{l,abc}})$. All these relationships can be summarized in (4.33). These equations have been presented earlier in detail in Sec. 3.4 and repeated below for convenience.

$$\mathrm{diag}(\hat{\mathbf{u}}_{\mathsf{L}}^{\mathsf{abc}})\mathbf{H}^\intercal \bar{\mathbf{i}}_{\mathsf{L}}^{\Delta} + \hat{\mathbf{s}}_{\mathsf{L}}^{\mathsf{Y}} = \mathrm{diag}(\hat{\mathbf{u}}_{\mathsf{L}}^{\mathsf{abc}})\bar{\mathbf{i}}_{\mathsf{L}}^{\mathsf{Y}}, \quad (4.33a)$$

$$\hat{\mathbf{s}}_{\mathsf{L}}^{\Delta} = \mathrm{diag}(\mathbf{H}\hat{\mathbf{u}}_{\mathsf{L}}^{\mathsf{abc}})\bar{\mathbf{i}}_{\mathsf{L}}^{\Delta}, \quad (4.33b)$$

$$\mathbf{i}_{\mathsf{L}}^{\mathsf{Y}} = \mathbf{Y}_{\mathsf{L0}}^{\mathsf{abc}}\mathbf{u}_0 + \mathbf{Y}_{\mathsf{LL}}^{\mathsf{abc}}\hat{\mathbf{u}}_{\mathsf{L}}^{\mathsf{abc}}, \quad (4.33c)$$

$$\hat{\mathbf{s}}^{\mathsf{f,abc/t,abc}} = \mathrm{diag}(\mathbf{A}_0^{\mathsf{f,abc/t,abc}}\mathbf{u}_0 + \mathbf{A}_{\mathsf{L}}^{\mathsf{f,abc/t,abc}}\hat{\mathbf{u}}_{\mathsf{L}}^{\mathsf{abc}})(\overline{\mathbf{Y}}_0^{\mathsf{f,abc/t,abc}}\bar{\mathbf{u}}_0 + \overline{\mathbf{Y}}_{\mathsf{L}}^{\mathsf{f,abc/t,abc}}\bar{\hat{\mathbf{u}}}_{\mathsf{L}}^{\mathsf{abc}}), \quad (4.33d)$$

$$s^{\mathsf{l,abc}} = \mathbf{u}_0{}^\intercal(\overline{\mathbf{Y}}_{00}^{\mathsf{abc}}\bar{\mathbf{u}}_0 + \overline{\mathbf{Y}}_{0\mathsf{L}}^{\mathsf{abc}}\bar{\hat{\mathbf{u}}}_{\mathsf{L}}^{\mathsf{abc}}) + \hat{\mathbf{u}}_{\mathsf{L}}^{\mathsf{abc}\intercal}(\overline{\mathbf{Y}}_{\mathsf{L}0}^{\mathsf{abc}}\bar{\mathbf{u}}_0 + \overline{\mathbf{Y}}_{\mathsf{LL}}^{\mathsf{abc}}\bar{\hat{\mathbf{u}}}_{\mathsf{L}}^{\mathsf{abc}}). \quad (4.33e)$$

Refer to Sec. 3.4 for information regarding above equations and its variables.

4.6.2 Multi-phase Economic Dispatch Problem

For dispatchable active and reactive power DGs, (4.34) presents a multi-phase variant of the single-phase ED problem in (4.3):

$$\min \quad \mathbf{c}_{\mathbf{p}_g^{\mathsf{Y}}}^{\mathsf{T}}\mathbf{p}_g^{\mathsf{Y}} + \mathbf{c}_{\mathbf{p}_g^{\Delta}}^{\mathsf{T}}\mathbf{p}_g^{\Delta} + \mathbf{c}_{\mathbf{q}_g^{\mathsf{Y}}}^{\mathsf{T}}\mathbf{q}_g^{\mathsf{Y}} + \mathbf{c}_{\mathbf{q}_g^{\Delta}}^{\mathsf{T}}\mathbf{q}_g^{\Delta} + \mathbf{c}_{\mathbf{p}^0}^{\mathsf{T}}\mathbf{p}^0 + \mathbf{c}_{\mathbf{q}^0}^{\mathsf{T}}\mathbf{q}^0 \tag{4.34a}$$

s.t.

$$\mathbf{1}_3^{\mathsf{T}}\mathbf{p}^0 + \mathbf{1}_{3n}^{\mathsf{T}}(\mathbf{p}_g^{\mathsf{Y}} + \mathbf{p}_g^{\Delta} - \mathbf{p}_l^{\mathsf{Y}} - \mathbf{p}_l^{\Delta}) = p^{\mathsf{l,abc}} : \lambda^{p,\mathsf{abc}} \tag{4.34b}$$

$$\mathbf{1}_3^{\mathsf{T}}\mathbf{q}^0 + \mathbf{1}_{3n}^{\mathsf{T}}(\mathbf{q}_g^{\mathsf{Y}} + \mathbf{q}_g^{\Delta} - \mathbf{q}_l^{\mathsf{Y}} - \mathbf{q}_l^{\Delta}) = q^{\mathsf{l,abc}} : \lambda^{q,\mathsf{abc}} \tag{4.34c}$$

$$|\mathbf{s}^{\mathsf{f,abc}}|^2 \leq (\mathbf{s}^{\mathsf{f,abc}})^2 \quad : \boldsymbol{\mu}^{+}_{s^{\mathsf{f,abc}}} \tag{4.34d}$$

$$|\mathbf{s}^{\mathsf{t,abc}}|^2 \leq (\mathbf{s}^{\mathsf{t,abc}})^2 \quad : \boldsymbol{\mu}^{+}_{s^{\mathsf{t,abc}}} \tag{4.34e}$$

$$\mathbf{v}_{\mathsf{L}}^{-,\mathsf{abc}} \leq \mathbf{v}_{\mathsf{L}}^{\mathsf{abc}} \leq \mathbf{v}_{\mathsf{L}}^{+,\mathsf{abc}} \quad : \boldsymbol{\mu}^{-}_{v_{\mathsf{L}}^{\mathsf{abc}}}, \boldsymbol{\mu}^{+}_{v_{\mathsf{L}}^{\mathsf{abc}}} \tag{4.34f}$$

$$\mathbf{p}_g^{\mathsf{Y}-} \leq \mathbf{p}_g^{\mathsf{Y}} \leq \mathbf{p}_g^{\mathsf{Y}+} \quad : \boldsymbol{\mu}^{-}_{\mathbf{p}_g^{\mathsf{Y}}}, \boldsymbol{\mu}^{+}_{\mathbf{p}_g^{\mathsf{Y}}} \tag{4.34g}$$

$$\mathbf{q}_g^{\mathsf{Y}-} \leq \mathbf{q}_g^{\mathsf{Y}} \leq \mathbf{q}_g^{\mathsf{Y}+} \quad : \boldsymbol{\mu}^{-}_{\mathbf{q}_g^{\mathsf{Y}}}, \boldsymbol{\mu}^{+}_{\mathbf{q}_g^{\mathsf{Y}}} \tag{4.34h}$$

$$\mathbf{p}_g^{\Delta-} \leq \mathbf{p}_g^{\Delta} \leq \mathbf{p}_g^{\Delta+} \quad : \boldsymbol{\mu}^{-}_{\mathbf{p}_g^{\Delta}}, \boldsymbol{\mu}^{+}_{\mathbf{p}_g^{\Delta}} \tag{4.34i}$$

$$\mathbf{q}_g^{\Delta-} \leq \mathbf{q}_g^{\Delta} \leq \mathbf{q}_g^{\triangle+} \quad : \boldsymbol{\mu}^{-}_{\mathbf{p}_g^{\Delta}}, \boldsymbol{\mu}^{+}_{\mathbf{p}_g^{\Delta}} \tag{4.34j}$$

The vector $\mathbf{c}_{(\mathbf{p}/\mathbf{q})_g^{\mathsf{Y}/\Delta}}/\mathbf{c}_{(\mathbf{p}/\mathbf{q})^0}$ represents marginal cost of providing energy from DGs/slack-bus, i.e. $(\mathbf{p}/\mathbf{q})_g^{\mathsf{Y}/\Delta}$/ $(\mathbf{p}/\mathbf{q})^0$. The problem (4.34) minimizes the overall cost for dispatching generation resources, with respect to the following constraints: 1) constraints (4.34b) and (4.34c) balances grid's active and reactive powers, 2) constraint (4.34d)/(4.34e) considers the square of the apparent power flow line limits in from/to directions, 3) the voltage magnitude $\mathbf{v}_{\mathsf{L}}^{\mathsf{abc}}$ is constrained in (4.34f), whereas active and reactive power of each wye-connected and delta-connected generators are constrained through (4.34g) – (4.34j). The variables listed to the right of the colon are the Lagrange multipliers and variables with superscript $+/-$ the respective maximum/minimum limits.

4.6.3 Multi-Phase Distribution Locational Marginal Price model

We follow the same strategy for developing DLMP model, as Sec. 4.2. First, we obtain a linear counterpart of (4.34) using the approximations developed in Sec. 3.4.2, repeated below for the convenience:

$$\tilde{\mathbf{v}}_{\mathsf{L}}{}^{\mathsf{abc}} = \hat{\mathbf{a}}^{\mathsf{abc}} + \mathbf{M}^{\mathbf{v}_{\mathsf{L}},\mathsf{Y}}\mathbf{s}_{\mathsf{L}}^{\mathsf{inj,Y}} + \mathbf{M}^{\mathbf{v}_{\mathsf{L}},\Delta}\mathbf{s}_{\mathsf{L}}^{\mathsf{inj},\Delta}, \tag{4.35a}$$

$$|\tilde{\mathbf{s}}^{\mathsf{f,abc}}|^2 = \hat{\mathbf{b}}^{\mathsf{abc}} + \mathbf{M}^{\mathbf{s}^{\mathsf{f}},\mathsf{Y}}\mathbf{s}_{\mathsf{L}}^{\mathsf{inj,Y}} + \mathbf{M}^{\mathbf{s}^{\mathsf{f}},\Delta}\mathbf{s}_{\mathsf{L}}^{\mathsf{inj},\Delta}, \tag{4.35b}$$

$$|\tilde{\mathbf{s}}^{\mathsf{t,abc}}|^2 = \hat{\mathbf{c}}^{\mathsf{abc}} + \mathbf{M}^{\mathbf{s}^{\mathsf{t}},\mathsf{Y}}\mathbf{s}_{\mathsf{L}}^{\mathsf{inj,Y}} + \mathbf{M}^{\mathbf{s}^{\mathsf{t}},\Delta}\mathbf{s}_{\mathsf{L}}^{\mathsf{inj},\Delta}, \tag{4.35c}$$

$$\tilde{p}^{\mathsf{l,abc}} = \hat{d}^{\mathsf{abc}} + \mathbf{M}^{p^{\mathsf{l}},\mathsf{Y}}\mathbf{s}_{\mathsf{L}}^{\mathsf{inj,Y}} + \mathbf{M}^{p^{\mathsf{l}},\Delta}\mathbf{s}_{\mathsf{L}}^{\mathsf{inj},\Delta}, \tag{4.35d}$$

$$\tilde{q}^{\mathsf{l,abc}} = \hat{e}^{\mathsf{abc}} + \mathbf{M}^{q^{\mathsf{l}},\mathsf{Y}}\mathbf{s}_{\mathsf{L}}^{\mathsf{inj,Y}} + \mathbf{M}^{q^{\mathsf{l}},\Delta}\mathbf{s}_{\mathsf{L}}^{\mathsf{inj},\Delta}, . \tag{4.35e}$$

Note that after replacing nonlinear constraints in (4.34) with liner approximations of (4.35), the resultant problem is now a multi-phase version of single-phase approximate quadratic program (4.20). This is because of the similar assumptions for cost functions in (4.34a) as **R. 4.2**.

Now following the similar procedure outlined before, we first obtain the Lagrangian of (4.34):

$$
\begin{aligned}
&\mathcal{L}^{\text{abc}}(\mathbf{p}_g^{\text{Y}}, \lambda^{p,\text{abc}}, \lambda^{q,\text{abc}}, \boldsymbol{\mu}^{+}_{s^{\text{f,abc}}}, \boldsymbol{\mu}^{+}_{s^{\text{t,abc}}}, \boldsymbol{\mu}^{-}_{\mathbf{v}_{\text{L}}^{\text{abc}}}, \boldsymbol{\mu}^{+}_{\mathbf{v}_{\text{L}}^{\text{abc}}}, \boldsymbol{\mu}^{-}_{\mathbf{p}_g^{\text{Y}}}, \boldsymbol{\mu}^{+}_{\mathbf{p}_g^{\text{Y}}}, \boldsymbol{\mu}^{-}_{\mathbf{q}_g^{\text{Y}}}, \boldsymbol{\mu}^{+}_{\mathbf{q}_g^{\text{Y}}}, \boldsymbol{\mu}^{-}_{\mathbf{p}_g^{\Delta}}, \boldsymbol{\mu}^{+}_{\mathbf{p}_g^{\Delta}}, \boldsymbol{\mu}^{-}_{\mathbf{q}_g^{\Delta}}, \boldsymbol{\mu}^{+}_{\mathbf{q}_g^{\Delta}}) \\
&= \mathbf{c}^{\mathsf{T}}_{\mathbf{p}_g^{\text{Y}}}\mathbf{p}_g^{\text{Y}} + \mathbf{c}^{\mathsf{T}}_{\mathbf{p}_g^{\Delta}}\mathbf{p}_g^{\Delta} + \mathbf{c}^{\mathsf{T}}_{\mathbf{q}_g^{\text{Y}}}\mathbf{q}_g^{\text{Y}} + \mathbf{c}^{\mathsf{T}}_{\mathbf{q}_g^{\Delta}}\mathbf{q}_g^{\Delta} + \mathbf{c}^{\mathsf{T}}_{\mathbf{p}^0}\mathbf{p}^0 + \mathbf{c}^{\mathsf{T}}_{\mathbf{q}^0}\mathbf{q}^0 \\
&- \lambda^{p,\text{abc}}\Big(\mathbf{1}_3^{\mathsf{T}}\mathbf{p}^0 + \mathbf{1}_{3n}^{\mathsf{T}}(\mathbf{p}_g^{\text{Y}} + \mathbf{p}_g^{\Delta} - \mathbf{p}_l^{\text{Y}} - \mathbf{p}_l^{\Delta}) - \tilde{p}^{\text{l,abc}}\Big) \\
&- \lambda^{q,\text{abc}}\Big(\mathbf{1}_3^{\mathsf{T}}\mathbf{q}^0 + \mathbf{1}_{3n}^{\mathsf{T}}(\mathbf{q}_g^{\text{Y}} + \mathbf{q}_g^{\Delta} - \mathbf{q}_l^{\text{Y}} - \mathbf{q}_l^{\Delta}) - \tilde{p}^{\text{l,abc}}\Big) \\
&- (\boldsymbol{\mu}^{+}_{s^{\text{f,abc}}})^{\mathsf{T}}\Big(|\tilde{\mathbf{s}}^{\text{f,abc}}|^2 - (\mathbf{s}^{\text{f,abc}})^2\Big) - (\boldsymbol{\mu}^{+}_{s^{\text{t,abc}}})^{\mathsf{T}}\Big(|\tilde{\mathbf{s}}^{\text{t,abc}}|^2 - (\mathbf{s}^{\text{t,abc}})^2\Big) \\
&- (\boldsymbol{\mu}^{+}_{\mathbf{v}_{\text{L}}^{\text{abc}}})^{\mathsf{T}}\Big(\tilde{\mathbf{v}}_{\text{L}}^{\text{abc}} - \mathbf{v}_{\text{L}}^{+,\text{abc}}\Big) + (\boldsymbol{\mu}^{-}_{\mathbf{v}_{\text{L}}^{\text{abc}}})^{\mathsf{T}}\Big(\tilde{\mathbf{v}}_{\text{L}}^{\text{abc}} - \mathbf{v}_{\text{L}}^{-,\text{abc}}\Big) - (\boldsymbol{\mu}^{+}_{\mathbf{p}_g^{\text{Y}}})^{\mathsf{T}}(\mathbf{p}_g^{\text{Y}} - \mathbf{p}_g^{\text{Y}+}) + (\boldsymbol{\mu}^{-}_{\mathbf{p}_g^{\text{Y}}})^{\mathsf{T}}\Big(\mathbf{p}_g^{\text{Y}} - \mathbf{p}_g^{\text{Y}-}\Big) \\
&- (\boldsymbol{\mu}^{+}_{\mathbf{q}_g^{\text{Y}}})^{\mathsf{T}}\Big(\mathbf{q}_g^{\text{Y}} - \mathbf{q}_g^{\text{Y}+}\Big) + (\boldsymbol{\mu}^{-}_{\mathbf{q}_g^{\text{Y}}})^{\mathsf{T}}\Big(\mathbf{q}_g^{\text{Y}} - \mathbf{q}_g^{\text{Y}-}\Big) - (\boldsymbol{\mu}^{+}_{\mathbf{p}_g^{\Delta}})^{\mathsf{T}}\Big(\mathbf{p}_g^{\Delta} - \mathbf{p}_g^{\Delta+}\Big) + (\boldsymbol{\mu}^{-}_{\mathbf{p}_g^{\Delta}})^{\mathsf{T}}\Big(\mathbf{p}_g^{\Delta} - \mathbf{p}_g^{\Delta-}\Big) \\
&- (\boldsymbol{\mu}^{+}_{\mathbf{q}_g^{\Delta}})^{\mathsf{T}}\Big(\mathbf{q}_g^{\Delta} - \mathbf{q}_g^{\Delta+}\Big) + (\boldsymbol{\mu}^{-}_{\mathbf{q}_g^{\Delta}})^{\mathsf{T}}\Big(\mathbf{q}_g^{\Delta} - \mathbf{q}_g^{\Delta-}\Big). \qquad (4.36)
\end{aligned}
$$

Using the similar methodology as single-phase equivalent grid model for deriving DLMPs, we also develop multi-phase grid's DLMP model. The DLMP model must represent components for both active and reactive power injections of wye/delta connections. We denote active power DLMP cleared at all grid buses for wye/delta connection as $\boldsymbol{\pi}_{\mathbf{p}}^{\text{Y, Grid}}/\boldsymbol{\pi}_{\mathbf{p}}^{\Delta,\text{Grid}}$ and reactive power DLMP for wye/delta connections as $\boldsymbol{\pi}_{\mathbf{q}}^{\text{Y, Grid}}/\boldsymbol{\pi}_{\mathbf{q}}^{\Delta,\text{Grid}}$. Similar to single-phase DLMP model, we desire grid cleared DLMP value to be decomposable into its energy, loss, congestion and voltage components. First, consider for wye connections, the final grid cleared DLMP $\boldsymbol{\pi}_{\mathbf{p}}^{\text{Y,Grid}}/\boldsymbol{\pi}_{\mathbf{q}}^{\text{Y, Grid}}$ is to be represented as a sum of its energy $\boldsymbol{\pi}_{\mathbf{p}}^{\text{E,Y}}/\boldsymbol{\pi}_{\mathbf{q}}^{\text{E, Y}}$, loss $\boldsymbol{\pi}_{\mathbf{p}}^{\text{Y, L}}/\boldsymbol{\pi}_{\mathbf{q}}^{\text{Y, L}}$, congestion $\boldsymbol{\pi}_{\mathbf{p}}^{\text{Y, C}}/\boldsymbol{\pi}_{\mathbf{q}}^{\text{Y, C}}$ and voltage components $\boldsymbol{\pi}_{\mathbf{p}}^{\text{Y, V}}/\boldsymbol{\pi}_{\mathbf{q}}^{\text{Y, V}}$, i.e.,

$$\boldsymbol{\pi}_{\mathbf{p}}^{\text{Y, Grid}} = \boldsymbol{\pi}_{\mathbf{p}}^{\text{Y,E}} + \boldsymbol{\pi}_{\mathbf{p}}^{\text{Y,L}} + \boldsymbol{\pi}_{\mathbf{p}}^{\text{Y,C}} + \boldsymbol{\pi}_{\mathbf{p}}^{\text{Y,V}} \qquad (4.37)$$

$$\boldsymbol{\pi}_{\mathbf{q}}^{\text{Y, Grid}} = \boldsymbol{\pi}_{\mathbf{q}}^{\text{Y,E}} + \boldsymbol{\pi}_{\mathbf{q}}^{\text{Y,L}} + \boldsymbol{\pi}_{\mathbf{q}}^{\text{Y,C}} + \boldsymbol{\pi}_{\mathbf{q}}^{\text{Y,V}} \qquad (4.38)$$

In order to derive the above form, recall from Sec. 4.2 DLMPs were defined as the marginal value of providing incremental demand at a specified bus. Using this definition, we can proceed to obtain, for wye connections, active power DLMPs $\boldsymbol{\pi}_{\mathbf{p}}^{\text{Y,Grid}}$ as:

$$
\begin{aligned}
\boldsymbol{\pi}_{\mathbf{p}}^{\text{Y, Grid}} &:= \frac{\partial \mathcal{L}^{\text{abc}}}{\partial \mathbf{p}_l^{\text{Y}}} = \lambda^{p,\text{abc}}\mathbf{1}_{3n} - (\frac{\partial \tilde{p}^{\text{l,abc}}}{\partial \mathbf{p}_l^{\text{Y}}})^{\mathsf{T}}\lambda^{p,\text{abc}} - (\frac{\partial \tilde{q}^{\text{l,abc}}}{\partial \mathbf{p}_l^{\text{Y}}})^{\mathsf{T}}\lambda^{q,\text{abc}} \\
&+ (\frac{\partial \tilde{s}^{\text{f,abc}}}{\partial \mathbf{p}_l^{\text{Y}}})^{\mathsf{T}}\boldsymbol{\mu}^{+}_{s^{\text{f,abc}}} + (\frac{\partial \tilde{s}^{\text{t,abc}}}{\partial \mathbf{p}_l^{\text{Y}}})^{\mathsf{T}}\boldsymbol{\mu}^{+}_{s^{\text{t,abc}}} + (\frac{\partial \tilde{\mathbf{v}}_{\text{L}}^{\text{abc}}}{\partial \mathbf{p}_l^{\text{Y}}})^{\mathsf{T}}(\boldsymbol{\mu}^{+}_{\mathbf{v}_{\text{L}}^{\text{abc}}} + \boldsymbol{\mu}^{-}_{\mathbf{v}_{\text{L}}^{\text{abc}}}), \qquad (4.39)
\end{aligned}
$$

and reactive power DLMPs $\boldsymbol{\pi}_{\mathbf{q}}^{\text{Y}}$ as:

$$
\begin{aligned}
\boldsymbol{\pi}_{\mathbf{q}}^{\text{Y, Grid}} &:= \frac{\partial \mathcal{L}^{\text{abc}}}{\partial \mathbf{q}_l^{\text{Y}}} = \lambda^{q,\text{abc}}\mathbf{1}_{3n} - (\frac{\partial \tilde{p}^{\text{l,abc}}}{\partial \mathbf{q}_l^{\text{Y}}})^{\mathsf{T}}\lambda^{p,\text{abc}} - (\frac{\partial \tilde{q}^{\text{l,abc}}}{\partial \mathbf{q}_l^{\text{Y}}})^{\mathsf{T}}\lambda^{q,\text{abc}} \\
&+ (\frac{\partial \tilde{s}^{\text{f,abc}}}{\partial \mathbf{q}_l^{\text{Y}}})^{\mathsf{T}}\boldsymbol{\mu}^{+}_{s^{\text{f,abc}}} + (\frac{\partial \tilde{s}^{\text{t,abc}}}{\partial \mathbf{q}_l^{\text{Y}}})^{\mathsf{T}}\boldsymbol{\mu}^{+}_{s^{\text{t,abc}}} + (\frac{\partial \tilde{\mathbf{v}}_{\text{L}}^{\text{abc}}}{\partial \mathbf{q}_l^{\text{Y}}})^{\mathsf{T}}(\boldsymbol{\mu}^{+}_{\mathbf{v}_{\text{L}}^{\text{abc}}} + \boldsymbol{\mu}^{-}_{\mathbf{v}_{\text{L}}^{\text{abc}}}), \qquad (4.40)
\end{aligned}
$$

Note that the above presented sensitivities $\frac{\partial(\cdot)}{\partial \mathbf{p}_l^{\text{Y}}/\mathbf{q}_l^{\text{Y}}}$ can be directly obtained from approximations in (4.35). Utilizing these sensitivities gives us the desired decomposition of (4.37) as:

$$\boldsymbol{\pi}_{\mathbf{p}}^{\mathsf{Y,E}} := \lambda^{p,\mathsf{abc}}\mathbf{1}_{3\mathsf{n}}, \tag{4.41a}$$
$$\boldsymbol{\pi}_{\mathbf{p}}^{\mathsf{Y,L}} := -(\mathbf{M}^{p^{\mathsf{l}},\mathsf{Y}})_{\mathbf{p}}^{\intercal}\lambda^{p,\mathsf{abc}} - (\mathbf{M}^{q^{\mathsf{l}},\mathsf{Y}})_{\mathbf{p}}^{\intercal}\lambda^{q,\mathsf{abc}}, \tag{4.41b}$$
$$\boldsymbol{\pi}_{\mathbf{p}}^{\mathsf{Y,C}} := (\mathbf{M}^{\mathbf{s}^{\mathsf{f}},\mathsf{Y}})_{\mathbf{p}}^{\intercal}\boldsymbol{\mu}_{s^{\mathsf{f}}}^{+} + (\mathbf{M}^{\mathbf{s}^{\mathsf{t}},\mathsf{Y}})_{\mathbf{p}}^{\intercal}\boldsymbol{\mu}_{s^{\mathsf{t}}}^{+}, \tag{4.41c}$$
$$\boldsymbol{\pi}_{\mathbf{p}}^{\mathsf{Y,V}} := (\mathbf{M}^{\mathbf{v}_{\mathsf{L}},\mathsf{Y}})_{\mathbf{p}}^{\intercal}(\boldsymbol{\mu}_{\mathbf{v}_{\mathsf{L}}}^{+} - \boldsymbol{\mu}_{\mathbf{v}_{\mathsf{L}}}^{-}), \tag{4.41d}$$

and of (4.40) as:

$$\boldsymbol{\pi}_{\mathbf{q}}^{\mathsf{Y,E}} := \lambda^{q,\mathsf{abc}}\mathbf{1}_{3\mathsf{n}}, \tag{4.42a}$$
$$\boldsymbol{\pi}_{\mathbf{q}}^{\mathsf{Y,L}} := -(\mathbf{M}^{p^{\mathsf{l}},\mathsf{Y}})_{\mathbf{q}}^{\intercal}\lambda^{p,\mathsf{abc}} - (\mathbf{M}^{q^{\mathsf{l}},\mathsf{Y}})_{\mathbf{q}}^{\intercal}\lambda^{q,\mathsf{abc}}, \tag{4.42b}$$
$$\boldsymbol{\pi}_{\mathbf{q}}^{\mathsf{Y,C}} := (\mathbf{M}^{\mathbf{s}^{\mathsf{f}},\mathsf{Y}})_{\mathbf{q}}^{\intercal}\boldsymbol{\mu}_{s^{\mathsf{f}}}^{+} + (\mathbf{M}^{\mathbf{s}^{\mathsf{t}},\mathsf{Y}})_{\mathbf{q}}^{\intercal}\boldsymbol{\mu}_{s^{\mathsf{t}}}^{+}, \tag{4.42c}$$
$$\boldsymbol{\pi}_{\mathbf{q}}^{\mathsf{Y,V}} := (\mathbf{M}^{\mathbf{v}_{\mathsf{L}},\mathsf{Y}})_{\mathbf{q}}^{\intercal}(\boldsymbol{\mu}_{\mathbf{v}_{\mathsf{L}}}^{+} - \boldsymbol{\mu}_{\mathbf{v}_{\mathsf{L}}}^{-}), \tag{4.42d}$$

where sub-matrices $\mathbf{M}_{\mathbf{p}/\mathbf{q}}^{(\cdot)}$ simply corresponds to active/reactive injection entries of $\mathbf{M}^{(\cdot)}$ in (4.35). For delta connections DLMPs, similar expressions exist after simply evaluating for active power: $\boldsymbol{\pi}_{\mathbf{p}}^{\Delta,\mathsf{Grid}} := \frac{\partial \mathcal{L}^{\mathsf{abc}}}{\partial \mathbf{p}_f^{\Delta}}$ and for reactive power: $\boldsymbol{\pi}_{\mathbf{q}}^{\Delta,\mathsf{Grid}} := \frac{\partial \mathcal{L}^{\mathsf{abc}}}{\partial \mathbf{q}_f^{\Delta}}$. Next, we demonstrate the implementation of multi-phase DLMP method on an unbalanced and multi-phase distribution grid.

Example 4.2

The proposed method is tested on the multi-phase and unbalanced IEEE 4-bus radial grid [47]. The readers are referred to the openDSS script file in Appendix A.1.3 for more information regarding the modeled grid. In example 3.8- 3.10 we provided verification of the *load-flow* solution and its approximation. Now we obtain DLMP for the modeled grid by including at bus n4 one DG between phase a and b (n4–ab) and another between phase a and ground (n4–a). In this way, we test the model for both delta and wye connections, where in this case delta and wye are simply a phase-phase and a phase-ground connection, respectively. The DGs are assumed to be operated as follows: 1) all DGs can control their per phase active and reactive power independently; 2) per-phase maximum and minimum active and reactive power dispatch for all DGs is constrained within $[0,\ 0.3]$ MW and $[-0.15,\ 0.15]$ MVar and; 3) marginal cost of active and reactive power for all DGs is set at 1 \$/MWh and 0.5 \$/MVarh. In order to obtain higher dispatch values from DGs, the marginal price of supplying active and reactive power to the grid (root-bus) is kept higher than DGs, at 10 \$/MWh and 5 \$/MVarh. Moreover, to demonstrate the full capability of the developed model, we simulate a scenario where both grid voltage at bus n4 and squared "from" line flow limits at the line connecting bus n3 and n4 are binding.

Table 4.4: Active (MW) and Reactive Power (MVar) Dispatch from DGs and root-bus.

	root-bus–a	root-bus–b	root-bus–c	n4–a	n4–ab
$\mathbf{p}_g^{\mathsf{Y}}/\mathbf{p}_g^{\Delta}$	0.257	0	0	0.297	0.300
$\mathbf{q}_g^{\mathsf{Y}}/\mathbf{q}_g^{\Delta}$	0.244	0	0	0.118	0.150

The active and reactive power outputs of DGs and the root-bus are presented in Ta-

ble. 4.4. Note that DGs are not dispatched equally, even though they share the exact same marginal cost. This is because due to voltage and line flow binding at bus n4. As injections from phase-ground (wye) connection has a higher impact on voltage reduction/increment (see example 3.10), DG with phase-ground connection is moved away from its full dispatch capabilities instead of DG with phase-phase connection. This property is also going to be analyzed later.

Fig. 4.6 and 4.7 shows DLMPs for all wye and delta connections. For wye connection, at n4–a, active power DLMP is equal to the marginal value of supplying power by the respective wye connected DG at n4–a (1 $/MWh). However, for delta connection, at n4–ab, the active power DLMP is 6.809, which is more than the marginal value of supplying power by the respective wye connected DG at n4–ab (1 $/MWh). This is because delta connected DG is dispatched to its maximum capabilities, hence the extra amount of power flows comes from the root-bus, which has a higher marginal cost of supplying power (10 $/MWh). The same observation holds true for reactive power DLMPs.

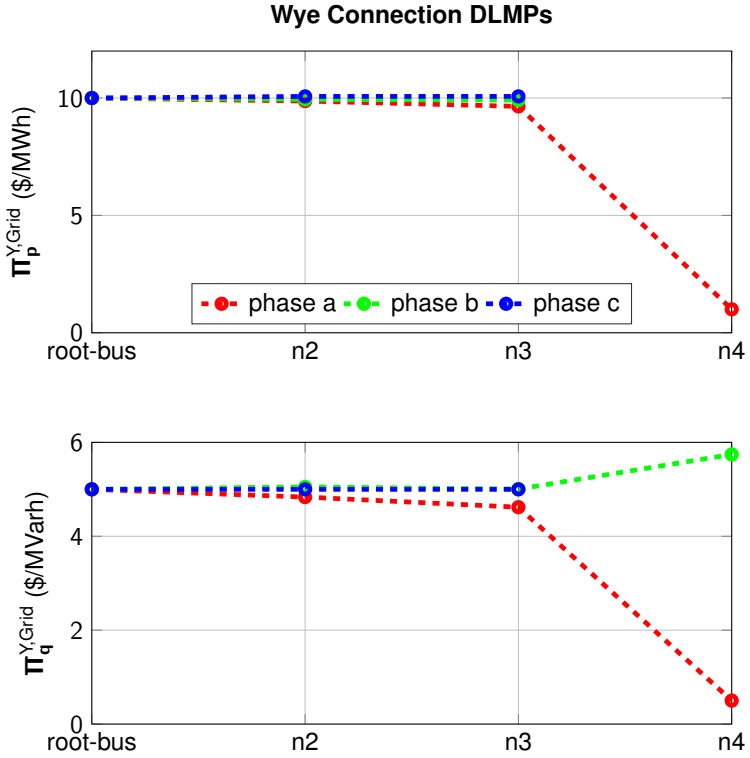

Figure 4.6: DLMPs for all phase-ground (wye) connections.

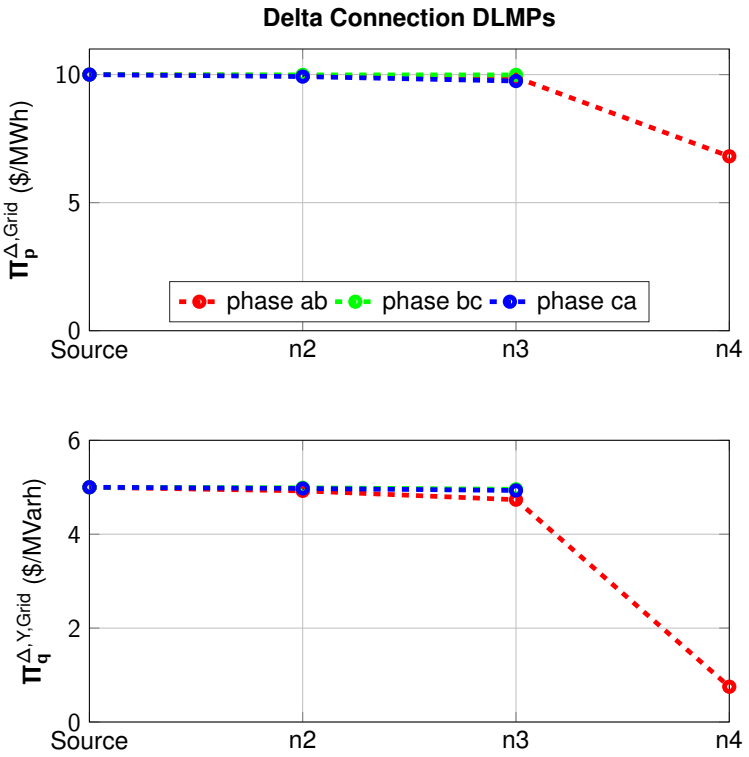

Figure 4.7: DLMPs for all phase-phase (delta) connections

For buses connected to DGs, Table 4.5 and 4.6 respectively present active and reactive power DLMPs (in bold) along with their breakdown in terms of their energy, congestion, losses, and voltage components. Moreover, the respective DG's marginal supply, i.e. $\frac{\partial \mathcal{L}^{\text{abc}}}{\partial \mathbf{p}_g^{\text{Y}/\Delta}} = \mathbf{c}_{\mathbf{p}_g^{\text{Y}/\Delta}} + \boldsymbol{\mu}^{+}_{\mathbf{p}_g^{\text{Y}/\Delta}} - \boldsymbol{\mu}^{-}_{\mathbf{p}_g^{\text{Y}/\Delta}}$ for active power and $\frac{\partial \mathcal{L}^{\text{abc}}}{\partial \mathbf{q}_g^{\text{Y}/\Delta}} = \mathbf{c}_{\mathbf{q}_g^{\text{Y}/\Delta}} + \boldsymbol{\mu}^{+}_{\mathbf{q}_g^{\text{Y}/\Delta}} - \boldsymbol{\mu}^{-}_{\mathbf{q}_g^{\text{Y}/\Delta}}$ for reactive power is also shown in Table 4.5 and 4.6.

Table 4.5: Active Power DLMPs ($/MWh) for wye- and delta-connection.

Bus–phase	$\boldsymbol{\pi}_{\mathbf{p}}^{\text{Y,E}}$	$\boldsymbol{\pi}_{\mathbf{p}}^{\text{Y,L}}$	$\boldsymbol{\pi}_{\mathbf{p}}^{\text{Y,C}}$	$\boldsymbol{\pi}_{\mathbf{p}}^{\text{Y,V}}$	$\boldsymbol{\pi}_{\mathbf{p}}^{\text{Y, Grid}}$	$\mathbf{c}_{\mathbf{p}_g^{\text{Y}}}$	$\boldsymbol{\mu}^{+}_{\mathbf{p}_g^{\text{Y}}} - \boldsymbol{\mu}^{-}_{\mathbf{p}_g^{\text{Y}}}$
root-bus–a	10	0	0	0	**10**	10	0
root-bus–b		0	0	0	**10**		0
root-bus–c		0	0	0	**10**		0
n4–a		-1.2384	-6.7292	-1.0324	**1**	1	0
Bus–phases	$\boldsymbol{\pi}_{\mathbf{p}}^{\Delta,\text{E}}$	$\boldsymbol{\pi}_{\mathbf{p}}^{\Delta,\text{Y}}$	$\boldsymbol{\pi}_{\mathbf{p}}^{\Delta,\text{C}}$	$\boldsymbol{\pi}_{\mathbf{p}}^{\Delta,\text{V}}$	$\boldsymbol{\pi}_{\mathbf{p}}^{\Delta,\text{Grid}}$	$\mathbf{c}_{\mathbf{p}_g^{\Delta}}$	$\boldsymbol{\mu}^{+}_{\mathbf{p}_g^{\Delta}} - \boldsymbol{\mu}^{-}_{\mathbf{p}_g^{\Delta}}$
n4–ab	10	-0.5464	-2.7120	0.0678	**6.8093**	1	5.8093

Table 4.6: Reactive Power DLMPs ($/MVarh) for wye- and delta-connection.

Bus–phase	$\boldsymbol{\pi}_{\mathbf{q}}^{\mathrm{Y,E}}$	$\boldsymbol{\pi}_{\mathbf{q}}^{\mathrm{Y,L}}$	$\boldsymbol{\pi}_{\mathbf{q}}^{\mathrm{Y,C}}$	$\boldsymbol{\pi}_{\mathbf{q}}^{\mathrm{Y,V}}$	$\boldsymbol{\pi}_{\mathbf{q}}^{\mathrm{Y,\,Grid}}$	$\mathbf{c}_{\mathbf{q}_g^{\mathrm{Y}}}$	$\boldsymbol{\mu}_{\mathbf{q}_g^{\mathrm{Y}}}^{+} - \boldsymbol{\mu}_{\mathbf{q}_g^{\mathrm{Y}}}^{-}$
root-bus–a	5	0	0	0	**5**	5	0
root-bus–b		0	0	0	**5**		0
root-bus–c		0	0	0	**5**		0
n4–a		-0.4064	-2.3664	-1.7272	**0.5**	0.5	0
Bus–phases	$\boldsymbol{\pi}_{\mathbf{p}}^{\Delta,\mathrm{E}}$	$\boldsymbol{\pi}_{\mathbf{q}}^{\Delta,\mathrm{Y}}$	$\boldsymbol{\pi}_{\mathbf{q}}^{\Delta,\mathrm{C}}$	$\boldsymbol{\pi}_{\mathbf{q}}^{\Delta,\mathrm{V}}$	$\boldsymbol{\pi}_{\mathbf{q}}^{\Delta,\mathrm{Grid}}$	$\mathbf{c}_{\mathbf{p}_q^{\Delta}}$	$\boldsymbol{\mu}_{\mathbf{p}_q^{\Delta}}^{+} - \boldsymbol{\mu}_{\mathbf{q}_g^{\Delta}}^{-}$
n4ab	5	-0.4860	-2.8847	-0.8779	**0.7514**	0.5	0.2514

As sum of both left and right side components to the final DLMPs (in bold) are equal in Table 4.5 & 4.6, this validates that the obtained DLMPs represent true marginal value of the delivered power. Also, one can observe that each DLMP component has a physical interpretation. For example, non-zero congestion components $\boldsymbol{\pi}_{(\cdot)}^{(\cdot),\mathrm{C}}$ is due to congestion at line connecting $\{$n–3a-n–4a$\}$. Similarly, the voltage magnitude is binding at location n4–a which is reflected upon $\boldsymbol{\pi}_{(\cdot)}^{(\cdot),\mathrm{V}}$. Note that the negative DLMP component reflect that the marginal increase in active/reactive power demand (decrease in active/reactive power injection) improves the overall grid dispatch cost. This also explains the reason for DG at location n4–a to dispatch active and reactive power below its maximum allowable limits.

From the above presented example, it is clear that DLMP at each phase is sensitive to individual phase-ground or phase-phase injections. This advocates the proposed DLMP model for each phase as it can present higher granularity and provide better knowledge of marginal value of supplying power to multi-phase and unbalanced distribution grids.

Chapter 5

Distribution Grid Market: Day-ahead Efficient Resource Allocation Dispatch

In this chapter, the developed solution algorithm and the price derivation of chapter 4 are used to organize a distribution grid market framework. First, we develop a multi-period ED, containing inter-temporal energy constraints from FLs. The underlying optimization problem resembles the same structure as the global power balance formulation used at the transmission level (wholesale) market, as discussed in detail in chapter 4. Then, using the concept of convexity in electricity market from chapter 2, we show that the proposed distribution grid market framework allocates the available flexibility resource efficiently.

The main contributions of this chapter is in proposing a distribution grid market framework which i) caters for both instantaneous (DGs) and inter-temporal energy constraints (FLs) ii) includes nonlinear power flow equations and iii) while efficiently allocating flexibility resources obtains a price structure which is physically interpretable and decomposable.

5.1 Local Distribution Grid Market: Overview

Fig. 5.1 presents the overview of the proposed local distribution grid market. The proposed local market aims to schedule flexible loads (FLs) and distributed generators (DGs) on a day-ahead basis. For the purpose of diversity and relevance to recent advances in inter-temporal load modeling, the proposed model is multi-period. This has the following advantages:

- it allows for a more accurate description of flexible load modeling, because closer to the consumption (distribution grids), static aggregated load modeling of transmission grids might not be accurate [48];
- it aids in scheduling flexibility resources with inter-temporal energy requirements; and
- it allows for a wide range of model applications and extensions, to be shown in the discussion part of this thesis (chapter 6).

Hence, the local market not only dispatches instantaneous power but also caters for energy planned over a certain planning horizon. In doing so, the cleared price from the local distribution grid market aims to obtain an optimal resource allocation for the entire planning horizon duration.

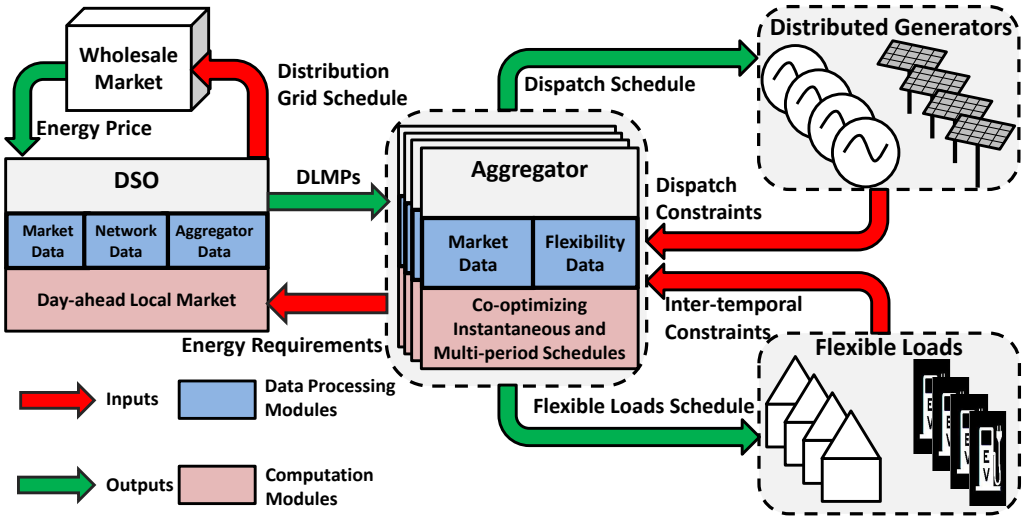

Figure 5.1: Overview of the proposed local distribution grid Market, to be cleared on a day-ahead basis. The input and output are marked with respect to their respective connected entities. For example, energy requirements to the DSO is an input from the aggregator, which is an output from aggregators after it has run its own optimization.

Holistically, the local distribution grid market is envisioned to operate as the following interaction between two main entities, i.e. the DSO and aggregators:

1. Aggregators obtain energy requirements and preferences from its contracted distributed generators (DGs) and flexible loads (FLs) and optimize their total energy requirements. Once computed, aggregators pass their energy requirements to the DSO.
2. On a day-ahead basis, the DSO collects information regarding aggregators' energy requirements, energy prices cleared at the wholesale market and its underlying grid. With this information, the DSO clears a spatio-temporal price, i.e., for each time interval of the planning horizon and buses of the grid. We term this price as distribution locational marginal price (DLMP).

Next, we describe the roles of the involved entities in the local distribution grid market.

5.2 Aggregator

We consider aggregator as a profit seeking entity, responsible for operating its contracted flexible loads. We assume that aggregator is economically rational, i.e. it maximizes its individual surplus. In particular, we assume that, similar to flexibility resources, aggregator aims to minimize the energy procurement cost while meeting the required energy requirements [41, 58, 35, 34]. The more involved aggregator formulations, such as risk aversion due to price uncertainties [16, 46] are considered out of scope for this thesis[1]. Finally, it is assumed that aggregator is a price-taking entity, with no market power. This is again a common assumption taken when large number of players exist in a market [59].

[1]Nevertheless, these uncertain formulations can also be cast as convex optimization problems[87, 11].

Remark 5.1. For notational convenience, we assume one aggregator for modeling the distribution grid local market. However, the methodology can be easily extended to generic number of aggregators along with DGs and FLs in the grid.

5.2.1 Models

We extend flexibility resource modeling presented in chapter 4 to represent FLs as planning over a time (t) horizon $\forall t \in \mathcal{T}$. However, similar to chapter 4, we keep DGs as a source of instantaneous power dispatch. The FLs are assumed to optimize their energy procurement cost of active powers for all $t \in \mathcal{T}$, i.e., $\mathbf{p}^{\mathsf{fl}}_t := (p^{\mathsf{fl}}_{1,t}, \dots, p^{\mathsf{fl}}_{n,t})^\intercal$ while keeping track of their state-of-charge (SOC) $\mathbf{ch}_t := (ch_{1,t}, \dots, ch_{n,t})^\intercal$, given an initial SOC $\mathbf{ch}_0$ before the beginning of planning horizon, i.e.,

$$\mathbf{ch}^{\mathsf{fl}}_t = \mathbf{ch}^{\mathsf{fl}}_0 + \mathbf{D}_t \mathbf{p}^{\mathsf{fl}}_t - \mathbf{z}_t, \tag{5.1}$$

More information regarding modeling of flexible loads is given in appendix A.3. As controlling reactive power $\mathbf{q}^{\mathsf{fl}}_t := (q^{\mathsf{fl}}_{1,t}, \dots, q^{\mathsf{fl}}_{n,t})^\intercal$ is not a usual load behavior, it is kept as uncontrollable and modeled simply through a specified power factor.

For modeling DGs, convention similar to chapter 4 is followed. However, we only consider instantaneous power dispatch from DG at each time interval t. Moreover, it is assumed that DGs optimize their instantaneous active powers $\mathbf{p}^{\mathsf{dg}}_t := (p^{\mathsf{dg}}_{1,t}, \dots, p^{\mathsf{dg}}_{n,t})^\intercal$ and reactive powers $\mathbf{q}^{\mathsf{dg}}_t := (q^{\mathsf{dg}}_{1,t}, \dots, q^{\mathsf{dg}}_{n,t})^\intercal$ independently. Aggregation of low voltage PV systems with controllable active and reactive power support to the grid can be considered as a practical application of these types of DGs [109].

As mentioned earlier, we assume that aggregator similar to its contracted DGs and FLs are price-taking, utility maximizing agents. To this end, the overall social welfare $w_{p,t}(\mathbf{p}^{\mathsf{fl}}_t, \mathbf{p}^{\mathsf{g}}_t)$ as the aggregate benefit of DGs and FLs from their active power procurement over the planning horizon $\mathcal{T}$ is:

$$w_{p,t}(\mathbf{p}^{\mathsf{fl}}_t, \mathbf{p}^{\mathsf{dg}}_t) = \sum_{t=1}^{\mathsf{n}_t} \Big(\mathbf{U}^{\mathsf{fl}}_t(\mathbf{p}^{\mathsf{fl}}_t) - \mathbf{C}^{\mathsf{dg}}_t(\mathbf{p}^{\mathsf{dg}}_t) \Big), \tag{5.2}$$

where $\mathbf{C}^{\mathsf{dg}}_t(\mathbf{p}^{\mathsf{g}}_t)$ and $\mathbf{U}^{\mathsf{fl}}_t(\mathbf{p}^{\mathsf{fl}}_t)$ are respective the cost (utility) of generation (consumption) of active power by aggregator's contracted DGs and FLs. For FLs, we model this utility simply as negative of the cost of purchasing energy from the wholesale market, i.e., $\mathbf{U}^{\mathsf{fl}}_t(\mathbf{p}^{\mathsf{fl}}_t) :=$ -$\mathbf{C}^{\mathsf{fl}}_t(\mathbf{p}^{\mathsf{fl}}_t)$. In the literature [59, 14, 56, 55, 105] there exists also other types of utility function models for FLs. However, the final aim is mostly to obtain a convex optimization problem through modeling of utility functions. Hence, the method developed in this thesis can be easily adapted to other utility function formulations. Similarly, social welfare from reactive power procurement of DGs amounts to:

$$w_{q,t}(\mathbf{q}^{\mathsf{dg}}_t) = -\sum_{t=1}^{\mathsf{n}_t} \mathbf{C}^{\mathsf{dg}}_t(\mathbf{q}^{\mathsf{dg}}_t). \tag{5.3}$$

Similar to definition of cost functions for instantaneous dispatch in chapter 4, we extend it to multi-period as:

Remark 5.2. For all $x \in \{\mathsf{dg}, \mathsf{fl}\}$ procuring power $y \in \{p, q\}$, costs are defined as $\mathbf{C}^x_t(\mathbf{y}^x_t) := \mathbf{c}^{x}_{y,t}{}^\intercal \cdot \mathbf{y}^x_t$, where marginal cost is of the form $\mathbf{c}^x_{y,t} := \mathbf{a}^x_{y,t} + \mathbf{B}^x_{y,t}\mathbf{y}^x_t$ with a positive price per unit vector $\mathbf{a}^x_{y,t} \in \mathbb{R}^n$ (in \$/MWh) and symmetric, positive definite matrix $\mathbf{B}^x_{y,t} \in \mathbb{R}^{n \times n}$ of

small positive price sensitivity coefficients (in \$/MWh^2), turning the social welfares introduced in (5.2) and (4.2) strictly convex. In the end, we also assume that the single-period cost function interpretations of **R. 4.2** holds true for the above presented muti-period cost functions.

5.2.2 Aggregator Problem

Now we collect all aggregator information from the above and formulate its utility maximization problem as:

$$\text{maximize} \quad \sum_{t\in T}\Big(w_{p,t}(\mathbf{p}_t^{\mathsf{fl}}, \mathbf{p}_t^{\mathsf{dg}}) + w_{q,t}(\mathbf{q}_t^{\mathsf{dg}})\Big) \tag{5.4a}$$

$$\text{subject to}$$

$$\mathbf{p}_t^{\mathsf{dg}-} \le \mathbf{p}_t^{\mathsf{dg}} \le \mathbf{p}_t^{\mathsf{dg}+} \qquad : \boldsymbol{\mu}_{\mathbf{p}_t}^{\mathsf{dg}-}, \boldsymbol{\mu}_{\mathbf{p}_t}^{\mathsf{dg}+} \tag{5.4b}$$

$$\mathbf{q}_t^{\mathsf{dg}-} \le \mathbf{q}_t^{\mathsf{dg}} \le \mathbf{q}_t^{\mathsf{dg}+} \qquad : \boldsymbol{\mu}_{\mathbf{q}_t}^{\mathsf{dg}-}, \boldsymbol{\mu}_{\mathbf{q}_t}^{\mathsf{dg}+} \tag{5.4c}$$

$$\mathbf{p}_t^{\mathsf{fl}-} \le \mathbf{p}_t^{\mathsf{fl}} \le \mathbf{p}_t^{\mathsf{fl}+} \qquad : \boldsymbol{\mu}_{\mathbf{p}_t}^{\mathsf{fl}-}, \boldsymbol{\mu}_{\mathbf{p}_t}^{\mathsf{fl}+} \tag{5.4d}$$

$$\mathbf{ch}_t^{\mathsf{fl}-} \le \mathbf{ch}_0^{\mathsf{fl}} + \mathbf{D}_t\mathbf{p}_t^{\mathsf{fl}} - \mathbf{z}_t \le \mathbf{ch}_t^{\mathsf{fl}+} : \boldsymbol{\mu}_{\mathbf{ch}_t}^{\mathsf{fl}-}, \boldsymbol{\mu}_{\mathbf{ch}_t}^{\mathsf{fl}+} \tag{5.4e}$$

$$\forall t \in \mathcal{T} = \{1, \dots, \mathsf{n}_t\}$$

Constraint (5.4d) limits dispatch capabilities of FLs within the allowable inter-temporal SOC constraints given in (5.4e). All DGs' active/reactive power are constrained through (5.4b)/(5.4c), respectively. The variables listed to the right of each constraint (behind colon) are their respective Lagrangian multipliers. The aggregator problem in (5.4) is a quadratic program (QP) because its objective function (5.4a) (see **R. 5.2**) along with constraints now which are affine in the decision variables, i.e., ($\mathbf{p}_t^{\mathsf{fl}}$, $\mathbf{q}_t^{\mathsf{dg}}$, $\mathbf{q}_t^{\mathsf{dg}}$). As discussed in chapter 4, this property is not mere a technicality, as it is going to be the cornerstone in our discussion on efficient resource allocation in the local distribution grid market. This is because, for the given a feasible solution ($\mathbf{p}_t^{*\mathsf{fl}}$, $\mathbf{q}_t^{*\mathsf{dg}}$, $\mathbf{q}_t^{*\mathsf{dg}}$) to (5.4) is a also a unique solution and a strict maximizer of (5.4). This is because QPs are strict convex programs and achieve a unique solution (see chapter 2.).

Remark 5.3. From (5.4) is can be seen that aggregator does not have information regarding grid conditions. Hence, they only are concerned with respect to energy requirements of its contracted FLs and DGs. Another assumption is that the aggregator has full observability and controllability over its respective FLs and DGs. Moreover, it is assumed that no delay or noise exists in the communication link between the aggregator and its contracted FLs and DGs. We do agree that at the current point in time this might be a strong assumption. However, as the *smart grid* promises to provide a higher level of communication and information exchange in the grid, the proposed framework of this thesis relies on this envisioned future development in the grid.

5.3 Distribution System Operator

The Distribution System Operator (DSO) is responsible for managing its underlying grid under its physical limits as well as providing energy to fixed loads $\mathbf{p}_t^{\mathsf{cl}} := (p_{1,t}^{\mathsf{cl}}, \dots, p_{n,t}^{\mathsf{cl}})^{\mathsf{T}}$. It is assumed that fixed loads are always met and there does not exist any extra utility to satisfy them [58].

As mentioned in Sec. 5.1, the DSO seeks to maximize the overall surplus of the grid. This is achieved as follows:

1. The DSO receives the marginal price at its respective root-bus from the wholesale market. Based on this price, it is assumed that at the root-bus of the grid, an equivalent generator exists which supplies grid's total active and reactive power. The marginal cost of supplying this power is then taken as the respective root-bus from the wholesale market.
2. The DSO assumes that the aggregator is economically rationale, i.e., within its allowable limits it maximizes the individual surplus. Note that this is directly in spirit with aggregator program introduced in 5.2.1.
3. Aggregator also submits its energy requirements along with the dispatch capabilities to the DSO. This assumption is true when there exists no privacy restriction between the DSO and aggregator. However, for the convex programs [35, 34] privacy constraints can also be introduced. Since this is not the main focus of this thesis, we don't discuss it here.

With this, the DSO formulates the overall surplus function of the grid as:

$$w_{p,t}(\mathbf{p}_t^{\mathsf{fl}}, \mathbf{p}_t^{\mathsf{g}}) = \Big(\mathbf{U}_t^{\mathsf{fl}}(\mathbf{p}_t^{\mathsf{fl}}) - \mathbf{C}_t^{\mathsf{g}}(\mathbf{p}_t^{\mathsf{g}})\Big), \tag{5.5}$$

where $\mathbf{p}_t^{\mathsf{g}} := (p_t^0, (\mathbf{p}_t^{\mathsf{dg}})^\intercal)^\intercal$ now collects all individual aggregator's DGs $\mathbf{p}^{\mathsf{dg}}$ and the root-bus p^0 with their cost of supplying energy as $\mathbf{C}^{\mathsf{g}}(\mathbf{p}^{\mathsf{g}})$. Similarly, for the reactive power, the overall social surplus becomes:

$$w_{q,t}(\mathbf{q}_t^{\mathsf{g}}) = -\mathbf{C}_t^{\mathsf{g}}(\mathbf{q}_t^{\mathsf{g}}), \tag{5.6}$$

with total reactive power generations: $\mathbf{q}_t^{\mathsf{g}} := (q_t^0, (\mathbf{q}_t^{\mathsf{dg}})^\intercal)^\intercal$. The assumption regarding the nature of cost function of active and reactive power at the root-bus are similar to the given for aggregator's DG Sec. 5.2.1.

5.3.1 Day-Ahead Local Distribution Grid Market

Incorporating the above assumption by the DSO and grid constraints, then under no uncertainty and perfect communication, the DSO aims to solve the following multi-period constrained social welfare maximization problem:

$$\begin{aligned}
&\text{maximize} \quad w_{p,t}(\mathbf{p}_t^{\mathsf{fl}}, \mathbf{p}_t^{\mathsf{g}}) + w_{q,t}(\mathbf{q}_t^{\mathsf{g}}) && && \text{(5.7a)}\\
&\text{subject to} \\
&\mathbf{1}_{\mathsf{N}}^\top \mathbf{p}_t^{\mathsf{g}} - \mathbf{1}_{\mathsf{n}}^\top(\mathbf{p}_t^{\mathsf{cl}} + \mathbf{p}_t^{\mathsf{fl}}) = p_t^{\mathsf{l}} && : \lambda_t^p && \text{(5.7b)}\\
&\mathbf{1}_{\mathsf{N}}^\top \mathbf{q}_t^{\mathsf{g}} - \mathbf{1}_{\mathsf{n}}^\top(\mathbf{q}_t^{\mathsf{cl}} + \mathbf{q}_t^{\mathsf{fl}}) = q_t^{\mathsf{l}} && : \lambda_t^q && \text{(5.7c)}\\
&|\mathbf{s}_t^{\mathsf{f}}|^2 \le (\mathbf{s}_t^{\mathsf{f}+})^2 && : \boldsymbol{\mu}_{s_t^{\mathsf{f}}}^+ && \text{(5.7d)}\\
&|\mathbf{s}_t^{\mathsf{t}}|^2 \le (\mathbf{s}_t^{\mathsf{t}+})^2 && : \boldsymbol{\mu}_{s_t^{\mathsf{t}}}^+ && \text{(5.7e)}\\
&\mathbf{v}_t^{L-} \le \mathbf{v}_t^{L} \le \mathbf{v}_t^{L+} && : \boldsymbol{\mu}_{\mathbf{v}_t^L}^-, \boldsymbol{\mu}_{\mathbf{v}_t^L}^+ && \text{(5.7f)}\\
&\mathbf{p}_t^{\mathsf{dg}-} \le \mathbf{p}_t^{\mathsf{dg}} \le \mathbf{p}_t^{\mathsf{dg}+} && : \boldsymbol{\mu}_{\mathbf{p}_t}^{\mathsf{dg}-}, \boldsymbol{\mu}_{\mathbf{p}_t}^{\mathsf{dg}+} && \text{(5.7g)}\\
&\mathbf{q}_t^{\mathsf{dg}-} \le \mathbf{q}_t^{\mathsf{dg}} \le \mathbf{q}_t^{\mathsf{dg}+} && : \boldsymbol{\mu}_{\mathbf{q}_t}^{\mathsf{dg}-}, \boldsymbol{\mu}_{\mathbf{q}_t}^{\mathsf{dg}+} && \text{(5.7h)}\\
&\mathbf{p}_t^{\mathsf{fl}-} \le \mathbf{p}_t^{\mathsf{fl}} \le \mathbf{p}_t^{\mathsf{fl}+} && : \boldsymbol{\mu}_{\mathbf{p}_t}^{\mathsf{fl}-}, \boldsymbol{\mu}_{\mathbf{p}_t}^{\mathsf{fl}+} && \text{(5.7i)}\\
&\mathbf{ch}_t^{\mathsf{fl}-} \le \mathbf{ch}_0^{\mathsf{fl}} + \mathbf{D}_t \mathbf{p}_t^{\mathsf{fl}} - \mathbf{z}_t \le \mathbf{ch}_t^{\mathsf{fl}+} && : \boldsymbol{\mu}_{\mathbf{ch}_t}^{\mathsf{fl}-}, \boldsymbol{\mu}_{\mathbf{ch}_t}^{\mathsf{fl}+} && \text{(5.7j)}\\
&\forall t \in \mathcal{T} = \{1, \dots, \mathsf{n}_t\}
\end{aligned}$$

for all $t \in \mathcal{T} = \{1, \ldots, \mathsf{n}_t\}$. Constraints (5.7b) and (5.7c) respectively present global active and reactive power balance of the distribution grid. Apparent power flowing in distribution grid lines from/to ends of the lines are constrained through (5.7d)/(5.7e). Refer to chapter 3 for definition of these grid quantities. Explanation of constraints related to flexibility resources [(5.7g)–(5.7g)] are provided in Sec. 5.2.1. The variables listed to the right of each constraint (behind colon) are their respective Lagrangian multipliers. Note that the optimization problem in (5.7) is a classical global energy balance formulation for calculating DLMPs [88, 82]. However, unlike transmission grid's single period, it deploys multi-period modeling as explained above for enhanced system controllability.

Remark 5.4. We solve the above non-convex problem using the trust-region based solution methodology presented in chapter 4. Recall that at each iteration of trust-region, we turn the above non-convex optimization problem into a quadratic program (QP) (see **R. 4.4** in chapter 4 for more details.). Recall that this is not done merely for convenience, as this also allows us to conclude that for a feasible solution of QP, we have an optimal and unique minimizer within the allowable trust-region.

5.3.2 Multi-Period Distribution Locational Marginal Prices

We extend the derivation of single-step of chapter 4 for multi-period case here. The solution of (5.7) can be obtained using the solution methodology proposed in chapter 4. The solution (resultant Lagrange multipliers) of (5.7) can then be utilized to clear DLMP at each time step t and grid buses. For active power procurement at each time step t, there exist active power DLMPs, i.e., $\boldsymbol{\pi}^{\mathsf{Grid}}_{\mathbf{p}_t}$, which are under equilibrium and completely representable for the whole grid as the sum of their (i) energy $\boldsymbol{\pi}^{\mathsf{E}}_{\mathbf{p}_t}$, (ii) loss $\boldsymbol{\pi}^{\mathsf{L}}_{\mathbf{p}_t}$, (iii) congestion $\boldsymbol{\pi}^{\mathsf{C}}_{\mathbf{p}_t}$ and (iv) voltage $\boldsymbol{\pi}^{\mathsf{V}}_{\mathbf{p}_t}$ components, i.e.,

$$\boldsymbol{\pi}^{\mathsf{Grid}}_{\mathbf{p}_t} = \boldsymbol{\pi}^{\mathsf{E}}_{\mathbf{p}_t} + \boldsymbol{\pi}^{\mathsf{L}}_{\mathbf{p}_t} + \boldsymbol{\pi}^{\mathsf{C}}_{\mathbf{p}_t} + \boldsymbol{\pi}^{\mathsf{V}}_{\mathbf{p}_t}. \tag{5.8}$$

uniquely determined as: $\boldsymbol{\pi}^{\mathsf{E}}_{\mathbf{p}_t} := c^0_{p,t}\mathbf{1}_{\mathsf{n}}$, $\boldsymbol{\pi}^{\mathsf{L}}_{\mathbf{p}_t} := -(\mathbf{M}^{p^{\mathsf{l}}})^{\intercal}_{\mathbf{p}_t} c^0_{p,t} - (\mathbf{M}^{q^{\mathsf{l}}})^{\intercal}_{\mathbf{p}_t} c^0_{q,t}$, $\boldsymbol{\pi}^{\mathsf{C}}_{\mathbf{p}_t} := (\mathbf{M}^{\mathbf{s}^{\mathsf{f}}})^{\intercal}_{\mathbf{p}_t}\boldsymbol{\mu}_{s^{\mathsf{f}}} + (\mathbf{M}^{\mathbf{s}^{\mathsf{t}}})^{\intercal}_{\mathbf{p}_t}\boldsymbol{\mu}_{s^{\mathsf{t}}}$ + and $\boldsymbol{\pi}^{\mathsf{V}}_{\mathbf{p}_t} := (\mathbf{M}^{\mathbf{v}_{\mathsf{L}}})^{\intercal}_{\mathbf{p}_t}(\boldsymbol{\mu}^{+}_{\mathbf{v}_{\mathsf{L}}} - \boldsymbol{\mu}^{-}_{\mathbf{v}_{\mathsf{L}}})$[2]. The explanation of this decomposition follows. Consider the KKT conditions to be satisfied by the solution of the market clearing problem (5.7):

$$\mathbf{c}^{\mathsf{fl}}_{p,t} + \lambda^p_t\mathbf{1}_{\mathsf{n}} - (\mathbf{M}^{p^{\mathsf{l}}})^{\intercal}_{\mathbf{p}_t}\lambda^p_t - (\mathbf{M}^{q^{\mathsf{l}}})^{\intercal}_{\mathbf{p}_t}\lambda^q_t + (\mathbf{M}^{\mathbf{s}^{\mathsf{f}}})^{\intercal}_{\mathbf{p}_t}\boldsymbol{\mu}_{s^{\mathsf{f}}} + (\mathbf{M}^{\mathbf{s}^{\mathsf{t}}})^{\intercal}_{\mathbf{p}_t}\boldsymbol{\mu}_{s^{\mathsf{t}}} + (\mathbf{M}^{\mathbf{v}_{\mathsf{L}}})^{\intercal}_{\mathbf{p}_t}(\boldsymbol{\mu}^{+}_{\mathbf{v}_{\mathsf{L}}} - \boldsymbol{\mu}^{-}_{\mathbf{v}_{\mathsf{L}}})$$
$$+ \boldsymbol{\mu}^{\mathsf{fl}+}_{\mathbf{p}_t} - \boldsymbol{\mu}^{\mathsf{fl}-}_{\mathbf{p}_t} + \overbrace{\mathbf{D}_t(\boldsymbol{\mu}^{\mathsf{fl}+}_{\mathbf{ch}_t} - \boldsymbol{\mu}^{\mathsf{fl}-}_{\mathbf{ch}_t})}^{t\in\mathcal{T}\setminus|\mathcal{T}|} = \mathbf{0}, \tag{5.9a}$$
$$\mathbf{c}^{\mathsf{g}}_{p,t} - \lambda^p_t\mathbf{1}_{\mathsf{N}} + (\mathbf{M}^{p^{\mathsf{l}}})^{\intercal}_{\mathbf{p}_t}\lambda^p_t + (\mathbf{M}^{q^{\mathsf{l}}})^{\intercal}_{\mathbf{p}_t}\lambda^q_t - (\mathbf{M}^{\mathbf{s}^{\mathsf{f}}})^{\intercal}_{\mathbf{p}_t}\boldsymbol{\mu}_{s^{\mathsf{f}}} - (\mathbf{M}^{\mathbf{s}^{\mathsf{t}}})^{\intercal}_{\mathbf{p}_t}\boldsymbol{\mu}_{s^{\mathsf{t}}} - (\mathbf{M}^{\mathbf{v}_{\mathsf{L}}})^{\intercal}_{\mathbf{p}}(\boldsymbol{\mu}^{+}_{\mathbf{v}_{\mathsf{L}}} - \boldsymbol{\mu}^{-}_{\mathbf{v}_{\mathsf{L}}})$$
$$- \boldsymbol{\mu}^{\mathsf{dg}+}_{\mathbf{p}_t} + \boldsymbol{\mu}^{\mathsf{dg}-}_{\mathbf{p}_t} = \mathbf{0}, \tag{5.9b}$$
$$\mathbf{c}^{\mathsf{g}}_{q,t} - \lambda^q_t\mathbf{1}_{\mathsf{N}} + (\mathbf{M}^{p^{\mathsf{l}}})^{\intercal}_{\mathbf{q}_t}\lambda^p_t + (\mathbf{M}^{q^{\mathsf{l}}})^{\intercal}_{\mathbf{q}_t}\lambda^q_t - (\mathbf{M}^{\mathbf{s}^{\mathsf{f}}})^{\intercal}_{\mathbf{q}_t}\boldsymbol{\mu}_{s^{\mathsf{f}}} - (\mathbf{M}^{\mathbf{s}^{\mathsf{t}}})^{\intercal}_{\mathbf{q}_t}\boldsymbol{\mu}_{s^{\mathsf{t}}} - (\mathbf{M}^{\mathbf{v}_{\mathsf{L}}})^{\intercal}_{\mathbf{q}}(\boldsymbol{\mu}^{+}_{\mathbf{v}_{\mathsf{L}}} - \boldsymbol{\mu}^{-}_{\mathbf{v}_{\mathsf{L}}})$$
$$- \boldsymbol{\mu}^{\mathsf{dg}+}_{\mathbf{q}_t} + \boldsymbol{\mu}^{\mathsf{dg}-}_{\mathbf{q}_t} = \mathbf{0}, \tag{5.9c}$$
$$\boldsymbol{\mu}_{s^{\mathsf{f}}}(|\tilde{\mathbf{s}}^{\mathsf{f}}|^2 - (\mathbf{s}^{\mathsf{f}+})^2) = 0, \tag{5.9d}$$
$$\boldsymbol{\mu}_{s^{\mathsf{f}}}(|\tilde{\mathbf{s}}^{\mathsf{t}}|^2 - (\mathbf{s}^{\mathsf{t}+})^2) = 0, \tag{5.9e}$$

[2]Matrix $\mathbf{M}^{[\cdot]}_{\mathbf{p}_t/\mathbf{q}_t}$ corresponds to active/reactive power parts of $\mathbf{M}^{[\cdot]}$. Marginal cost of active/reactive power supply at the root-bus is $c^0_{p,t}/c^0_{q,t}$.

$$\boldsymbol{\mu}^{+}_{\mathbf{v}^{\mathsf{L}}_t}(\tilde{\mathbf{v}}^{\mathsf{L}}_t - \mathbf{v}^{L+}_t) = \mathbf{0}, \tag{5.9f}$$

$$\boldsymbol{\mu}^{-}_{\mathbf{v}^{\mathsf{L}}_t}(-\tilde{\mathbf{v}}^{\mathsf{L}}_t + \mathbf{v}^{L-}_t) = \mathbf{0}, \tag{5.9g}$$

$$\boldsymbol{\mu}^{\mathsf{dg}+}_{\mathbf{p}_t}(\mathbf{p}^{\mathsf{dg}}_t - \mathbf{p}^{\mathsf{dg}+}_t) = \mathbf{0}, \tag{5.9h}$$

$$\boldsymbol{\mu}^{\mathsf{dg}-}_{\mathbf{p}_t}(-\mathbf{p}^{\mathsf{dg}}_t + \mathbf{p}^{\mathsf{dg}+}_t) = \mathbf{0}, \tag{5.9i}$$

$$\boldsymbol{\mu}^{\mathsf{dg}+}_{\mathbf{q}_t}(\mathbf{q}^{\mathsf{dg}}_t - \mathbf{q}^{\mathsf{dg}+}_t) = \mathbf{0}, \tag{5.9j}$$

$$\boldsymbol{\mu}^{\mathsf{dg}-}_{\mathbf{q}_t}(-\mathbf{q}^{\mathsf{dg}}_t + \mathbf{q}^{\mathsf{dg}+}_t) = \mathbf{0}, \tag{5.9k}$$

$$\boldsymbol{\mu}^{\mathsf{fl}+}_{\mathbf{p}_t}(\mathbf{p}^{\mathsf{fl}}_t - \mathbf{p}^{\mathsf{fl}+}_t) = \mathbf{0}, \tag{5.9l}$$

$$\boldsymbol{\mu}^{\mathsf{fl}-}_{\mathbf{p}_t}(-\mathbf{p}^{\mathsf{fl}}_t + \mathbf{p}^{\mathsf{fl}+}_t) = \mathbf{0}, \tag{5.9m}$$

$$\boldsymbol{\mu}^{\mathsf{fl}+}_{\mathbf{ch}_t}(\mathbf{ch}^{\mathsf{fl}}_0 + \mathbf{D}_t\mathbf{p}^{\mathsf{fl}}_t - \mathbf{z}_t - \mathbf{ch}^{\mathsf{fl}+}_t) = \mathbf{0}, \tag{5.9n}$$

$$\boldsymbol{\mu}^{\mathsf{fl}-}_{\mathbf{ch}_t}(-\mathbf{ch}^{\mathsf{fl}}_0 - \mathbf{D}_t\mathbf{p}^{\mathsf{fl}}_t + \mathbf{z}_t + \mathbf{ch}^{\mathsf{fl}-}_t) = \mathbf{0}, \tag{5.9o}$$

$$\forall t \in \mathcal{T} = \{1, \dots, \mathsf{n}_t\},$$

along with all primal feasible conditions of (5.7) and non-negative Lagrange multipliers. Note that as stationary condition (5.9a) contains inter-temporal constraints, the last term only exists for non-terminal period, i.e., $\mathcal{T} \setminus |\mathcal{T}|$, else its zero [58]. Now, we proceed with the similar line of derivation for obtaining DLMP, as presented in chapter 4 for single-step.

For active powers, the only stationary condition of KKT in (5.9) is (5.9b). This gives us the following equivalence:

$$c^0_{p,t} = -\lambda^p_t. \tag{5.10}$$

Now let respective marginal values of DGs and FLs be,

$$\begin{aligned} \boldsymbol{\pi}^{\mathsf{Flex}}_{\mathbf{p}^{\mathsf{fl}}_t} &:= -\mathbf{c}^{\mathsf{fl}}_{p,t} - \boldsymbol{\mu}^{\mathsf{fl}+}_{\mathbf{p}_t} + \boldsymbol{\mu}^{\mathsf{fl}-}_{\mathbf{p}_t} - \overbrace{\mathbf{D}_t(\boldsymbol{\mu}^{\mathsf{fl}+}_{\mathbf{ch}_t} - \boldsymbol{\mu}^{\mathsf{fl}-}_{\mathbf{ch}_t})}^{t \in \mathcal{T} \setminus |\mathcal{T}|} \\ \boldsymbol{\pi}^{\mathsf{Flex}}_{\mathbf{p}^{\mathsf{dg}}_t} &:= \mathbf{c}^{\mathsf{dg}}_{p,t} + \boldsymbol{\mu}^{\mathsf{dg}+}_{\mathbf{p}_t} - \boldsymbol{\mu}^{\mathsf{dg}-}_{\mathbf{p}_t} \in \mathbb{R}^{\mathsf{n}} \end{aligned} \tag{5.11}$$

As the definitions in (5.11) represent internal constraints of the flexibility resources, the cleared DLMPs $\boldsymbol{\pi}^{\mathsf{Grid}}_{\mathbf{p}_t}$, which is a grid equilibrium, must satisfy the following condition:

$$\boldsymbol{\pi}^{\mathsf{Flex}}_{\mathbf{p}^{\mathsf{fl}}_t} = \boldsymbol{\pi}^{\mathsf{Grid}}_{\mathbf{p}_t} = \boldsymbol{\pi}^{\mathsf{Flex}}_{\mathbf{p}^{\mathsf{dg}}_t}. \tag{5.12}$$

After substituting (5.10) in [(5.9a), (5.9b)] and then utilizing (5.12), we recover the individual components of grid cleared DLMPs, $\boldsymbol{\pi}^{\mathsf{Grid}}_{\mathbf{p}_t}$, as proposed in (5.8). Moreover, from (5.12) we have also shown that these components exists in equilibrium with internal flexibility resources' marginal value of supplying power. Hence, the obtain DLMP value is representative of both flexibility resources' internal constraints as well as grid conditions.

Similar to active power DLMPs $\boldsymbol{\pi}^{\mathsf{Grid}}_{\mathbf{p}_t}$, reactive power DLMPs $\boldsymbol{\pi}^{\mathsf{Grid}}_{\mathbf{q}_t}$ can be derived using a similar method, i.e. evaluating the marginal cost of supplying reactive power at the root-bus, $c^0_{q,t}$ with its corresponding stationary condition of (5.9c).

5.4 Distribution Grid Market: Efficient Resource Allocation

This section shows that the proposed local distribution grid market is able to achieve efficient flexible resource allocation. This means that the cleared DLMPs of the local market in (5.12),

optimizing the overall system dispatch in (5.7), achieves exactly same dispatch as to when aggregator maximizes its individual surplus with the inclusion of DLMPs obtained from (5.7). To show this, we make following assumptions:

- We assume that the DSO considers that the aggregator behave economically rational, i.e., it maximizes its individual surplus. Note that this assumption is directly in spirit of our defined entities in the distribution grids, i.e., the DSO and aggregator (see Sec. 5.1). Hence, with the clearance of price at the respective buses of aggregators, it naturally has to include this price in its original problem (5.4).
- We assume that no uncertainty in this grid cleared price exists as well as in predicting local flexibility resources' states by aggregators.

In principle, we need to show that under above assumptions, the DSO cleared DLMPs ($\boldsymbol{\pi}^{\text{Grid}}_{\mathbf{p}_t}$, $\boldsymbol{\pi}^{\text{Grid}}_{\mathbf{q}_t}$) correspond to a unique solution, maximizing the overall social welfare (5.7) as well as aggregator's individual surplus. To this end, consider individual aggregator maximization problem, after the inclusion of grid cleared DLMPs:

$$\begin{aligned}
\text{maximize} \quad & \sum_{t\in\mathcal{T}} -\Big((\boldsymbol{\pi}^{\text{Grid}}_{\mathbf{p}_t})^{\mathsf{T}}\mathbf{p}^{\text{dg}}_t + (\boldsymbol{\pi}^{\text{Grid}}_{\mathbf{p}_t})^{\mathsf{T}}\mathbf{p}^{\text{fl}}_t + (\boldsymbol{\pi}^{\text{Grid}}_{\mathbf{q}_t})^{\mathsf{T}}\mathbf{q}^{\text{dg}}_t\Big) && \text{(5.13a)}\\
\text{subject to} \quad & \mathbf{p}^{\text{dg}-}_t \le \mathbf{p}^{\text{dg}}_t \le \mathbf{p}^{\text{dg}+}_t && : \boldsymbol{\mu}^{\text{dg}-}_{\mathbf{p}_t}, \boldsymbol{\mu}^{\text{dg}+}_{\mathbf{p}_t} && \text{(5.13b)}\\
& \mathbf{q}^{\text{dg}-}_t \le \mathbf{q}^{\text{dg}}_t \le \mathbf{q}^{\text{dg}+}_t && : \boldsymbol{\mu}^{\text{dg}-}_{\mathbf{q}_t}, \boldsymbol{\mu}^{\text{dg}+}_{\mathbf{q}_t} && \text{(5.13c)}\\
& \mathbf{p}^{\text{fl}-}_t \le \mathbf{p}^{\text{fl}}_t \le \mathbf{p}^{\text{fl}+}_t && : \boldsymbol{\mu}^{\text{fl}-}_{\mathbf{p}_t}, \boldsymbol{\mu}^{\text{fl}+}_{\mathbf{p}_t} && \text{(5.13d)}\\
& \mathbf{ch}^{\text{fl}-}_t \le \mathbf{ch}^{\text{fl}}_0 + \mathbf{D}_t\mathbf{p}^{\text{fl}}_t - \mathbf{z}_t \le \mathbf{ch}^{\text{fl}+}_t && : \boldsymbol{\mu}^{\text{fl}-}_{\mathbf{ch}_t}, \boldsymbol{\mu}^{\text{fl}+}_{\mathbf{ch}_t} && \text{(5.13e)}\\
& \forall t \in \mathcal{T} = \{1, \dots, \mathsf{n}_t\}
\end{aligned}$$

As the overall DSO problem (5.7) has a strictly convex cost function (**R. 5.2**), the inclusion of DLMPs (linear in ($\mathbf{p}^{\text{dg}}_t, \mathbf{q}^{\text{dg}}_t, \mathbf{p}^{\text{fl}}_t$)) also makes the cost function of individual aggregator problem (5.13a) strictly convex. Combining this with affine constraints [(5.13b)–(5.13e)], the individual aggregator problem (5.13) is then also a QP, with a unique minimizer ($\mathbf{p}^{\text{dg}*}_t, \mathbf{q}^{\text{dg}*}_t, \mathbf{p}^{\text{fl}*}_t$) satisfying its following necessary and sufficient KKT conditions (5.14):

$$\begin{aligned}
& \boldsymbol{\pi}^{\text{Grid}}_{\mathbf{p}_t} + \boldsymbol{\mu}^{\text{fl}+}_{\mathbf{p}_t} - \boldsymbol{\mu}^{\text{fl}-}_{\mathbf{p}_t} + \overbrace{\mathbf{D}_t(\boldsymbol{\mu}^{\text{fl}+}_{\mathbf{ch}_t} - \boldsymbol{\mu}^{\text{fl}-}_{\mathbf{ch}_t})}^{t\in\mathcal{T}\setminus|\mathcal{T}|} = \mathbf{0}, && \text{(5.14a)}\\
& \boldsymbol{\pi}^{\text{Grid}}_{\mathbf{p}_t} - \boldsymbol{\mu}^{\text{dg}+}_{\mathbf{p}_t} + \boldsymbol{\mu}^{\text{dg}-}_{\mathbf{p}_t} = \mathbf{0}, && \text{(5.14b)}\\
& \boldsymbol{\pi}^{\text{Grid}}_{\mathbf{q}_t} - \boldsymbol{\mu}^{\text{dg}+}_{\mathbf{q}_t} + \boldsymbol{\mu}^{\text{dg}-}_{\mathbf{q}_t} = \mathbf{0}, && \text{(5.14c)}\\
& \boldsymbol{\mu}^{\text{dg}+}_{\mathbf{p}_t}(\mathbf{p}^{\text{dg}}_t - \mathbf{p}^{\text{dg}+}_t) = \mathbf{0}, && \text{(5.14d)}\\
& \boldsymbol{\mu}^{\text{dg}-}_{\mathbf{p}_t}(-\mathbf{p}^{\text{dg}}_t + \mathbf{p}^{\text{dg}+}_t) = \mathbf{0}, && \text{(5.14e)}\\
& \boldsymbol{\mu}^{\text{dg}+}_{\mathbf{q}_t}(\mathbf{q}^{\text{dg}}_t - \mathbf{q}^{\text{dg}+}_t) = \mathbf{0}, && \text{(5.14f)}\\
& \boldsymbol{\mu}^{\text{dg}-}_{\mathbf{q}_t}(-\mathbf{q}^{\text{dg}}_t + \mathbf{q}^{\text{dg}+}_t) = \mathbf{0}, && \text{(5.14g)}\\
& \boldsymbol{\mu}^{\text{fl}+}_{\mathbf{p}_t}(\mathbf{p}^{\text{fl}}_t - \mathbf{p}^{\text{fl}+}_t) = \mathbf{0}, && \text{(5.14h)}\\
& \boldsymbol{\mu}^{\text{fl}-}_{\mathbf{p}_t}(-\mathbf{p}^{\text{fl}}_t + \mathbf{p}^{\text{fl}+}_t) = \mathbf{0}, && \text{(5.14i)}\\
& \boldsymbol{\mu}^{\text{fl}+}_{\mathbf{ch}_t}(\mathbf{ch}^{\text{fl}}_0 + \mathbf{D}_t\mathbf{p}^{\text{fl}}_t - \mathbf{z}_t - \mathbf{ch}^{\text{fl}+}_t) = \mathbf{0}, && \text{(5.14j)}\\
& \boldsymbol{\mu}^{\text{fl}-}_{\mathbf{ch}_t}(-\mathbf{ch}^{\text{fl}}_0 - \mathbf{D}_t\mathbf{p}^{\text{fl}}_t + \mathbf{z}_t + \mathbf{ch}^{\text{fl}-}_t) = \mathbf{0}, && \text{(5.14k)}
\end{aligned}$$

$$\forall t \in \mathcal{T} = \{1, \ldots, \mathsf{n}_t\},$$

along with the primal feasible (5.13b), (5.13e) and all Lagrange multipliers non-negative constraints.

Observe that the grid cleared DLMPs, $\boldsymbol{\Pi}^{\mathsf{Grid}}_{\mathbf{p}_t}$, deployed in the individual problems of (5.14) are in equilibrium with $\boldsymbol{\Pi}^{\mathsf{Flex}}_{\mathbf{p}^{\mathsf{fl}}_t}$ of (5.11). This means that from (5.12), we can substitute [(5.14a)–(5.14c)] using (5.8) for both active/reactive power DLMPs $\boldsymbol{\Pi}^{\mathsf{Grid}}_{\mathbf{p}_t}/\boldsymbol{\Pi}^{\mathsf{Grid}}_{\mathbf{q}_t}$:

$$\begin{aligned}
\boldsymbol{\Pi}^{\mathsf{Grid}}_{\mathbf{p}_t} &:= \lambda^p_t \mathbf{1}_{\mathsf{n}} - (\mathbf{M}^{p^{\mathsf{l}}})^{\intercal}_{\mathbf{p}_t} \lambda^p_t - (\mathbf{M}^{q^{\mathsf{l}}})^{\intercal}_{\mathbf{p}_t} \lambda^q_t + (\mathbf{M}^{\mathbf{s}^{\mathsf{f}}})^{\intercal}_{\mathbf{p}_t} \boldsymbol{\mu}_{s^{\mathsf{f}}} + (\mathbf{M}^{\mathbf{s}^{\mathsf{t}}})^{\intercal}_{\mathbf{p}_t} \boldsymbol{\mu}_{s^{\mathsf{t}}} + (\mathbf{M}^{\mathbf{v}_{\mathsf{L}}})^{\intercal}_{\mathbf{p}_t} (\boldsymbol{\mu}^{+}_{\mathbf{v}_{\mathsf{L}}} - \boldsymbol{\mu}^{-}_{\mathbf{v}_{\mathsf{L}}}) \\
\boldsymbol{\Pi}^{\mathsf{Grid}}_{\mathbf{q}_t} &:= \lambda^q_t \mathbf{1}_{\mathsf{N}} - (\mathbf{M}^{p^{\mathsf{l}}})^{\intercal}_{\mathbf{q}_t} \lambda^p_t - (\mathbf{M}^{q^{\mathsf{l}}})^{\intercal}_{\mathbf{q}_t} \lambda^q_t + (\mathbf{M}^{\mathbf{s}^{\mathsf{f}}})^{\intercal}_{\mathbf{q}_t} \boldsymbol{\mu}_{s^{\mathsf{f}}} + (\mathbf{M}^{\mathbf{s}^{\mathsf{t}}})^{\intercal}_{\mathbf{q}_t} \boldsymbol{\mu}_{s^{\mathsf{t}}} + (\mathbf{M}^{\mathbf{v}_{\mathsf{L}}})^{\intercal}_{\mathbf{q}} (\boldsymbol{\mu}^{+}_{\mathbf{v}_{\mathsf{L}}} - \boldsymbol{\mu}^{-}_{\mathbf{v}_{\mathsf{L}}})
\end{aligned} \tag{5.15}$$

Now substituting (5.15) in aggregator KKTs (5.14), we can see that individual aggrgattor KKT conditions are in fact embedded in the overall KKT conditions of the DSO problem (5.9). This means that a valid overall solution $(\mathbf{p}^{\mathsf{dg}**}_t, \mathbf{q}^{\mathsf{dg}**}_t, \mathbf{p}^{\mathsf{fl}**}_t)$, satisfying (5.9), is also a solution to (5.14). On the other hand, the individual problem (5.13) does not contain any grid constraints, so a valid individual solution $(\mathbf{p}^{\mathsf{dg}*}_t, \mathbf{q}^{\mathsf{dg}*}_t, \mathbf{p}^{\mathsf{fl}*}_t)$ to (5.14) may not necessarily satisfy (5.9). However, $\boldsymbol{\Pi}^{\mathsf{Grid}}_{\mathbf{p}_t}$ shared among the individual and overall problem is obtained around a unique operating point, due to strictly convex subproblem (see **R. 5.4**), making the overall solution $(\mathbf{p}^{\mathsf{dg}**}_t, \mathbf{q}^{\mathsf{dg}**}_t, \mathbf{p}^{\mathsf{fl}**}_t)$ of (5.9) unique. Moreover, as the individual aggregator problem (5.13) is also a strictly convex problem (see (5.13)), it also constitutes a unique solution $(\mathbf{p}^{\mathsf{dg}*}_t, \mathbf{q}^{\mathsf{dg}*}_t, \mathbf{p}^{\mathsf{fl}*}_t)$. Due to this uniqueness, both the individual aggregator problem solution and the overall DSO-run local distribution grid market solution are similar, i.e. $(\mathbf{p}^{\mathsf{dg}**}_t, \mathbf{q}^{\mathsf{dg}**}_t, \mathbf{p}^{\mathsf{fl}**}_t) = (\mathbf{p}^{\mathsf{dg}*}_t, \mathbf{q}^{\mathsf{dg}*}_t, \mathbf{p}^{\mathsf{fl}*}_t)$.

5.4.1 Final Organization of the Proposed Local Market

In the end, we collect the above mentioned framework to describe the final working of the proposed distribution grid market framework as:

1. The DSO forecasts its daily underlying grid demand along with the cost to supply it using the marginal-cost at the root-bus, i.e., $c^0_{p,t}/c^0_{q,t}$;
2. Aggregator submits their energy requirements to the DSO; and
3. on a day-ahead basis, the DSO, assuming that the underlying aggregator is a price taker, economically rationale entity, clears DLMPs for each interval and pass them to aggregators.

Next, we present some discussion related to the proposed local markets.

5.5 Simulation Setup and Results

The proposed method is tested on the IEEE 33-bus distribution system [4]. The modified configuration of the grid is shown in Fig. 5.2. We assume each flexibility bus is an aggregator, having a contracted DG/FL. A realistic scenario with DGs and FLs operating under different cost functions and dispatch capabilities are simulated as follows.

- The active and reactive power dispatch for DGs are within range $[0, 0.5]$ MW and $[-0.3, 0.3]$ MVar, with marginal cost of active and reactive power set at 10 \$/MWh and 3 \$/MVarh for the whole day.

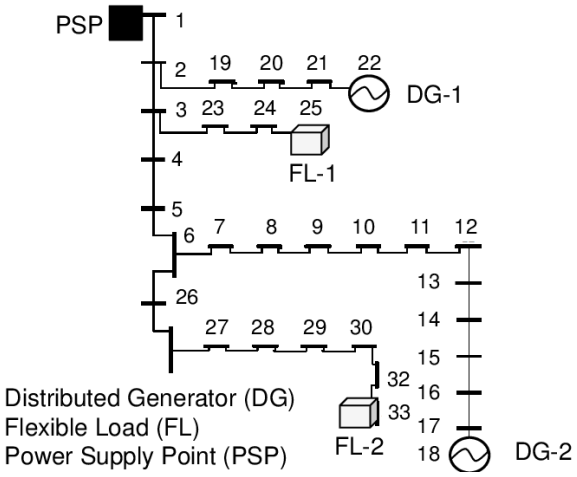

Figure 5.2: The modified 33-bus distribution grid with two FLs and two DGs, with PSP (root-bus) connection from the transmission grid. For fully exploring the proposed method FL-1 and DG-1 are placed closer to the root-bus, whereas FL-2 and DG-2 are placed far from the root-bus.

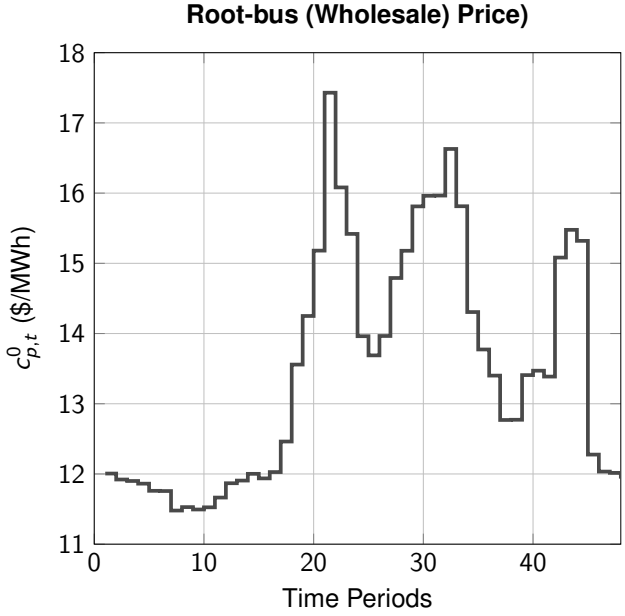

Figure 5.3: The wholesale market price, at the respective substation root-bus $c^0_{p,t}$, in half-hour granularity, taken from [25].

- The active power dispatch for FLs is kept within the range $[-1.47, 0]$ MW. This range is derived from the RC thermal flexible building models, given in appendix A.3.
- For constructing utility function of FLs as negative of the cost function, we take the day-ahead cleared price from the wholesale market at their respective root-bus of the grid. In this way, the aggregator problem with FLs is simply a cost minimization problem [41, 58, 34, 35].
- A small value of price sensitivity coefficient of 1e-4 \$/MWh^2(MVarh^2) is chosen to keep

all cost functions strictly convex. This value is in line with the price sensitivity coefficients assumed for european distribution grids in [58]. Note that a considerably large value of these coefficients makes flexible resources to dispatch their schedule more conservatively, as then the quadratic term (Hessian) dominates their respective cost functions (see **R. 5.2**). More information on obtaining these coefficients is provided in [41, 99].

- We take day-ahead wholesale price, similar to FLs, to deliver power by the DSO from its respective root-bus. This is because recall that in Sec. 5.3 it was assumed that the root-bus serves as an equivalent DG, to be dispatched by the DSO. As this equivalent DG is located at the root-bus, similar to FLs, it is assumed that it is dispatched using the day-ahead price at its respective bus, cleared from the wholesale market. Since there exists no reactive power price in wholesale market, we simply take marginal price for providing reactive power at root-bus as 3 $/MVarh. Note that this is also the value used for dispatch DGs.

Parameters of the trust-region in Algorithm 1 are taken from [27]. All simulations are performed on a 2.4-GHz processor with 64-GB RAM. Optimization problems are solved using YALMIP [65] with GUROBI [30] as a solver. Power flows for the trust-region evaluation steps in Algorithm 1 are performed using MATPOWER [84]. To explore the proposed method in detail, we simulate three scenarios with the resultant active power DLMPs along with dispatch quantities presented in Fig. 5.4 and Fig. 5.5, respectively.

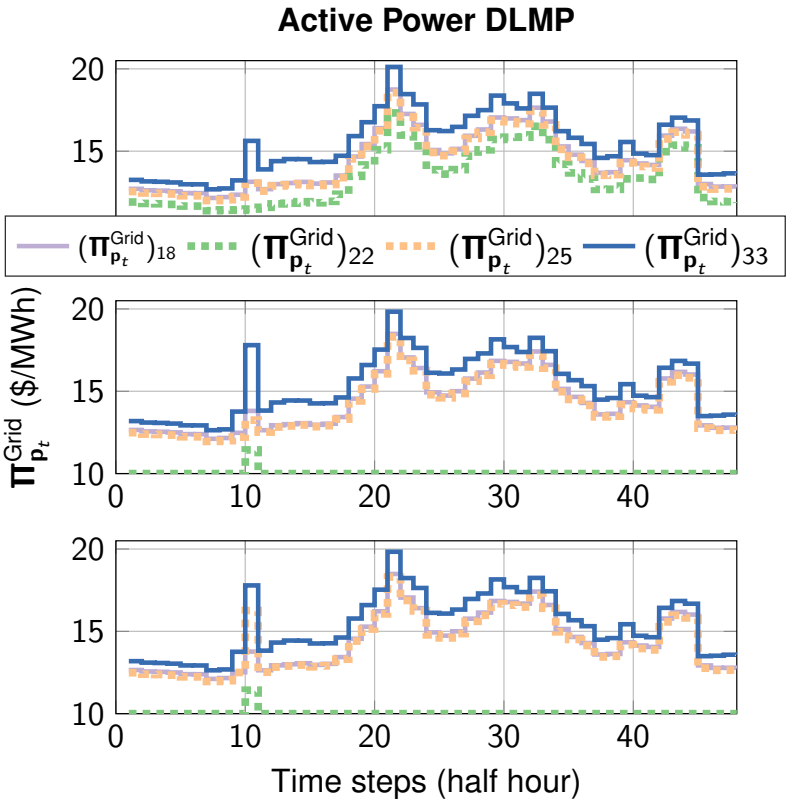

Figure 5.4: Active power DLMPs for *Scenario* 1 (top), 2 (middle) and 3 (bottom) for all flexible buses.

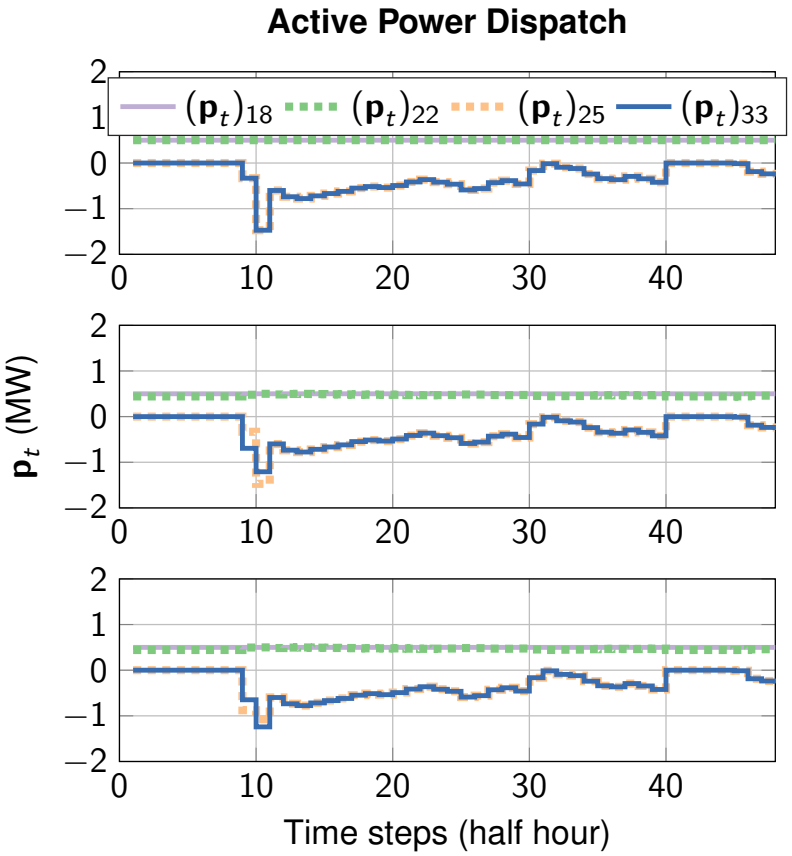

Figure 5.5: Active power dispatch values for *Scenario* 1 (top), 2 (middle) and 3 (bottom) for all flexible buses. Above, each individual time series only refers to flexibility resource dispatch connected at the bus. For example, time series $(\mathbf{p}_t)_{18}$ refers to dispatch by DG1.

5.5.1 *Scenario 1* – No Voltage and Congestion Binding

Scenario 1 is simulated by relaxing all nodal voltages and line flow constraints. In doing so we only show the effect of losses in the obtained DLMPs. As dispatching power from DGs is cheaper than supplying from the root-bus, i.e. 10 \$/MWh $< c^0_{p,t}$, $\forall t \in T$, they are fully dispatched for the whole time horizon in this scenario. However, this does not imply that buses with DGs also experience lower DLMPs. This is because whenever DGs are dispatch fully, the extra MW amount comes from the higher marginal cost providing the root-bus. The interesting case is experience at step 10, where FLs draw a large amount of energy due to its internal energy requirements[3]. This higher power drawn by FLs also increases DLMPs. This is because higher power causes higher losses in the grid, raising the loss component of the grid and consequently DLMPs.

[3]These energy requirements originate due to pre-cooling of the office space (from 5 am), to remain within the comfortable temperature throughout the day (see [35] for details.

5.5.2 *Scenario 2* – Only Voltage Binding

Scenario 2 constrains all nodal voltage magnitude between 0.92 and 1.05 p.u., causing an increase in DLMPs at time step 10 for FL2 as higher loading at bus 33 binds lower voltage limits. As a consequence, FL2 draws lesser power at time step 10, as compared to *Scenario 1*. The same dispatch phenomenon is observed for DG1 (bus 22), where active power dispatch is reduced from its upper limit (as compared to *Scenario* 1)in order to respect upper voltage limits. An interesting observation can then be made regarding DLMPs at bus 22, i.e., now being fully served by its local DG (DG1) the DLMP value at the bus is equal to marginal cost of DG1, i.e., 10 \$/MWh. However, around time step 10, where higher grid loading occurs from FLs, DGs (both DG1 and DG2) are able to dispatch to their maximum limits. Similar, to *Scenario* 1, this causes the extra MW amount at the DG buses to be satisfied by root-bus and consequently raising DLMP around time-step 10.

5.5.3 *Scenario 3* – Voltage and Congestion Binding

Scenario 3 constrains the distribution line serving FL1 by 1.6 MVA. This scenario is implemented to demonstrate the capability of the proposed model to handle the most strict conditions of the grid, as all constraints are active. Note that this rarely happens in the current distribution grids due to small number of FLs and DGs. However, studies in [100, 58] have shown that with higher integration of these devices, voltage and congestion limits are going to be binding more than usual. From results (Fig. 5.5 and 5.4) it can be seen that, as compared to *Scenario 1* & *2*, congestion limit causes FL1 to draw less power than it would have desired at time step 10. Consequently, DLMP value at bus corresponding to FL1 can be seen to increase, as congestion component in the DLMP calculation is nonzero due to the binding line flows at the respective buses.

Table 5.1: DLMPs for scenario 1 (top), 2 (middle) and 3 (bottom) at time step $t = 10$ and bus i.

i	$\boldsymbol{\pi}^{\mathsf{E}}_{\mathbf{p}_t}$	$\boldsymbol{\pi}^{\mathsf{L}}_{\mathbf{p}_t}$	$\boldsymbol{\pi}^{\mathsf{C}}_{\mathbf{p}_t}$	$\boldsymbol{\pi}^{\mathsf{V}}_{\mathbf{p}_t}$	$\boldsymbol{\pi}^{\mathsf{Grid}}_{\mathbf{p}_t}$	$\mathbf{c}^{\mathsf{dg/fl}}_{p,t}$	$\boldsymbol{\pi}^{\mathsf{M}}_{\mathbf{p}_t}$	$\boldsymbol{\pi}^{\mathsf{D}}_{\mathbf{p}_t}$	$\boldsymbol{\pi}^{\mathsf{Flex}}_{\mathbf{p}_t^{\mathsf{dg/fl}}}$
18	11.52	1.62	0	0	**13.14**	10	3.14	–	**13.14**
22		-0.04	0	0	**11.48**		1.48	–	**11.48**
25		1.53	0	0	**13.06**	-11.52	-2.84	27.42	**13.06**
33		4.10	0	0	**15.63**		-1.41	28.56	**15.63**
18	11.52	1.45	0	0.83	**13.80**	10	3.80	–	**13.80**
22		-0.04	0	-0.04	**11.44**		1.44	–	**11.44**
25		1.48	0	0.24	**13.25**	-11.52	-2.67	27.44	**13.25**
33		3.50	0	2.78	**17.80**		0	29.32	**17.80**
18	11.52	1.42	0	0.82	**13.77**	10	3.77	–	**13.77**
22		-0.05	0	-0.04	**11.42**		1.42	–	**11.42**
25		1.26	0.23	3.25	**16.26**	-11.52	0	27.79	**16.26**
33		3.50	0	2.76	**17.79**		0	29.32	**17.79**

For time step 10 and all scenarios, we present active power DLMP values in Table 5.1. In Table 5.1, $\boldsymbol{\pi}^{\mathsf{M}}_{\mathbf{p}_t} = \boldsymbol{\mu}^{\mathsf{fl}+/\mathsf{dg}+}_{\mathbf{p}_t} - \boldsymbol{\mu}^{\mathsf{fl}-/\mathsf{dg}-}_{\mathbf{p}_t}$, and $\boldsymbol{\pi}^{\mathsf{D}}_{\mathbf{p}_t} = \mathbf{D}_t(\boldsymbol{\mu}^{\mathsf{fl}+}_{\mathbf{ch}_t} - \boldsymbol{\mu}^{\mathsf{fl}-}_{\mathbf{ch}_t})$. Table 5.1 also shows the market equilibrium of the proposed model in Sec. 5.3. This is shown in bold values of Table 5.1, where it can be observed that flexible DLMPs representing the internal flexible bus

dynamics exist in equilibrium with the grid cleared DLMPs, i.e., $\boldsymbol{\Pi}^{\text{Grid}}_{\mathbf{p}_t} = \boldsymbol{\Pi}^{\text{Flex}}_{\mathbf{p}_t^{\text{dg/fl}}}$. Similar to the physical intuition presented in chapter 4 for single time-step DLMPS, we observe consistent behavior for multi-period DLMPS. For example, non-zero congestion components $\boldsymbol{\Pi}^{\text{C}}_{\mathbf{p}_t}$ is observed for line connecting FL1, i.e., bus 25. Similarly, the voltage magnitude is binding only for *Scenario* 2 and 3 which is reflected upon the respective DLMP voltage component $\boldsymbol{\Pi}^{\text{V}}_{\mathbf{p}_t}$. Moreover, note that the negative DLMP component reflects that the marginal increase in active/reactive power demand (decrease in active/reactive power injection) improves the overall grid dispatch cost. This is why DG1 (bus 22) is dispatched below its maximum allowable limits, except for time-step 10, where it has to dispatch more power to meet grid constraints.

Chapter 6

Conclusions and Outlook

This chapter outlines the main conclusion from this thesis. It lays down the important features of the presented work in the previous chapters. We also discuss the relevance of the presented method with respect to some of the practical work done in this field. Building on it, at the end of this chapter, we provide an outlook on how to integrate this work in future grids and also some possibilities to improve the theoretical foundation of this thesis.

6.1 Discussion

6.1.1 The Proposed Work: Overview

In this thesis, chapter 3 and 4 presented:

- local approximation methodology, given a feasible *load-flow* solution; and
- global approximation methodology, which interpolates a linear function between a given *load-flow* solution and no-load conditions.

Both these above mentioned approximation techniques were adopted to calculate DLMPs, for:

- single-phase equivalent grid models, in case of a balanced portion of the distribution; and
- multiphase grid models, with consideration of unbalanced loadings and missing phases.

Moreover, by formulating single time-step DLMP (chapter 4) and multi-period DLMP (chapter 5) formulations, the proposed methods cater for:

- instantaneous energy dispatch, examples of such system consists of DGs with costs to generate power; and
- planned time-horizon dispatch, examples of such system consists of FLs having inter-temporal energy constraints.

The final calculated DLMPs expressed marginal cost of delivering both active and reactive powers to grid buses, i.e. the cost of sending extra watt/var to the respective bus. Moreover, this marginal cost was decomposable into their respective energy, loss, congestion and voltage components. Through a tractable solution methodology and power flow feasibility properties we showed that the obtained DLMPs are in equilibrium with the grid conditions. We also showed that the proposed DLMPs maximizing the overall social welfare of the grid also maximized the individual social welfare of the flexibility resources (DGs, DLMPs).

6.1.2 Practical Implications: Connection to Wholesale Market

The local distribution grid market proposed in this thesis can be simply extended to co-exist with the current wholesale day-ahead energy markets [1]. This can be achieved by merely adjusting the organization structure of the local distribution grid market of chapter 5 as:

1. Aggregators purchase/sell energy from/to the wholesale market.
2. The schedule from aggregators are then submitted to the local DSO.
3. The DSO can then proceed to run its local market (as proposed in chapter 5) and formulate DLMPs which are then passed on to aggregators
4. Aggregators can then include these DLMPs into their individual energy planning and proceed with their participation in the day-ahead wholesale market.

Note that this is also how most of the aggregators operate, i.e., they purchase energy from the wholesale market and sell to their contracted customers. Note that the above method simply introduces an additional layer, i.e., DLMPs, into the already established aggregator-customers link. The main improvements from introducing this link is that, through DLMPs, the DSO can indirectly influence aggregators to schedule their loads within the allowable grid conditions. Moreover, with the talks of handing over the future DSO with more "transactive" actions, the proposed methods of chapter 4 and 5 can be simply adopted to construct a local distribution grid market.

Another interesting observation from the presented DLMP formulation of this thesis is the discovery of reactive power price $\boldsymbol{\pi}_{\mathbf{q}_t}$. Similar to active power, reactive power DLMPs are also recovered using the forecast of the marginal cost of reactive power supply at the root-bus. However, whether this marginal cost of supplying reactive power at the root-bus is made available by existing wholesale markets is still a topic of ongoing discussion [12, 28, 111]. Nevertheless, the presented model is flexible enough to provide an option of pricing reactive power only as a function of its marginal value at the root-bus, i.e. $c^0_{q,t}$. If this information is not available at the root-bus, this price can simply be set to zero. We take this as a flexibility provided by the proposed methodology of this thesis.

6.1.3 Relevance to "Smart Grid" Promises

Now we discuss whether the proposed formulation aids in achieving the promises of "smart grids". A possible application of the proposed day-ahead local market, described in chapter 5 is in developing a grid-friendly demand response and congestion management programs. This is possible because the cleared DLMP at a particular node automatically reflects its contribution of delivered energy towards system losses, congestion and voltage violations. Hence, the submitted schedules by aggregators can be simply evaluated by the DSO and eventually drive day-to-day scheduling as well as future investments in the smart grid technologies towards grid-friendly areas. This is going to help in increasing the lifetime of grid assets as the overall cost-effective operation, as aggregator scheduling is influenced to better utilize the grid. Similar analysis for lossless DLMPs can be found in [35, 34, 41, 58].

6.1.4 Diversity and Extensions

The proposed model of chapter 5 represents flexibility resources for both instantaneous and multi-period dispatch. This allows for multiple extensions of the proposed method. For example, similar to inter-temporal constraints of FLs, the formulation can be extended with generic

energy storage systems, DGs with ramp-up/down limitations [12, 37]. In this way, the proposed formulation not only allows to cater for the already deployed large set of various assets, but also for an extension in the case of the development of future smart grid devices to be integrated in distribution grids.

Similarly, the proposed method handles for multiple grid types, i.e., multiphase lines, unbalanced loadings and mixture of wye/delta connections. In this way, the method can be altered by the DSO to reflect its current grid conditions and hence calculate accurate DLMPs.

6.2 Future Research Directions

We hope that the work presented in this thesis is going to motivate academia and industry in the pursuit of having an improved technical and economical operation of future distribution grids. To this end, we believe there are certain aspects of the work to be expanded in the future works. These expansions are listed below.

6.2.1 Solution Algorithms

We attempted to obtain a solution algorithm, which combines the mature technologies (*load-flow* problem) with approximations to interpret the final price in terms of physical grid components (energy, loss, voltage and congestion). However, the power flow feasibility check is included in the solution algorithm as a separate step. For the practical grids, it is shown that power flow feasibility is always respected. One of the future works in this direction exists in the form of embedding power flow security (mostly steady state voltage security) constraints into the proposed AQP of this thesis. In this way, the overall time required for implementing the solution algorithm can be minimized, as there exists then no need to implement a feasibility check of the approximated solution by projecting it to the *load-flow* problem. There has been some recent works, which integrates stability constraints in the optimal power flow [20, 107]. However, more work is still required to reflect them in a market-based framework and translate them into prices as proposed in this thesis.

6.2.2 Decentralized Calculations

There has been enormous literature discussing a decentralized/distributed operation of power systems. For example see [77] for exhaustive literature review on the decentralized/distributed optimization and control in power systems for transmission systems. However, there has been a limited focus on adapting these works in the context of DLMP calculation, even though closer to the consumption (distribution grids) there exists a higher need to preserve privacy. Moreover, by distributing/decentralizing the calculation, the solution algorithms can also be executed faster. We presented some preliminary work in [35, 34], which presented privacy preserving algorithm for obtaining optimal DLMPs under uncertain load dynamics. However, these works considered a simplified power flow calculations. Hence, one future direction regarding the proposed work is to to obtain meaningful and interpretable DLMPs in a distributed/decentralized manner.
Need for a faster solution algorithm, for real-time or on-line DLMP calculations whereas for improved distributed solutions to cater for nonlinearities

6.2.3 Price Volatility

This thesis only addressed day-ahead distribution grid market to clear DLMPs for the entire planning horizon. However, from the presented results and the theory presented in this thesis, one can observe that DLMPs vary based on the grid conditions. This means that there value might be higher/lower at certain grid locations, this could mean that some nodes may pay or get paid higher or lower depending, purely based on where they are located. Even though DLMPs reflect truest cost of delivering power to a certain bus, this might not be acceptable in the current distribution grid retail structures (tariffs), which is designed to reflect one price (equal for all) for a certain customer type (residential, commercial and industrial). In this regards, in a much similar manner to transmission grids [38, 39], hedging rights might be obtain to offset this DLMP volatility. We have done some preliminary work in this regards, however it does not reflect nonlinear power flow. Hence, one of the future works might be to look at removing the volatility of DLMPs. The main goal of removing this volatility could then be to keep the physical power flow feasibility of DLMP, while maintaining revenue adequacy of the local distribution grid along with proper merchandising surplus distribution by the DSO among market participants.

Appendix A

Appendix

A.1 Codes

A.1.1 Modified 3 bus MATPOWER case file

The deployed three-bus grid in this thesis has been taken from the meshed grid given in [76]. However, the line connecting bus 1 and 3 has been removed to make the grid radial.

```
function mpc = case3
%% MATPOWER Case Format : Version 2
mpc.version = '2';
%%-----  Power Flow Data  -----%%
%% system MVA base
mpc.baseMVA = 1;
%% bus data
%   bus_i   type    Pd  Qd  Gs  Bs      area    Vm      Va      baseKV  zone
    Vmax    Vmin
mpc.bus = [
1       3       0   0   0   0       1       1.5     0       12.6    1       1.5
    1.5;
2       1       1   1   0   0       1       1.0     0       12.6    1       1.5
    0.8;
3       1       0   0   0   0       1       1.0     0       12.6   1        1.5
    0.8;
];
%% generator data
%   bus Pg  Qg      Qmax    Qmin    Vg      mBase   status  Pmax    Pmin    Pc1
    Pc2 Qc1min  Qc1max  Qc2min  Qc2max  ramp_agc    ramp_10 ramp_30 ramp_q  apf
mpc.gen = [
1   0.1 0.1     500     0       1.5     100     1.0       332.4 0   0   0   0
    0   0   0   0   0   0   0   0;
3   0.1 0.1    500     0       1.0     100     1.0       140    0   0   0   0
    0   0   0   0   0   0   0   0;
];
%% branch data
%   fbus    tbus    r       x       b   rateA   rateB   rateC   ratio   angle
    status  angmin  angmax
mpc.branch = [
1       2       0.1     0.1     0   50     600     600     0    0   1   -360
    360;
```

```
2       3       0.1     0.1     0   50     600     600     0    0   1   -360
    360;
];
%%-----  OPF Data  -----%%
%% generator cost data
%   1   startup shutdown    n   x1  y1  ... xn  yn
%   2   startup shutdown    n   c(n-1)  ... c0
mpc.gencost = [
2   0   0   2   10  1e-4    0;
2   0   0   2   10  1e-4    0;
2   0   0   2   1   1e-4    0;
2   0   0   2   1   1e-4    0;
];
```

A.1.2 Modified 33-bus MATPOWER case file

The following code is used for implementing 33-bus system for single-period (chapter 4) and multi-period (chapter 5) ED problem. For implementing *Scenario-2* of Sec. 4.5.1, make marginal cost of FLs as 15 $/MWh.

```
function mpc = case33_DGs_FLs
%CASE33d    Power system data for 33 bus radial distribution systm.

%% MATPOWER Case Format : Version 2
mpc.version = '2';

%%-----  Power Flow Data  -----%%
%% system MVA base
mpc.baseMVA = 10;

%% bus data
%   bus_i   type    Pd  Qd  Gs  Bs  area    Vm  Va  baseKV  zone    Vmax    Vmin
mpc.bus = [
1   3   0    0      0   0   1   1   0   12.66   1   1.05    0.8;
2   1   0.1  0.06   0   0   1   1   0   12.66   1   1.5     0.8;
3   1   0.09 0.04   0   0   1   1   0   12.66   1   1.5 0.8;
4   1   0.12 0.08   0   0   1   1   0   12.66   1   1.5 0.8;
5   1   0.06 0.03   0   0   1   1   0   12.66   1   1.5 0.8;
6   1   0.06 0.02   0   0   1   1   0   12.66   1   1.5 0.8;
7   1   0.2  0.1    0   0   1   1   0   12.66   1   1.5 0.8;
8   1   0.2  0.1    0   0   1   1   0   12.66   1   1.5 0.8;
9   1   0.06 0.02   0   0   1   1   0   12.66   1   1.5 0.8;
10  1   0.06 0.02   0   0   1   1   0   12.66   1   1.5 0.8;
11  1   0.045 0.03  0   0   1   1   0   12.66   1   1.5 0.8;
12  1   0.06  0.035 0   0   1   1   0   12.66   1   1.5 0.8;
13  1   0.06  0.035 0   0   1   1   0   12.66   1   1.5 0.8;
14  1   0.12 0.08   0   0   1   1   0   12.66   1   1.5 0.8;
15  1   0.06 0.01   0   0   1   1   0   12.66   1   1.5 0.8;
16  1   0.06 0.02   0   0   1   1   0   12.66   1   1.5 0.8;
17  1   0.06 0.02   0   0   1   1   0   12.66   1   1.5 0.8;
18  1   0.09 0.04   0   0   1   1   0   12.66   1   1.5 0.8;
19  1   0.09 0.04   0   0   1   1   0   12.66   1   1.5 0.8;
20  1   0.09 0.04   0   0   1   1   0   12.66   1   1.5 0.8;
21  1   0.09 0.04   0   0   1   1   0   12.66   1   1.5 0.8;
```

```
22  1   0.09 0.04   0   0   1   1   0   12.66   1   1.5    0.8;
23  1   0.09 0.05   0   0   1   1   0   12.66   1   1.5    0.8;
24  1   0.42 0.0    0   0   1   1   0   12.66   1   1.5 0.8;
25  1   0.42 0.0    0   0   1   1   0   12.66   1   1.5 0.8;
26  1   0.06 0.025  0   0   1   1   0   12.66   1   1.5 0.8;
27  1   0.06 0.025  0   0   1   1   0   12.66   1   1.5    0.8;
28  1   0.06 0.02   0   0   1   1   0   12.66   1   1.5 0.8;
29  1   0.12 0.07   0   0   1   1   0   12.66   1   1.5 0.8;
30  1   0.2  0.6    0   0   1   1   0   12.66   1   1.5 0.8;
31  1   0.15 0.07   0   0   1   1   0   12.66   1   1.5 0.8;
32  1   0.21 0.1    0   0   1   1   0   12.66   1   1.5 0.8;
33  1   0.02 0.03   0   0   1   1   0   12.66   1   1.5 0.8;
];

%% generator data
%   bus Pg  Qg  Qmax    Qmin    Vg  mBase   status      Pmax    Pmin    Pc1 Pc2
    Qc1min  Qc1max  Qc2min  Qc2max  ramp_agc    ramp_10 ramp_30 ramp_q  apf
mpc.gen = [
%   1   500 0   150 -200    1.05    100 1   800 0   0   0   0   0       0   0
    0   0   0   0   0;
1   2.78    0               100     -100        1.05    100 1       100     0
          0   0   0   0   0   0   0   0   0   0   0; %PSP
18  0.50    0.00        0.30    0           1       100 1       0.50     0
          0  0   0   0   0   0   0   0   0   0   0; %DG1
22  0.50    0.00        0.30    0           1       100 1       0.50     0
          0  0   0   0   0   0   0   0   0   0   0; %DG2
25  -1.0    0     0 0           1       100  1   0 -1.4725       0   0   0   0
    0   0   0   0   0   0   0; %FL1
33  -1.0    0     0 0           1       100  1   0 -1.4725       0   0   0   0
    0   0   0   0   0   0   0; %FL2
];

%% branch data
%   fbus    tbus    r   x   b   rateA   rateB   rateC   ratio   angle   status
    angmin  angmax
mpc.branch = [
1   2   0.005752591 0.002976124 0   130 130 130 0   0   1   -360    360;
2   3   0.030759517 0.015666764 0   130 130 130 0   0   1   -360    360;
3   4   0.022835666 0.011629967 0   130 130 130 0   0   1   -360    360;
4   5   0.023777793 0.01211039  0   130 130 130 0   0   1   -360    360;
5   6   0.051099481 0.044111518 0   130 130 130 0   0   1   -360    360;
6   7   0.011679881 0.038608497 0   130 130 130 0   0   1   -360    360;
7   8   0.106778574 0.077061012 0   130 130 130 0   0   1   -360    360;
8   9   0.064264305 0.046170471 0   130 130 130 0   0   1   -360    360;
9   10  0.062642099 0.046170471 0   130 130 130 0   0   1   -360    360;
10  11  0.012266371 0.004055514 0   130 130 130 0   0   1   -360    360;
11  12  0.023359763 0.007724195 0   130 130 130 0   0   1   -360    360;
12  13  0.091592232 0.072063371 0   130 130 130 0   0   1   -360    360;
13  14  0.033791794 0.044479634 0   130 130 130 0   0   1   -360    360;
14  15  0.036873985 0.03281847  0   130 130 130 0   0   1   -360    360;
15  16  0.046563544 0.034003928 0   130 130 130 0   0   1   -360    360;
16  17  0.08042397  0.107377542 0   130 130 130 0   0   1   -360    360;
17  18  0.045671331 0.035813312 0   130 130 130 0   0   1   -360    360;
2   19  0.010232375 0.009764431 0   130 130 130 0   0   1   -360    360;
19  20  0.093850842 0.084566834 0   130 130 130 0   0   1   -360    360;
```

```
20  21  0.025549741 0.029848586 0   130 130 130 0   0   1   -360    360;
21  22  0.044230064 0.058480517 0   130 130 130 0   0   1   -360    360;
3   23  0.028151509 0.019235617 0   130 130 130 0   0   1   -360    360;
23  24  0.056028491 0.044242542 0   130 130 130 0   0   1   -360    360;
24  25  0.055903706 0.043743402 0   130 130 130 0   0   1   -360    360;
6   26  0.012665683 0.006451387 0   130 130 130 0   0   1   -360    360;
26  27  0.017731957 0.009028199 0   130 130 130 0   0   1   -360    360;
27  28  0.066073688 0.058255904 0   130 130 130 0   0   1   -360    360;
28  29  0.050176072 0.043712206 0   130 130 130 0   0   1   -360    360;
29  30  0.031664208 0.016109751 0   130 130 130 0   0   1   -360    360;
30  31  0.06079528  0.060084005 0   130 130 130 0   0   1   -360    360;
31  32  0.01937288  0.022579856 0   130 130 130 0   0   1   -360    360;
32  33  0.021275852 0.033080519 0   130 130 130 0   0   1   -360    360;
];

%% generator cost data
%   1   startup shutdown    n   x1  y1  ... xn  yn
%   2   startup shutdown    n   c(n-1)  ... c0
mpc.gencost = [
2   0   0   2   12.06   1e-4;
2   0   0   2   10  1e-4;
2   0   0   2   10  1e-4;
2   0   0   2   10  1e-4;
2   0   0   2   10  1e-4;
2   0   0   2   3   1e-4;
2   0   0   2   3   1e-4;
2   0   0   2   3   1e-4;
2   0   0   2   0   0;
2   0   0   2   0   0;
];
```

A.1.3 Modified 4 bus openDSS script file

```
clear
! IEEE modified 4-bus test case
! Originally given at OPENDSS Website, developed by Alan Dunn and Steve Sparling
new circuit.4bus   basekV=12.47 phases=3
~ mvasc3=200000 200000
new linecode.mtx601 nphases=3  Units=mi
~ rmatrix=[0.4576  |0.1559  0.4666  |0.1535  0.158  0.4615  ]
~ xmatrix=[1.078  |0.5017  1.04828  |0.3849  0.4236  1.065  ]
~ cmatrix=[0  |0  0  |0  0  0  ]
new linecode.mtx602 nphases=2  Units=mi
~ rmatrix=[0.4576  |0.1559  0.4666]
~ xmatrix=[1.078  |0.5017  1.04828]
~ cmatrix=[0  |0  0 ]
! **** 12.47 KV LINE
new line.line1 phases=3 bus1=sourcebus bus2=n2 linecode=mtx601 Length=2000
    units=ft
! **** 3-PHASE STEP-DOWN TRANSFORMER 12.47 to 4.16 KV Ygrd-Ygrd (remove ''\''
    when inputing the code as .dss file)
new transformer.t1  phases=3   windings=2  xhl=2
~ wdg=1 bus=n2.1.2.3 conn=wye kV=12.47 kVA=6000 \%r=.55     xht=1
~ wdg=2 bus=n3.1.2.3 conn=wye   kV=4.16  kVA=6000  \%r=.55   xlt=1
```

```
! **** 4.16 KV LINE
new line.line2 phases=3 bus1=n3.1.2 bus2=n4.1.2 linecode=mtx602 Length=2500
    units=ft
! **** SINGLE PHASE WYE-CONNECTED DELTA-CONNECTED (LINE-LINE) LOADS with 4.16
    KV-LL RATING
new load.load1 phases=1 bus1=n4.1.0 kV=2.4018 kW=400 kvar=200 vminpu=0.75
    model=1
new load.load2 phases=1 bus1=n4.1.2 kV=4.16 kW=400 kvar=200 vminpu=0.75 model=1
set voltagebases=[12.47, 4.16]
set controlmode=OFF
calcvoltagebases
solve
```

A.2 DLMP Model for Convexified OPF

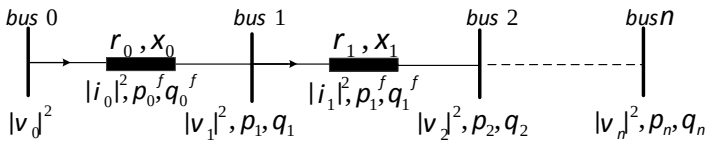

Figure A.1: Notations used to represent branch flow convexified power flow model of the radial grid [57]. For line connecting bus j and k, squared line current, active power flow, reactive power flow, resistance and reactance are represented as: $i_j^{sq} := |i_j|^2$, p_j^f, q_j^f, r_j and x_j, respectively. For bus j, squared voltage, active power injection and reactive power injection are represented as: $v_j^{sq} := |v_j|^2$, p_j and q_j, respectively.

A.2.1 Convexified DLMP Formulation

In order to aid in developing branch flow convexification method [4, 57, 26], we adopt scalar notation here to represent a radial grid in Fig. A.1. We formulate convexified ACOPF for a generic injections (p_j, q_j) at each bus j and single time-step in (A.1)[1]. In (A.1), s_j^f and $c_j^p(\cdot)$ / $c_j^q(\cdot)$ are respectively the scalar version of the complex line flow "from" and cost function given in (3.14) and Sec. 4.1.1. For more information regarding the formulation, interested readers are referred to [57]. Constraints [(A.1b)–(A.1e)] represent AC power flow relaxation. The constraint (A.1e) is actually a second order cone constraint, if satisfied as an equality constraint makes the relaxation exact [26]. For detailed information on SOCP, interested readers are

[1]The full formulation (analogous to (4.3)) which considers FLs/DGs along with inter-temporal energy and actuator constraints is a straight forward procedure and is left out here for exposition simplicity and brevity.

referred to [57, 26].

$$\max \quad -\sum_{j=1}^{n} \left(c_j^p(p_j) + c_j^q(q_j)\right) \tag{A.1a}$$

s.t.

$$p_j^f = p_{j+1}^f + r_j i_j^{sq} - p_{j+1} \qquad : \lambda_j^p \tag{A.1b}$$

$$q_j^f = q_{i+1}^f + x_j i_j^{sq} - q_{j+1} \qquad : \lambda_j^q \tag{A.1c}$$

$$v_j^{sq} = v_{j+1}^{sq} + 2(r_j p_j^f + x_j q_i^f) - (r_j^2 + x_j^2) i_j^{sq} : \lambda_j^v \tag{A.1d}$$

$$\frac{(p_j^f)^2 + (q_j^f)^2}{v_j^{sq}} \leq i_j^{sq} \qquad : \mu_j^i \tag{A.1e}$$

$$(p_j^f)^2 + (q_j^f)^2 \leq (s_j^{f+})^2 \qquad : \mu_j^s \tag{A.1f}$$

$$v_j^{sq-} \leq v_j^{sq} \leq v_j^{sq+} \qquad : \mu_j^{v-}, \mu_j^{v+} \tag{A.1g}$$

$$\forall j \in \{0, \ldots, n-1\}$$

Now considering an exact solution of (A.1), the following KKT conditions are then satisfied:

$$\begin{aligned}
c_j^p + \lambda_j^p &= 0 \\
c_j^q + \lambda_j^q &= 0 \\
\lambda_{j-1}^p = \lambda_j^p + 2r_j\lambda_j^v - 2p_j^f(\beta_j + \mu_j^s) &= 0 \\
\lambda_{j-1}^q = \lambda_j^q + 2x_j\lambda_j^v - 2q_j^f(\beta_j + \mu_j^s) &= 0 \\
r_j\lambda_j^p + x_j\lambda_j^q - (r_j^2 + x_j^2) + \mu_j^i &= 0 \\
\mu_j^i \frac{(p_j^f)^2 + (q_j^f)^2}{(v_j^{sq})^2} + \mu_j^{v+} - \mu_j^{v-} + \lambda_j^v - \lambda_{j-1}^v &= 0 \\
\forall j \in \{1, \ldots, n\}
\end{aligned}$$

Along with the primal feasible (A.1) and non-negative Lagrange multipliers conditions. In (A.2), we have $\beta_j := \frac{\mu_j^i}{v_j^{sq}}$.

For active power, consider DLMP at bus j to be defined as λ_j^p. Then from (A.2), we have DLMP at bus (j) λ_j^p dependent upon DLMP at its ancestor-bus $(j-1)$ λ_{j-1}^p, along with other terms which are only dependent on the bus (j) $2r_j\lambda_j^v$ and the line connecting the bus (j) and its ancestor-bus $(j-1)$ $2p_j^f(\beta_j + \mu_j^s)$. Same explanation holds for the reactive power DLMP at bus (j), i.e., λ_j^q.

DLMP Representation Issues

The DLMP value obtained from the above mentioned convexified formulation (A.2) might be interpreted as follows: a marginal change in injection at bus (j) only requires a marginal change of injections at its own bus (j) and its ancestor-bus $(j-1)$, while leaving reset of the grid unaffected. However, this interpretation is not physically true. As it has been shown in [82, Proposition 3.3] that a marginal change in the injection at bus j also affects variables (e.g. voltages, line flows) at buses other than its ancestor-bus $(j-1)$. Moreover, Lagrange multipliers λ_j^v and μ_j^i do not have straight forward interpretation. In light of these representation issues, we

adopt global power balance formulation and its trust-region based iterative linearization for calculating DLMPs.

A.3 Flexible Load Model

Table A.1: Flexible Load Model Nomenclature

Notation	Description
wi, ri	number of walls and rooms
T_{wi}, T_{ri}, T_{si}	Temperature of walls, rooms and air supply
C_{wi}, C_{ri}	Transmittance of window i and absorptivity coefficient of wall
R_{ij}	Thermal resistance between node i
A^{i}_{ri}, A_{wi}	Total area of window i and total area of the wall wi
$q''_{rad_{ri}}$, $\dot{q}_{int_{ri}}$	Solar radiation and internal heat generation in the room
N_{wi}, N_{ri}	The set of all connected nodes to walls and the room
r_i	Equal to 0 for internal and 1 for peripheral walls
$x(t)$	Temperature state [deg C]
$ch(t)$	State of the charge [–]
$u_{m,t}$	Air mass flow energy schedule [kg/sec]
$z(t)$	External and internal disturbances
$p_{\text{heat},t}$, $p_{\text{fan},t}$	Heating and fan power [kW]
ρ, Δp, c_{p}	Air density, pressure difference across the fan, and air specific heat capacity

In the existing literature, (1) data driven models [72, 73], (2) high fidelity physical models [18, 98, 19] and (3) resistance-capacitance (R-C) based physical models [67, 21] of buildings are found. Data driven models provide good performance when operated within trained (historical) data sets. Hence, the main drawback of these models exists in the form of high data requirements, covering range of operating and ambient conditions. High fidelity physical building models represent accurate complex thermal interactions within a building. Applications of these models are mainly limited to the estimation of annual, monthly or weekly energy consumption. The main disadvantages of these types of models are their size and complexity. Hence, they cannot be easily incorporated into optimization problems, which is necessary for quantifying load shifting potential.

For buildings, the R-C model is designed to achieve controllability. These types of models attempt to mitigate issues related to data driven and high fidelity models. Even though R-C models represent a simplified form of high fidelity physical models, they still provide accurate enough prediction of important thermal states of the building. Compared to their counterparts, R-C models are computationally tractable. This property has been specially useful in the utilization of control theory in building operations [66, 81, 32, 33, 69, 80]. Hence in this thesis, an R-C based physical model is used to predict thermal states and energy requirements of the building.

Zone Model

An R-C (lumped) model of a zone consists of thermal resistances and thermal capacitances, representing heat transfer and heat storage, respectively. Each node in a zone is represented by one temperature (thermal) state. These buses are connected with each other through thermal resistances, and to the ground through thermal capacitances. From A.2, it can also

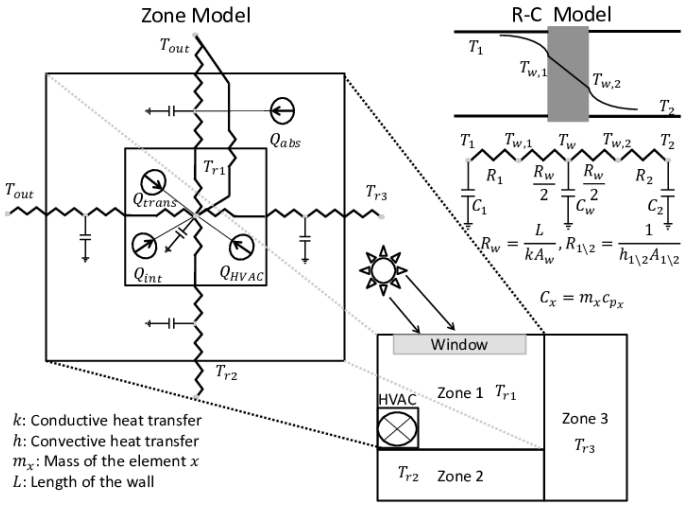

Figure A.2: Simple R-C model representing interpretation of walls and its surrounding environment (top right). The translation of one zone, into an R-C thermal network (left). For simplification, zone 1 is assumed to contain only one room. The injections Q_{HVAC}, Q_{abs} and Q_{int} represent the second, third and fourth term of (A.2b), respectively. Similarly, Q_{trans} is evaluated using the second term of (A.2a).

be observed that heat flows are represented by current injections, whereas temperatures as voltages. The differential equations representing temperature evolutions of walls and room are:

$$\frac{dT_{wi}}{dt} = \frac{1}{C_{wi}}\Big(\sum_{j\in N_{wi}} \frac{T_j - T_{wi}}{R_{ij}} + r_i \alpha_{wi} A_{wi} q''_{rad_{ri}}\Big), \tag{A.2a}$$

$$\frac{dT_{ri}}{dt} = \frac{1}{C_{ri}}\Big(\sum_{j_{\in N_{ri}}} \frac{T_j - T_{ri}}{R_{ij}} + \dot{m}_{ri} c_p (T_{si} - T_{ri}) + w_i \tau^i_{ri} A^i_{ri} q''_{rad_{ri}} + \dot{q}_{int}\Big), \tag{A.2b}$$

The total number of state equations to represent one zone are $n = wi + ri$. There are two sources of disturbances in the model: (i) external disturbances, experienced due to solar radiation $q''_{rad_{ri}}$ and (ii) internal disturbances, caused by electronic components and occupancy $\dot{q}_{int}$. More details regarding parameters of the R-C model and their units can be found in [67]. From (A.2), the temperature of the zone x_t can be expressed as a nonlinear combination with the Heating Ventillation and Air-Conditioning (HVAC) mass flow rate $u(t)$ as:

$$x(t+1) = x(t) + g(x(t), u(t)) - z(t). \tag{A.3}$$

The expression shown above is of nonlinear nature. Since the most efficient controllers are obtained for linear systems, the nonlinear model described above is linearized and discretized using sequential quadratic programing and zero order hold, respectively [68]. In [68], it is shown that linearizing around the usual operating point does not introduce significant errors. This is mainly because the temperature range of the building is normally not very large. Another simplification made in obtaining an equivalent flexible load model is that only aggregated room temperature is concerned, i.e., we omit the effect of wall temperatures. This is done because from experiments it has been observed that wall temperature are always moving very slowly and hence can be assumed constant. Hence, we obtain the resultant discrete time linear system at step k becomes:

The above equation in a sequential form, i.e., as a linear combination of previous and current state,

$$ch_t = ch_0^{\text{fl}} + \sum_{t'<t-1} dp_{t'}^{\text{fl}} - \sum_{t'\leq t} z_{t'}, \tag{A.4}$$

where ch_t is now an equivalent state of charge of the room temperature. This state of flexible load ch_t at time period t is then represented sum of its initial state ch_0 and the amount it deviates due to flexible load provision till period $t-1$, $p_{t'}^{\text{fl}}$ and the disturbance it experiences up to time period t, i.e., z_t. Interested readers are directed to [41, Sec. III], [58, Sec. III] regarding the above shown representation of flexible loads. In (A.4), $p_t^{\text{fl}} = p_{\text{heat},t}(u_t) + p_{\text{fan},t}(u_t)$, where it is assumed that a variable frequency drive fan based HVAC system is available for flexibile consumption. In principle, by modulating the fan speed $\dot{m}_{ri}$, the energy consumption as well as the temperature of the room is controlled. Hence, the electrical power consumed for heating $p_{\text{heat},t}$ and fan $p_{\text{fan},t}$ as a function of control variable is given as:

$$p_{\text{heat},t} = \frac{u_t c_{\text{p}}(T_{si} - T_{ri})}{\eta}, \tag{A.5a}$$

$$p_{\text{fan},t} = \frac{u_t \Delta p}{\rho}. \tag{A.5b}$$

Finally, the above flexible load state equations can be compactly represented as the vector of all n flexible loads states in the grid,

$$\mathbf{ch}_t^{\text{fl}} = \mathbf{ch}_0^{\text{fl}} + \mathbf{D}_t \mathbf{p}_t^{\text{fl}} - \mathbf{z}_t, \tag{A.6}$$

where $\mathbf{D}_t$ places parameter d recursively in its entries to reflect inter-temporal flexible load consumption so that the state ch_t is dependent on both previous and current time steps.

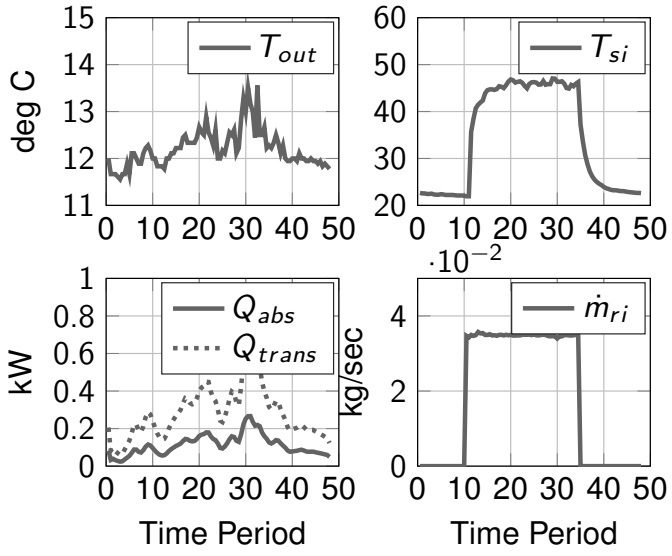

Figure A.3: Measurements used for conducting flexible load's zone model identification.

Identification & Validation

As an initial guess, the R-C thermal model is first developed using typical values of construction materials. In order to adjust the developed theoretical model to represent the actual thermal behavior of the zone, parameters of the model are adjusted. This is performed using the "fmincon" function in Matlab. In particular, optimal parameters are found which minimizes the least square error between the simulated and the actual temperature of the zone. The identified parameters are then used to simulate the thermal behavior of the zone. Chapter A.4 shows a comparison between the measured temperature of an actual commercial building's zone [67] and the simulated temperature using the identified parameters. The maximum absolute error of only 0.46 deg C is observed in A.4, which has a negligible effect on users. To quantify the performance of the obtained model, two metrics are defined: (1) the mean absolute percentage error (MAPE) and (2) the mean absolute error (MAE).

$$\text{MAPE} = \frac{1}{N}\sum_{k=1}^{N}\frac{|T_{ri} - T_{mi}|}{T_{mi}} \times 100 \tag{A.7a}$$

$$\text{MAE} = \frac{1}{N}\sum_{k=1}^{N}|T_{ri} - T_{mi}|. \tag{A.7b}$$

In (A.7), T_{mi} and N are the measured temperature of the zone and time duration of the experiment (24 hr), respectively. The MAPE and MAE for the model comes out to be 0.30% and 0.21, respectively. These values show that the modeled temperature evolution is close to the actual one.

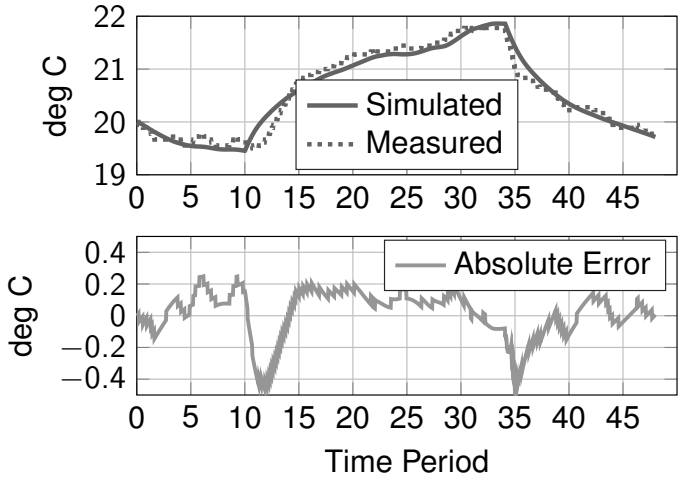

Figure A.4: Comparison between the simulated and actual temperature profile (top), along with the absolute error (bottom).

A.3.1 Practicality of the Adopted Flexible Model

The main advantages of adopting the proposed model to the Building-Resistance-Capacitance-Modeling (BRCM) toolbox [96] is that: (1) it automates the connection of zone differential equation, and (2) it allows for benchmarking and comparing of control/optimization techniques for building simulation [33, 95, 13, 32]. Hence, the zone model described in A.3, is shown to

be translatable to BRCM using the description provided below. The advantage of the BRCM toolbox comes from its ability to separate the dynamic thermal model (heat transfer between rooms, walls etc.) and the static external heat flux (EHF) model (solar and internal gains etc.) of the building. Keeping the similar notation of A.3, the BRCM represents the interaction of thermal states (temperatures), ch_t with the aggregated EHF inputs, q_t as:

$$\dot{ch}_t = Ach_t + Bq_t(x_t, u(t), z_t). \tag{A.8}$$

In principle, q_t can be considered as a response in the form of heat due to the influence of control inputs ($u(t)$) and disturbances ($\hat{d}_t$) on the system. For n_u number of inputs, the thermal model in A.8 is discretized in order to obtain a bilinear model of the system (the time varying product of states and disturbances with control inputs)[2]

$$x_{t+1} = Ax_t + B_u u_t + E_z z_t + \sum_{i=1}^{n_u} (E_{zu,i}\hat{d}_k + B_{xu,i}x_k)u_{k,i}, \tag{A.9}$$

In order to bring the model of (A.9) into the presented zone model in A.3, two simplifications can be performed: (1) it is assumed that the temperature experienced by the outside of the walls, solar irradiation and heat gains are known in advance (from historical data), and (2) only the HVAC's mass flow is taken as a control input. Under these assumptions, the input dependent state B_{xu} and disturbance $E_{\hat{d}u,i}$ matrices are concatenated into A and E, respectively. The resultant discrete time linear state space model then becomes:

$$x_{t+1} = Ax_t + B_u u_t + z_t \tag{A.10}$$

As a validation, A.5 shows the comparison between the simulated zone models and the measured temperature. It can be observed that the BRCM toolbox represents a close similarity to the actual temperature evolution. This validation enforces that the BRCM provides an extensible, yet comprehensive tool for modeling the thermal dynamics of a building.

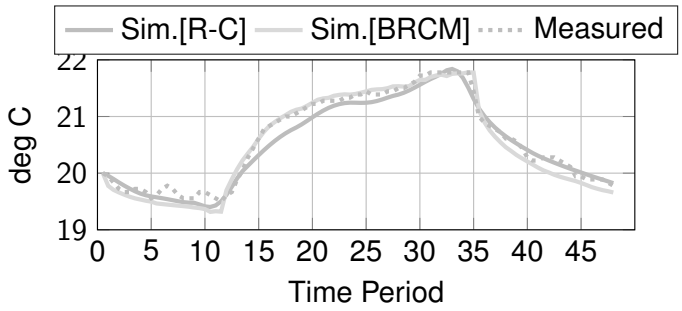

Figure A.5: Temperature profiles of simulated zone models, using BRCM and R-C model((A.10)), and their comparison with the actual measurements [67].

[2]Refer to [96] for the more information regarding the thermal model and its corresponding matrices of BRCM.

Bibliography

[1] Pennsylvania, Jersey, Maryland Power Pool (PJM). Overview of the energy market: Pjm, 2017. URL: http://pjm.com/~/media/committees-groups/committees/mrc/20160824/20160824-item-01-day-ahead-overview.ashx.

[2] T. Ackermann, G. Andersson, and L. Söder. Distributed generation: a definition. *Electric Power Systems Research*, 57(3):195 – 204, 2001. URL: http://www.sciencedirect.com/science/article/pii/S0378779601001018, doi:https://doi.org/10.1016/S0378-7796(01)00101-8.

[3] L. Bai, J. Wang, C. Wang, C. Chen, and F. F. Li. Distribution locational marginal pricing (dlmp) for congestion management and voltage support. *IEEE Transactions on Power Systems*, PP(99):1–1, 2017. doi:10.1109/TPWRS.2017.2767632.

[4] M. Baran and F. F. Wu. Optimal sizing of capacitors placed on a radial distribution system. *IEEE Transactions on Power Delivery*, 4(1):735–743, 1989. doi:10.1109/61.19266.

[5] M. Bazrafshan and N. Gatsis. Comprehensive modeling of three-phase distribution systems via the bus admittance matrix. *IEEE Transactions on Power Systems*, PP(99):1–1, 2017. doi:10.1109/TPWRS.2017.2728618.

[6] M. Bazrafshan and N. Gatsis. *Convergence of the Z-Bus method and existence of unique solution in single-phase distribution load-flow*, pages 851–855. Institute of Electrical and Electronics Engineers Inc., United States, 4 2017. doi:10.1109/GlobalSIP.2016.7905963.

[7] A. Bernstein and E. Dall'Anese. Linear power-flow models in multiphase distribution networks: Preprint. In *IEEE International Conference on Innovative Smart Grid Technologies (ISGT Europe 2017)*, May 2017. URL: http://www.osti.gov/scitech/servlets/purl/1361015.

[8] A. Bernstein, C. Wang, E. Dall'Anese, J.-Y. L. Boudec, and C. Zhao. Load-flow in multiphase distribution networks: Existence, uniqueness, non-singularity and linear models. *arXiv preprint arXiv:1702.03310*, 2017.

[9] S. Bolognani and F. Dörfler. Fast power system analysis via implicit linearization of the power flow manifold. In *Proc. 53rd Annual Allerton Conference on Communication, Control, and Computing*, 2015. doi:10.1109/ALLERTON.2015.7447032.

[10] S. Bolognani and S. Zampieri. On the existence and linear approximation of the power flow solution in power distribution networks. *IEEE Transactions on Power Systems*, 31(1):163–172, Jan. 2016. doi:10.1109/TPWRS.2015.2395452.

[11] S. Boyd and L. Vandenberghe. *Convex optimization*. Cambridge University Press, Cambridge, UK and New York, 2004.

[12] M. Caramanis, E. Ntakou, W. W. Hogan, A. Chakrabortty, and J. Schoene. Co-optimization of power and reserves in dynamic T&D power markets with nondispatchable renewable generation and distributed energy resources. *Proceedings of the IEEE*, 104(4):807–836, 2016. doi:10.1109/JPROC.2016.2520758.

[13] S. Chatzivasileiadis, M. Bonvini, J. Matanza, R. Yin, T. S. Nouidui, E. C. Kara, R. Parmar, D. Lorenzetti, M. Wetter, and S. Kiliccote. Cyber-physical modeling of distributed resources for distribution system operations. *Proc. IEEE*, 104(4):789–806, 2016. arXiv:arXiv:1505.00078v1, doi:10.1109/JPROC.2016.2520738.

[14] L. Chen, N. Li, S. H. Low, and J. C. Doyle. Two market models for demand response in power networks. In *2010 First IEEE International Conference on Smart Grid Communications*, pages 397–402, Oct 2010. doi:10.1109/SMARTGRID.2010.5622076.

[15] T. H. Chen, M. S. Chen, K. J. Hwang, P. Kotas, and E. A. Chebli. Distribution system power flow analysis-a rigid approach. *IEEE Transactions on Power Delivery*, 6(3):1146–1152, Jul 1991. doi:10.1109/61.85860.

[16] A. J. Conejo, M. Carrión, and J. M. Morales. *Decision Making Under Uncertainty in Electricity Markets*, volume 153. Springer US, Boston, MA, 2010. doi:10.1007/978-1-4419-7421-1.

[17] A. Conn, N. Gould, and P. Toint. *Trust Region Methods*. Society for Industrial and Applied Mathematics, 2000. doi:10.1137/1.9780898719857.

[18] D. B. Crawley, J. W. Hand, M. Kummert, and B. T. Griffith. Contrasting the capabilities of building energy performance simulation programs. *Build. Environ.*, 43(4):661–673, apr 2008. doi:10.1016/j.buildenv.2006.10.027.

[19] D. B. Crawley, L. K. Lawrie, F. C. Winkelmann, W. F. Buhl, Y. J. Huang, C. O. Pedersen, R. K. Strand, R. J. Liesen, D. E. Fisher, M. J. Witte, and J. Glazer. EnergyPlus: Creating a new-generation building energy simulation program. *Energy Build.*, 33(4):319–331, 2001. doi:10.1016/S0378-7788(00)00114-6.

[20] B. Cui and X. A. Sun. A New Voltage Stability-Constrained Optimal Power Flow Model: Sufficient Condition, SOCP Representation, and Relaxation. *ArXiv e-prints*, May 2017. arXiv:1705.10372.

[21] David Sturzenegger. *Model Predictive Building Climate Control - Steps Towards Practice*. Ph.d. thesis, ETH Zurich, 2012. URL: http://tinyurl.com/hldpwq7.

[22] Department of Energy. United states electricity industry primer, 2015. URL: https://www.energy.gov/sites/prod/files/2015/12/f28/united-states-electricity-industry-primer.pdf.

[23] W. El-Khattam and M. Salama. Distributed generation technologies, definitions and benefits. *Electric Power Systems Research*, 71(2):119 – 128, 2004. URL: http://www.sciencedirect.com/science/article/pii/S0378779604000240, doi:https://doi.org/10.1016/j.epsr.2004.01.006.

[24] Energy independence and security act of 2007. Smart grid, 2010. URL: https://www.gpo.gov/fdsys/pkg/PLAW-110publ140/pdf/PLAW-110publ140.pdf.

[25] Energy Market Company. Market data: Price information, 2017. URL: https://www.emcsg.com/MarketData/PriceInformation.

[26] M. Farivar and S. H. Low. Branch flow model: Relaxations and convexification–part i. *IEEE Transactions on Power Systems*, 28(3):2554–2564, Aug 2013. doi:10.1109/TPWRS.2013.2255317.

[27] A. M. Giacomoni and B. F. Wollenberg. Linear programming optimal power flow utilizing a trust region method. In *North American Power Symposium 2010*, pages 1–6, Sept 2010. doi:10.1109/NAPS.2010.5619970.

[28] J. B. Gil, T. G. S. Roman, J. J. A. Rios, and P. S. Martin. Reactive power pricing: a conceptual framework for remuneration and charging procedures. *IEEE Transactions on Power Systems*, 15(2):483–489, May 2000. doi:10.1109/59.867129.

[29] J. J. Grainger and W. D. Stevenson. *Power System Analysis*. McGraw-Hill, New York, 1994.

[30] I. Gurobi Optimization. Gurobi optimizer reference manual, 2016. URL: http://www.gurobi.com.

[31] Gurobi Optimization Inc. Gurobi optimizer quick start guide, 2016.

[32] M. Gwerder, D. Gyalistras, C. Sagerschnig, R. S. Smith, and D. Sturzenegger. Final Report : Use of Weather And Occupancy Forecasts For Optimal Building Climate Control (OptiControl). Technical Report September, ETH Zürich, 2010. URL: http://www.opticontrol.ethz.ch/Lit/Gyal_10_Rep-OptiCtrlFinalRep.pdf.

[33] M. Gwerder, D. Gyalistras, C. Sagerschnig, R. S. Smith, and D. Sturzenegger. Final Report : Use of Weather And Occupancy Forecasts For Optimal Building Climate Control – Part II : Demonstration (OptiControl-II). Technical Report September, ETH Zürich, 2013. URL: http://www.opticontrol.ethz.ch/Lit/Gwer_13_Rep-OptiCtrl2FinalRep.pdf.

[34] S. Hanif, H. B. Gooi, T. Massier, T. Hamacher, and T. Reindl. Distributed congestion management of distribution grids under robust flexible buildings operations. *IEEE Transactions on Power Systems*, page 1, 2017. doi:10.1109/TPWRS.2017.2660065.

[35] S. Hanif, T. Massier, H. B. Gooi, T. Hamacher, and T. Reindl. Cost optimal integration of flexible buildings in congested distribution grids. *IEEE Transactions on Power Systems*, 2016. doi:10.1109/TPWRS.2016.2605921.

[36] G. Heydt. The Next Generation of Power Distribution Systems. *IEEE Trans. Smart Grid*, 1(3):225–235, 2010. doi:10.1109/TSG.2010.2080328.

[37] G. T. Heydt, B. H. Chowdhury, M. L. Crow, D. Haughton, B. D. Kiefer, F. Meng, and B. R. Sathyanarayana. Pricing and control in the next generation power distribution system. *IEEE Transactions on Smart Grid*, 3(2):907–914, 2012. doi:10.1109/TSG.2012.2192298.

[38] W. W. Hogan. Contract networks for electric power transmission. *Journal of regulatory economics*, 4(3):211–242, 1992. doi:10.1007/BF00133621.

[39] W. W. Hogan. Electricity market design - financial transmission rights, up to congestion transactions and multi–settlement systems, 2012.

[40] Z. Hu, H. Cheng, Z. Yan, and F. Li. An iterative lmp calculation method considering loss distributions. *IEEE Transactions on Power Systems*, 25(3):1469–1477, 2010. doi:10.1109/TPWRS.2010.2041799.

[41] S. Huang, Q. Wu, S. S. Oren, R. Li, and Z. Liu. Distribution locational marginal pricing through quadratic programming for congestion management in distribution networks. *IEEE Transactions on Power Systems*, 30(4):2170–2178, 2015. doi:10.1109/TPWRS.2014.2359977.

[42] International Renewable Energy Agency. Global ev outlook 2017, 2017. URL: https://www.iea.org/publications/freepublications/publication/GlobalEVOutlook2017.pdf.

[43] International Renewable Energy Agency. Renewable capacity statistics, 2018. URL: http://www.irena.org/-/media/Files/IRENA/Agency/Publication/2018/Mar/IRENA_RE_Capacity_Statistics_2018.pdf.

[44] R. A. Jabr. A primal-dual interior-point method to solve the optimal power flow dispatching problem. *Optimization and Engineering*, 4(4):309–336, Dec 2003. URL: https://doi.org/10.1023/B:OPTE.0000005390.63406.1e, doi:10.1023/B:OPTE.0000005390.63406.1e.

[45] James McCalley. Optimization Intro: Steady-State Analysis - Power System Operation and Control (Fall 2012), 2012. URL: http://home.engineering.iastate.edu/~jdm/ee553/ee553schedule.htm.

[46] J. Y. Joo and M. D. Ilić. Multi-layered optimization of demand resources using lagrange dual decomposition. *IEEE Trans. on Smart Grid*, 4(4):2081–2088, Dec 2013. doi:10.1109/TSG.2013.2261565.

[47] W. H. Kersting. Radial distribution test feeders. *IEEE Transactions on Power Systems*, 6(3):975–985, Aug 1991. doi:10.1109/59.119237.

[48] W. H. Kersting. *Distribution System Modeling and Analysis, Third Edition*. CRC Press, Boca Raton, 2012.

[49] H. Khodr, F. Olsina, P. D. O.-D. Jesus, and J. Yusta. Maximum savings approach for location and sizing of capacitors in distribution systems. *Electric Power Systems Research*, 78(7):1192 – 1203, 2008. doi:https://doi.org/10.1016/j.epsr.2007.10.002.

[50] D. S. Kirschen and G. Strbac. *Fundamentals of power system economics*. John Wiley & Sons, Chichester West Sussex England and Hoboken NJ, 2004.

[51] N. C. Koutsoukis, D. O. Siagkas, P. S. Georgilakis, and N. D. Hatziargyriou. Online reconfiguration of active distribution networks for maximum integration of distributed generation. *IEEE Transactions on Automation Science and Engineering*, 14(2):437–448, April 2017. doi:10.1109/TASE.2016.2628091.

[52] L. Kristov and P. D. Martini. 21st century electric distribution system operations, 2014. URL: http://resnick.caltech.edu/docs/21st.pdf.

[53] H. W. Kuhn and A. W. Tucker. Nonlinear programming. In *Proceedings of the Second Berkeley Symposium on Mathematical Statistics and Probability*, pages 481–492, Berkeley, Calif., 1951. University of California Press. URL: https://projecteuclid.org/euclid.bsmsp/1200500249.

[54] F. Li and R. Bo. Dcopf-based lmp simulation: Algorithm, comparison with acopf, and sensitivity. *IEEE Transactions on Power Systems*, 22(4):1475–1485, 2007. doi:10.1109/TPWRS.2007.907924.

[55] N. Li, L. Chen, and M. A. Dahleh. Demand response using linear supply function bidding. *IEEE Transactions on Smart Grid*, 6(4):1827–1838, July 2015. doi:10.1109/TSG.2015.2410131.

[56] N. Li, L. Chen, and S. H. Low. Optimal demand response based on utility maximization in power networks. In *2011 IEEE Power and Energy Society General Meeting*, pages 1–8, July 2011. doi:10.1109/PES.2011.6039082.

[57] N. Li, L. Chen, and S. H. Low. Exact convex relaxation of opf for radial networks using branch flow model. In *2012 IEEE Third International Conference on Smart Grid Communications (SmartGridComm)*, pages 7–12, Nov 2012. doi:10.1109/SmartGridComm.2012.6485951.

[58] R. Li, Q. Wu, and S. S. Oren. Distribution locational marginal pricing for optimal electric vehicle charging management. *IEEE Transactions on Power Systems*, 29(1):203–211, 2014. doi:10.1109/TPWRS.2013.2278952.

[59] J. Lian, D. Wu, K. Kalsi, and H. Chen. Theoretical framework for integrating distributed energy resources into distribution systems. In *2017 IEEE Power Energy Society General Meeting*, pages 1–5, July 2017. doi:10.1109/PESGM.2017.8274331.

[60] E. Litvinov. Design and operation of the locational marginal prices-based electricity markets. *IET Generation, Transmission & Distribution*, 4(2):315, 2010. doi:10.1049/iet-gtd.2009.0046.

[61] E. Litvinov, T. Zheng, G. Rosenwald, and P. Shamsollahi. Marginal loss modeling in lmp calculation. *IEEE Transactions on Power Systems*, 19(2):880–888, 2004. doi:10.1109/TPWRS.2004.825894.

[62] Y. Liu, J. Li, and L. Wu. Distribution system restructuring: Distribution lmp via unbalanced acopf. *IEEE Transactions on Smart Grid*, PP(99):1–1, 2017. doi:10.1109/TSG.2016.2647692.

[63] Y. Liu, J. Li, and L. Wu. Distribution system restructuring: Distribution lmp via unbalanced acopf. *IEEE Transactions on Smart Grid*, PP(99):1–1, 2017. doi:10.1109/TSG.2016.2647692.

[64] Y. Liu, J. Li, L. Wu, and Q. Liu. Ex-post real-time distribution lmp based on state estimation. In *2016 IEEE Power and Energy Society General Meeting (PESGM)*, pages 1–5, July 2016. doi:10.1109/PESGM.2016.7741682.

[65] J. Löfberg. Yalmip: A toolbox for modeling and optimization in matlab. In *2004 IEEE International Symposium on Computer-Aided Control System Design*, pages 284–289, Piscataway, NJ, 2004. IEEE. doi:10.1109/CACSD.2004.1393890.

[66] Y. Ma, A. Kelman, A. Daly, and F. Borrelli. Predictive Control for Energy Efficient Buildings with Thermal Storage: Modeling, Stimulation, and Experiments. *IEEE Control Syst.*, 32(1):44–64, 2012. doi:10.1109/MCS.2011.2172532.

[67] M. Maasoumy. *Controlling Energy-Efficient Buildings in the Context of Smart Grid: A Cyber Physical System Approach*. PhD thesis, University of California, Berkeley, 2013. URL: http://www.eecs.berkeley.edu/Pubs/TechRpts/2013/EECS-2013-244.html.

[68] M. Maasoumy, A. Pinto, and A. Sangiovanni-Vincentelli. Model-Based Hierarchical Optimal Control Design for HVAC Systems. In *ASME 2011 Dyn. Syst. Control Conf. Bath/ASME Symp. Fluid Power Motion Control. Vol. 1*, pages 271–278, 2011. doi:10.1115/DSCC2011-6078.

[69] M. Maasoumy, C. Rosenberg, A. Sangiovanni-Vincentelli, and D. S. Callaway. Model predictive control approach to online computation of demand-side flexibility of commercial buildings HVAC systems for Supply Following. In *2014 Am. Control Conf.*, pages 1082–1089. IEEE, jun 2014. doi:10.1109/ACC.2014.6858874.

[70] P. D. Martini. Making the distribution grid more open, efficient and resilient, 2015. URL: https://www.energy.gov/sites/prod/files/2015/04/f21/05-Mar2015EAC-GridMod-DeMartini.pdf.

[71] E. Martinot, L. Kristov, and J. D. Erickson. Distribution system planning and innovation for distributed energy futures. *Current Sustainable/Renewable Energy Reports*, 2(2):47–54, Jun 2015. URL: https://doi.org/10.1007/s40518-015-0027-8, doi:10.1007/s40518-015-0027-8.

[72] J. L. Mathieu, D. S. Callaway, and S. Kiliccote. Variability in automated responses of commercial buildings and industrial facilities to dynamic electricity prices. *Energy Build.*, 43(12):3322–3330, 2011. doi:10.1016/j.enbuild.2011.08.020.

[73] J. L. Mathieu, P. N. Price, S. Kiliccote, and M. A. Piette. Quantifying changes in building electricity use, with application to demand response. *IEEE Trans. Smart Grid*, 2(3):507–518, 2011. doi:10.1109/TSG.2011.2145010.

[74] K. K. Mehmood, S. U. Khan, S.-J. Lee, Z. M. Haider, M. K. Rafique, and C.-H. Kim. A real-time optimal coordination scheme for the voltage regulation of a distribution network including an oltc, capacitor banks, and multiple distributed energy resources. *International Journal of Electrical Power and Energy Systems*, 94:1 – 14, 2018. URL: http://www.sciencedirect.com/science/article/pii/S0142061517309092, doi:https://doi.org/10.1016/j.ijepes.2017.06.024.

[75] G. Mokryani. Active distribution networks planning with integration of demand response. *Solar Energy*, 122:1362 – 1370, 2015. URL: http://www.sciencedirect.com/science/article/pii/S0038092X15006076, doi:https://doi.org/10.1016/j.solener.2015.10.052.

[76] D. K. Molzahn. *Application of Semidefinite Optimization Techniques to Problems in Electric Power Systems*. dissertation, University of Wisconsin-Madison Department of Electrical and Computer Engineering, August 2013.

[77] D. K. Molzahn, F. Dörfler, H. Sandberg, S. H. Low, S. Chakrabarti, R. Baldick, and J. Lavaei. A survey of distributed optimization and control algorithms for electric power systems. *IEEE Transactions on Smart Grid*, 8(6):2941–2962, Nov 2017. doi:10.1109/TSG.2017.2720471.

[78] Network-Enabled Optimization System (NEOS). Types of optimization problems: Taxonomy. NEOS, 2017. URL: https://neos-guide.org/content/optimization-taxonomy.

[79] J. Nocedal and W. Stephen, J. *Springer Series in Operations Research: Numerical Optimization*. Springer, USA, 2006.

[80] F. Oldewurtel, C. N. Jones, and M. Morari. A tractable approximation of chance constrained stochastic MPC based on affine disturbance feedback. In *Proc. IEEE Conf. Decis. Control*, pages 4731–4736, 2008. doi:10.1109/CDC.2008.4738806.

[81] F. Oldewurtel, A. Parisio, C. N. Jones, D. Gyalistras, M. Gwerder, V. Stauch, B. Lehmann, and M. Morari. Use of model predictive control and weather forecasts for energy efficient building climate control. *Energy Build.*, 45:15–27, feb 2012. doi:10.1016/j.enbuild.2011.09.022.

[82] A. Papavasiliou. Analysis of distribution locational marginal prices. *IEEE Transactions on Smart Grid*, 2017. doi:10.1109/TSG.2017.2673860.

[83] F. Pilo and e. a. Jupe. *Working Group C6.19: Planning and optimization methods for active distribution systems*. Cigre C6, 08 2014.

[84] D. Z. Ray, E. M. S. Carlos, and J. T. Robert. Matpower: Steady-state operations, planning, and analysis tools for power systems research and education. *IEEE Transactions on Power Systems*, 26(1):12–19, 2011. doi:10.1109/TPWRS.2010.2051168.

[85] D. Roger and M. Davis. Reference guide: The open distribution system simulator(opendss), 2018. URL: svn.code.sf.net/p/electricdss/code/trunk/Distrib/Doc/OpenDSSManual.pdf.

[86] T. Samad, E. Koch, and P. Stluka. Automated Demand Response for Smart Buildings and Microgrids: The State of the Practice and Research Challenges. *Proc. IEEE*, 104(4):726–744, 2016. doi:10.1109/JPROC.2016.2520639.

[87] S. Sarykalin, G. Serraino, and S. Uryasev. *Value-at-Risk vs. Conditional Value-at-Risk in Risk Management and Optimization*, chapter Chapter 13, pages 270–294. INFORMS, 2008. doi:10.1287/educ.1080.0052.

[88] F. C. Schweppe, M. C. Caramanis, R. D. Tabors, and R. E. Bohn. *Spot Pricing of Electricity*. The Kluwer International Series in Engineering and Computer Science, Power Electronics & Power Systems. Springer US, Boston, MA, 1988.

[89] V. R. Simoni and G. L. Torres. A sequential *l*-1 quadratic programming method for robust nonlinear optimal power flow solution. In *2014 Power Systems Computation Conference*, pages 1–7, Aug 2014. doi:10.1109/PSCC.2014.7038398.

[90] P. M. Sotkiewicz and J. M. Vignolo. Nodal pricing for distribution networks: efficient pricing for efficiency enhancing dg. *IEEE Transactions on Power Systems*, 21(2):1013–1014, May 2006. doi:10.1109/TPWRS.2006.873006.

[91] A. A. Sousa, G. L. Torres, and C. A. Canizares. Robust optimal power flow solution using trust region and interior-point methods. *IEEE Transactions on Power Systems*, 26(2):487–499, May 2011. doi:10.1109/TPWRS.2010.2068568.

[92] State of Hawaii Public Utilities Commission. Exhibit a: Commission's inclinations on the future of hawaii's electric utilities, 2014. URL: http://www.puc.hawaii.gov/wp-content/uploads/2014/04/Commissions-Inclinations.pdf.

[93] State of New York, Department of Public Service. Developing the rev market in new york: Dps staff straw proposal on track one issues, 2014. URL: http://documents.dps.ny.gov/public/Common/ViewDoc.aspx?DocRefId=%7BCA26764A-09C8-46BF-9CF6-F5215F63EF62%7D.

[94] S. Stoft. *Power System Economics: Designing Markets for Electricity*. Wiley, 2002.

[95] D. Sturzenegger, D. Gyalistras, M. Morari, and R. S. Smith. Model Predictive Climate Control of a Swiss Office Building: Implementation, Results, and Cost-Benefit Analysis. *IEEE Trans. Control Syst. Technol.*, 24(1):1–12, 2016. doi:10.1109/TCST.2015.2415411.

[96] D. Sturzenegger, V. Semeraro, D. Gyalistras, and R. S. Smith. Building Resistance-Capacitance Modeling (BRCM) ToolBox, 2012. URL: http://www.brcm.ethz.ch.

[97] J. Taylor. *Convex Optimization of Power Systems*. Convex Optimization of Power Systems. Cambridge University Press, 2015. URL: https://books.google.com.sg/books?id=hlW2oAEACAAJ.

[98] TRNSYS. Trnsys 17 - A Transient System Simulation Program. Technical report, Solar Energy Laboratory, Univ. of Wisconsin-Madison, 2013. URL: http://sel.me.wisc.edu/trnsys/features/t17_1_updates.pdf.

[99] R. A. Verzijlbergh, L. J. de Vries, and Z. Lukszo. Renewable energy sources and responsive demand. do we need congestion management in the distribution grid? *IEEE Transactions on Power Systems*, 29(5):2119–2128, 2014. doi:10.1109/TPWRS.2014.2300941.

[100] R. A. Verzijlbergh, M. O. W. Grond, Z. Lukszo, J. G. Slootweg, and M. D. Ilic. Network impacts and cost savings of controlled EV charging. *IEEE Transactions on Smart Grid*, 3(3):1203–1212, 2012. doi:10.1109/TSG.2012.2190307.

[101] C. Wang, A. Bernstein, J. Y. L. Boudec, and M. Paolone. Explicit conditions on existence and uniqueness of load-flow solutions in distribution networks. *IEEE Transactions on Smart Grid*, PP(99):1–1, 2017. doi:10.1109/TSG.2016.2572060.

[102] W. Wang and N. Yu. Lmp decomposition with three-phase dcopf for distribution system. In *2016 IEEE Innovative Smart Grid Technologies - Asia (ISGT-Asia)*, pages 1–8, Nov 2016. doi:10.1109/ISGT-Asia.2016.7796352.

[103] W. Warwick, T. Hardy, M. Hoffman, and J. Homer. Electricity distribution system baseline report, 2016. URL: https://www.energy.gov/sites/prod/files/2017/01/f34/Electricity%20Distribution%20System%20Baseline%20Report.pdf.

[104] A. Wood, B. Wollenberg, and G. Sheblé. *Power Generation, Operation, and Control*. Wiley, 2013.

[105] Y. Xu, N. Li, and S. H. Low. Demand response with capacity constrained supply function bidding. *IEEE Transactions on Power Systems*, 31(2):1377–1394, March 2016. doi:10.1109/TPWRS.2015.2421932.

[106] R. Yang and Y. Zhang. Three-phase ac optimal power flow based distribution locational marginal price. In *2017 IEEE Power Energy Society Innovative Smart Grid Technologies Conference (ISGT)*, pages 1–5, April 2017. doi:10.1109/ISGT.2017.8086032.

[107] M. Yao, J. L. Mathieu, and D. K. Molzahn. Using demand response to improve power system voltage stability margins. In *2017 IEEE Manchester PowerTech*, pages 1–6, June 2017. doi:10.1109/PTC.2017.7980798.

[108] S. Yu, H. D. Nguyen, and K. S. Turitsyn. Simple certificate of solvability of power flow equations for distribution systems. In *2015 IEEE Power Energy Society General Meeting*, pages 1–5, July 2015. doi:10.1109/PESGM.2015.7286371.

[109] H. Yuan, F. Li, Y. Wei, and J. Zhu. Novel linearized power flow and linearized opf models for active distribution networks with application in distribution lmp. *IEEE Transactions on Smart Grid*, page 1, 2016. doi:10.1109/TSG.2016.2594814.

[110] Z. Yuan, M. R. Hesamzadeh, and D. Biggar. Distribution locational marginal pricing by convexified acopf and hierarchical dispatch. *IEEE Transactions on Smart Grid*, PP(99):1–1, 2016. doi:10.1109/TSG.2016.2627139.

[111] J. Zhong and K. Bhattacharya. Toward a competitive market for reactive power. *IEEE Transactions on Power Systems*, 17(4):1206–1215, Nov 2002. doi:10.1109/TPWRS.2002.805025.

[112] R. D. Zimmerman. *Comprehensive distribution power flow: modeling, formulation, solution algorithms and analysis*. Ph.d., School of Electrical Engineering, Ithaca, NY, USA, 1995.

[113] R. D. Zimmerman and C. E. Murillo-Sánchez. *MATPOWER 6.0 User's Manual*. Power Systems Engineering Research Center (PSERC), Dec 2016. URL: http://www.pserc.cornell.edu/matpower/manual.pdf.